1-1-2013

Functional Block Copolymers for Applications in Advanced Materials, Energy Storage, and Lithography

Christopher George Hardy
University of South Carolina

FUNCTIONAL BLOCK COPOLYMERS FOR APPLICATIONS IN ADVANCED MATERIALS, ENERGY STORAGE, AND LITHOGRAPHY

by

Christopher George Hardy

Bachelor of Science
North Carolina State University, 2009

Submitted in Partial Fulfillment of the Requirements

For the Degree of Doctor of Philosophy in

Chemistry

College of Arts and Sciences

University of South Carolina

2013

Accepted by:

Chuanbing Tang, Major Professor

Brian Benicewicz, Committee Member

Harry Ploehn, Committee Member

Daniel Reger, Committee Member

Lacy Ford, Vice Provost and Dean of Graduate Studies

DEDICATION

In loving memory of my grandfathers, Carl Greene Hardy, Jr. and George Harvey Rouse.

ACKNOWLEDGEMENTS

First, I would like to thank my advisor, Prof. Chuanbing Tang, for his guidance and constant support during my graduate studies at the University of South Carolina. The opportunity to learn from such a knowledgeable, enthusiastic, and assiduous person has proved invaluable in my development as a scientist.

I would also like to thank my research committee – Prof. Brian Benicewicz, Prof. Harry Ploehn, and Prof. Daniel Reger – for their advice, conversations, and encouragement during graduate school. Further, the research collaborations formed with the Benicewicz and Ploehn groups were instrumental in the research presented herein.

I am very appreciative of the experiences shared and friendships formed with other graduate students and post-docs at USC. Members of Tang lab – especially Lixia, Kejian, Perry, Jiuyang, Yali, Yi, and Jeff – I owe you all a lot of thanks for your help throughout the years. I would also like to thank Anand, Atri, Brandon, and Kai (χ) for your help both within and outside of lab.

The friendships that have continued from before and developed during my stay in Columbia are also very much cherished. Phil, Cory, Mark, Max, Jason, Chad, MD Mains, Buck, Taylor, and the One Hit Wonders – may the good times we have shared and friendships we have formed in years past continue into the future.

Finally, I would like to thank my family – my grandparents and my parents, my brother and sister, Terri, and Mr. Bighead (Oliver) – your support throughout my academic career allowed me to reach this stage. Thank you all very much!

ABSTRACT

Block copolymers spontaneously self-assembly into a wide variety of ordered nanostructures on the length scale of 5 - 100 nm due to the thermodynamic immiscibility between the covalently linked, chemically distinct polymer chains. Incorporating desirable functional groups into block copolymer systems can lead to confinement of the functional group to a specific domain upon microphase separation of the block copolymer. The resulting materials display desirable characteristics of the functional group in a well-ordered nanostructure. Such systems have been utilized in a wide variety of applications including catalysis, ceramic materials, and membranes. This dissertation is focused on the synthesis, characterization, self-assembly and materials processing of various functionalized block copolymer systems. An assortment of monomers functionalized with specific groups were prepared and polymerized by a variety of polymerization techniques including atom transfer radical polymerization, reversible addition-fragmentation chain transfer polymerization, and ring-opening metathesis polymerization. Self-assembly of the functionalized block copolymers led to well-defined nanostructures in bulk and thin films. Depending upon the functional group incorporated, the ordered materials were utilized in various applications including ordered catalysts, energy storage, and templates for nanolithography.

TABLE OF CONTENTS

LIST OF TABLES

LIST OF FIGURES

CHAPTER 1

OVERVIEW

1.1 BACKGROUND

Block copolymers are a class of intriguing soft materials comprised of at least two covalently linked polymer chains.[1] Thermodynamic immiscibility between these chemically distinct blocks leads to a variety of ordered nanostructures with periodicity at the scale of 10 - 100 nm.[2] Such length scales enable block copolymers for use in many potential applications including templates for lithography, microelectronic devices, membranes, data storage systems, photonic crystals, etc.[3-12] The simplest coil-coil diblock copolymers typically self-assemble into body-centered cubic spheres, hexagonally packed cylinders, gyroid structures and lamellae, as seen in Figure 1.1.[13-15] Microphase-separated structures of block copolymers are dictated by three experimental parameters including the degree of polymerization (N), the volume fraction of the blocks (f), and the Flory–Huggins interaction parameter (χ).[16-19] The chemical nature of the blocks determines χ, which essentially describes segment-segment interactions.

Other than AB diblock copolymers which have been well developed for more than three decades, there are many other strategies for developing novel block copolymer systems. Linear ABC triblock copolymers have received significant attention because of the existence of the wide range of potential morphologies such as periodic arrays of core/shell spheres and cylinders, tetragonal lattices of cylinders, and novel bi-continuous

and tri-continuous ordered mesophases, as seen in Figure 1.1.[20, 21] As opposed to one binary interaction parameter, one volume fraction and a single block sequence for AB diblock copolymers, the greater diversity in morphology afforded by ABC triblock copolymers is due to their three binary interaction parameters, two independent volume fractions and three different block sequences.[22-27] Blends of diblock copolymers such as A-B/B-C and A-B/C-D have also been explored in searching for novel architectures.[28, 29] However, these systems are somewhat limited due to the occurrence of macrophase separation. In a related approach, supramolecular interactions have been employed in A-B/B'-C type block copolymer blends to improve compatibility and limit macrophase separation, as the B/B' interaction (typically hydrogen bonding) allows the B and B' block to form a homogenous domain, which in turn allows for microphase separation to occur between the A, B/B', and C block fractions.[30-32]

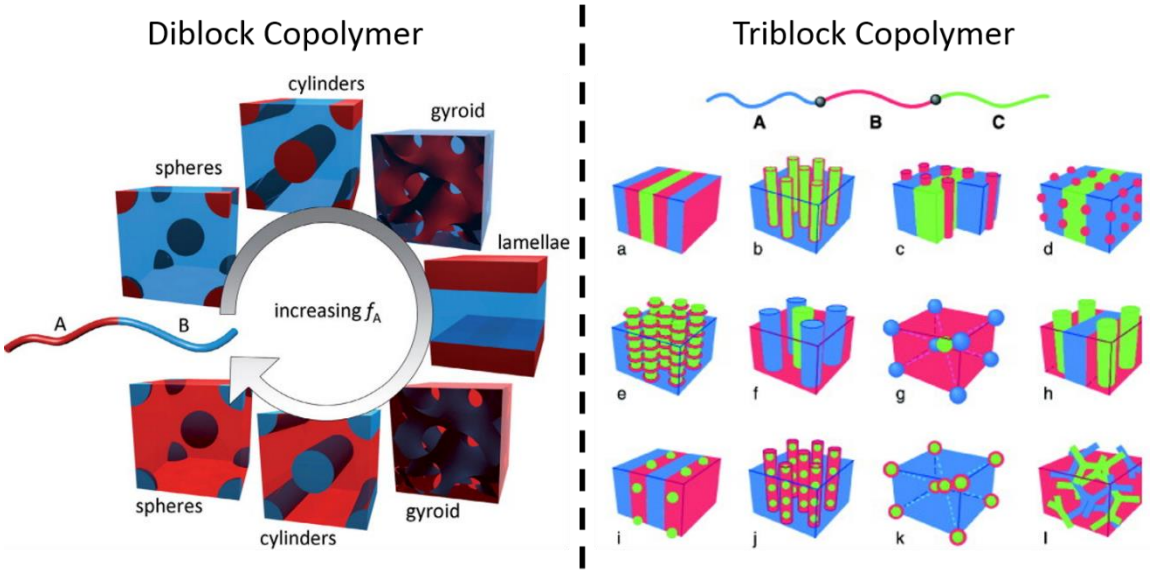

Figure 1.1. Various architectures of diblock and triblock copolymers.[33]

In the past 20 years, various controlled radical polymerization techniques, mainly atom transfer radical polymerization (ATRP),[34-40] reversible addition-fragmentation chain transfer polymerization (RAFT),[41, 42] and nitroxide-mediated polymerization (NMP),[43, 44] have been utilized to prepare well-defined polymers with predetermined molecular weight, narrow molecular weight distribution, controlled functionalities and architectures. In parallel, non-radical based living/controlled polymerization techniques such as ring-opening metathesis polymerization (ROMP) have also drawn significant attention in developing multifunctional polymers with precisely controlled structures.[45] As each of these polymerization techniques preserves the polymer end-group, block copolymers can be easily prepared by chain extension with a second monomer, as shown in Scheme 1.1. Separately, the polymer end-groups can be modified to react with a second end-functionalized polymer chain, which also serves as an effective way to prepare block copolymers. While the chain extension route is often preferred due to simplicity, polymer coupling can be utilized when chain extension is not possible due to the inability for a particular polymerization method to polymerize a specific monomer.

Scheme 1.1. Preparation of block copolymers by chain extension (*Route 1*) and polymer coupling (*Route 2*).

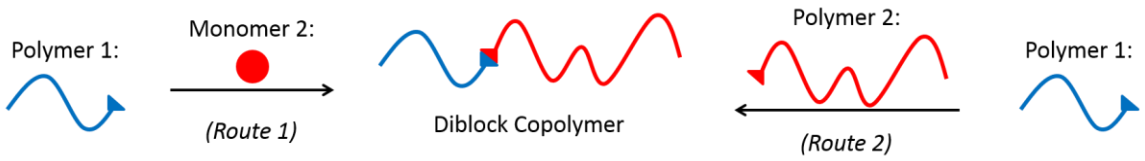

1.2 Dissertation Outline

The goal of this thesis is to discover novel functional block copolymers for applications in advanced materials, energy storage, and lithography. Various desired

functional groups have been incorporated into the side-chain, end-chain, and/or linker between polymer chains to confine the functional group either within a specific domain or at the junction between domains within a microphase separated polymer film.

Chapters 2-4 involve incorporation of metallocene moieties into the side-chain of block copolymers. Specifically, the second chapter is a review on the synthesis and applications of side-chain metallocene-containing polymers prepared by living and controlled polymerization techniques. This review discusses the synthetic challenges that the metallopolymer field has struggled over the years, and details the synthetic techniques that have led to the successful incorporation of metallocene units into polymeric structures. The third chapter covers the preparation, polymerization, and properties of several ferrocene-containing (meth)acrylate monomers. The fourth chapter details the preparation and self-assembly of ferrocene-containing triblock copolymers, and their use in the templated synthesis of ordered iron oxide nanoparticles.

In Chapters 5-6, conjugated oligoaniline moieties were incorporated into block copolymer systems for use as all-organic nanodielectric materials. Specifically, the fifth chapter summarizes the incorporation of oligoaniline moieties onto the side-chain of diblock copolymers in which one block is electrically insulating, while the oligoaniline-containing block is electrically conductive. The synthesis, self-assembly, and dielectric properties were studied. The sixth chapter details incorporating oligoaniline units at the end-chains of electrically insulating polystyrene. The oligoaniline domains form conductive nanodomains upon microphase separation, which results in enhanced dielectric properties.

In Chapters 7-8, block copolymer systems are developed to produce highly dense nanoporous films for use as templates in nanolithography. In the seventh chapter, a photocleavable linker is placed within the two blocks of poly(ethylene oxide)-*block*-polystyrene (PEO-*b*-PS). Nanoporous films are obtained after microphase separation, photoexposure, and removal of PEO. A lower molecular weight for the linear diblock copolymer PEO-*b*-PS is realized, as macroscopic dewetting occurs below a molecular weight threshold. In the eighth chapter, a grafted block copolymer system is developed to target low feature sizes that prove impossible for the linear diblock copolymer PEO-*b*-PS system.

1.3 REFERENCES

1. Bates, F. S.; Fredrickson, G. H. *Annu. Rev. Phys. Chem.* **1990,** 41, 525-557.
2. Bates, F. S.; Fredrickson, G. H. *Phys. Today* **1999,** 52, 32-38.
3. Albert, J. N. L.; Epps III, T. H. *Mater. Today* **2010,** 13, 24-33.
4. Bang, J.; Jeong, U.; Ryu, D. Y.; Russell, T. P.; Hawker, C. J. *Adv. Mater.* **2009,** 21, 4769-4792.
5. Hadjichristidis, N.; Pispas, S.; Floudas, G., *Block Copolymers: Synthetic Strategies, Physical Properties, and Applications*. John Wiley & Sons, Inc.: Hoboken, NJ, 2003.
6. Hamley, I. W., *The Physics of Block Copolymers*. Oxford University Press: Oxford, U.K., 1998.
7. Hamley, I. W. *Prog. Polym. Sci.* **2009,** 34, 1161-1210.
8. Kim, H.-C.; Park, S.-M.; Hinsberg, W. D. *Chem. Rev.* **2010,** 110, 146-177.
9. Lazzari, M.; Liu, G.; Lecommandoux, S., *Block Copolymers in Nanoscience*. Wiley-VCH: Weinheim, 2007.
10. Park, C.; Yoon, J.; Thomas, E. L. *Polymer* **2003,** 44, 6725-6760.
11. Park, M.; Harrison, C.; Chaikin, P. M.; Register, R. A.; Adamson, D. H. *Science* **1997,** 276, 1401-1404.
12. Tang, C.; Tracz, A.; Kruk, M.; Zhang, R.; Smilgies, D.-M.; Matyjaszewski, K.; Kowalewski, T. *J. Am. Chem. Soc.* **2005,** 127, 6918-6919.
13. Fredrickson, G. H.; Bates, F. S. *Annu. Rev. Mater. Sci.* **1996,** 26, 501-550.
14. Helfand, E. *Macromolecules* **1975,** 8, 552-556.
15. Leibler, L. *Macromolecules* **1980,** 13, 1602-1617.
16. Hajduk, D. A.; Harper, P. E.; Gruner, S. M.; Honeker, C. C.; Kim, G.; Thomas, E. L.; Fetters, L. J. *Macromolecules* **1994,** 27, 4063-4075.
17. Helfand, E.; Wasserman, Z. R. *Macromolecules* **1978,** 11, 960-966.
18. Helfand, E.; Wasserman, Z. R. *Macromolecules* **1980,** 13, 994-998.

19. Matsushita, Y.; Mori, K.; Saguchi, R.; Nakao, Y.; Noda, I.; Nagasawa, M. *Macromolecules* **1990,** 23, 4313-4316.
20. Mogi, Y.; Kotsuji, H.; Kaneko, Y.; Mori, K.; Matsushita, Y.; Noda, I. *Macromolecules* **1992,** 25, 5408-5411.
21. Mogi, Y.; Nomura, M.; Kotsuji, H.; Ohnishi, K.; Matsushita, Y.; Noda, I. *Macromolecules* **1994,** 27, 6755-6760.
22. Bailey, T. S.; Pham, H. D.; Bates, F. S. *Macromolecules* **2001,** 34, 6994-7008.
23. Bang, J.; Kim, S. H.; Drockenmuller, E.; Misner, M. J.; Russell, T. P.; Hawker, C. J. *J. Am. Chem. Soc.* **2006,** 128, 7622-7629.
24. Chen, H.-Y.; Fredrickson, G. H. *J. Chem. Phys.* **2002,** 116, 1137-1146.
25. Nakazawa, H.; Ohta, T. *Macromolecules* **1993,** 26, 5503-5511.
26. Rzayev, J.; Hillmyer, M. A. *J. Am. Chem. Soc.* **2005,** 127, 13373-13379.
27. Tang, C.; Bang, J.; Stein, G. E.; Fredrickson, G. H.; Hawker, C. J.; Kramer, E. J.; Sprung, M.; Wang, J. *Macromolecules* **2008,** 41, 4328-4339.
28. Abetz, V.; Goldacker, T. *Macromol. Rapid Commun.* **2000,** 21, 16-34.
29. Kimishima, K.; Jinnai, H.; Hashimoto, T. *Macromolecules* **1999,** 32, 2585-2596.
30. Tang, C.; Hur, S.-m.; Stahl, B. C.; Sivanandan, K.; Dimitriou, M.; Pressly, E.; Fredrickson, G. H.; Kramer, E. J.; Hawker, C. J. *Macromolecules* **2010,** 43, 2880-2889.
31. Tang, C.; Lennon, E. M.; Fredrickson, G. H.; Kramer, E. J.; Hawker, C. J. *Science* **2008,** 322, 429-432.
32. Tang, C.; Sivanandan, K.; Stahl, B. C.; Fredrickson, G. H.; Kramer, E. J.; Hawker, C. J. *ACS Nano* **2010,** 4, 285-291.
33. Botiz, I.; Darling, S. B. *Mater. Today* **2010,** 13, 42-51.
34. Wang, J.-S.; Matyjaszewski, K. *J. Am. Chem. Soc.* **1995,** 117, 5614-5615.
35. Percec, V.; Barboiu, B. *Macromolecules* **1995,** 28, 7970-7972.
36. Kato, M.; Kamigaito, M.; Sawamoto, M.; Higashimura, T. *Macromolecules* **1995,** 28, 1721-1723.
37. Matyjaszewski, K.; Xia, J. *Chem. Rev.* **2001,** 101, 2921-2990.
38. Tsarevsky, N. V.; Matyjaszewski, K. *Chem. Rev.* **2007,** 107, 2270-2299.
39. Matyjaszewski, K. *Macromolecules* **2012,** 45, 4015-4039.
40. Matyjaszewski, K.; Tsarevsky, N. V. *Nat. Chem.* **2009,** 1, 276-288.
41. Chiefari, J.; Chong, Y. K.; Ercole, F.; Krstina, J.; Jeffery, J.; Le, T. P. T.; Mayadunne, R. T. A.; Meijs, G. F.; Moad, C. L.; Moad, G.; Rizzardo, E.; Thang, S. H. *Macromolecules* **1998,** 31, 5559-5562.
42. Moad, G.; Mayadunne, R. T. A.; Rizzardo, E.; Skidmore, M.; Thang, S. H. *Macromol. Symp.* **2003,** 192, 1-12.
43. Hawker, C. J.; Bosman, A. W.; Harth, E. *Chem. Rev.* **2001,** 101, 3661-3688.
44. Nicolas, J.; Guillaneuf, Y.; Lefay, C.; Bertin, D.; Gigmes, D.; Charleux, B. *Prog. Poly. Sci.* **2013,** 38, 63-235.
45. Bielawski, C. W.; Grubbs, R. H., Living Ring-Opening Metathesis Polymerization. In *Controlled and Living Polymerizations*, Wiley-VCH: Weinheim, Germany, 2010; pp 297-342.

CHAPTER 2

SIDE-CHAIN METALLOCENE-CONTAINING POLYMERS BY LIVING AND CONTROLLED POLYMERIZATIONS[†]

[†] Hardy, C. G.; Ren, L.; Zhang, J.; Tang, C. *Israel Journal of Chemistry* **2012**, *53*, 230-245. Reprinted here with permission of publisher.

2.1 ABSTRACT

This review summarizes recent work on side-chain metallocene-containing polymers prepared by controlled and living polymerizations, which include living anionic polymerization (LAP), ring-opening metathesis polymerization (ROMP) and controlled radical polymerization (CRP) such as atom transfer radical polymerization (ATRP), reversible addition fragmentation chain transfer polymerization (RAFT), and nitroxide-mediated polymerization (NMP). The majority of efforts in the field are focused on side-chain ferrocene-containing polymers, while cobaltocenium-containing polymers have recently started to draw attention. Future direction on the development of other metallocene-containing polymers is discussed.

2.2 INTRODUCTION

Over the past sixty years, metallopolymers have been developed to combine the synthetic efficiency and versatility of an organic polymer framework with the unique redox, responsive, and catalytic properties of inorganic metals.[1-18] Among a variety of metallopolymers, metallocene-containing polymers attract significant attention in materials science due to their high thermal stability, fully reversible redox chemistry and many other fascinating properties that arise from their unique sandwich-like structures.[19-25] Following the discovery of ferrocene in 1950s, metallocene-functionalized macromolecules including oligomers, polymers and dendrimers have found uses in applications such as catalysts, redox sensors, magnetic materials, ceramic materials, nanolithography, and biomedical systems.[26-30] These metallocene-containing macromolecules serve to bridge together several fields of chemistry including inorganic, organic, polymer or dendrimer chemistry and materials science.

Generally, there are two major classes of metallocene-containing polymers: main-chain polymers with the metallocene as an integral part of polymer backbone (Figure 2.1A) and side-chain metallocene-containing polymers in which the entire metallocene moiety is a pendant group (Figure 2.1B). Other much less developed metallocene-containing polymers include: embedded side-chain polymers in which the polymer backbone crosses the same cyclopentadiene ring in one metallocene unit (Figure 2.1C) and unbridged metallocene-containing polymers in which the polymer backbone directly connects the metal center (Figure 2.1D).

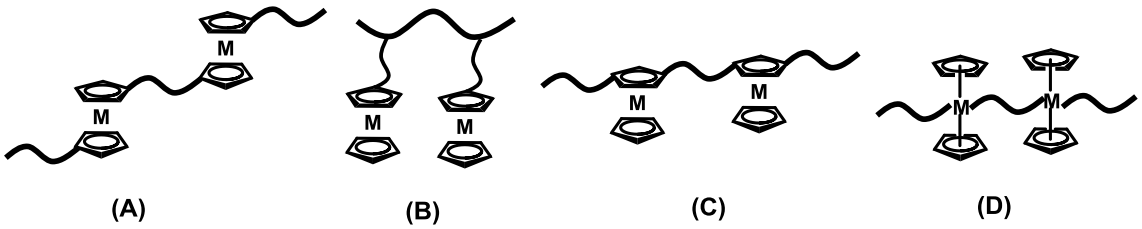

Figure 2.1. Four different classes of metallocene-containing polymers.

Early efforts involved the preparation of side-chain ferrocene-containing polymers, such as poly(vinylferrocene), due to facile electrophilic substitution of ferrocene.[31-33] There were also studies of ferrocene-containing acrylate and methacrylate monomers that were polymerized by conventional techniques such as free radical, cationic, and anionic polymerization.[34-36] However, these techniques generally produced low molecular weight polymers (< 10,000 g/mol) that lack the control of molecular weight and molecular weight distribution. The synthetic challenges have halted more interest in studying these side-chain metallocene-containing polymers as prepared by conventional polymerization techniques.

During the late 1970s and 1980s there was much work on how poly(vinylferrocene) was prepared by both electrochemical polymerization and plasma polymerization techniques.[37-43] Films of the redox-active polymers were formed onto electrode surfaces when these polymers precipitated during the polymerization. The degree of polymerization and the film thickness was relative to the length of time that the current was applied, as the chain growth continued at the outer surface of the polymer film. These modified electrodes served as model systems in understanding electron propagation (charge transport) in redox active polymer films.[44, 45]

In the early 1990s, seminal work on strained, ring-tilted metallocenophanes reported by Manners and coworkers opened a new era in the field of ferrocene-containing polymers, that is, to develop well-defined high molecular weight main-chain ferrocene-containing polymers by anionic ring-opening polymerization.[46] A wide array of elements have been used to link the two cyclopentadienyl (Cp) rings of ferrocene including elements from Groups 4, 10, and 13-16. This allows for incorporation of additional desired functionalities in the polymer main chain. Ferrocenylsilanes, in which a silicon atom is used to bridge the two Cp rings, have been the most widely studied system. A variety of block copolymers have been prepared in which the additional blocks contain various repeat units including styrene, isoprene, (meth)acrylates, and different substituted ferrocenophanes. For example, Scheme 2.1 details the synthetic route of triblock copolymer polyisoprene-*block*-polystyrene-*block*-polyferrocenylsilane (PI-*b*-PS-*b*-PFS) prepared by anionic ring-opening polymerization.[47] This field has flourished over the last two decades as a variety of main-chain ferrocene-containing polymers and block polymers have been developed.[26-30, 48, 49] These ferrocene-containing polymers have been

used in a wide range of applications including magnetic ceramics, variable refractive index sensors, nonlinear optical materials, and plasma etch resistant materials.

Scheme 2.1 Synthesis of triblock copolymer PI-*b*-PS-*b*-PFS prepared by anionic ring-opening polymerization (PI represents three different isoprene units in the main chain).

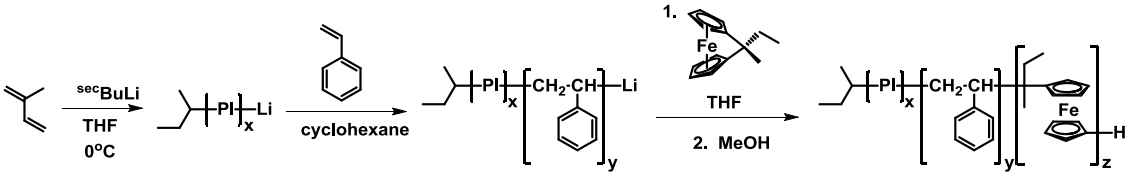

Although the last two decades have witnessed rapid development of main-chain ferrocene-containing polymers, the side-chain ferrocene-containing polymers have only gained attention until recently. Well-defined side-chain metallocene-containing polymers and block copolymers have been synthesized by living anionic polymerization (LAP)[50, 51] and ring-opening metathesis polymerization (ROMP),[52] as well as by controlled/living radical polymerization (CRP) techniques[53-55] including atom transfer radical polymerization (ATRP),[56-58] reversible addition-fragmentation chain transfer polymerization (RAFT),[55] and nitroxide-mediated polymerization (NMP).[59, 60] This mini-review aims to give an overview of side-chain metallocene-containing polymers prepared by various living and controlled polymerization techniques and some of their properties. This article does not aim to be exhaustive as only recent or well-representative examples have been chosen to illustrate individual synthetic routes or properties. Reviews on main-chain metallocene-containing polymers and extensive earlier reviews on side-chain metallocene-containing systems can be found elsewhere.[61, 62] Metallopolymers containing ligated metals in the side chain have also been developed and have been reviewed elsewhere.[63] This review will be limited to the classic metallocene structure,

that is, a metal atom sandwiched between two cyclopentadiene rings. There is an abundance of work in which metal clusters, especially organometallic metal carbonyl compounds, are present as pendant groups; however, these pendant groups are beyond the scope of this mini-review.

2.3 Side-Chain Ferrocene-Containing Polymers

2.3.1 Free Radical Polymerization

Early work on side-chain ferrocene-containing polymers was focused on the free radical polymerization (FRP) of vinylferrocene (VFc).[64, 65] Initial attempts at polymerizing VFc by FRP led to low molecular weight polymers under long reaction time. Rate law and mechanistic studies[66, 67] showed that the first-order chain termination occurred as opposed to the second-order bimolecular termination, leading to a rate law of $r = k[M]^{1.1}[I]^{1.1}$ instead of the expected rate law of $r = k[M]^{1}[I]^{0.5}$ expected for vinyl monomers. It was believed that the metal center adjacent to the active double bond can effectively quench the radical propagating step through internal electron transfer (Scheme 2.2). By inserting an alkyl spacer between the ferrocene moiety and the polymerization site, Pittman et al. found that this electron transfer could be avoided. Ferrocene-containing monomers ferrocenylmethyl acrylate (FMA) and ferrocenylmethyl methacrylate (FMMA) were developed and polymerized by FRP, leading to high molecular weight polymers (Scheme 2.3).[31, 32] The internal electron transfer reaction occurred for VFc provides particularly important information in designing monomers not only for free radical polymerizations, but also for controlled and living polymerizations.

Scheme 2.2. Internal electron transfer mechanism of vinylferrocene.

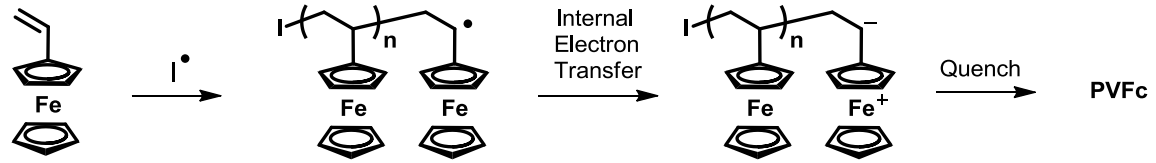

Scheme 2.3. Free radical polymerization of ferrocenylmethyl acrylate and ferrocenylmethyl methacrylate.

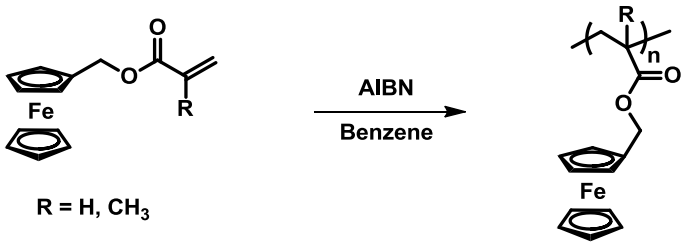

2.3.2 LIVING ANIONIC POLYMERIZATION

Attention soon turned to living anionic polymerization (LAP), as it is well known to produce polymers with well-controlled molecular weights and a narrow molecular weight distribution. Additionally, LAP could be used to produce well-defined block copolymers that can spontaneously self-assemble into an assortment of nanostructures upon microphase separation.[50, 51] Nanostructures containing metallic domains were of high interest as these materials hold great promise for catalysis, nanotechnology, and nanosensing devices.

Pittman et al. first attempted anionic polymerization of FMA and FMMA monomers in the 1970s, but achieved limited success. High molecular weight homopolymers FMMA (>700,000 g/mol) were produced using $LiAlH_4$-initiated anionic polymerization.[34] Block copolymers with methyl methacrylate, acrylonitrile, and styrene

were also prepared.[35] However, the polymerizations were not well controlled as polydispersity indexes (PDI) mostly fell in the range of 2-3. FMA and VFc were shown to be inactive towards anionic polymerization.[36]

Rehahn et al. have recently made great improvements to the anionic polymerization of FMMA. Various polymerization conditions were tried, and as shown in Scheme 2.4, it was found that a true living polymerization system existed when FMMA was initiated by 1,1-diphenylhexyllithium (DPH-Li) in THF in the presence of LiCl at -78 ^{o}C.[68] It was noted that high monomer purity was a strict requirement, as any impurities can lead to problems during polymerization. Homopolymers with molecular weights ranging from 5,000 g/mol to 100,000 g/mol were produced with PDI between 1.03-1.05. Diblock copolymer polystyrene-*block*-poly(ferrocenylmethyl methacrylate) (PS-*b*-PFMMA) was prepared by living anionic polymerization of styrene with the use of sec-butyllithium followed by end-capping with 1,1-diphenylethylene, and finally, by adding in FMMA, LiCl, and THF at -78 ^{o}C. Clean molecular weight shifts with negligible remaining macroinitiator, along with low PDI, were observed by gel permeation chromatography. These experiments proved that the polymerizations were indeed well-controlled and living. A series of block copolymers PS-*b*-PFMMA were prepared in which the molecular weight fraction of polystyrene was varied between 0.1 and 0.43. Surprisingly, thermal annealing produced poor microphase separation. Solvent annealing in a dichloromethane atmosphere at room temperature allowed for partial ordering. Diblock copolymer poly((1,1'-dimethylsilyacylobutant)-*block*-poly(ferrocenylmethyl methacrylate)) (PDMSB-*b*-PFMMA) was also prepared by Rehahn and his coworkers with a similar polymerization route to the synthesis of PS-*b*-

PFMMA.[69] The silicon-containing fraction is interesting due to its potential to serve as a functional material; this is especially useful for the development of ceramics. High chain-extension efficiencies, low PDI, and moderate molecular weights for the diblock copolymers were obtained.

Scheme 2.4. Synthesis of block copolymers PS-*b*-PFMMA by living anionic polymerization.

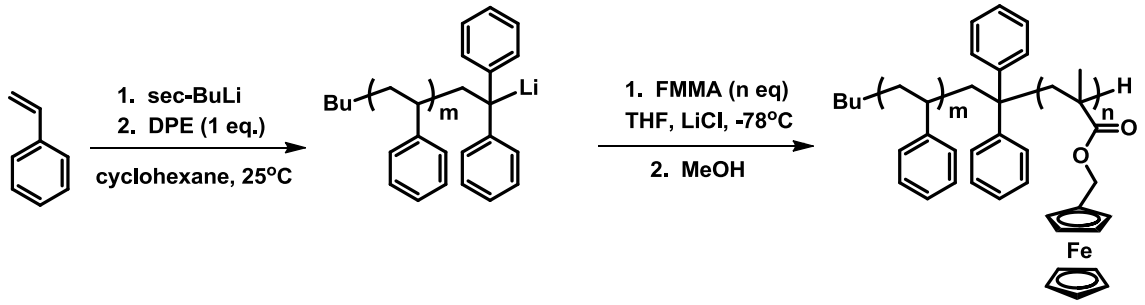

It was not until 1997 that Nuyken et al. reported that VFc could be polymerized by anionic polymerization.[70] A thorough study was carried out in which the initiator, solvent, and reaction temperature were varied in order to find a suitable system for polymerization. It was found that *n*- and *sec*-butyl lithium served as reasonable initiators in a THF solvent at -45 ^{o}C. True living polymerizations were proved for low molecular weight polymers (3,000-5,000 g/mol), as the initiation was instantaneous; molecular weight was controlled by the [monomer]:[initiator] ratio; molecular weight increased linearly with conversion; polydispersity was low (< 1.1); and molecular weight increased upon sequential monomer addition. Furthermore, well-controlled block copolymers with styrene, methyl methacrylate, and propylene sulfide were synthesized. However, it was noted that the LAP of VFc was somewhat limited to low molecular weight polymers; the polymerization rate slowed at ~ 40% monomer conversion and completely stopped at around 75% monomer conversion when targeting molecular weights above 8,000 g/mol.

Upon supplying additional monomers to the reaction system, the polymerization instantaneously proceeded until the monomer conversion again reached high conversion. Polyvinylferrocene with low molecular weights (3,000-5,000 g/mol) had low PDI (< 1.1); however, when higher molecular weights were targeted (> 10, 000 g/mol), the PDI increased significantly (> 1.5). Clearly, the control was problematic, as polymers and block copolymers containing VFc fraction were limited by low molecular weight of the organometallic fraction.

Scheme 2.5. Synthesis of PVFc, PVFc-*b*-PMMA, and PVFc-*b*-P2VP by living anionic polymerization.

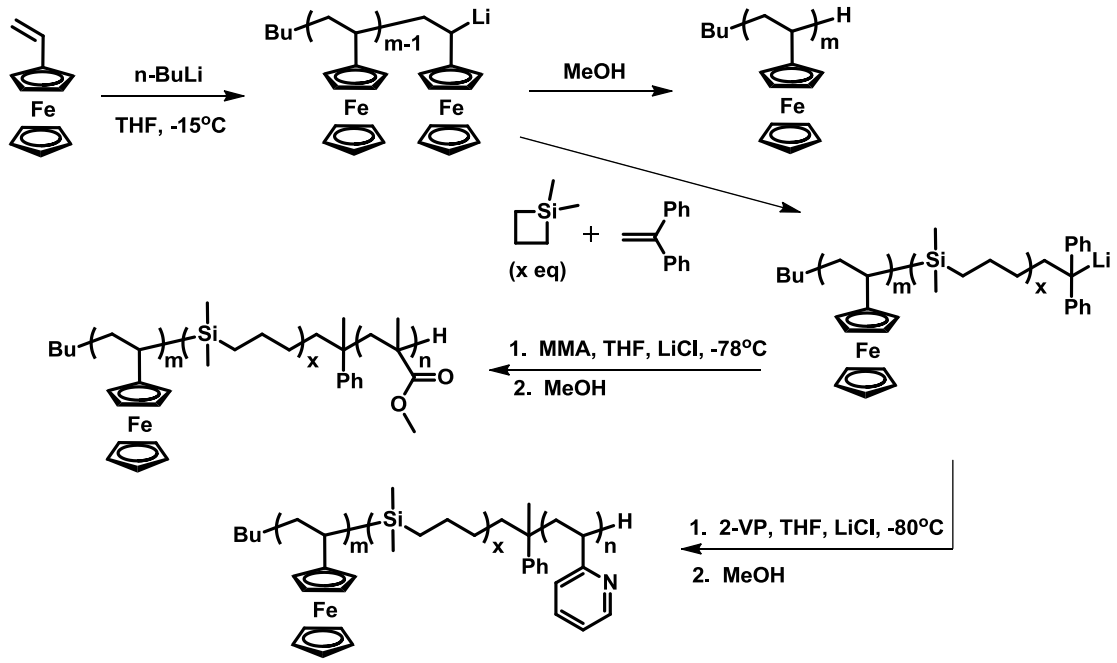

A recent study by Rehahn et al. reported that the highly active propagating species at the initial stage became much less active as the polymerization proceeded, ultimately ending in a deactivated, "sleeping" state prior to quantitative conversion of VFc.[71] To obtain higher molecular weight homopolymers, sequential addition of VFc can be carried out, allowing for additional chain growth while maintaining low PDI. For diblock

copolymer synthesis, direct second monomer addition resulted in broad PDI due to the presence of both active and "sleeping" chain ends. In order to obtain a single macro-anion species before chain extension, a "carbanion-pump" technique was employed to effectively end-cap the polymer chains. It was found that both the active and "sleeping" chain ends can be reactivated by end-capping with 1,1-dimethylsilacyclobutant (DMSB) and 1,1-diphenylethylene (DPE) (Scheme 2.5). The end-capped polyvinylferrocene served as an efficient macroinitiator to produce block copolymers with methyl methacrylate (MMA) and 2-vinylpyridine (2VP). A PVFc-*b*-PMMA diblock copolymer with PVFc molecular weight of 20,400 g/mol and PMMA molecular weight of 81,000 g/mol was produced while maintaining a polydispersity of 1.02.

2.3.3 Ring-Opening Metathesis Polymerization

In the early 1990s, Schrock and coworkers demonstrated that ferrocene-containing norbornene (Fc-NBE) monomers could be successfully polymerized by ring-opening metathesis polymerization (ROMP). A molybdenum-based metal catalyst ($Mo(CH\text{-}t\text{-}Bu)(NAr)(O\text{-}t\text{-}Bu)_2$) was used to initiate the ROMP of the Fc-NBE monomers in THF at room temperature.[72] The polymerization was complete in less than 30 minutes after addition of the monomers and quenched by addition of pivaldehyde. The homopolymers were well controlled and exhibited PDI between 1.1-1.2. Solution cyclic voltammetry studies showed that the side-chain ferrocene redox centers were electronically isolated from each other and were fully capable of participating in electron exchange with the electrode. Moreover, it was discovered that the polymers became insoluble and coated the surface of the electrode when the neutral ferrocene moieties were oxidized to cationic ferrocenium. Schrock et al. proceeded to bind a triblock

copolymer containing PFc-NBE, NBE, and a norbornene-triethoxysilane (NBE-TES) group to platinum, indium tin oxide, and n-doped silicon electrode surfaces through siloxane bond formation.[73] Triblock copolymers PNBE-*b*-PFc-NBE-*b*-P(NBE-TES) and P(Fc-NBE)-*b*-PNBE-*b*-P(NBE-TES) were constructed in which the Fc-NBE and NBE blocks were alternated, which effectively located the ferrocene-containing block either directly onto the surface of the electrode or had the redox-active block separated from the electrode by the NBE block. Synthesis of triblock copolymer PNBE-*b*-P(Fc-NBE)-*b*-P(NBE-TES) is shown in Scheme 2.6. Attachment of the triblock polymer through the siloxane peripheral group proved successful; however, the polymers did not create a uniform monolayer on the electrode surface. Thus, the ferrocene moieties were capable of penetrating to the electrode surface and undergo electrochemical reactions with the electrode. Though it is beyond the scope of this article, it is worth recognizing that Schrock et al. also demonstrated that several other metal centers, including cobalt, tungsten, zinc, palladium, platinum, lead, and tin could be bound to norbornene monomers and successfully polymerized by ROMP.[74-77]

Scheme 2.6. Synthesis of triblock copolymer PNBE-*b*-P(Fc-NBE)-*b*-P(NBE-TES) by ROMP.

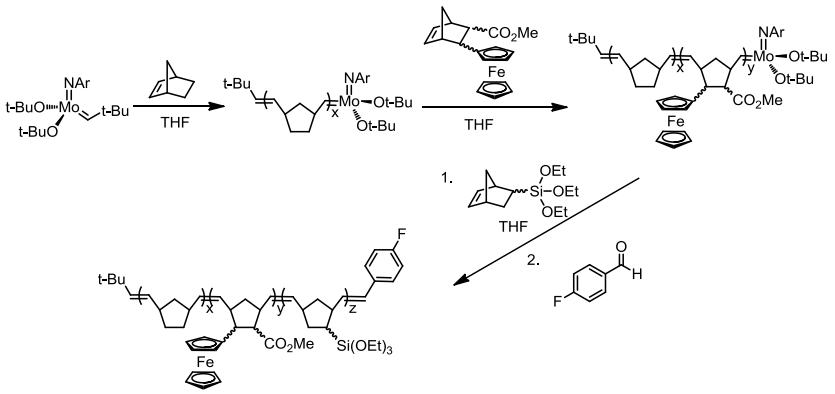

Soon after the groundbreaking work of Schrock, Mirkin et al. polymerized ferrocene-containing norbornene monomers using a much less sensitive ruthenium-based catalyst. Gold nanoparticles were modified to contain a norbornene group, which served as an initiation site for ROMP.[78] A block copolymer that had two separate ferrocene-containing fractions was grown from the gold nanoparticle. The two blocks differed in that the second block had an alkyl spacer between the ferrocene center and the norbornene moiety (Figure 2.2). The electron donating methyl group at the alpha position to the ferrocene effectively shifted the half-wave potential to a more negative value, as the oxidized, electron deficient ferrocenium cation was stabilized (Figure 2.2). These results showed how ROMP could be used to functionalize nanoparticles with multiple polymeric layers of functionalized norbornene monomers.

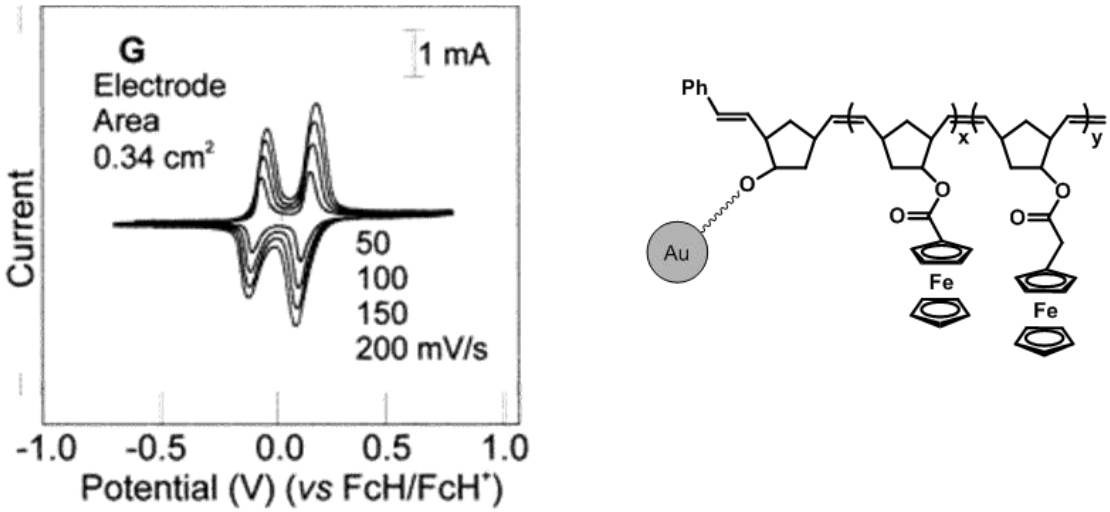

Figure 2.2. Structure and electrochemical properties of a gold nanoparticle coated with two layers of side-chain ferrocene-norbornene polymers.

Soon after, Mirkin and coworkers synthesized a novel amphiphilic norbornene monomer that contained not only a ferrocene moiety, but also a quaternary ammonium

salt in the linker between the ferrocene and norbornene groups. This monomer was shown to be easily polymerized using a commercially available ruthenium-based catalyst in a variety of organic solvents (Scheme 2.7).[79] Cyclic voltammetry studies showed that both the monomer and polymer exhibited fully reversible redox chemistry. The polymer was found to be soluble in both organic and aqueous solutions. Water soluble, redox-active polymers have promising biological applications, especially for electrochemically based diagnostic uses.

Scheme 2.7. Polymerization of an amphiphilic ferrocene-containing norbornene monomer by ROMP.

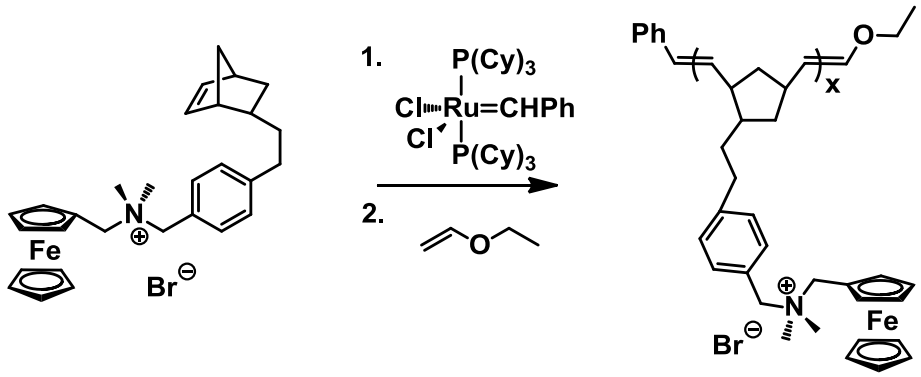

In the past decade, much work in side-chain cationic cylopentadienyliron arene (CIA) complex-containing polymers prepared using ROMP has been carried out by Abd-El-Aziz and coworkers.[1, 80, 81] Strictly, these iron complexes are not metallocenes. However, they also satisfy the 18-e rule and thus are included here. Initially, it was shown that embedded CIA-containing polymers enhanced the solubility in organic media as compared to their organic counterparts.[80, 82] Shortly after, cationic CIA-norbornene derivatives containing both one and two CIA groups were prepared and successfully polymerized by ROMP in the presence of Grubbs' first generation catalyst.[83, 84] Additionally, the 6-membered ring of the CIA moiety has been further derivatized by

methyl or arene groups. The linker between the CIA group and the norbornene has also been modified by various arene units. These various monomers are given in Figure 2.3.

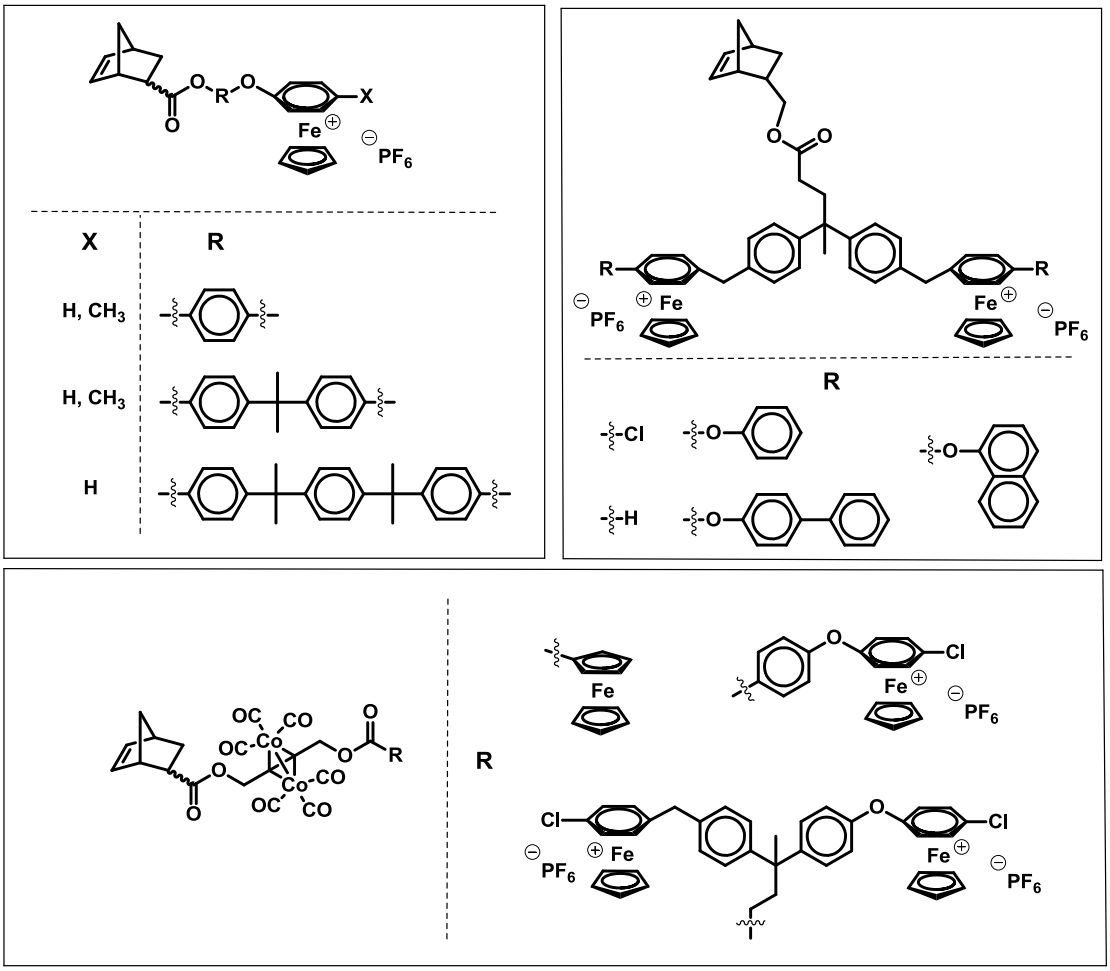

Figure 2.3. Various ferrocene- and cylopentadienyliron arene complex-containing norbornene monomers.

As the polymerization of each substituted norbornene monomer proceeded in a timely and well-controlled manner, it was apparent that the steric effect of the arene rings and the additional CIA moiety did not adversely affect the polymerization.[83, 84] Furthermore, cyclic voltammetry studies showed a fully reversible redox potential for the CIA group depending upon whether the phenyl group was methylated. The metallic

fraction could be removed from the polymer chain by photolytic decoordination, resulting in completely organic polymers. An example of the polymerization and photolytic decoordination of a model monomer is shown in Scheme 2.8. The polymers after decoordination showed to be more thermally stable than their metallic counterparts. Thermal stability was further enhanced by the incorporation of bulky aromatic groups. These rigid aromatic groups effectively increased the glass transition temperatures of the polymers.

Recently, Abd-El-Aziz et al. have prepared both neutral ferrocene and cationic CIA functionalized norbornene derivatives in which the linker between the organometallic fraction and the norbornene group was further functionalized by carbonyl cobalt moieties (Figure 2.3).[85] This illustrated how the linker between the active polymerization site and the side-chain termini can be further modified to contain additional functional groups. The mixed organoiron/organocobalt polymers ranged in molecular weights between 4,500 and 69,000 g/mol and contained PDI between 1.2 - 1.8. The CIA/carbonyl cobalt polymer showed a fully reversible redox potential corresponding to the ferrocenium group and an irreversible electrochemical process corresponding to the cobalt moiety. Thermal analysis showed degradation of the carbonyl cobalt group at 130 ^{o}C and polymer backbone degradation above 350^{o}C.

Scheme 2.8. Synthesis and subsequent photolytic decoordination of a cylopentadienyliron arene complex-containing polymer by ROMP.

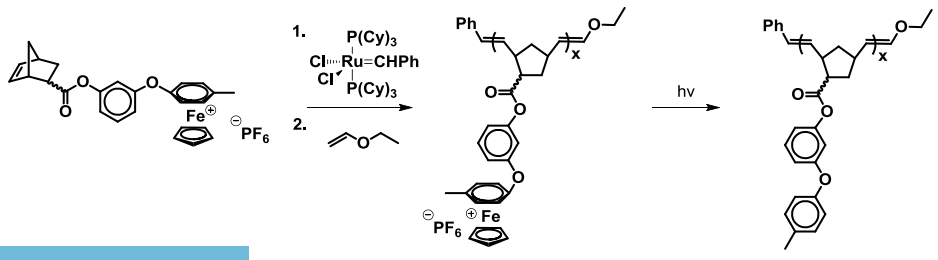

2.3.4 CONTROLLED/LIVING RADICAL POLYMERIZATION (CRP) TECHNIQUES

CRP allows the synthesis of well-defined polymers with controlled molar mass, narrow molecular weight distribution, and well-defined architectures and functionalities.[86-90] Atom transfer radical polymerization (ATRP),[53, 91-100] reversible addition fragmentation chain transfer (RAFT) polymerization,[101-105] and nitroxide-mediated polymerization (NMP)[106, 107] are three of the most widely used CRP methods, and all involve a fast dynamic equilibrium between dormant species and active radical species to provide control. The conditions of the polymerization, including ATRP using transition metal complexes, NMP using nitroxides, and RAFT using dithioesters, are selected so that the equilibrium between dormant and active species is strongly shifted toward dormant species in order to establish a low concentration of propagating radicals and reduce proportion of unavoidable termination reactions. CRP is compatible with a wide range of monomers including acrylates, methacrylates, styrene, etc. Over the last one and half decades, CRP has been well established as a major tool to prepare polymers with predetermined molecular weight, low polydispersity and controlled architectures. All these three most important CRP techniques have been used to polymerize metallocene-containing monomers.

2.3.4.1 NITROXIDE-MEDIATED POLYMERIZATION

The first report of controlled/living radical polymerization of a ferrocene-containing monomer appeared in 1999 by Plenio and coworkers. They attempted to polymerize VFc using 2, 2, 6, 6-tetramethyl-piperidine-1-oxyl (TEMPO) and azobisisobutyronitrile (AIBN).[108] However, the obtained results were similar to the work

of Pittman et al. in the late 1970s. It was found that the homopolymerizations of VFc by the radical pathway were limited in that only low molecular weight polymers could be obtained. When polymerizations exceeded 40% monomer conversion, the polydispersity quickly rose to above 1.7. These results can be attributed to the internal electron transfer mechanism as discussed above. The same group also prepared random copolymers of VFc and styrene, and observed that though higher molecular weight polymers could be obtained, the amount of VFc they could incorporate into the random copolymer was severely limited. As higher fractions of VFc were introduced, the maximum conversion decreased and the polydispersity increased.

2.3.4.2 Reversible Addition Fragmentation Chain Transfer Polymerization

Lu et al. has recently shown that the RAFT polymerization technique can be used to prepare well-controlled side-chain ferrocene-containing homo- and block copolymers. A novel styrene-derivatized monomer containing both an aldehyde group and a ferrocene moiety was synthesized and shown to exhibit a well-controlled polymerization using a chain transfer agent 2-cyanopropyl-2-yl dithiobenzoate (CPDB).[109] The resulting homopolymer displayed a PDI below 1.2 with molecular weights under 10,000 g/mol. It was noted that at above 60% conversion the polymerization slowed down dramatically. However, by stopping the polymerization below 60%, the group was able to chain extend with styrene to develop a diblock copolymer with a PDI of 1.32. Furthermore, the chain-extension efficiency was high, as no macroinitiator was left as shown by GPC. Recently, the same group reported an amphiphilic copolymer from their ferrocene/aldehyde monomer and poly(ethylene oxide).[110] A monomethoxy-terminated PEO-based macro-chain transfer agent was chain extended with the ferrocene/aldehyde monomer. A series

of diblock copolymers were synthesized in which the degree of polymerization of the organometallic fraction was varied between 10 and 43. The aldehyde group was then reacted with a model drug (BHA) containing an aminooxy group to investigate the drug delivery capabilities of the copolymer (Scheme 2.9). Electrochemical studies showed that the half wave potential shifted to a more negative value after the complexation of aldehyde with the drug compound. The amount of drug loading could be calculated simply by measuring the change in potential response by cyclic voltammetry. Solution self-assembly studies were shown to form micelles with an organometallic core and a poly(ethylene oxide) shell when the diblock copolymer was dissolved in THF and added to an aqueous solution. The micelles were not disassembled after complexation with the drug or after oxidizing the ferrocene group to ferrocenium. This report is another example of how the linker between the active polymerization site and the ferrocene group can be further modified to incorporate additional desirable functional groups. In this case, the aldehyde group served as an attachment site for biomolecules while the ferrocene moiety provided an electrochemical probe.

Scheme 2.9. RAFT polymerization of an amphiphilic copolymer with one block containing side chain ferrocene and aldehyde functionalities and subsequent loading with a model drug.

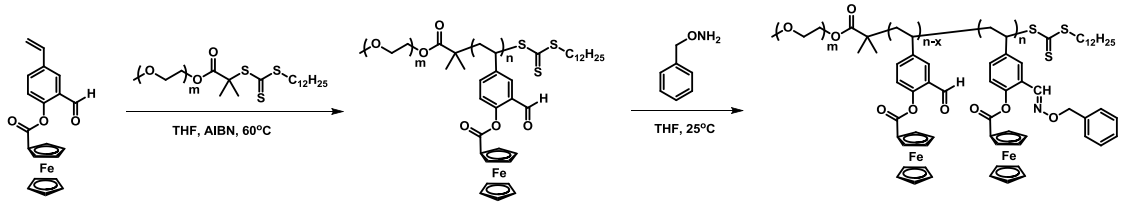

2.3.4.3 ATOM TRANSFER RADICAL POLYMERIZATION

The discovery of ATRP by Matyjaszewski and his coworkers, almost simultaneously by Sawamoto and his coworkers is one of the most important achievements in the field of polymer science.[53, 86-97] The seminal and systematic work with the great depth by Matyjaszewski and his coworkers has pushed ATRP as the most widely used and successful CRP technique. ATRP differs significantly from other CRP techniques through the use of a copper catalyst. It involves an activation process. During this process, the halogen atom is transferred from the domain species to the catalyst while copper (I) is oxidized to copper (II). However, the rate constant of deactivation (k_{deact}) is at least five orders of magnitude higher than the rate constant of activation (k_{act}). The majority of the time the equilibrium is in the dormant species state, thus resulting in an extremely low concentration of radicals. This minimizes undesirable termination reactions although the rate constant of termination (k_t) is similar to that in free radical polymerization. ATRP is a robust technique to precisely control the chemical composition and architecture of polymers as well as the uniform growth of polymer chains, while tolerating a wide range of monomers.

ATRP has been recently used to prepare side-chain metallocene-containing polymers.[111-117] In 2005, surface-initiated ATRP was used to graft 2-methacryloyloxyethyl ferrocenecarboxylate (MAEFc) from quartz and ITO substrates. The resulting polymers showed living characteristics with polydispersities below 1.3. Furthermore, it was noted that the redox films were electrochemically active, showing fully reversible redox signals.[115] This indicated that the electrolyte had excellent permeability into the polymer film and that the metallopolymer had full access to the ITO

electrode. In a separate study by Pyun and his coworkers, ferrocene-containing homo- and block copolymers were also grafted from ITO. Their study illustrated that the electrochemical communication between the ferrocene units and the ITO electrode can be modified by inserting a polymer spacer between the two components.[112] The electrochemistry of the system greatly varied depending upon whether the ferrocene block was directly connected to the ITO surface (Figure 2.4a), or whether it was separated by a non-electroactive block (PMMA) (Figure 2.4b). It was observed that when there was a PMMA block between the organometallic fraction and the ITO surface, the cathodic and anodic peaks were largely separated and significantly broadened. This revealed that the PMMA block effectively impeded electrochemical communication between the ferrocene moieties and the ITO electrode.

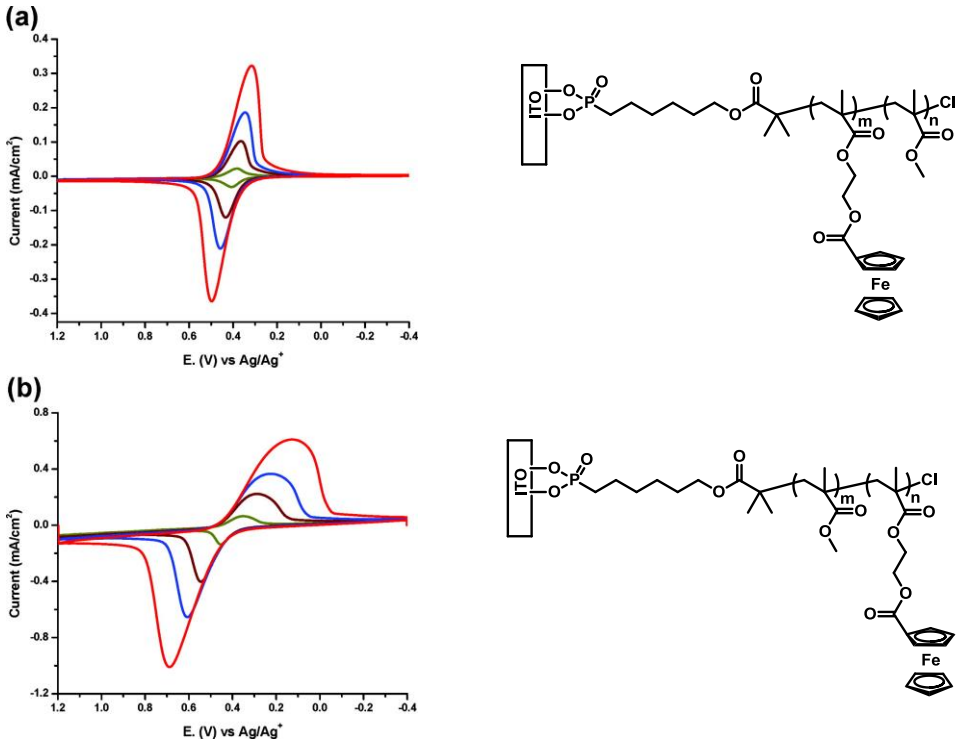

Figure 2.4. Structure and CV of diblock copolymers (a) PMAEFc-*b*-PMMA and (b) PMMA-*b*-PMAEFc grafted from ITO.

We have recently reported a systematic study on ATRP of side-chain ferrocene (meth)acrylates in which the length of the alkyl spacer between the (meth)acrylate unit and the ferrocene moiety was varied.[114] Acrylates with alkyl spacers between 1 and 8 methylene repeat units were synthesized. Ferrocene-containing methacrylate monomers with two different alkyl units were synthesized. It was found that most ferrocene (meth)acrylates were polymerized in a well-controlled fashion with narrow polydispersities using a Cu(I)Cl/bipyridine catalyst system, except the monomer with a triazole linker (Scheme 2.10). The monomer with only one methylene group between the iron center and the acrylate group exhibited a high polydispersity upon polymerization (PDI=1.7), which can be attributed to the occurrence of internal electron transfer. Generally, as the length of the alkyl spacer increased, the polymerization rate decreased. Additionally, the rate of polymerization for the methacrylate monomer was much faster than that of the corresponding acrylate. With the increase of the length of the linkers there was a decrease in difference between the half-wave potential of the monomer and the corresponding polymer. This is discussed in detail in the following chapter.

Scheme 2.10. ATRP of ferrocene-containing (meth)acrylates with various linkers.

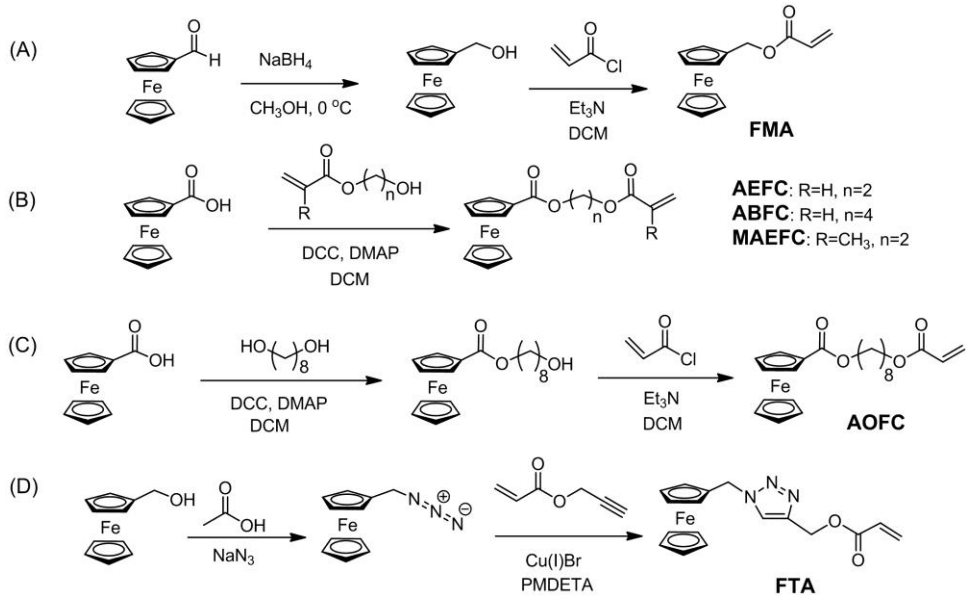

2.4 Side-Chain Cobaltocenium-Containing Polymers

While 18-e ferrocene side-chain polymers have received much attention over the years, by comparison, there have been far fewer examples of polymers containing isoelectronic 18-e cationic cobaltocenium unit. 19-e Cobaltocene was first synthesized[118-120] during the enormous activities following the discovery of 18-e ferrocene. The ionization potential of cobaltocene is 5.56 eV,[121] only slightly above that of alkali metals, so that cobaltocene can lose an electron readily to form very stable 18-e cobaltocenium cation.[5] Comparing cobaltocenium and ferrocene, the key difference is that cobaltocenium is cationic, associated with counter-ions, while ferrocene is a neutral metallocene. The choice of counter ions dictates the solubility of cobaltocenium. Smaller inorganic anions (e.g. halogen, PF_6^-) make cobaltocenium water soluble, while cobaltocenium with bulky organic anions (e.g. BPh_4^-) is hydrophobic. Cobaltocenium is in the higher Co(III) oxidation state, more inert toward oxidation than ferrocene (in lower

Fe(II) oxidation state). It is extremely difficult to remove an electron from the formal Co(III) center in a cobaltocenium ion, with the $E_{1/2}$ of the Co(III)/Co(IV) couple falling at ca. 2.7 V vs ferrocene.[122, 123] The cobaltocenium moiety could be electrochemically monitored through its Nernstian Co(III)/Co(II) couple expected to fall at ca. –1.6 V vs ferrocene.

Given the ease oxidation of cobaltocene and the great inertness of cobaltocenium salts, electrophilic substitution of pre-formed cobaltocene and cobaltocenium is virtually impossible.[124, 125] Substituted cyclopentadiene, particularly methylcyclopentadiene, is often used to prepare substituted cobaltocenium.[124-147] Some efforts have been recently focused on cobaltocenium-containing dendrimer synthesis.[148-155] Although limited early work produced low molecular weight main-chain cobaltocenium polymers (mostly oligomers due to their poor solubility) by step-growth polymerization, explicit characterization of macromolecular structures was often missing.[6,126, 135-138, 155-158] Nevertheless, these cobaltocenium compounds, dendrimers and polymers have shown promising properties such as thermal/chemical stability,[137, 150] active redox/sensing,[139, 141, 142] biomedical activity,[144, 154, 159-162] the use for ion-exchange[163] and molecular electronics,[148] etc.

Scheme 2.11. PtBA-*b*-P(HEA-*r*-AECoPF6) by ATRP and post-polymerization modification.

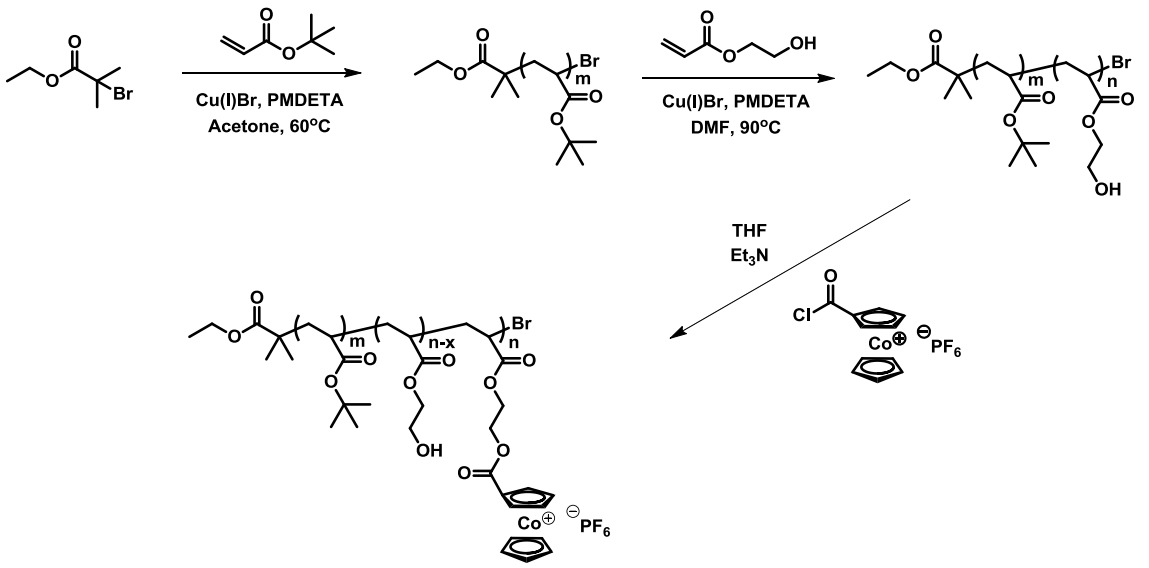

We have developed a class of side-chain cobaltocenium containing polymers.[113, 164] As shown in Scheme 2.12, we modified a reported procedure[125] to synthesize highly pure cobaltocenium monocarboxylic acid, while removing any 1,1'-dicarboxycobaltocenium. This is a vital step toward side-chain cobaltocenium polymers, as trace contamination with 1,1'-disubstitued cobaltocenium could result in crosslinked polymers. The monocarboxycobaltocenium can be readily converted into relatively stable cobaltocenium acyl chloride under reflux of thionyl chloride. Our initial studies were focused on a post-polymerization modification strategy in which a parent homo- or block copolymer was prepared that contained a reactive side group.[113] For example, well-defined poly(tert-butyl acrylate)-*block*-poly(2-hydroxyethyl acrylate) (PtBA-*b*-PHEA) was synthesized using ATRP. The hydroxyl groups of the PHEA block were then reacted with cobaltocenium mono-acid halide under basic conditions, resulting P*t*BA-*b*-poly(2-acryloyloxyethyl cobaltoceniumcarboxylate hexafluorophosphate)(P*t*BA-*b*-PAECoPF6),

as shown in Scheme 2.11. The esterification yields generally ranged from 60-80%. Even though quantitative substitution was not obtained, intriguing solution self-assembly results were observed. As shown in Figure 2.5, the morphology of block copolymer micelles depended on the use of solvents, as it was found that vesicles were formed when the block copolymers were dissolved in a mixture of acetone and water. However, when the block copolymers were dissolved in acetone and chloroform, very uniform (in diameter) and rigid nanotubes were produced.

Scheme 2.12. Synthesis of highly pure cobaltocenium mono-carboxylic acid.

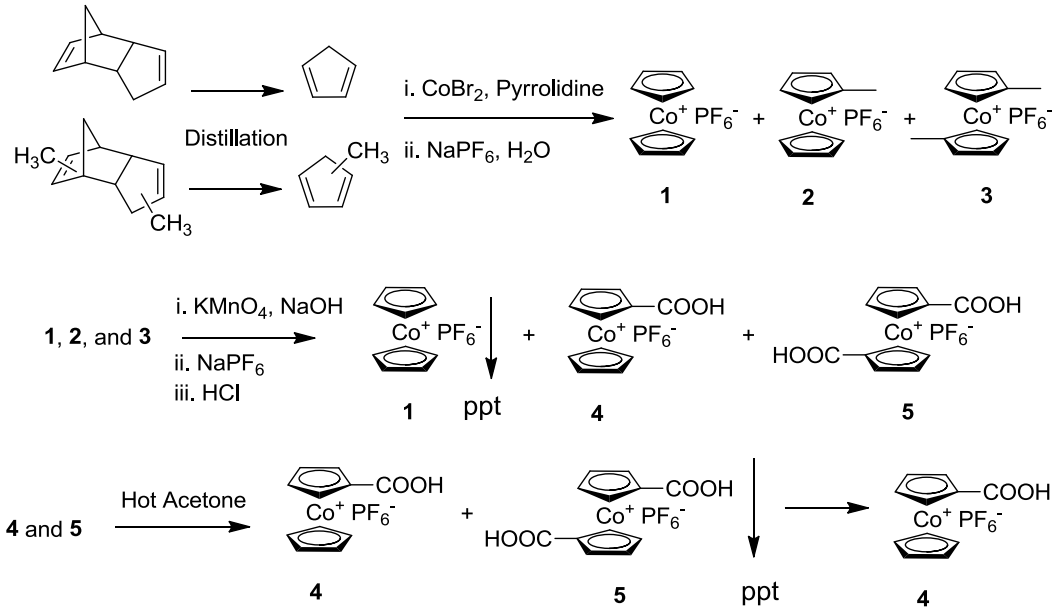

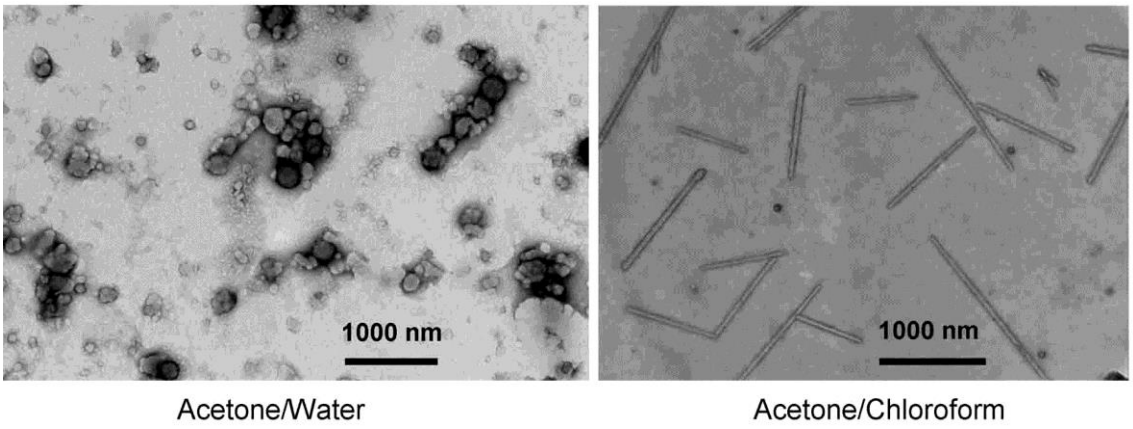

Figure 2.5. TEM micrographs of P*t*BA-*b*-PAECoPF6 self-assembled micelles in the mixture of (a) acetone/water and (b) acetone/chloroform.

In a separate study, we showed that a cobaltocenium acrylate monomer could be polymerized by free radical polymerization, as shown in Scheme 2.13.[164] The resulting polymers showed tunable solubility by changing the counter ion. Cobaltocenium polymers with a hexafluorophosphate counter ion were hydrophilic, whereas polymers containing a tetraphenylborate counter ion were hydrophobic. Cyclic voltammetry studies showed that the polymers exhibited fully reversible redox potentials. Our current efforts are being undertaken at polymerizing novel cobaltocenium-containing (meth)acrylate or norbornene monomers by RAFT or ROMP, respectively. Additionally, both solution and thin film self-assembly studies are underway.

Scheme 2.13. Synthesis and radical polymerization of 2-acryloyloxyethyl cobaltoceniumcarboxylate hexafluorophosphate and an Ion-exchange Process.

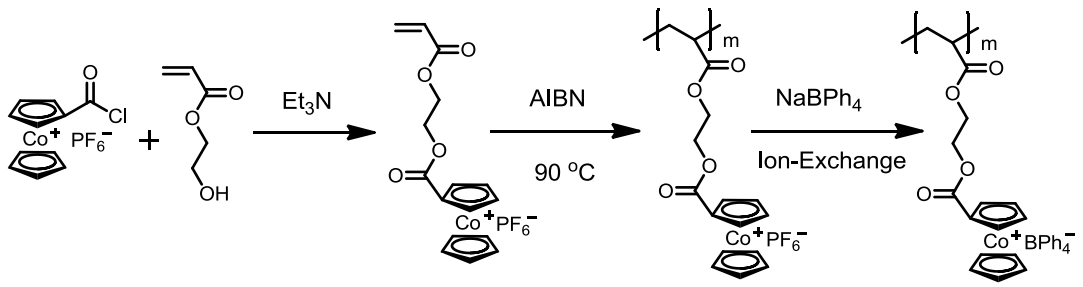

Recently, a report of a side-chain cyclopentadienyl-cobalt-cyclobutadiene (CpCoCb) polymer was described by Ragogna and coworkers.[117] Although not metallocene, this 18-electron complex is electronically neutral and isoelectronic to ferrocene and cobaltocenium. The cyclobutadiene ring was derivatized either by four phenyl rings or methyl groups. Both an acrylate and methacrylate monomer containing methylated cyclobutadiene rings were synthesized. An acrylate monomer containing a phenylated cyclobutadiene ring was also synthesized. Although both acrylic monomers were polymerizable by free radical polymerization, only the phenylated cyclobutadiene cobalt acrylic monomer showed some activity for ATRP (Scheme 2.14). A Cu(I)Br/PMDETA system was used in benzene at 80°C. Though the reaction time was very long (4 days), the oligomers retained a low polydispersities (PDI<1.2). The oligomers were shown to be well soluble in organic solvents. The methylated Cb ring polymers were thermally stable to 235°C while the phenylated Cb ring oligomers were stable to 360°C.

Scheme 2.14. ATRP attempts of neutral cobaltocene (meth)acrylate monomers.

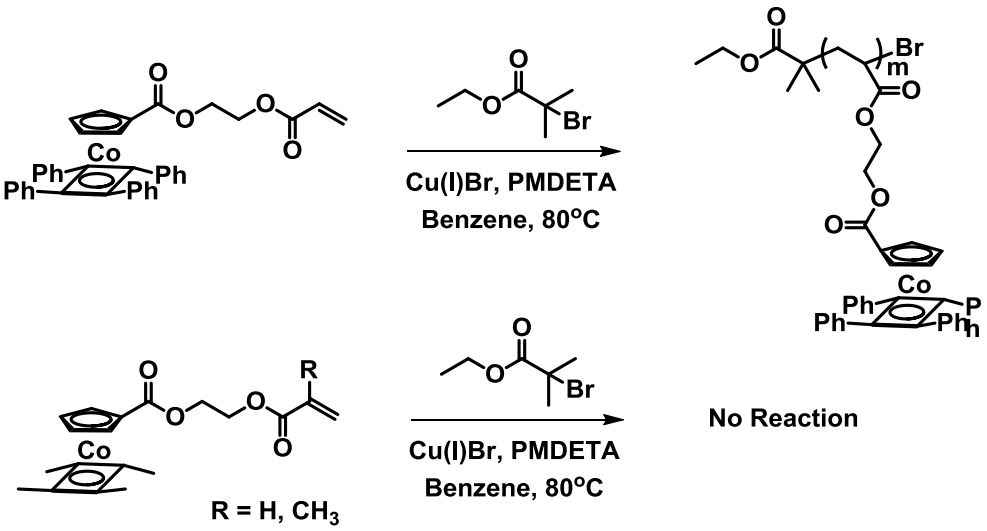

2.5 SUMMARY AND OUTLOOK

Over the past twenty years, there has been a re-emergence of research in the field of metallopolymers with novel materials for applications ranging from biomedical applications to nanotechnology. This mini-review is focused on the synthesis of side-chain metallocene containing polymers prepared using living/controlled polymerization techniques. It was not until recently that these polymers have been synthesized using controlled/living radical polymerization techniques. However, interesting synthetic and self-assembly studies have already shown great promise for side-chain metallocene-containing polymers. These side-chain metallocene polymers offer notable advantages, including the ability to further functionalize the metallocene rings and the spacer between the polymer backbone, as well as the counter ion (if charged). In the past ten years it has been shown how the ability to further functionalize the linker between the polymer backbone and the metallocene moiety can lead to multi-functional materials. These materials have displayed interesting results in developing many applications.

While most of current efforts are devoted to studying side-chain ferrocene-containing polymers, our recent work and others open a new avenue to develop cobaltocenium-containing polymers.[113, 164-166] We have started an ambitious program on developing side-chain cobaltocenium-containing polymers and already discovered a lot of fascinating properties, functions and applications that ferrocene-containing polymers do not have. Currently we are working on the development of various macromolecular architectures containing cobaltocenium moiety.

Scheme 2.15. Metallocenes and their unexplored polymers prepared by direct polymerization or post-polymerization modification.

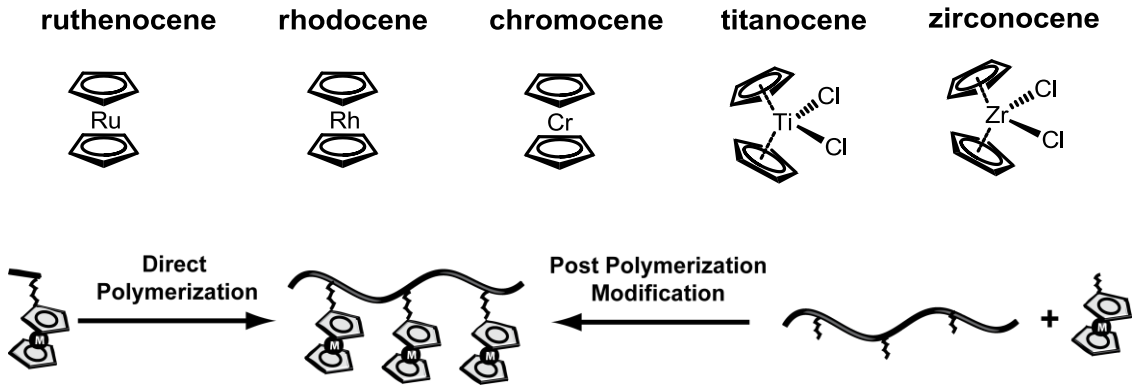

Future work should pay more attention to other metallocene-containing polymers such as ruthenocene, rhodocene, titanocene, and chromocene. Preparation of substituted metallocene derivatives of monomers is very important, as they can be used to prepare polymers by either post-polymerization modification or direct polymerization (Scheme 2.15). Ruthenocene is an 18-e metallocene, isoelectronic to ferrocene and cobaltocenium. In principle, it is possible to carry out electrophilic substitution on ruthenocene to prepare derivatives or monomers.[167] Similar to cobaltocene, 19-e rhodocene is not stable. Compared with cobaltocenium, the even more negative reduction potential of rhodocenium indicates its high stability.[168] Therefore, it is very likely that both rhodocene and rhodecenium can not undergo electrophlic substitution. The use of substituted cyclopentadiene is probably the only way to prepare substituted rhodocene. Chromocene is a 16-e metallocene, which is 2-electron short of 18-electron rule. Thus chromocene is highly reducing. The preparation of substituted chromocene also requires the use of substituted cyclopentadiene. Group IVB metallocenes have the cyclopentadiene groups facing the metal atom but present in a distorted tetrahedral arrangement such as titanocene (dichloride) and zirconocene (dichloride). These distorted metallocenes could

be incorporated as a pendant group into a polymer framework.[169, 170] The work in this direction is almost unexplored. These various metallocenes share the high thermal stability and reversible redox chemistry as ferrocene, though the redox potentials, solubility, and magnetic properties may differ substantially. The future of this field is very promising as multi-functional materials are becoming ever important for the development of high-demand devices and niche applications.

2.6 Acknowledgements

This work is supported by the University of South Carolina start-up fund.

2.7 References

1. A. S. Abd-El-Aziz, *Macromol. Rapid Commun.*, **2002**, *23*, 995-1031.
2. A. S. Abd-El-Aziz and I. Manners, *Frontiers in Transition Metal-Containing Polymers*, Wiley, Hoboken, NJ, 2007.
3. J. B. Beck, J. M. Ineman and S. J. Rowan, *Macromolecules*, **2005**, *38*, 5060-5068.
4. M. Burnworth, L. Tang, J. R. Kumpfer, A. J. Duncan, F. L. Beyer, G. L. Fiore, S. J. Rowan and C. Weder, *Nature*, **2011**, *472*, 334-337.
5. K. J. Calzia and G. N. Tew, *Macromolecules*, **2002**, *35*, 6090-6093.
6. R. B. Grubbs, *J. Polym. Sci. Part A: Polym. Chem.*, **2005**, *43*, 4323-4336.
7. B. J. Holliday and T. M. Swager, *Chem. Commun.*, **2005**, 23-36.
8. F. Jakle, *Chem. Rev.*, **2010**, *110*, 3985-4022.
9. P. Y. Keng, B. Y. Kim, I.-B. Shim, R. Sahoo, P. E. Veneman, N. R. Armstrong, H. Yoo, J. E. Pemberton, M. M. Bult, J. J. Griebelt, E. L. Ratcliff, K. G. Nebesny and J. Pyun, *ACS Nano*, **2009**, *3*, 3143-3157.
10. B. D. Korth, P. Keng, I. Shim, S. Bowles, K. Nebesny, C. Tang, T. Kowalewski and J. Pyun, *J. Am. Chem. Soc.*, **2006**, *128*, 6562-6563.
11. N. Madhavan, W. Sommer and M. Weck, *Chem. Soc. Rev.*, **2011**, *40*, 129-137.
12. L. A. Mıinea, L. B. Sessions, K. D. Ericson, D. S. Glueck and R. B. Grubbs, *Macromolecules*, **2004**, *37*, 8967-8972.
13. U. S. Schubert and C. Eschbaumer, *Angew. Chem., Int. Ed.*, **2002**, *41*, 2892-2926.
14. U. S. Schubert, G. R. Newkome and I. Manners, *Metal-Containing and Metallosupramolecular Polymers and Materials*, American Chemical Society, Washington, DC, 2006.
15. R. Shunmugam, G. J. Gabriel, K. A. Aamer and G. N. Tew, *Macromol. Rapid Comm.*, **2010**, *31*, 784-793.
16. G. R. Whittell, M. D. Hager, U. S. Schubert and I. Manners, *Nature Mater.*, **2011**, *10*, 176-188.

17. G. R. Whittell and I. Manners, *Adv. Mater.*, **2007**, *19*, 3439-3468.
18. I. Manners, *Synthetic Metal-Containing Polymers*, Wiley-VCH, Weinheim, 2004.
19. P. Stepnicka, *Ferrocenes: Ligands, Materials and Biomolecules*, 2008.
20. A. Togni and R. Halterman, *Metallocenes: Synthesis - Reactivity - Applications*, 1998.
21. A. Togni and T. Hayashi, *Ferrocenes: Homogeneous Catalysis, Organic Synthesis, Materials Science*, 1995.
22. I. Manners, *Science*, **2001**, *294*, 1664-1666.
23. R. D. A. Hudson, *J. Organomet. Chem.*, **2001**, *637-639*, 47-69.
24. M. A. Vorotyntseva and S. V. Vasilyeva, *Adv. Coll. Interface Sci.*, **2008**, *139*, 97-149.
25. X. Wang, G. Guerin, H. Wang, Y. Wang, I. Manners and M. A. Winnik, *Science*, **2007**, *317*, 644-647.
26. H. D. Abruna, *Coord. Chem. Rev.*, **1988**, *86*, 135-189.
27. M. A. Hempenius, F. F. Brito and G. J. Vancso, *Macromolecules*, **2003**, *36*, 6683-6688.
28. Y. Ma, W.-F. Dong, M. A. Hempenius, H. Mohwald and G. J. Vancso, *Nature Mater.*, **2006**, *5*, 724-729.
29. E. W. Neuse, *Macromol. Symp.*, **2001**, *172*, 127-138.
30. G. R. Whittell and I. Manners, *Adv. Mater.*, **2007**, *19*, 3439-3468.
31. C. U. Pittman, J. C. Lai, D. P. Vanderpool, M. Good and R. Prado, *Macromolecules*, **1970**, *3*, 746-754.
32. C. U. Pittman, R. L. Voges and W. B. Jones, *Macromolecules*, **1971**, *4*, 298-302.
33. C. U. Pittman, R. L. Voges and W. R. Jones, *Macromolecules*, **1971**, *4*, 291-297.
34. C. U. Pittman and A. Hirao, *J. Polym. Sci. Pol. Chem.*, **1977**, *15*, 1677-1686.
35. C. U. Pittman and A. Hirao, *J. Polym. Sci. Pol. Chem.*, **1978**, *16*, 1197-1209.
36. C. U. Pittman and C. C. Lin, *J. Polym. Sci. Pol. Chem.*, **1979**, *17*, 271-275.
37. J. B. Flanagan, S. Margel, A. J. Bard and F. C. Anson, *J. Am. Chem. Soc.*, **1978**, *100*, 4248-4253.
38. A. Merz and A. J. Bard, *J. Am. Chem. Soc.*, **1978**, *100*, 3223-3224.
39. P. Daum, J. R. Lenhard, D. R. Rolison and R. W. Murray, *J. Am. Chem. Soc.*, **1980**, *102*, 4649-4653.
40. R. J. Nowak, F. A. Schultz, M. Umana, R. Lam and R. W. Murray, *Anal. Chem.*, **1980**, *52*, 315-321.
41. P. Daum and R. W. Murray, *J. Phys. Chem.*, **1981**, *85*, 389-396.
42. M. Umana, P. Denisevich, D. R. Rollson, S. Nakahama and R. W. Murray, *Anal. Chem.*, **1981**, *53*, 1170-1175.
43. R. W. Murray, *Ann. Rev. Mater. Sci.*, **1984**, *14*, 145-169.
44. H. D. Abruna, Y. Kiya and J. C. Henderson, *Phys. Today*, **2008**, *61*, 43-47.
45. B. Ulgut and H. D. Abruna, *Chem. Rev.*, **2008**, *108*, 2721-2736.
46. D. A. Foucher, B. Z. Tang and I. Manners, *J. Am. Chem. Soc.*, **1992**, *114*, 6246.
47. V. P. Chuang, J. Gwyther, R. A. Mickiewicz, I. Manners and C. A. Ross, *J. Am. Chem. Soc.*, **2009**, *9*, 4364-4369.
48. R. Rulkens, A. Lough and I. Manners, *J. Am. Chem. Soc.*, **1994**, *116*, 797-798.
49. R. Rulkens, A. J. Lough, I. Manners, S. R. Lovelace, C. Grant and W. E. Geiger, *J. Am. Chem. Soc.*, **1996**, *118*, 12683-12695.

50. M. Szwarc, *Nature*, **1956**, *178*, 1168-1169.
51. N. Hadjichristidis, M. Pitsikalis, S. Pispas and H. Iatrou, *Chem. Rev.*, **2001**, *101*, 3747-3792.
52. M. R. Buchmeiser, *Chem. Rev.*, **2000**, *100*, 1565-1604.
53. K. Matyjaszewski and J. Xia, *Chem. Rev.*, **2001**, *101*, 2921-2990.
54. M. Kamigaito, T. Ando and M. Sawamoto, *Chem. Rev.*, **2001**, *101*, 3689-3745.
55. J. Chiefari, Y. K. Chong, F. Ercole, J. Krstina, J. Jeffery, T. P. Le, R. T. A. Mayadunne, G. F. Meijs, C. L. Moad, G. Moad, E. Rizzardo and S. H. Thang, *Macromolecules*, **1998**, *31*, 5559-5562.
56. J.-S. Wang and K. Matyjaszewski, *J. Am. Chem. Soc.*, **1995**, *117*, 5614-5615.
57. V. Percec and B. Barboiu, *Macromolecules*, **1995**, *28*, 7970-7972.
58. M. Kato, M. Kamigaito, M. Sawamoto and T. Higashihara, *Macromolecules*, **1995**, *28*, 1721-1723.
59. C. J. Hawker, A. W. Bosman and E. Harth, *Chem. Rev.*, **2001**, *101*, 3661-3688.
60. M. K. Georges, R. P. N. Veregin, P. M. Kazmaier and G. K. Hamer, *Macromolecules*, **1993**, *26*, 2897-2898.
61. P. Nguyen, P. Gomez-Elipe and I. Manners, *Chem. Rev.*, **1999**, *99*, 1515-1548.
62. C. U. Pittman, *J. Inorg. Organomet. Polym. Mater.*, **2005**, *15*, 33-55.
63. R. Shunmugam and G. N. Tew, *Macromol. Rapid Commun.*, **2008**, *29*, 1355-1362.
64. F. S. Arimoto and A. C. Haven, *J. Am. Chem. Soc.*, **1955**, *77*, 6295-6297.
65. J. C. Lai, T. Rounsefell and C. U. Pittman, *J. Polym. Sci. Pol. Chem.*, **1971**, *9*, 651-662.
66. M. George and G. Hayes, *J. Polym. Sci. Pol. Chem.*, **1975**, *13*, 1049-1070.
67. M. George and G. Hayes, *J. Polym. Sci. Pol. Chem.*, **1976**, *14*, 475-488.
68. M. Gallei, B. Schmidt, R. Klein and M. Rehahn, *Macromol. Rapid Commun.*, **2009**, *30*, 1463-1469.
69. M. Gallei, S. Tockner, R. Klein and M. Rehahn, *Macromol. Rapid Commun.*, **2010**, *31*, 889-896.
70. O. Nuyken, V. Burkhardt and C. Hubsch, *Macromol. Chem. Phys.*, **1997**, *198*, 3353-3363.
71. M. Gallei, R. Klein and M. Rehahn, *Macromolecules*, **2010**, *43*, 1844-1854.
72. D. Albagli, G. Bazan, M. S. Wrighton and R. R. Schrock, *J. Am. Chem. Soc.*, **1992**, *114*, 4150-4158.
73. D. Albagli, G. C. Bazan, R. R. Schrock and M. S. Wrighton, *J. Am. Chem. Soc.*, **1993**, *115*, 7328-7334.
74. V. Sankaran, C. C. Cummins, R. R. Schrock, R. E. Cohen and R. J. Silbey, *J. Am. Chem. Soc.*, **1990**, *112*, 6858-6859.
75. V. Sankaran, J. Yue, R. E. Cohen, R. J. Silbey and R. R. Schrock, *Chem. Mater.*, **1993**, *5*, 1133-1142.
76. C. C. Cummins, M. D. Beachy, R. R. Schrock, M. G. Vale, V. Sankaran and R. E. Cohen, *Chem. Mater.*, **1991**, *3*, 1153-1163.
77. C. Chan, G. S. W. Craig, R. R. Schrock and R. E. Cohen, *Chem. Mater.*, **1992**, *4*, 885-894.
78. K. J. Watson, J. Zhu, S. T. Nguyen and C. A. Mirkin, *J. Am. Chem. Soc.*, **1999**, *121*, 462-463.

79. K. J. Watson, S. T. Nguyen and C. A. Mirkin, *J. Organomet. Chem.*, **2000**, *606*, 79-83.
80. A. S. Abd-El-Aziz, E. K. Todd, R. M. Okasha and T. E. Wood, *Macromol. Rapid Commun.*, **2002**, *23*, 743-748.
81. A. S. Abd-El-Aziz, E. K. Todd, R. M. Okasha, P. O. Shipman and T. E. Wood, *Macromolecules*, **2005**, *38*, 9411-9419.
82. A. S. Abd-El-Aziz, E. K. Todd and G. Z. Ma, *J. Polym. Sci. Pol. Chem.*, **2001**, *39*, 1216-1231.
83. A. S. Abd-El-Aziz, L. J. May, J. A. Hurd and R. M. Okasha, *J. Polym. Sci. Pol. Chem.*, **2001**, *39*, 2716-2722.
84. A. S. Abd-El-Aziz, R. M. Okasha, L. J. May and J. Hurd, *J. Polym. Sci. Pol. Chem.*, **2006**, *44*, 3053-3070.
85. A. S. Abd-El-Aziz, D. J. Winram, P. O. Shipman and L. Bichler, *Macromol. Rapid Commun.*, **2010**, *31*, 1992-1997.
86. K. Matyjaszewski, ed., *Controlled/living radical polymerization. Progress in ATRP, NMP, and RAFT, ACS Symp. Ser.*, American Chemistry Society, San Francisco, 2000.
87. K. Matyjaszewski, ed., *Advances in Controlled/living radical polymerization, ACS Symp. Ser.*, American Chemistry Society, Washington, D.C., 2003.
88. K. Matyjaszewski, ed., *Controlled/Living Radical Polymerization. From Synthesis to Materials*, American Chemical Society, Washington, DC, 2006.
89. A. A. Gridnev and S. D. Ittel, **2001**, *101*, 3611-3660.
90. K. Matyjaszewski and T. P. Davis, eds., *Handbook of radical polymerization*, John Wiley & Sons, Hoboken, 2002.
91. J. S. Wang and K. Matyjaszewski, *J. Am. Chem. Soc.*, **1995**, *117*, 5614-5615.
92. M. Kamigaito, T. Ando and M. Sawamoto, *Chem. Rev.*, **2001**, *101*, 3689-3745.
93. K. A. Davis and K. Matyjaszewski, *Adv. Polym. Sci.*, **2002**, *159*, 1-169.
94. T. E. Patten and K. Matyjaszewski, *Adv. Mater.*, **1998**, *10*, 901-915.
95. C. Tang, L. Bombalski, M. Kruk, M. Jaroniec, K. Matyjaszewski and T. Kowalewski, *Adv. Mater.*, **2008**, *20*, 1516-1522.
96. C. Tang, B. Dufour, T. Kowalewski and K. Matyjaszewski, *Macromolecules*, **2007**, *40*, 6199-6205.
97. C. Tang, T. Kowalewski and K. Matyjaszewski, *Macromolecules*, **2003**, *36*, 1465-1473.
98. P. A. Wilbon, Y. Zheng, K. Yao and C. Tang, *Macromolecules*, **2010**, *43*, 8747-8754.
99. Y. Zheng, K. Yao, J. Lee, D. Chandler, J.-F. Wang, C.-P. Wang, F.-X. Chu and C. Tang, *Macromolecules*, **2010**, *43*, 5922-5924.
100. B. Dufour, C. Tang, K. Koynov, Y. Zhang, T. Pakula and K. Matyjaszewski, *Macromolecules*, **2008**, *41*, 2451-2458.
101. G. Moad, E. Rizzardo and S. H. Thang, *Aust. J. Chem.*, **2005**, *58*, 379-410.
102. J. Chiefari, Y. K. Chong, F. Ercole, J. Krstina, J. Jeffery, T. P. Le, R. T. A. Mayadunne, G. F. Meijs, C. L. Moad, G. Moad, E. Rizzardo and S. H. Thang, *Macromolecules*, **1998**, *31*, 5559-5562.
103. J. Chiefari, R. T. A. Mayadunne, C. L. Moad, G. Moad, E. Rizzardo, A. Postma, M. Skidmore and S. H. Thang, *Macromolecules*, **2003**, *36*, 2273-2283.

104. C. Tang, T. Kowalewski and K. Matyjaszewski, *Macromolecules*, **2003**, *36*, 8587-8589.
105. L. A. McCullough, B. Dufour, C. Tang, R. Zhang, T. Kowalewski and K. Matyjaszewski, *Macromolecules*, **2007**, *40*, 7745-7747.
106. C. J. Hawker, A. W. Bosman and E. Harth, *Chem. Rev.*, **2001**, *101*, 3661-3688.
107. D. Benoit, V. Chaplinski, R. Braslau and C. J. Hawker, *J. Am. Chem. Soc.*, **1999**, *121*, 3904-3920.
108. M. Baumert, J. Frohlich, M. Stieger, H. Frey, R. Mulhaupt and H. Plenio, *Macromol. Rapid Commun.*, **1999**, *20*, 203-209.
109. M. Shi, A.-L. Li, H. Liang and J. Lu, *Macromolecules*, **2007**, *40*, 1891-1896.
110. Z.-P. Xiao, Z.-H. Cai, H. Liang and J. Lu, *J. Mater. Chem.*, **2011**, *20*, 8375-8381.
111. M. Droulia, A. Anastasaki, A. Rokotas, M. Pitsikalis and P. Paraskevopoulou, *J. Polym. Sci. Pol. Chem.*, **2011**, *49*, 3080-3089.
112. B. Y. Kim, E. L. Ratcliff, N. R. Armstrong, T. Kowalewski and J. Pyun, *Langmuir*, **2010**, *26*, 2083-2092.
113. L. Ren, C. G. Hardy and C. Tang, *J. Am. Chem. Soc.*, **2010**, *132*, 8874-8875.
114. C. G. Hardy, L. Ren, T. C. Tamboue and C. Tang, *J. Polym. Sci. A Polym. Chem.*, **2011**, *49*, 1409-1420.
115. T. Sakakiyama, H. Ohkita, O. Masataka, S. Ito, Y. Tsujii and T. Fukuda, *Chem. Lett.*, **2005**, *34*, 1366-1367.
116. C. Feng, Z. Shen, D. Yang, Y. Li, J. Hu, G. Lu and X. Huang, *J. Polym. Sci. Pol. Chem.*, **2009**, *47*, 4346-4357.
117. P. Chadha and P. J. Ragogna, *Chem. Commun.*, **2011**, *47*, 5301-5303.
118. G. Wilkinson, *J. Am. Chem. Soc.*, **1952**, *74*, 6148-6149.
119. E. O. Fischer and R. Jira, *Z. Naturforsch.*, **1953**, *8b*, 327-328.
120. E. O. Fischer and R. Jira, *Z. Naturforsch.*, **1953**, *8b*, 1-2.
121. G. E. Herberich, E. Bauer and J. Schwarzer, *J. Organomet. Chem.*, **1969**, *17*, 445-452.
122. D. R. Laws, J. Sheats, A. L. Rheingold and W. E. Geiger, *Langmuir*, **2010**, *26*, 15010-15021.
123. J. C. Swarts, D. Laws and W. E. Geiger, *Organometallics*, **2005**, *24*, 341-343.
124. J. E. Sheats, *J. Organomet. Chem. Libr.*, **1979**, *7*, 461-521.
125. J. E. Sheats and M. D. Rausch, *J. Org. Chem.*, **1970**, *35*, 3245-3249.
126. J. E. Sheats, in *Organometallic Polymers [Symposium]*, eds. C. E. J. Carraher, J. E. Sheats and J. Pittman, C. P., 1978, pp. 87-94.
127. J. E. Sheats, J. Carraher, C. E. , J. Pittman, C. P. , M. Zeldin and B. Currell, *Inorganic and Metal-Containing Polymeric Materials*, Plenum, New York, 1985.
128. J. E. Sheats and G. Hlatky, *J. Chem. Ed.*, **1983**, *60*, 1015-1016.
129. J. E. Sheats, G. Hlatky and R. S. Dickson, *J. Organomet. Chem.*, **1979**, *173*, 107-115.
130. J. E. Sheats and T. Kirsch, *Syn. Inorg. Met. Org. Chem.*, **1973**, *3*, 59-62.
131. J. E. Sheats, D. Latini, K. T. Micai, A. Lang, A. Jones, S. Furyk, C. Geraci, E. Sellitto, A. L. Rheingold and I. Guzei, *PMSE Preprints*, **2002**, *86*, 70-71.
132. J. E. Sheats, W. Miller and T. Kirsch, *J. Organomet. Chem.*, **1975**, *91*, 97-104.
133. J. E. Sheats, W. Miller, M. D. Rausch, S. A. Gardner, P. S. Andrews and F. A. Higbie, *J. Organomet. Chem.*, **1975**, *96*, 115-121.

134. J. E. Sheats, E. J. Sabol, Jr., D. Z. Denney and N. El Murr, *J. Organomet. Chem.*, **1976**, *121*, 73-80.
135. C. E. J. Carraher, W. Venable, H. S. Blaxall and J. E. Sheats, *J. Macrom. Sci., Chem.*, **1980**, *A14*, 571-579.
136. C. E. J. Carraher, G. F. Peterson, J. E. Sheats and T. Kirsch, *Makrom. Chem.*, **1974**, *175*, 3089-3096.
137. C. E. J. Carraher, G. F. Peterson, J. E. Sheats and T. Kirsch, *J. Macrom. Sci., Chem.*, **1974**, *A8*, 1009-1022.
138. C. E. J. Carraher and J. E. Sheats, *Makrom. Chem.*, **1973**, *166*, 23-29.
139. I. d. Peso, B. Alonso, F. Lobete, C. M. Casado, I. Cuadrado and J. L. d. Barrio, *Inorg. Chem. Commun.*, **2002**, *5*, 288-291.
140. B. Gonzalez, I. Cuadrado, C. M. Casado, B. Alonso and C. J. Pastor, *Organometallics*, **2000**, *19*, 5518-5521.
141. B. Gonzalez, I. Cuadrado, B. Alonso, C. M. Casado, M. Moran and A. E. Kaifer, *Organometallics*, **2002**, *21*, 3544-3551.
142. P. D. Beer, D. Hesek, J. E. Kingston, D. K. Smith, S. E. Stokes and M. G. B. Drew, *Organometallics*, **1995**, *14*, 3288-3295.
143. Y. Wang, S. Mendoza and A. E. Kaifer, *Inorg. Chem.*, **1998**, *37*, 317-320.
144. A. Maurer, H. B. Kraatz and N. Metzler-Nolte, *Eur. J. Inorg. Chem.*, **2005**, 3207-3210.
145. N. E. Murr, *J. Organomet. Chem.*, **1981**, *208*, C9-C11.
146. N. El Murr, *J. Organomet. Chem.*, **1976**, *112*, 177-187.
147. N. El Murr, *J. Organomet. Chem.*, **1976**, *112*, 189-199.
148. D. Astruc, C. Ornelas and J. Ruiz, *Acc. Chem. Res.*, **2008**, *41*, 841-856.
149. C. Ornelas, J. Ruiz and D. Astruc, *Organometallics*, **2009**, *28*, 276-2723.
150. C. M. Casado, B. Gonzalez, I. Cuadrado, B. Alonso, M. Moran and J. Losada, *Angew. Chem., Int. Ed.*, **2000**, *39*, 2135-2138.
151. K. Takada, D. J. Díaz, H. D. Abruna, I. Cuadrado, B. Gonzalez, C. M. Casado, B. Alonso, M. Moran and J. Losada, *Chem. Euro. J.*, **2001**, *7*, 1109-1117.
152. B. Gonzalez, C. M. Casado, B. Alonso, I. Cuadrado, M. Moran, Y. Wang and A. E. Kaifer, *Chem. Commun.*, **1998**, 2569-2570.
153. D. Sobransingh and A. E. Kaifer, *Langmuir*, **2006**, *22*, 10540-10544.
154. F. Noor, A. Wustholz, R. Kinscherf and N. Metzler-Nolte, *Angew. Chem., Int. Ed.*, **2005**, *44*, 2429-2432.
155. R. A. Simon, T. E. Mallouk, K. A. Daube and M. S. Wrighton, *Inorg. Chem.*, **1985**, *24*, 3119-3126.
156. E. W. Neuse, in *Organometallic Polymers [Symposium]*, eds. C. E. J. Carraher, J. E. Sheats and J. Pittman, C. P., 1978, pp. 95-100.
157. C. U. Pittman, O. E. Ayers, S. P. McManus, J. E. Sheats and C. E. Whitten, *Macromolecules*, **1971**, *4*, 360-362.
158. C. U. Pittman, O. E. Ayers, B. Suryanarayanan, S. P. McManus and J. E. Sheats, *Makrom. Chem.*, **1974**, *175*, 1427-1437.
159. J. T. Chantson, M. Vittoria, V. Falzacappa, S. Crovella and N. Metzler-Nolte, *ChemMedChem*, **2006**, *1*, 1268-1274.
160. F. Noor, R. Kinscherf, G. A. Bonaterra, S. Walczak, S. Wolfl and N. Metzler-Nolte, *ChemBioChem*, **2009**, *10*, 493-502.

161. G. Gasser, I. Ott and N. Metzler-Nolte, *J. Med. Chem.*, **2010**, *54*, 3-25.
162. N. Metzler-Nolte, *Chimia*, **2007**, *61*, 736-741.
163. T. Ito and T. Kenjo, *Bull. Chem. Soc. Jap.*, **1968**, *41*, 614-619.
164. L. Ren, C. G. Hardy, S. Tang, D. B. Doxie, N. Hamidi and C. Tang, *Macromolecules*, **2010**, *43*, 9304-9310.
165. U. F. J. Mayer, J. B. Gilroy, D. O'Hare and I. Manners, *J. Am. Chem. Soc.* , **2009**, *131*, 10382-10383.
166. J. B. Gilroy, S. K. Patra, J. M. Mitchels, M. A. Winnik and I. Manners, *Angew. Chem., Int. Ed.*, **2011**, *50*, 5851-5855.
167. T. C. Willis and J. E. Sheats, *J. Polym. Sci. Polym. Chem. Ed.*, **1984**, *22*, 1077-1084.
168. N. El Murr, J. E. Sheats, W. E. Geiger and J. D. L. Holloway, *Inorg. Chem.*, **1979**, *18*, 1443-1446.
169. B. Heurtefeu, C. c. Bouilhac, Ã. r. Cloutet, D. Taton, A. Deffieux and H. Cramail, *Prog. Polym. Sci.*, **2011**, *36*, 89-126.
170. C. Carraher, *J. Inorg. Organomet. Polym. Mater.*, **2005**, *15*, 121-145.

CHAPTER 3

SIDE-CHAIN FERROCENE-CONTAINING (METH)ACRYLATE POLYMERS: SYNTHESIS AND PROPERTIES[†]

[†] Hardy, C. G.; Ren, L.; Tamboue T. C.; Tang C. *Journal of Polymer Science: Polymer Chemistry* **2011**, *49*, 1409-1420. Reprinted here with permission of publisher.

3.1 ABSTRACT

A comprehensive investigation on the synthesis and properties of a series of ferrocene-containing (meth)acrylate monomers and their polymers that differ in the linkers between the ferrocene unit and the backbone was carried out. The side-chain ferrocene-containing polymers were prepared via atom transfer radical polymerization (ATRP). The kinetic studies indicated polymerization of most monomers followed a "controlled"/living manner. The polymerization rates were affected by the vinyl monomer structures, and decreased with an increase of the linker length. Methacrylate polymerization was much faster than acrylate polymerization. The optical absorption of monomers and polymers was affected by the linkers. Thermal properties of these polymers can be tuned by controlling the length of the linker between the ferrocene unit and the backbone. By increasing the length of the linker, the glass transition temperature ranged from over 100 ^{o}C to – 20 ^{o}C. Electrochemical properties of both monomers and polymers were characterized.

3.2 INTRODUCTION

Among a variety of metallopolymers,[1-14] metallocene-containing polymers have attracted significant attention in materials science due to their interesting properties that arise from their unique sandwich-like structures.[15-25] After the discovery of ferrocene, macromolecules, including oligomers, polymers and dendrimers, functionalized with metallocene moieties have quickly found uses in applications such as catalysts, redox sensors, nanoceramic materials, nanolithography, and biomedical applications.[26-30] These metallocene-containing macromolecules can be seen as bridging together several sub-

fields of chemistry including inorganic, organic, polymer or dendrimer chemistry as well as materials science.

Generally, there are two classes of metallocene polymers: side-chain metallocene-containing polymers with the metallocene unit as a pendant group, and main-chain metallocene-containing polymers with the metallocene as an integral part of polymer backbone.[18] Earlier studies of ferrocene-functionalized polymers were focused on side-chain polymers such as poly(vinylferrocene) due to facile electrophilic substitution of ferrocene. A few acrylate and methacrylate monomers have been polymerized by conventional techniques such as free radical, cationic, and anionic polymerization.[31-38] However, most of these organometallic polymers developed in the 1970s and 1980s lacked control on molecular weight, molecular weight distribution, and were incapable of producing advanced topology such as block copolymers. Since then, side-chain ferrocene-containing polymers have been much less explored. Meanwhile, a seminal work on strained, ring-tilted metallocenophanes reported by Manners and coworkers in the early 1990s opened a new era in the field of ferrocene-containing polymers, that is, to develop well-defined high molecular weight main-chain ferrocene-containing polymers by anionic ring-opening polymerization.[39] This field has been flourishing over the last two decades.[40, 41] A variety of main-chain ferrocene-containing polymers have been developed. These ferrocene-containing polymers have found applications in magnetic ceramics, variable refractive index sensors, nonlinear optical materials, plasma etch resistant materials, etc.[42, 43]

Although the last two decades have witnessed the rapid rampage of main-chain ferrocene-containing polymers, the once first-developed side-chain ferrocene-containing

polymers have recently started to draw attention again, especially well-defined polymers and block copolymers such as those synthesized by anionic polymerization[44] and ring-opening metathesis polymerization (ROMP).[45, 46] The last fifteen years have also witnessed explosive growth of controlled/living radical polymerization (CRP) techniques[47-49] as means to prepare polymers with predetermined molecular weight, low polydispersity, high functionality and diverse architectures. These techniques include nitroxide-mediated polymerization (NMP),[50, 51] reversible addition-fragmentation chain transfer (RAFT) polymerization,[47] and atom transfer radical polymerization (ATRP).[52-54] However, little work has been done in the use of CRP to prepare side-chain ferrocene-containing vinyl polymers and to further explore their properties.[47-49] To develop side-chain ferrocene-containing polymers for broader applications, a comprehensive investigation on polymerization of different ferrocene monomers and their properties is needed.

Herein we report an exploration of ATRP on a series of ferrocene-containing acrylate and methacrylate monomers. Different linkers were intentionally placed between the ferrocene unit and the vinyl ester group, hoping that these linkers can alter the physicochemical properties. The monomers with different alkyl linkers were prepared by effective esterification reactions between mono-substituted ferrocene and functional (meth)acrylates. A copper catalyzed [3+2] cycloaddition of an azide and an alkyne[55] was also used to prepare a novel ferrocene acrylate monomer containing a triazole group as the linker. These monomers were then polymerized by ATRP with all polymerization kinetics studied by nuclear magnetic resonance (NMR) and gel permeation chromatography (GPC). The optical properties of monomers and polymers were explored

by Fourier transform infrared spectroscopy (FTIR) and UV-vis spectroscopy. The thermal properties of polymers were studied using differential scanning calorimetry (DSC) and thermogravimetric analysis (TGA). The electrochemical properties of monomers and polymers were studied using cyclic voltammetry (CV).

3.3 Results and Discussion

Synthesis of Ferrocene-Containing (Meth)acrylate Monomers. (Meth)acrylate monomers with different linkers between the pendant ferrocene unit and the vinyl ester group were prepared by efficient halide displacement, DCC coupling, or copper catalyzed [3+2] cycloaddition reactions. These reactions were demonstrated to produce high quality monomers in high yield from commercially available materials.[56, 57] The synthesis of FMA employed an efficient halide displacement chemistry by using hydroxymethylferrocene and acryloyl chloride in the presence of triethylamine (**Scheme 3.1A**). Instead of repeated recrystallization to purify the mixture as seen in a previous report,[35] the crude product was extracted with a potassium carbonate solution to remove excess triethylamine and resulting salts, followed by passing through a basic alumina column to separate out unreacted hydroxymethylferrocene. As shown in the ^{1}H NMR (**Figure 3.1A**), the peaks at 4.0~4.4 ppm corresponded to cyclopentadienyl (Cp) rings from the ferrocene unit, and the signals at 5.8, 6.1, and 6.4 ppm were assigned to the double bond. The methylene protons of FMA exhibited a singlet at a chemical shift of 5.0 ppm. The successful synthesis of this monomer was further verified by ^{13}C NMR, FT-IR, UV-Vis, and mass spectrum analysis.

Scheme 3.1. Synthesis of Ferrocene-Containing (Meth)acrylate Monomers. (A) FMA Prepared by Esterification Reaction; (B) AEFC, ABFC and MAEFC Prepared by DCC Catalyzed Esterification Reaction; (C) AOFC Prepared by Esterification Reaction; (D) FTA Prepared by Click Reaction.

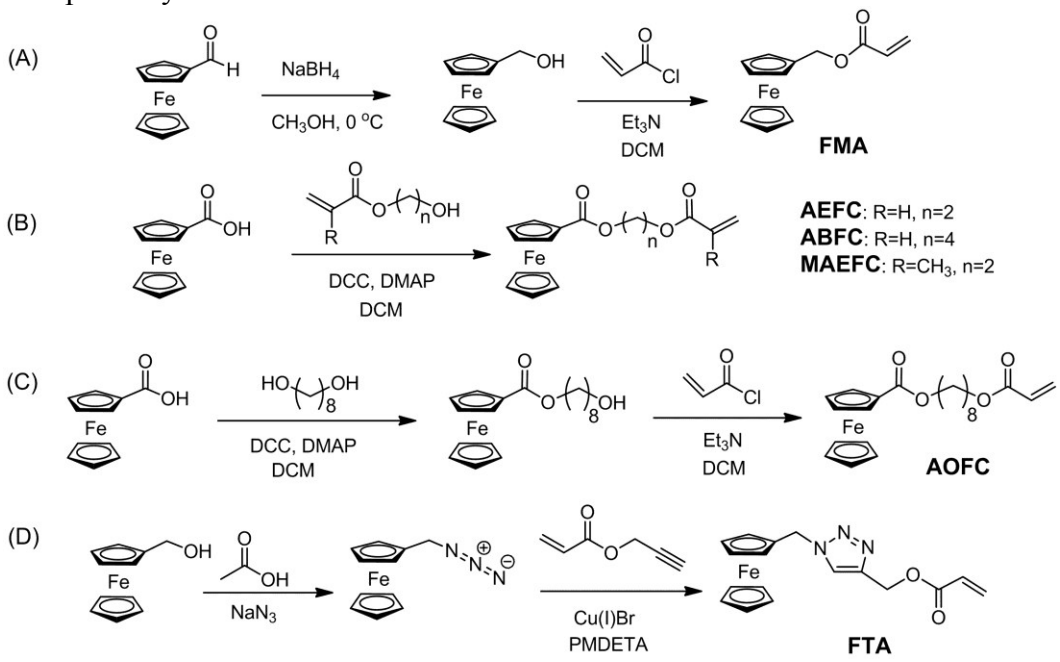

Synthesis of AEFC, ABFC, and MAEFC were all involved with a one-step reaction utilizing the DCC catalyzed esterification reactions of ferrocenecarboxylic acid and appropriate hydroxyl-containing acrylate (2-hydroxyethyl acrylate and 4-hydroxyethyl acrylate) or methacrylate (2-hydroxyethyl methacrylate) as shown in **Scheme 3.1B**. **Figures 3.1B, 3.1C** and **3.1D** show the ^{1}H NMR spectra of AEFC, MAEFC and ABFC, respectively. The chemical shifts of the Cp protons were located at 4.2, 4.4, and 4.8 ppm, while the alkyl groups were clearly assigned in the spectra. ^{13}C NMR, mass spectrum analysis, FT-IR, and UV-Vis further provided unambiguous evidence for the formation of pure ferrocene-containing vinyl monomers. This is a convenient and efficient pathway to synthesize ferrocene monomers, as simple column chromatography was sufficient to separate and purify desirable products.

To obtain a monomer with the longest linker (C8) between the ferrocene unit and the vinyl ester group involved in this work, a synthetic route involving both DCC coupling and halide displacement reactions was carried out, as shown in **Scheme 3.1C**. The first step was an esterification reaction to obtain hydroxyoctylferrocene by DCC coupling between ferrocenecarboxylic acid and 1, 8-octanediol. A large excess of diol was necessary to avoid the formation of two ferrocene moieties linked by the C8. This hydroxyoctylferrocene was then reacted with acryloyl chloride via a halide displacement reaction in the presence of triethylamine, yielding AOFC. **Figure 3.1E** shows the ^{1}H NMR of AOFC, and each proton was clearly assigned.

In order to evaluate how linkers other than alkyl groups affect the polymerization, a new ferrocene-containing acrylate with a triazole group as the linker, FTA, was synthesized from azidomethylferrocene and propargyl acrylate through a copper catalyzed [3+2] cycloaddition reaction, as shown in **Scheme 3.1D**. Azidomethylferrocene was synthesized by reacting hydroxymethylferrocene and sodium azide in the presence of acetic acid. Azidomethylferrocene was then reacted with propargyl acrylate in the presence of a copper (I) catalyst, yielding the desired product, FTA, in an exceptionally high yield. Protons from Cp rings and double bond exhibited similar chemical shifts to other ferrocene monomers, along with a strong singlet at 7.5 ppm corresponding to the characteristic triazole proton (**Figure 3.1F**). Also, there were two singlets at 5.2-5.3 ppm from the protons at the alpha carbon next to the ferrocene moiety and protons next to the ester group. ^{13}C NMR, FT-IR, and UV-Vis further demonstrate the purity of FTA.

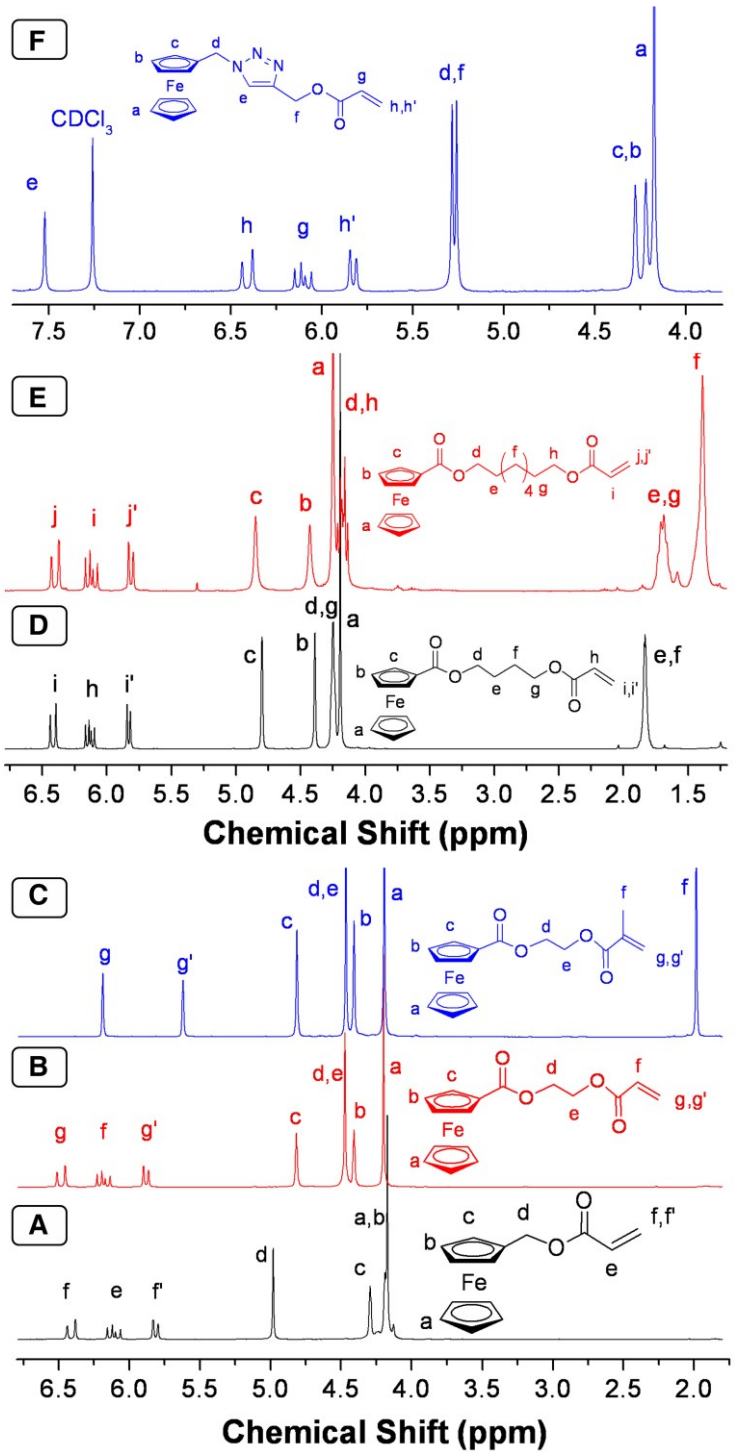

Figure 3.1. ^{1}H NMR ($CDCl_3$) of FMA (a), AEFC (b), MAEFC (c), ABFC (d), AOFC (e), and FTA (f).

Atom Transfer Radical Polymerization of Ferrocene (Meth)acrylate Monomers. ATRP was used to polymerize the six different ferrocene monomers. The polymerization conditions were kept the same for all monomers in order to compare the kinetics and monomer activities. Copper(I) chloride, bpy, and EBiB were used as the catalyst, ligand, and initiator respectively. The polymerization was carried out in toluene with a molar ratio [monomer]:[EBiB]:[Cu(I)Cl]:[bpy] of 100:1:2:4 at 90°C, as shown in **Scheme 3.2**. To demonstrate whether ATRP of these ferrocene-containing monomers follows a controlled and "living" nature, all polymerization kinetics was investigated. Samples were taken out of the reaction flask under the protection of nitrogen gas at periodic intervals. The conversion of monomers was determined from ^{1}H NMR analysis of crude reaction mixtures by comparing the integration area of peaks at 5.8-6.5 ppm (double bond from monomer) and the peaks from Cp rings (4.0~4.8 ppm). The semilogarithmic plots are shown in **Figure 3.2**. Each polymerization showed a linear kinetic plot as the reaction time increased, indicating a controlled/living polymerization. As shown in a representative plot (AOFC polymerization) in **Figure 3.3**, the GPC-based molecular weight increased linearly with monomer conversion calculated from ^{1}H NMR analysis, further confirming the living nature of the polymerization. All other polymers showed similar linear relationship between molecular weight and reaction conversion.

Scheme 3.2. Side-Chain Ferrocene-Containing Polymers Prepared by ATRP: PAEFC (n=2, R=H), PABFC (n=4, R=H), PAOFC (n=8, R=H), and PMAEFC (n=2, R=CH_3).

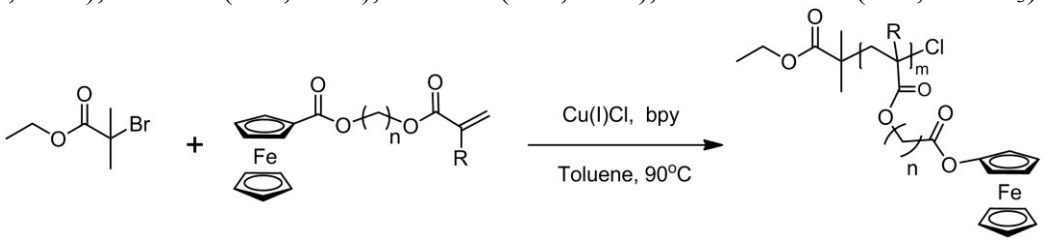

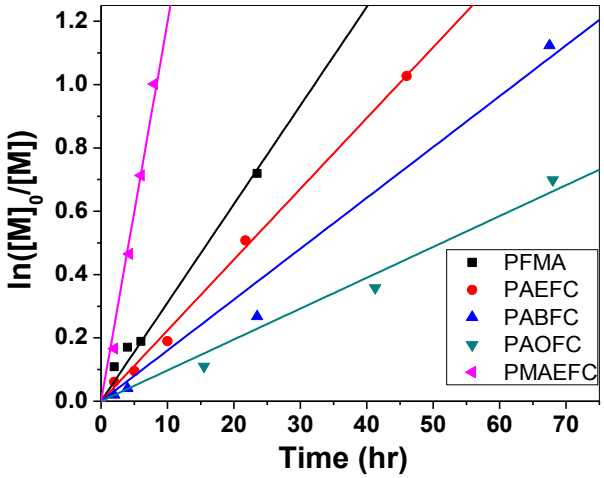

Figure 3.2. Semilogarithmic kinetic plots of polymerization of FMA, AEFC, ABFC, AOFC, and MAEFC monomers by ATRP.

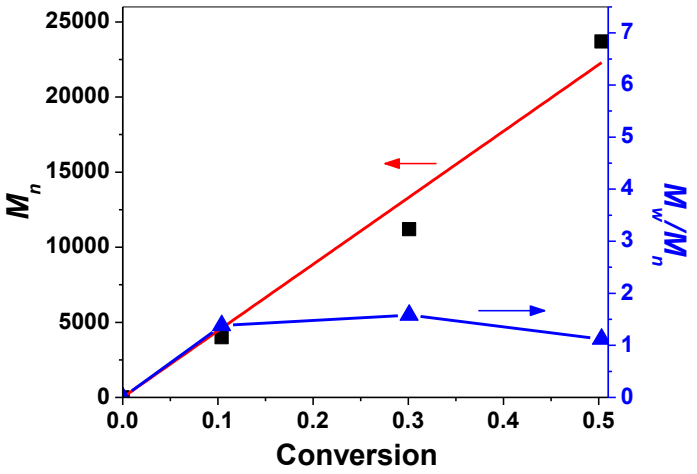

Figure 3.3. A representative plot of molecular weight (M_n, GPC) and monomer conversion (^{1}H NMR): ATRP of AOFC.

One of the goals of this study was to determine the effects of the length of alkyl linkers on the polymerization kinetics and monomer reactivities. For acrylate monomers, it was found that as the length of alkyl linkers increased, the polymerization rate decreased, which was confirmed with the decrease of the slopes of the semilogarithmic kinetic plots (**Figure 3.2**). **Table 3.1** shows the polymerization conditions and results of

obtained polymers. Overall, the conversion of the monomers was controlled at about 50~60%. The FMA monomer showed the highest activity while AOFC exhibited slowest polymerization: ~50% conversion after ~68 hours. This is somewhat unexpected, as the bulky ferrocene unit would have exerted a steric effect to slow down the polymerization for monomer FMA. However, the steric effect of alkyl linkers, especially long alkyl chains, should also play an important role in controlling the polymerization. It was demonstrated that acrylates with long alkyl side group have a lower rate constant of termination compared with those with short alkyl groups such as methyl acrylate. This is due to the ability of the long alkyl group to effectively screen the radical end of the growing polymer chains and therefore reduce bimolecular termination.[58-60] However, the screening effect also slows down the rate of chain propagation. This screening effect likely explains the control of polymerization on ferrocene-containing acrylates. Indeed, PFMA has a much higher polydispersity (PDI=1.7) probably due to the ability of the short linker to transfer the radical from the growing chain end to the ferrocene metal center[61]. In contrast, even after more than 60 hours of polymerization, the polymerization of AOFC still progressed nicely, indicating a low rate constant of termination as well as low activity of the monomer. The final polymer PAOFC has a PDI as low as 1.12. It should be pointed out that hydrophobicity of monomers due to long alkyl chains in less polar solvents (e.g. toluene in this work) seemed not to play a strong role in the ferrocene monomers, although early work on polymerization of dodecyl or octadecyl acrylates indicated the formation of heterogeneous catalyst system.[58-60] The reduced effect of long alkyl hydrophobicity in our monomers was probably due to the presence of the ferrocene

group, which is soluble in almost all organic solvents. This was clearly confirmed with formation of homogeneous catalyst system in all polymerizations.

Table 3.1. ATRP of Ferrocene-Containing Monomers

Monomer	[M]:[I]:[C]:[L][a]	Solvent	Ligand	Time (h)	Conv. (%)[b]	M_n[c]	M_n[d]	M_w/M_n[d]
FMA	100:1:2:4	Toluene	bpy	23.5	51.3	13800	6630	1.71
AEFC	100:1:2:4	Toluene	bpy	46	64.2	21100	4950	1.26
ABFC	100:1:2:4	Toluene	bpy	67.5	67.5	24000	10500	1.58
AOFC	100:1:2:4	Toluene	bpy	68	50.3	20700	23700	1.12
MAEFC	100:1:2:4	Toluene	bpy	8	63.3	21700	5250	1.25

[a][M]:[I]:[C]:[L]: molar concentration ratio of monomer : initiator : catalyst : ligand. Initiator: ethyl 2-bromoisobutyrate bromide; catalyst: Cu(I)Cl; ligand: 2,2'-dipyridyl. [b]Monomer conversion determined by ^{1}H NMR. [c]Molecular weight obtained from ^{1}H NMR using conversion of monomer. [d]Obtained from GPC using polystyrenes as standards.

As expected, the ferrocene-containing methacrylate monomer MAEFC showed a much faster polymerization than acrylate monomers. A 63% conversion was achieved in 8 h. The polymerization proceeded in a living nature as confirmed from the linear kinetic plot. The PDI of homopolymer PMAEFC was reasonably low (1.25). Other methacrylate

monomers with different linkers were not studied in this work. We expect that the control should be similar to the acrylate polymerization, although with much faster kinetics.

The polymerization of monomer FTA under similar reaction conditions completely failed. No polymers were obtained after 48 hours. ATRP and click chemistry have been combined in previous reports utilizing post polymer modification either at the end of the polymer chain or at the side chains.[62] For end-group modification, the terminal alkyl halide from a polymer synthesized by ATRP can be converted into an azide group and then reacted with an alkyne group to attach various functional groups or add additional block segments.[63-65] ATRP initiators have also been designed to have a terminal azide that can also be used for a click reaction after the polymerization is complete.[66] For side-chain modification, monomers containing an azide or protected alkyne side group can be polymerized, and then reacted under typical click chemistry conditions to modify the side-chain with desired functionalities.[67, 68] Though there were reports of monomers containing a triazole group in the linker being successfully polymerized by ROMP,[69, 70] NMP[71] and RAFT,[71-73] there have been almost no such accounts on ATRP of triazole-containing monomers. This is not unexpected, given that the triazole group may have sophisticated complexation with copper catalysts, possibly suppressing the polymerization. In addition, the triazole group imparted additional steric effect on the monomer activity. A possible solution is to use a much more active ligand such as Me_6Tren (tris(2-(dimethylamino)ethyl)amine), which is currently in progress.

All obtained ferrocene polymers were soluble in most conventional solvents such as toluene, THF, chloroform, dichloromethane, dimethylformamide, etc. **Figure 3.4** shows ^{1}H NMR spectra of five obtained homopolymers: PFMA, PAEFC, PABFC,

PAOFC and PMAEFC. All NMR spectra show characteristic ferrocene peaks at 5.8~6.5 ppm and peaks from polymer backbone at 0.8~2.5 ppm. All other peaks from the alkyl linkers were clearly assigned.

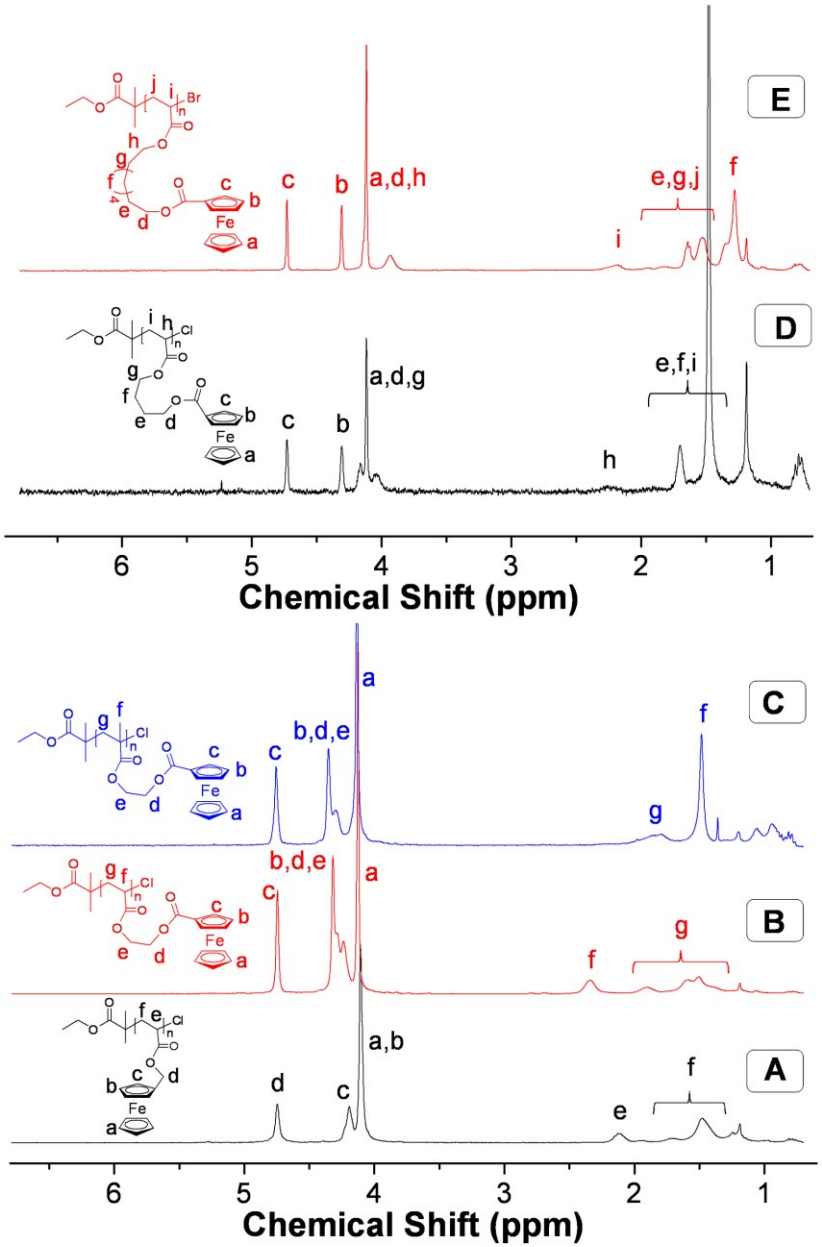

Figure 3.4. ^{1}H NMR ($CDCl_3$) of PFMA (a), PAEFC (b), PMAEFC (c), PABFC (d), and PAOFC (e) prepared by ATRP.

Optical Properties of Ferrocene Vinyl Monomers and Side-Chain Ferrocene-Containing Polymers. Generally, monomers showed similar absorption peaks to their corresponding polymers. All monomers and polymers exhibited major characteristic peaks at ~3100 cm^{-1} for C–H stretching from Cp rings, peaks at ~2960 cm^{-1} for all other C-H stretching, peaks at ~1710 cm^{-1} for C=O stretching. With the increase of the alkyl linker length, the absorption intensity of C-H stretching (non-Cp rings) increased.

Typipcally, monomers and their corresponding polymers have similar absorption peaks, as observed by UV-Vis. FMA, PFMA and FTA showed three characteristics absorption peaks from ferrocene at ~235 nm, ~325 nm and ~445 nm resulting from the π-π* transition, the ring MO-MO* tranisition, and the d-d* transition, respectively.[74, 75] All other monomers and polymers (AEFC, ABFC, AOFC, MAEFC and their polymers) showed the following peaks: ~235 nm, ~263 nm, ~308 nm, ~345 nm, ~445 nm. The π-π* transition remains at ~235 nm. The origin of peak at ~263 nm is believed to be from the ring MO-MO* transition. The difference between these monomers and polymers is primarily due to the structures of linkers. It has been established that the ring MO-MO* transition is considerably affected by substitutions on the Cp rings.[74, 75] Both FMA and FTA have a $–CH_2–$ connected with ferrocene, while AEFC, ABFC, AOFC and MAEFC have an ester group connected with ferrocene. The absorption intensity of peaks at ~445 nm is almost same for all monomers and polymers. This is consistent with the notion that the wavelength of the band maximum at ~445 nm is insensitive to substitutions on the Cp rings.[74] Absorption at 308 nm is due to the intermolecular charge transfer excitation to solvents. It is not clear why absorption at 308 nm disappeared from FMA, PFMA and FTA spectra.

Thermal Properties of Side-Chain Ferrocene-Containing Polymers. The thermal properties of ferrocene-containing (meth)acrylate polymers were characterized with the aid of DSC and TGA. Thermal behaviors of these homopolymers exhibited a strong correlation with the alkyl linkers. As shown in **Figure 3.5**, PAOFC, which contains the longest alkyl linker, showed the lowest T_g at ~ –20°C, while PABFC and PAEFC with shorter alkyl linkers exhibited T_g at 20°C and 60°C, respectively. T_g of the acrylate polymer PFMA, which contains the shortest linker, was somehow ambiguous in the DSC traces. It seemed to have two different "T_g" like transitions at 101 °C and 132 °C. It is not very clear the origins of these transitions. Compared with acrylate polymers, methacrylate polymers PMAEFC with the same length of alkyl linker exhibited an expected and noticeable higher T_g at ~70°C. Clearly, the longer the linker between the bulky ferrocene unit and the backbone, the lower the T_g of the polymers. This is in agreement with the notion that longer linkers reduced the rotation barriers of (meth)acrylate polymers and therefore decreased the T_g.

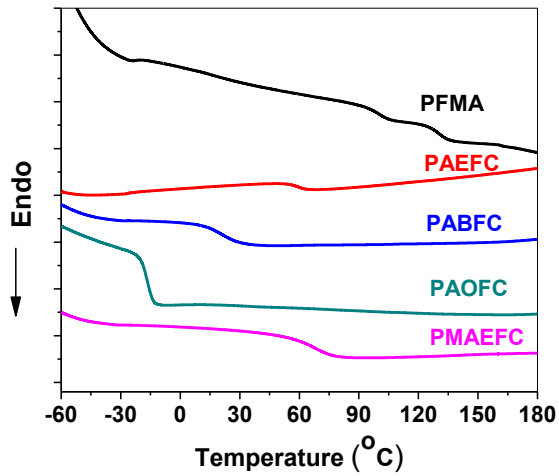

Figure 3.5. DSC traces of PFMA, PAEFC, PABFC, PAOFC and PMAEFC homopolymers polymerized by ATRP.

The thermal stability of side-chain ferrocene-containing polymers was carried out using TGA. As shown in **Figure 3.6**, all homopolymers had at least three weight-loss stages. All polymers were stable below 220 ^{o}C. The onset temperature of major weight loss ranged from 220 ^{o}C to 300 ^{o}C. Most of polymer backbone and organic side group decomposed when heated to 450-480 ^{o}C. Above these temperatures, appreciable weight loss was observed, and was mostly due to the decomposition of the Cp ring from the ferrocene moiety. As expected, the final weight percent of the homopolymers decreased as the increase of the linker length. PFMA exhibited quite different weight loss behavior than the other four homopolymers. The first stage of weight loss occurred at 220-380^{o}C, followed by the largest weight loss at 380-500 ^{o}C. The different weight loss behavior of PFMA was probably due to the difference in the linker structure compared with the other four polymers. PAEFC, PABFC, PAOFC, and PMAEFC have two ester groups located at the alpha position of both the ferrocene unit and the polymer main chain while PFMA has only one ester group located at the alpha position of the polymer main chain.

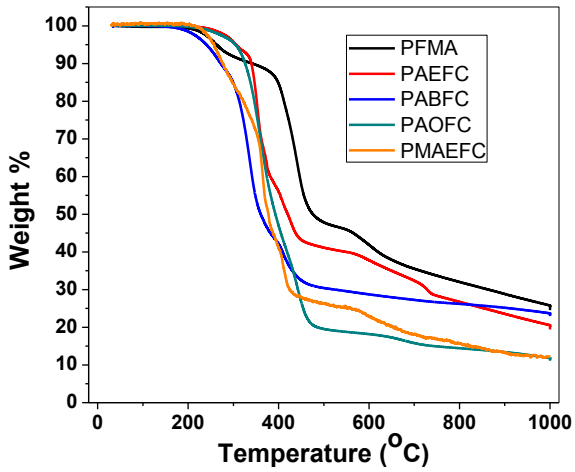

Figure 3.6. TGA curves of side-chain ferrocene-containing polymers: PFMA, PAEFC, PABFC, PAOFC and PMAEFC at a heating rate of 10 ^{o}C/min from 40 ^{o}C to 1000 ^{o}C.

Electrochemical Properties of Ferrocene (Meth)acrylate Monomers and Side-Chain Ferrocene-Containing Polymers. It is well known that ferrocene has a reversible redox potential that can be utilized for electrochemical sensing.[24, 25] Thus, the electrochemical properties of side-chain ferrocene-containing monomers and polymers were also studied. All cyclic voltammograms were recorded in the presence of *n*-Bu_4NPF_6 electrolytes using dichloromethane as the solvent. Generally, all monomers and polymers exhibited one-electron transfer, as evidenced by single oxidation and reduction peaks as shown in **Figure 3.7**. The equal anodic and cathodic peak currents indicated that all monomers showed reversible redox behavior. However, most of side-chain ferrocene-containing polymers showed irreversible redox behavior, as the reduction peak currents were smaller than the oxidation currents. The anodic voltammetric behavior of ferrocene (Fe(II)) polymers may be deteriorated by the insolubility of their oxidized form (Fe(III), ferrocenium polymers) in dichloromethane. The one-electron oxidation of Fe(II) then resulted in the deposition of electrogenerated ferrocenium polymers on the electrode surface.

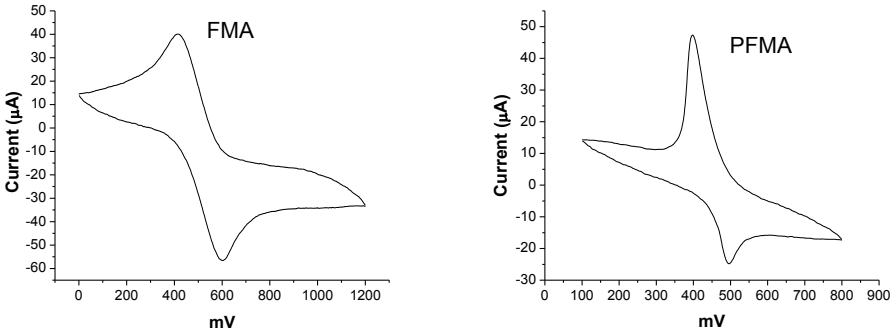

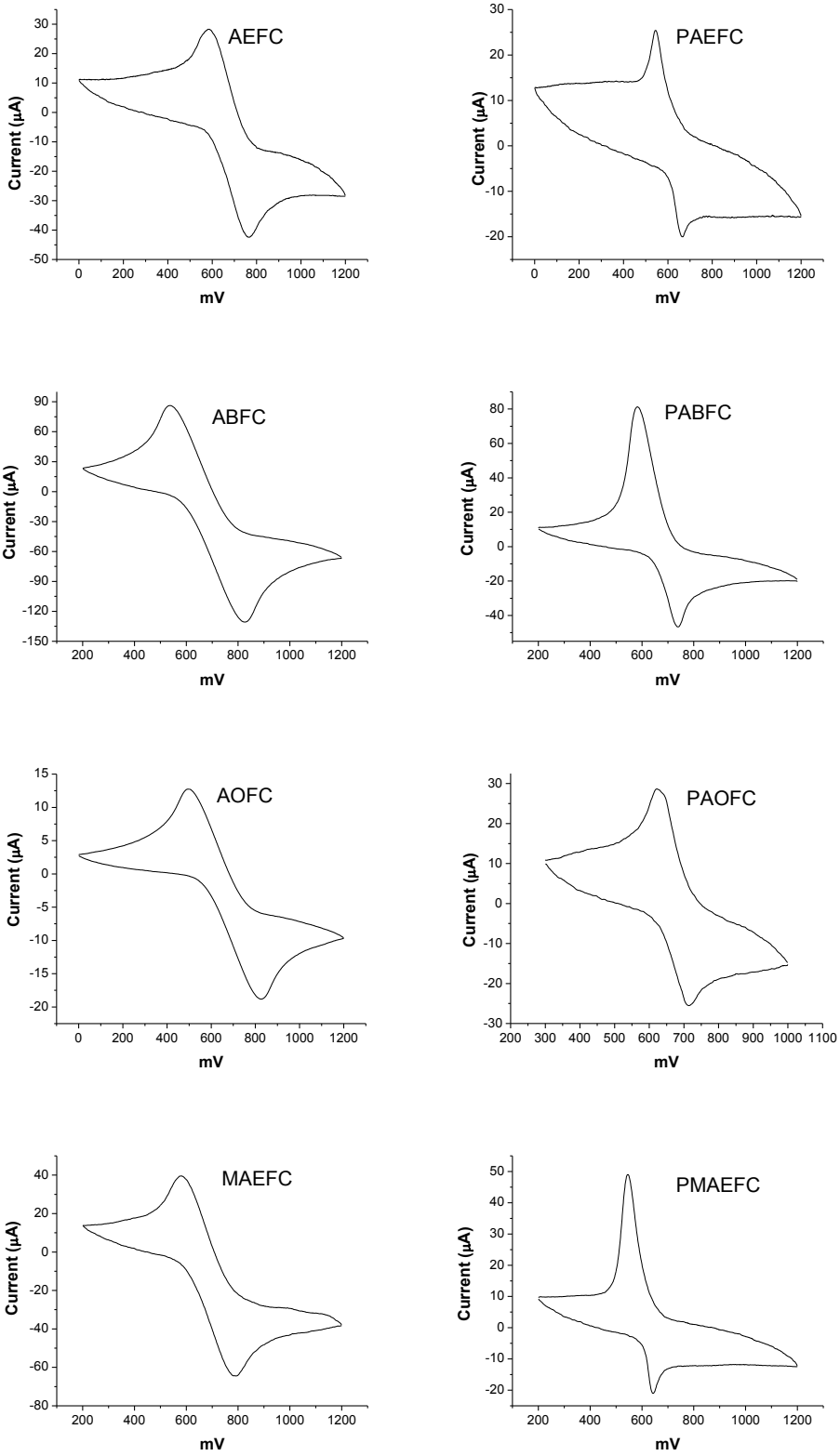

Figure 3.7. Cyclic voltammograms of FMA, AEFC, ABFC, AOFC and MAEFC monomers and their corresponding homopolymers.

The linkers between the ferrocene unit and double bond in the monomers or backbone of polymers had an influence on the half-wave potential ($E_{1/2}$).[76] When electron-donating groups such as alkyl groups are adjacent to the Cp ring, there is a shift to a more negative potential. This is due to the stabilizing effect that an electron donating group has on the reduced ferrocenium state. Electron-withdrawing groups such as carbonyls shift the potential more positively, as the reduced ferrocenium state is less favored. This trend was observed in both the ferrocene-containing monomers and polymers, as the potential of FMA and PFMA shifted more negatively than the other ferrocene (meth)acrylates that contain an alpha carbonyl (**Figure 3.8** and **Table 3.2**). With the increase of the linker length, the difference in electrochemical potential between monomers and polymers decreased. PABFC and PAOFC exhibited very similar redox behaviors to the corresponding monomers ABFC and AOFC, respectively. In addition, PAEFC and PMAEFC also displayed similar redox properties, indicating that the additional methyl group in methacrylate polymers had a minimal impact on electrochemical behaviors. As previously reported,[77] the half-wave potential ($E_{1/2}$) of the polymers slightly shifted from the corresponding monomers due to the ferrocene moiety being attached to a polymer backbone which changed the diffusion coefficient and affected the oxidation and reduction potentials, especially for PFMA, PAEFC and PMAEFC polymers.

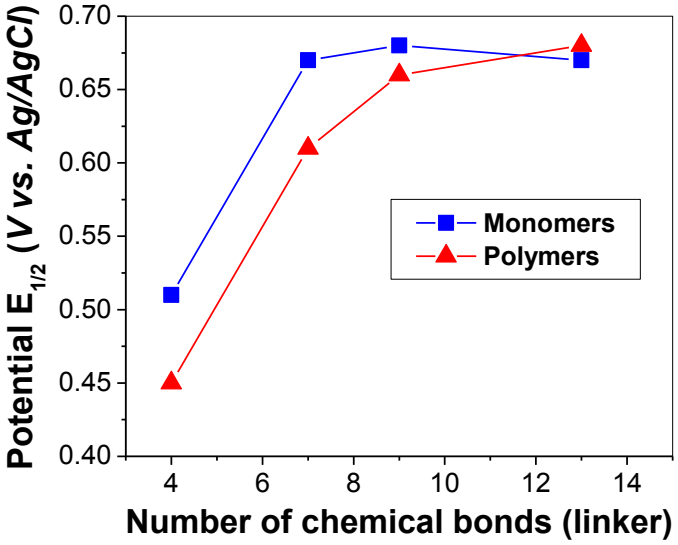

Figure 3.8. Correlation curves of acrylate monomers and polymers: half wave redox potential *vs.* the length of linkers.

Table 3.2. Electrochemical Properties of Side-Chain Ferrocene-Containing Monomers and Polymers

Pot, V	FMA	PFMA	AEFC	PAEFC	ABFC	PABFC	AOFC	PAOFC	MAEFC	PMAEFC
E_{oxd}	0.42	0.40	0.58	0.54	0.54	0.58	0.50	0.63	0.58	0.54
E_{red}	0.60	0.50	0.76	0.67	0.82	0.73	0.83	0.72	0.79	0.64
$E_{1/2}$	0.51	0.45	0.67	0.61	0.68	0.66	0.67	0.68	0.69	0.60

3.4 EXPERIMENTAL

Materials. Toluene (Acros) was dried over molecular sieves and distilled prior to use. *N,N'*-Dicyclohexylcarbodiimide (DCC, 99%), 4-(dimethylamino)pyridine (DMAP, 99%), 2-bromoisobutyryl bromide (97%), acryloyl chloride (96%), ethyl 2-bromoisobutyrate (EBiB, 97%) and propargyl acrylate (95%) from Alfa Aesar, ferrocenecarboxylic acid (97%), copper(I) chloride (99.999%), *N,N,N',N',N''*-pentamethyldiethylenetriamine (PMDETA) and sodium azide from Aldrich,

ferrocenecarboxaldehyde (98%), 2-hydroxyethyl acrylate (97%), 2-hydroxyethyl methacrylate (97%), 4-hydroxybutyl acrylate (96%), 2,2'-dipyridyl (bpy, 99%) and 1,8-octanediol (96%), triethylamine (99%) from Acros, and all other reagents were used as received unless otherwise noted.

Characterization. ^{1}H (300 MHz) and ^{13}C (75 MHz) NMR spectra were recorded on a Varian Mercury 300 NMR spectrometer with tetramethylsilane (TMS) as an internal reference. Mass spectrometry was conducted on a Waters Micromass Q-Tof mass spectrometer, and the ionization source was positive ion electrospray. Ultraviolet-visible spectroscopy (UV-Vis) was carried out on a Shimadzu UV-2450 spectrophotometer with a 10.00 mm quartz cuvette using tetrahydrofuran (THF) as solvent and monochromatic light of various wavelengths over a range of 190-900 nm. GPC was performed at room temperature on a Varian system equipped with a Varian 356-LC refractive index detector and a Prostar 210 pump. The columns were STYRAGEL HR1, HR2 (300 X 7.5 mm) from Waters. HPLC grade THF was used as eluent at a flow rate of 1 mL/min. THF and samples were filtered through microfilters with pore size of 0.2 μm (Teflon, 17 mm Syringes Filters, National Scientific, USA). Polystyrene standards were used for calibration. FT-IR spectra were recorded on a PerkinElmer Spectrum 100 FT-IR spectrometer equipped with a Universal ATR sampling accessory. Thermal transitions of the polymers were recorded using DSC on a TA Instruments Q2000 in a temperature range from -70 to 200 ^{o}C at a heating rate of 10 ^{o}C/min under constant nitrogen flow at a rate of 50 mL/min. About 5 mg samples were added to an aluminum hermetic pan and sealed. The data was collected on the second heating run. TGA was conducted on a TA Instruments Q5000 using a heating rate of 10 ^{o}C/min from 40 to 1000 ^{o}C under constant

nitrogen flow. CV was carried out on a BAS CV-50W Voltametric Analyzer at a scan rate of 50 mV s^{-1} with dichloromethane as solvent, 0.1 M tetra-*n*-butylammonium hexafluorophosphate (n-Bu_4NPF_6) as electrolyte, glassy carbon as a working electrode, platinum as a counter electrode, and Ag/Ag(I)Cl as a reference electrode.

Synthesis of Ferrocene-Containing (Meth)acrylate Monomers.

Hydroxymethylferrocene. Ferrocenecarboxaldehyde (10.1 g, 47.19 mmol) was added to methanol (270 mL) under nitrogen atmosphere and cooled to 0 ^oC. Sodium borohydride (4.52 g, 119.48 mmol) was added portion-wise over 2 hours to the solution, and stirred at room temperature overnight. The reaction mixture was quenched with aqueous ammonium chloride solution (0.5 M, 250 mL) and stirred for 30 min. Then, saturated sodium chloride solution (50 mL) was added and stirred for 5 min. The reaction mixture was extracted with dichloromethane (3 x 200 mL). The organic fractions were combined, dried over magnesium sulfate, filtered, and vacuum dried to afford hydroxymethylferrocene as a yellow solid (10.02 g, 97%). ^1H NMR ($CDCl_3$), δ (TMS, ppm): 4.33 (d, J = 5.01 Hz, 2H, CH_2Fc), 4.24 and 4.18 (9H, C*H* of Fc), 1.57 (s, 1H, CH_2OH). FT-IR (cm^{-1}): 3210, 3087, 2955, 1453, 1237, 1191, 1104, 987, 807.

Ferrocenemethyl acrylate (FMA). Hydroxymethylferrocene (3.7 g, 17.12 mmol) and triethylamine (30 mL, 215.24 mmol) were dissolved in dry dichloromethane (200 mL) and cooled to 0 ^oC. Acryloyl chloride (3.0 mL, 36.46 mmol) was added to the solution dropwise over 30 min and allowed to stir at 0 ^oC for two hours. The solution was then allowed to stir at room temperature overnight before washing with saturated potassium carbonate solution (2 x 300 mL). The organic layers were combined, dried

over magnesium sulfate, filtered, and concentrated. The product was passed through a basic alumina column using dichloromethane as solvent. The solution was collected, concentrated, and vacuum dried to afford a yellow solid (4.11 g, 89%). ^{1}H NMR ($CDCl_3$), δ (TMS, ppm): 6.44 (d, *J* = 18.1 Hz, 1H, vinyl *H*), 6.15 (dd, *J* = 10.38 and 17.31 Hz, 1H, vinyl *H*), 5.83 (d, *J* = 10.4 Hz, 1H, vinyl *H*), 4.98 (s, 2H, C*H*$_2$Fc), 4.29 and 4.17 (m, 7H, C*H* of Fc). ^{13}C NMR($CDCl_3$), δ (TMS, ppm): 166.1 (*C*=O), 130.6 and 128.5 (COO*C*H=*C*H$_2$), 81.2 (C_q of Fc), 69.6, 68.8, and 68.5 (*C*H of Fc), 62.9 (Fc*C*H$_2$). FT-IR (cm^{-1}): 3101, 2954, 1713, 1622, 1410, 1264, 1177, 1041, 817. MS (EI), m/z calcd for $C_{14}H_{14}O_2Fe$ 270.11; found 270 (M^+).

2-(Acryloyloxy)ethyl ferrocenecarboxylate (AEFC). Ferrocenecarboxylic acid (2.01 g, 8.74 mmol), 2-hydroxyethyl acrylate (1.3 mL, 11.33 mmol) and DMAP (0.13 g, 1.06 mmol) were dissolved in 100 mL dry dichloromethane, purged with N_2 gas, and cooled to 0 °C. DCC (2.15 g, 10.44 mmol) was dissolved in dry DCM (20 mL) and added dropwise to the solution over one hour, then stirred at room temperature for 24 hours. The solution was filtered, concentrated, and the mixture was separated by column chromatography (silica gel, eluent: 12:1 hexane/ethyl acetate). The product was collected, concentrated, and vacuum dried, yielding a yellow solid (2.0 g, 70%). ^{1}H NMR ($CDCl_3$), δ (TMS, ppm): 6.51 (d, *J* = 18.27 Hz, 1H, vinyl *H*), 6.23 (dd, *J* = 10.41 Hz and 17.31 Hz, 1H, vinyl *H*), 5.90 (d, *J* = 11.37 Hz, 1H, vinyl *H*), 4.20-4.82 (m, 9H, C*H* of Fc), 4.47 (s, 4H, COOC*H*$_2$C*H*$_2$COO). ^{13}C NMR($CDCl_3$), δ (TMS, ppm): 171.6 (Fc*C*OOCH$_2$), 165.9 (CH$_2$*C*OOCH=CH$_2$), 131.5 and 128.1 (COO*C*H=*C*H$_2$), 70.5 (C_q of Fc), 71.5, 70.2, 69.8 (*C*H of Fc), 62.5 and 61.9 (COO*C*H$_2$*C*H$_2$COO). FT-IR (cm^{-1}): 3112,

2951, 1707, 1619, 1464, 1408, 1264, 1148, 818. MS (EI), m/z calcd for $C_{16}H_{16}O_4Fe$ 328.14; found 328 (M^+).

4-(Acryloyloxy)butyl ferrocenecarboxylate (ABFC). This compound was prepared as an orange solid from ferrocenecarboxylic acid (2.75 g, 11.957 mmol), 4-hydroxybutyl acrylate (2.0 mL, 14.44 mmol), DMAP (0.18 g, 1.47 mmol), and DCC (2.96 g, 14.35 mmol) in dry dichloromethane (100 mL) following a similiar procedure used for AEFC synthesis. Yield: 3.19 g (75%). ^{1}H NMR ($CDCl_3$), δ (TMS, ppm): 6.44 (d, *J* = 17.32 Hz, 1H, vinyl *H*), 6.16 (dd, *J* = 10.4 Hz and 17.3 Hz, 1H, vinyl *H*), 5.84 (d, *J* = 7.8 Hz, 1H, vinyl *H*), 4.19-4.80 (m, 9H, C*H* of Fc), 4.39 (s, 4H, COOC*H*$_2$(CH$_2$)$_2$C*H*$_2$COO), 1.83 (s, 4H, COOCH$_2$(C*H*$_2$)$_2$CH$_2$COO). ^{13}C NMR ($CDCl_3$), δ (TMS, ppm): 171.7 (Fc*C*OOCH$_2$), 166.3 (CH$_2$*C*OOCH=CH$_2$), 130.8 and 128.4 (COO*C*H=*C*H$_2$), 71.1 (*C*$_q$ of Fc), 71.3, 70.1, 69.7 (*C*H of Fc), 64.1 and 63.6 (COO*C*H$_2$CH$_2$CH$_2$*C*H$_2$COO), 25.6 and 25.5 (COOCH$_2$*C*H$_2$*C*H$_2$CH$_2$COO). FT-IR (cm^{-1}): 3112, 2962, 1710, 1635, 1411, 1273, 1190, 1132, 812. MS (EI), m/z calcd for $C_{18}H_{20}O_4Fe$ 356.20; found 356 (M^+).

Hydroxyoctylferrocene. Ferrocenecarboxylic acid (1.5 g, 6.52 mmol), 1, 8-octanediol (3.81 g, 26.10 mmol), and DMAP (0.32 g, 2.61 mmol) were dissolved in dry dichloromethane (100 mL), purged with nitrogen gas, and cooled to 0 ^{o}C. DCC (5.37 g, 26.07 mmol) was added to the solution and allowed to stir for 30 minutes at 0 ^{o}C, then stirred at room temperature for 24 hours. The solution was filtered, concentrated, and the mixture was separated by column chromatography (silica gel, eluent: 9:1 hexane/ethyl acetate). The product was collected, concentrated, and vacuum dried at room temperature, yielding an orange solid (1.79 g, 77%). ^{1}H NMR ($CDCl_3$), δ (TMS, ppm):

4.19-4.80 (m, 9H, C*H* of Fc), 4.22 (s, 2H, FcCOOCH_2), 3.65 (m, 2H, CH_2OH), 1.72 (m, 2H, FcCOOCH$_2$CH_2), 1.56 (m, 2H, CH$_2$CH_2OH), 1.32-1.37 (m, 8H, COOCH$_2$CH$_2$(CH_2)$_4$). FT-IR (cm^{-1}): 3220, 3086, 2940, 1236, 1190, 1105, 986, 812.

8-(Acryloyloxy)octyl ferrocencarboxylate (AOFC). Hydroxyoctylferrocene (1.45 g, 4.05 mmol) and triethylamine (2.3 mL, 16.5 mmol) were dissolved in dry dichloromethane (125 mL) and cooled to 0^{o}C. Acryloyl chloride (0.7 mL, 8.66 mmol) was added to the solution dropwise over 30 min. The solution was allowed to stir at room temperature for 24 hours. The resulting solution was extracted with saturated potassium carbonate solution (3 X 150 mL). The organic layers were combined, dried over magnesium sulfate, filtered, and concentrated. The organic products were separated using column chromatography (silica gel, eluent: 9:1 hexane/ethyl acetate). Yield = 1.36 g (82%). ^{1}H NMR (CDCl$_3$), δ (TMS, ppm): 6.43 (d, *J* = 18.39 Hz, 1H, vinyl *H*), 6.17 (dd, *J* = 10.4 Hz and 17.3 Hz, 1H, vinyl *H*), 5.83 (d, *J* = 11.43 Hz, 1H, vinyl *H*), 4.24-4.84 (m, 9H, C*H* of Fc), 4.18 (4H, COOCH_2(CH$_2$)$_6$CH_2COO), 1.69 (m, 4H, COOCH$_2$CH_2(CH$_2$)$_4$CH_2CH$_2$COO), 1.39 (m, 8H, COOCH$_2$CH$_2$(CH_2)$_4$CH$_2$CH$_2$COO). ^{13}C NMR (CDCl$_3$), δ (TMS, ppm): 171.8 (Fc*C*OOCH$_2$), 166.4 (CH$_2$*C*OOCH=CH$_2$), 130.5 and 128.6 (COO*C*H=*C*H$_2$), 71.5 (C_q of Fc), 71.1, 70.1, 69.7 (*C*H of Fc), 64.6 and 64.2 (COO*C*H$_2$(CH$_2$)$_6$*C*H$_2$COO), 25.6-29.2 (COOCH$_2$(*C*H$_2$)$_6$CH$_2$COO). FT-IR (cm^{-1}): 3101, 2937, 2857, 1712, 1635, 1460, 1406, 1270, 1190, 1136, 812. MS (EI), m/z calcd for $C_{22}H_{28}O_4Fe$ 412.30; found 412 (M^+).

2-(Methacryloyloxy)ethyl ferrocenecarboxylate (MAEFC). This compound was prepared as an orange solid from ferrocenecarboxylic acid (2.02 g, 8.78 mmol), 2-hydroxyethyl methacrylate (1.3 mL, 10.72 mmol), DMAP (0.13 g, 1.06 mmol), and DCC

(2.15 g, 10.43 mmol) in dry dichloromethane (100 mL) following a similiar procedure used for AEFC synthesis. Yield: 2.40 g (80%). ^{1}H NMR ($CDCl_3$), δ (TMS, ppm): 6.19 (s,1H, vinyl *H*), 5.62 (s,1H, vinyl *H*), 4.20-4.82 (m, 9H, C*H* of Fc), 4.47 (s, 4H, COOCH_2CH_2COO), 1.98 (s, 3H, COOC(CH_3)=CH_2). ^{13}C NMR($CDCl_3$), δ (TMS, ppm): 170.2 (Fc*C*OOCH_2), 167.1 (CH_2*C*OOCH=CH_2), 136.3 and 126.0 (COOC(*C*H_3)=*C*H_2), 70.6 (C_q of Fc), 71.4, 70.2, 69.8 (*C*H of Fc), 62.6 and 61.9 (COO*C*H_2*C*H_2COO), 18.2 (COOC(*C*H_3)=CH_2). FT-IR (cm^{-1}): 3108, 2958, 1705, 1638, 1467, 1280, 1146, 821. MS (EI), m/z calcd for $C_{17}H_{18}O_4Fe$ 342.17; found 342 (M^+).

Azidomethylferrocene. Hydroxymethylferrocene (3.8 g, 17.59 mmol), sodium azide (6.86 g, 105.52 mmol), and glacial acetic acid (190 mL) were added to a round bottom flask under nitrogen flow and heated to 50 ^{o}C for 3.5 hours. After the solution cooled to room temperature, dichloromethane (500 mL) was added and the organic layer was extracted with saturated sodium bicarbonate solution (3 X 300 mL) followed by extraction with deionized water (300 mL). The organic fractions were combined, dried over anhydrous magnesium sulfate, filtered, and vacuum dried. Yield = 4.14 g (97.6 %). ^{1}H NMR ($CDCl_3$), δ (TMS, ppm): 4.23-4.16 (7H, C*H* of Fc), 4.12 (s, 2H, FcCH_2N_3). FT-IR (cm^{-1}): 3105, 2944, 2100, 1450, 1259, 1106, 1036, 1000, 854. MS (EI), m/z calcd for $C_{11}H_{11}N_3Fe$ 241.1; found 241 (M^+).

Ferrocenylmethyl triazole methyl acrylate (FTA). Copper (I) bromide (0.116 g, 0.81 mmol) was added to a round bottom flask and purged with nitrogen for 10 min. PMDETA (0.2 mL, 0.97 mmol) and dry deoxygenated THF (1.0 mL) were added and stirred for 10 min. In a separate round bottom flask, propargyl acrylate (1.2 mL, 10.86 mmol) and azidomethylferrocene (1.95 g, 8.09 mmol) were dissolved in dry THF (100

mL) and deoxygenated by nitrogen bubbling for 25 min. This degassed solution was then transferred to the flask containing the copper complex and allowed to stir at room temperature overnight. The resulting mixture was filtered and passed through a basic alumina column. All solutions were concentrated and vacuum dried at room temperature. Yield = 2.53 g (90%). ^{1}H NMR ($CDCl_3$), δ (TMS, ppm): 7.52 (s, 1H, NC*H*=C), 6.4388 (d, *J* = 17.28 Hz, 1H, vinyl *H*), 6.15 (dd, *J* = 10.41 Hz and 17.28 Hz, 1H, vinyl *H*), 5.85 (d, *J* = 10.41 Hz, 1H, vinyl *H*), 5.28 (s, 2H, CH=CC*H*2OC=O), 5.26 (s, 2H, FcCH_2N), 4.28-4.17 (m, 9H, C*H* of Fc). ^{13}C NMR($CDCl_3$), δ (TMS, ppm): 165.9 (*C*OOCH=CH_2), 142.5 (N*C*H=C), 131.5 (NCH=*C*), 128.0 and 123.2 (COO*C*H=*C*H_2), 80.7 (C_q of Fc), 69.1, 68.9, and 68.9 (*C*H of Fc), 57.7 (Fc*C*H2N), 50.1 (COO*C*H_2C). FT-IR (cm^{-1}): 3122, 2976, 1722, 1635, 1546, 1445, 1406, 1333, 1296, 1226, 1177, 1104, 1052, 984, 821. MS (EI), m/z calcd for $C_{17}H_{17}N_3O_2Fe$ 351.22; found 351 (M^+).

General Polymerization Procedure and Kinetic Study. For a typical polymerization, the ferrocene-containing (meth)acrylate (100 molar eq.), Cu(I)Cl (2 molar eq.), and 2,2'-dipyridyl (bpy) (4 molar eq.) were added to a 10-mL Schlenk flask and degassed by purging with nitrogen. Distilled toluene (1 mL) was added to a 5 mL round bottom flask and degassed by bubbling the solution with nitrogen gas for 10 min. Ethyl 2-bromoisobutyrate (EBiB) (1 molar eq.) was added directly to the Schlenk flask followed by addition of the degassed toluene. The mixture was further degassed by nitrogen bubbling for 5 min. The reaction was stirred at room temperature for 15 min before the flask was placed in an oil bath preheated to 90 ^{o}C. An initial sample was taken in order to accurately determine the reaction conversion by ^{1}H NMR. Samples were periodically taken over the course of the polymerization for ^{1}H NMR and GPC analysis.

The polymerization was quenched by placing the Schlenk flask in an ice bath. The mixtures were then passed through a short neutral alumina plug, concentrated, and precipitated into hexane at least two times and vacuum dried.

3.5 CONCLUSIONS

A series of ferrocene-containing acrylate and methacrylate monomers were prepared using either simple esterification reactions or a copper catalyzed [3+2] cycloaddition reaction. With the exception of a triazole-containing ferrocene acrylate, all monomers were successfully polymerized using atom transfer radical polymerization (ATRP). The kinetic studies showed the polymerization followed a controlled/"living" nature. Most polymers had controlled molecular weights and low polydispersity. It was found the length of the linkers played a key role in the kinetics of the polymerization, as longer linkers between the ferrocene moiety and the vinyl ester of monomers slowed down polymerization. It was also found that ferrocene-containing methacrylate monomers exhibited much faster polymerization than the corresponding acrylate monomers. Optically properties of these polymers showed a structural dependence. Thermal properties of all homopolymers showed a tunable glass transition temperature depending on the length of linkers. Cyclic voltammetry studies showed reversible redox chemistry for the ferrocene-containing monomers, but irreversible redox chemistry for the corresponding polymers in dichloromethane. The irreversible redox was due to the limited solubility of ferrocenium polymers. The electrochemical properties were generally influenced by the linkers. The synthesis and characterization of ferrocene-containing (meth)acrylate monomers and polymers in this work may pave the way to develop a variety of side-chain ferrocene-containing polymers with different

functionalities and architectures, which have the promise to regenerate new interests in the field of organometallic polymers.

3.6 ACKNOWLEDGMENT

We would like to acknowledge the University of South Carolina for providing start-up fund.

3.6 REFERENCES

1. Abd-El-Aziz, A. S.; Manners, I., *Frontiers in Transition-Metal-Containing Polymers*. Wiley: Hoboken, NJ, 2007.
2. Andres, P. R.; Schubert, U. S. **2004,** 16, 1043-1068.
3. Beck, J. B.; Ineman, J. M.; Rowan, S. J. **2005,** 38, 5060-5068.
4. Calzia, K. J.; Tew, G. N. **2002,** 35, 6090-6093.
5. Hofmeier, H.; Schubert, U. S. **2005**, 2423-2432.
6. Holliday, B. J.; Swager, T. M. **2005**, 23-26.
7. Manners, I., *Synthetic Metal-Containing Polymers*. Wiley-VCH: Weinheim, 2004.
8. Manners, I. **2004,** 294, 1664-1666.
9. Newkome, G. R.; He, E.; Moorefield, C. N. **1999,** 99, 1689-1746.
10. Schubert, U. S.; Eschbaumer, C. **2002,** 41, 2892-2926.
11. Whittell, G. R.; Manners, I. **2007,** 19, 3439-3468.
12. Shunmugam, R.; Gabriel, G. J.; Aamer, K. A.; Tew, G. N. **2010,** 31, 784-793.
13. Grubbs, R. B. *J. Polym. Sci., Part A: Polym. Chem.* **2005,** 43, 4323-4336.
14. Mıinea, L. A.; Sessions, L. B.; Ericson, K. D.; Glueck, D. S.; Grubbs, R. B. *Macromolecules* **2004,** 37, 8967-8972.
15. Abd-El-Aziz, A. S. *Macromol. Rapid Commun.* **2002,** 23, 995-1031.
16. Astruc, D.; Chardac, F. **2001,** 101, 2991-3023.
17. He, F.; Gadt, T.; Jones, M.; Scholes, G.; Manners, I.; Winnik, M. A. **2009,** 42, 7953-7960.
18. Hudson, R. D. **2001**, 637-639.
19. Nguyen, P.; Gomez-Elipe, P.; Manners, I. **1999,** 99, 1515-1548.
20. Ren, L.; Hardy, C. G.; Tang, C. **2010,** 132, 8874-8875.
21. Sheats, J. E.; Carraher, J., C. E. ; Pittman, J., C. P. ; Zeldin, M.; Currell, B., *Inorganic and Metal-Containing Polymeric Materials*. Plenum: New York, 1985.
22. Sheats, J. E.; Rausch, M. D. **1970,** 35, 3245-3249.
23. Stepnicka, P., *Ferrocenes: ligands, materials and biomolecules*. John Wiley & Sons: West Sussex, 2008.
24. Togni, A.; Halterman, R., *Metallocenes: Synthesis - Reactivity - Applications*. Wiley-VCH: Weinheim, 1998.
25. Togni, A.; Hayashi, T., *Ferrocenes: homogeneous catalysis, organic synthesis, materials science*. VCH Publishers: New York, 1995.

26. Rider, D. A.; Manners, I. **2007,** 47, 165-195.
27. Kaifer, A. E. **2007,** 32, 5015-5027.
28. Ornelas, C.; Ruiz, J.; Astruc, D. **2009,** 28, 2716-2723.
29. Ornelas, C.; Ruiz, J.; Belin, C.; Astruc, D. **2008,** 131, 590-601.
30. Sobransingh, D.; Kaifer, A. E. **2006,** 22, 10540-10544.
31. Arimoto, F. S.; Haven, A. C. *J. Am. Chem. Soc.* **1955,** 77, 6295-6297.
32. Deschenaux, R.; Izvolensk, V.; Turpin, F.; Guillon, D.; Heinrich, B. **1996**, 439-440.
33. Pittman, C. U. **1967,** 5, 2927-2937.
34. Pittman, C. U.; Ayers, O. E.; McManus, S. P.; Sheats, J. E.; Whitten, C. E. **1971,** 4, 360-362.
35. Pittman, C. U.; Jr, n.; Vanderpool, D. P.; Good, M. J.; Prados, R. **1970,** 3, 746-754.
36. Pittman, C. U.; Voges, R. L.; Jones, W. R. **1971,** 4, 298-302.
37. Rausch, M. D.; Coleman, L. E., Jr. **1958,** 23, 107-108.
38. Wright, M. E. **1990,** 9, 853-856.
39. Foucher, D. A.; Tang, B. Z.; Manners, I. **1992,** 114, 6246-6248.
40. Rulkens, R.; Lough, A. J.; Manners, I. **1994,** 116, 797-798.
41. Rulkens, R.; Lough, A.-J.; Manners, I.; Lovelace, S. R.; Grant, C.; Geiger, W. E. **1996,** 118, 12683-12695.
42. Chuang, V. P.; Gwyther, J.; Mickiewicz, R. A.; Manners, I.; Ross, C. A. **2009,** 9, 4364-4369.
43. Zhao, D.; Ren, B.; Liu, S.; Liu, X.; Tong, Z. **2006**, 779-781.
44. Gallei, M.; Schmidt, B. V. K. J.; Klein, R.; Rehahn, M. **2009,** 30, 1463-1469.
45. Albagli, D.; Bazan, G.; Wrighton, M. S.; Schrock, R. R. **1992,** 114, 4150-4158.
46. Watson, K. J.; Zhu, J.; Nguyen, S. T.; Mirkin, C. A. **1998,** 121, 462-463.
47. Chiefari, J.; Chong, Y. K.; Ercole, F.; Krstina, J.; Jeffery, J.; Le, T. P. T.; Mayadunne, R. T. A.; Meijs, G. F.; Moad, C. L.; Moad, G.; Rizzardo, E.; Thang, S. H. *Macromolecules* **1998,** 31, 5559-5562.
48. Kamigaito, M.; Ando, T.; Sawamoto, M. **2001,** 101, 3689-3745.
49. Matyjaszewski, K.; Xia, J. **2001,** 101, 2921-2990.
50. Georges, M. K.; Veregin, R. P. N.; Kazmaier, P. M.; Hamer, G. K. **1993,** 26, 2897-2898.
51. Hawker, C. J.; Bosman, A. W.; Harth, E. **2001,** 101, 3661-3688.
52. Kato, M.; Kamigaito, M.; Sawamoto, M.; Higashimura, T. **1995,** 28, 1721-1723.
53. Percec, V.; Barboiu, B. **1995,** 28, 7970-7972.
54. Wang, J.-S.; Matyjaszewski, K. **1995,** 117, 5614-5615.
55. Kolb, H. C.; Finn, M. G.; Sharpless, K. B. **2001,** 40, 2004-2021.
56. Feng, C.; Shen, Z.; Yang, D.; Li, Y.; Hu, J.; Lu, G.; Huang, X. **2009,** 47, 4346-4357.
57. Kim, B. Y.; Ratcliff, E. L.; Armstrong, N. R.; Kowalewski, T.; Pyun, J. **2009,** 26, 2083-2092.
58. Beers, K. L.; Matyjaszewki, K. **2001,** 38, 731-739.
59. Qin, S.; Matyjaszewki, K.; Xu, H.; Sheiko, S. S. **2003,** 36, 605-612.
60. Qin, S.; Saget, J.; Pyun, J.; Jia, S.; Kowalewski, T.; Matyjaszewki, K. **2003,** 36, 8969-8977.

61. Pittman Jr., C. U. **2005,** 15, 33-55.
62. Golas, P.; Matyjaszewki, K. **2010,** 39, 1338-1354.
63. Lutz, J. F.; Boerner, H. G.; Weichenhan, K. **2005,** 26, 514-518.
64. Lutz, J. F.; Boerner, H. G.; Weichenhan, K. **2006,** 39, 6376-6383.
65. Mantovani, G.; Ladmiral, V.; Tao, L.; Haddleton, D. M. **2005,** 16, 2089-2091.
66. Urien, M.; Erothu, H.; Cloutet, E.; Hiorns, R. C.; Vignau, L.; Cramail, H. **2008,** 41, 7033-7040.
67. Ladmiral, V.; Mantovani, G.; Clarkson, G. J.; Cauet, S.; Irwin, J. L.; Haddleton, D. M. **2006,** 128, 4823-4830.
68. Sumerlin, B. S.; Tsarevsky, N. V.; Louche, G.; Lee, R. Y.; Matyjaszewki, K. **2005,** 38, 7540-7545.
69. Binder, W. H.; Kluger, C. **2004,** 37, 9321-9330.
70. Binder, W. H.; Sachsenhofer, R. **2007,** 28, 15-54.
71. Nulwala, H.; Takizawa, K.; Odukale, A.; Khan, A.; Thibault, R. J.; Taft, B. R.; Lipshutz, B. H.; Hawker, C. J. **2009,** 42, 6068-6074.
72. Nulwala, H.; Burke, D. J.; Khan, A.; Serrano, A.; Hawker, C. J. **2010,** 43, 5474-5477.
73. Thibault, R. J.; Takizawa, K.; Lowenheilm, P.; Helms, B.; Mynar, J. L.; Frechet, J. M. J.; Hawker, C. J. **2006,** 128, 12084-12085.
74. Scott, D. R.; Becker, R. S. **1961,** 35, 516-531.
75. Akiyama, T.; Sugimori, A.; Hermann, H. **1973,** 46, 1855-1859.
76. Astruc, D.; Ornelas, C.; Ruiz, J. **2009,** 15, 8936-8944.
77. Yan, F.; Higashihara, T.; Mosurkal, R.; Li, L.; Yang, K.; Faust, R.; Kumar, J. **2008,** 45, 910-913.

CHAPTER 4

SELF-ASSEMBLY OF WELL-DEFINED FERROCENE TRIBLOCK COPOLYMERS AND THEIR TEMPLATE SYNTHESIS OF ORDERED IRON OXIDE NANOPARTICLES[†]

[†] Hardy, C. G.; Ren, L.; Tang, C. *Chemical Communications* **2013**, 49, 4373-4375. Reprinted here with permission of publisher.

4.1 ABSTRACT

Well-defined ferrocene-containing triblock copolymers were synthesized by atom transfer radical polymerization and were found to self-assemble into highly ordered hexagonal arrays of cylinders via solvent annealing. The thin films were further used as a template and converted into highly ordered iron oxide nanoparticles (α-Fe_2O_3) by UV/ozonolysis and thermal pyrolysis.

4.2 INTRODUCTION

Ordered arrays of transition metal oxide nanoparticles with controlled size, spacing, and arrangement have recently received much attention due to their potential applications in high-density nanoelectronic technologies such as flash memory devices, magnetic data storage devices and catalyst sites for organized molecular wires.[1-3] These technologies utilize well-ordered metal particles at the nano-level. Current "top-down" lithographic practices, employed by the microelectronic industry, face the escalating production cost as a function of decreasing feature size. As a result of the limitations in current lithography, various "bottom-up" techniques are being developed to create well-defined nanostructures on the 5-50 nm level.[4] Block copolymer (BCP) nanolithography is of particular interest due to the ability of BCPs to spontaneously self-assembly into a variety of well-defined nanodomains including spheres, cylinders, lamellae, and bicontinuous gyroids in the bulk state.[5-11] The morphology of diblock copolymers is dictated by three parameters including the degree of polymerization (N), the volume fraction of each block (f), and the Flory-Huggins interaction parameter (χ).[12-14]

Self-assembly of BCPs in thin films are affected by 2D confinement as well as substrate/polymer and polymer/surface interactions. There are several strategies to

prepare highly ordered BCP films including topographical or chemical graphoepitaxy, the use of external forces such as electrical field, magnetic field, directional solidification, and solvent annealing.[15-19] Directional solvent evaporation, in which the oriented growth and positions of microdomains are controlled by the rate and directionality of solvent evaporation, is a simple and fast way to produce ordered nanostructures. Russell group utilized diblock copolymer poly(ethylene oxide)-*b*-polystyrene (PEO-*b*-PS) to obtain the long-range order of nearly defect-free perpendicular cylinders by solvent annealing in a high humidity atmosphere.[17, 20-22] By combining long-range order obtained from the PEO-*b*-PS diblock copolymer with the photodegradability of poly(methyl methacrylate) (PMMA), thin films of triblock copolymer PEO-*b*-PMMA-*b*-PS were demonstrated to form highly ordered arrays of nanopores by solvent annealing and subsequent etching.[23] Many other block copolymers based on PEO and PS have been also developed to form ordered arrays of nanodomains.[24-30]

Arrays of transition metal oxide nanoparticles have been prepared using a wide variety of techniques including deposition of metal nanoparticles, evaporation of thin metal films, and degradation of organometallic BCPs.[31-34] These methods have shown to be effective in producing metal nanoparticles with controllable size; however, many of these systems are not capable of achieving long-range order. To address this issue, a few groups utilized diblock copolymer polystyrene-*b*-poly(4-vinylpyridine) (PS-*b*-P4VP) to form ordered thin films of perpendicular, hexagonal cylinders by solvent annealing.[35, 36] Upon complexation of a metal precursor through electrostatic interactions between an iron complex and the protonated nitrogen of P4VP, the metal center could be spatially positioned into the minor domain. Similarly, diblock copolymer PEO-*b*-PS was used to

create a highly ordered nanoporous film after self-assembly and a surface reconstruction process.[37] A solution containing iron nitrate was then spin coated onto the nanoporous film, essentially filling the pores with the metal complex. Upon pyrolysis or oxygen plasma treatment to remove organic matter, iron oxide nanoparticles were deposited onto the substrate.

Herein, we report a method to fabricate highly ordered arrays of iron oxide nanoparticles through self-assembly of organometallic triblock copolymer poly(ethylene oxide)-*b*-poly(2-(methacryloyloxy)ethyl ferrocenecarboxylate)-*b*-polystyrene (PEO-*b*-PMAEFc-*b*-PS), as shown in Scheme 4.1. Different from main-chain poly(ferrocenyl silane)-based polymer systems,[33, 34] there is no silicon atom present in the block containing the ferrocene in our system. Thus, upon removal of the organic compounds, pure iron oxide could be obtained, instead of a mixture of silicon and iron oxides from the poly(ferrocenyl silane) systems. Since the metallocene moiety is covalently bonded to the side-chain of the middle block, the metallic precursor is automatically positioned into the cylindrical domain upon self-assembly. This approach bypasses the metal complexation and/or surface modification steps as reported in other studies.[35, 36, 37] Furthermore, by chemically attaching the metal precursor into BCPs, it could preclude metal residues to diffuse out of cylindrical domains or to stay on top of films. In addition, ferrocene is expected to uniformly distribute within each cylinder, which could translate into iron oxide nanoparticles with uniform size after removal of organic materials.

Scheme 4.1. Preparation of ordered BCP films and their template synthesis of iron oxide nanoparticles.

4.3 Results and Discussion

Triblock copolymer PEO-*b*-PMAEFc-*b*-PS was prepared using atom transfer radical polymerization (ATRP) as outlined in Figure 4.1 and detailed in the experimental section. Briefly, a monofunctional PEO ATRP macroinitiator (**1**) was used for chain extension with ferrocene-containing monomer MAEFc to give diblock copolymer PEO-*b*-PMAEFc (**2**), which was then chain extended with styrene, resulting in triblock copolymer PEO-*b*-PMAEFc-*b*-PS (**3a-c**). Upon chain extension with MAEFc, signature peaks appeared between between 4.0-4.8 ppm in the ^{1}H NMR (Figure 4.4), attributed to the cylopentadienyl protons and the methylene protons in side chain.[38] Upon further chain extension with styrene, characteristic peaks between 6.1-7.4 ppm from phenyl protons appeared. Three separate chain extensions with styrene were preformed from the same diblock copolymer PEO-*b*-PMAEFc (**2**) in order to find the appropriate compositions (Table 4.1) that would lead to highly ordered hexagonal arrays of cylinders. Monomodal traces with increase in molecular weight were obtained for each sequential chain extension (Figure 4.1). The relative degree of polymerization and molecular weight of each block was determined using ^{1}H NMR based on the known molecular weight of the starting PEO block (5,000 g/mol).

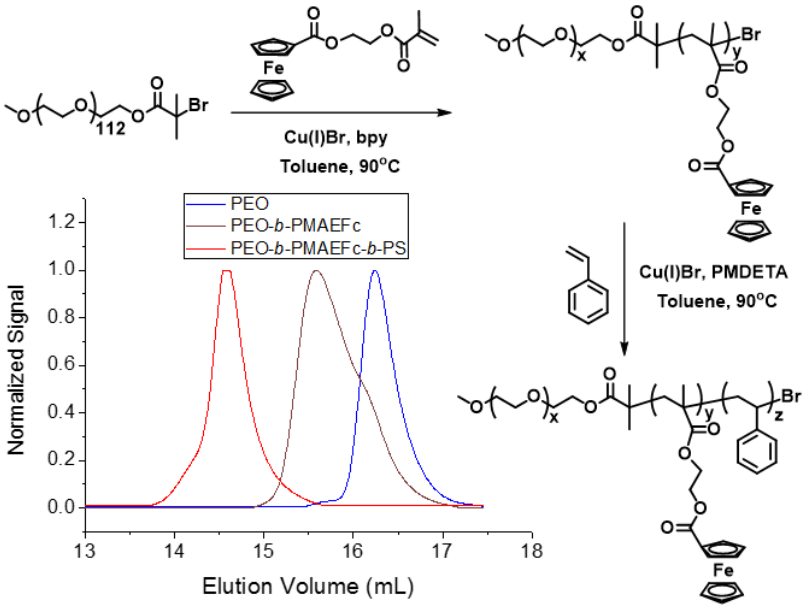

Figure 4.1. Synthesis of triblock copolymer PEO-*b*-PMAEFc-*b*-PS by ATRP and GPC overlay of PEO (**1**), PEO-*b*-PMAEFc (**2**), and PEO-*b*-PMAEFc-*b*-PS (**3**).

1.5 wt% solution of triblock copolymer PEO-*b*-PMAEFc-*b*-PS (**3a-c**) in toluene was spin-coated onto cleaned silicon wafer substrates. The films (thickness ~60 nm) were then annealed in the presence of toluene vapour and a controlled humidity environment (85-90% relative humidity) to induce microphase separation and ordering. Perpendicular hexagonal arrays of cylinders with grain sizes of over 3 µm × 3 µm were obtained for triblock copolymer **3b** (81 wt% PS) after solvent annealing for 12 hours (Figures 4.2A and 4.2B). Notably, incorporation of the PMAEFc block did not disrupt the order that is usually observed for PEO-*b*-PS diblock copolymer systems. The PEO/PMAEFc domains have a diameter of 24 nm (without tip deconvolution) and a spacing of 45 nm, embedded in PS matrix. Triblock copolymers **3a** (47 wt% PS) and **3c** (87 wt% PS) resulted in disorganized morphology after annealing, as seen in Figures 4.5 and 4.6.

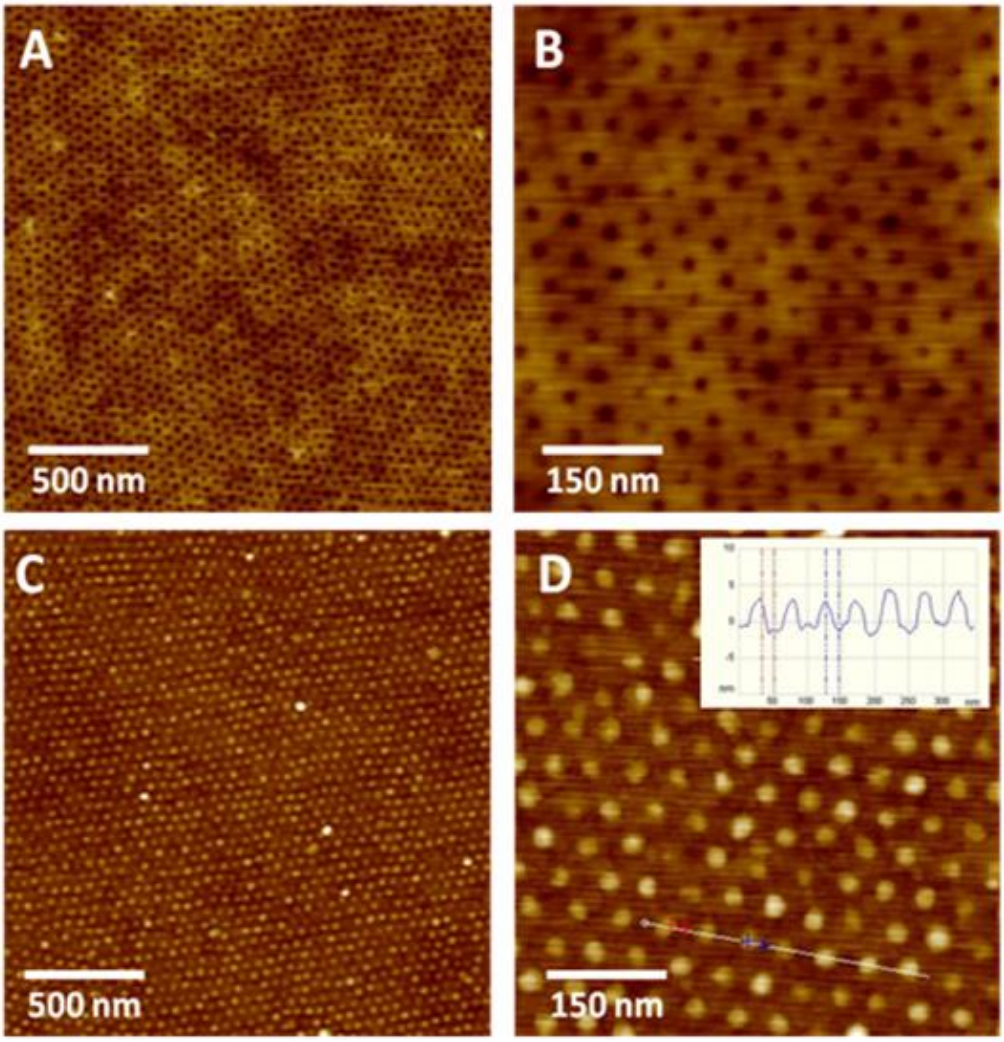

Figure 4.2. (A,B) AFM height images of the triblock copolymer PEO-*b*-PMAEFc-*b*-PS (**3b**) film after annealing; and (C, D) AFM height images of iron oxide nanoparticles obtained after UV/O and pyrolysis of triblock copolymer PEO-*b*-PMAEFc-*b*-PS.

The thin films were then exposed to UV/ozone (UV/O) and pyrolyzed at 1200 ^{o}C to degrade organic components and convert into iron oxide nanoparticles. Figures 4.2C and 2D show the AFM images of the ordered iron oxide nanoparticles. The average diameter and height of nanodots are 25 (±3) nm and 4.3 (±1.5) nm (Figure 4.2D, inset), respectively. The spacing for the nanoparticles was maintained at 45 nm, indicating the perseverance of ordering templated from BCP films. The ferrocene units in the cylinders

were converted into inorganic iron oxide and aggregated within the domains without the loss of ordering.

A previous study[35] has shown that simple UV/O treatment at room temperature to degrade iron oxide precursors resulted in non-crystalline iron oxides due to the amorphous nature of the iron oxide. Upon pyrolysis, crystalline iron oxide was obtained, as confirmed by both X-ray photoelectron spectroscopy (XPS) and X-ray diffraction (XRD). XPS was utilized to determine the chemical nature of the newly formed nanoparticles (Figure 4.3A and Figure 4.7). The XPS spectra of iron oxide nanoparticles showed Fe($2p_{3/2}$) and Fe($2p_{1/2}$) peaks at 710.5 eV and 723.9 eV, respectively, with both shake-up peaks ~8 eV higher. Furthermore, the peak at 710.5 eV had a distinct shoulder at 709.5 eV. The shoulder at 709.5 eV and the shake-up peak at 718.5 eV suggested the formation of α-Fe_2O_3.[39, 40] As shown in Figure 4.3B, the XRD patterns of our nanoparticles showed strikingly high order peaks at 2θ = 24.1°, 33.2°, 35.6°, 40.8°, 49.5°, 54.2°, 62.4°, and 64.0°, which are consistent with the value of JCPDS card 33-0664, and could be indexed to the pure hexagonal phase of hematite ((012), (104), (110), (113), (024), (116), (214), and (300)).[41] Our results are also in good agreement with the formation of α-Fe_2O_3, as confirmed from early reported diffraction patterns (Table 4.2).[35, 42-45]

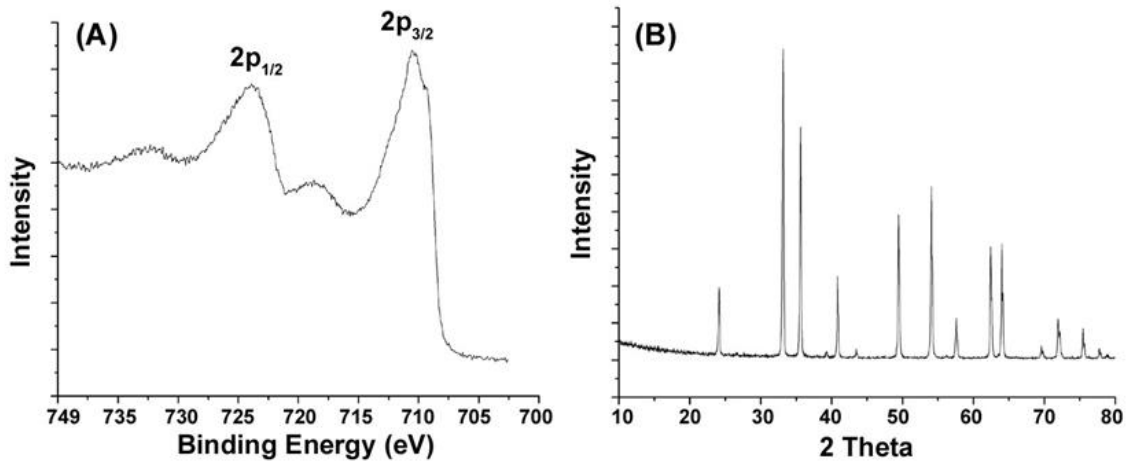

Figure 4.3. (A) XPS and (B) XRD spectra of iron oxide nanoparticles obtained after UV/O and pyrolysis of triblock copolymer PEO-*b*-PMAEFc-*b*-PS (**3b**).

4.4 EXPERIMENTAL

Materials. All reagents were purchased from Alfa Aesar and Aldrich and used as received unless otherwise noted. 2-(Methacryloyloxy)ethyl ferrocenecarboxylate (MAEFc) and ATRP macroinitiator PEO-Br were prepared according to reported procedures.[46,47] Styrene was distilled before use. AIBN was recrystallized from diethyl ether before use.

Characterization. ^{1}H NMR (300 MHz) spectra were recorded on a Varian Mercury 300 spectrometer with tetramethylsilane (TMS) as an internal reference. GPC was performed at 50^{o}C on a Varian system equipped with a Varian 356-LC refractive index detector and a Prostar 210 pump. The columns were STYRAGEL HR1, HR2 (300 × 7.5 mm) from Waters. HPLC grade DMF was used as eluent with 0.01 wt% LiBr at a flow rate of 0.8 mL/min. Polystyrene standards were used for calibration. Atomic force microscopy (AFM) was conducted on a Nanoscope V Multimode instrument, operating under tapping mode. 1.5 weight % solutions of the block copolymers in toluene were spin-coated onto cleaned silicon wafers. X-ray photoelectron spectroscopy (XPS)

measurements were conducted using a Kratos AXIS Ultra DLD XPS system equipped with a monochromatic Al K^+ source. The energy scale of the system was calibrated using Au foil with Au4f scanned for the Al radiation and Cu foil with Cu2p scanned for Mg radiation resulting in a difference of 1081.70 ± 0.025 eV between these two peaks. The binding energy was calibrated using an Ag foil with Ag3d5/2 set at 368.21 ± 0.025 eV for the monochromatic Al X-ray source. The monochromatic Al K^+ source was operated at 15 keV and 120 W. The pass energy was fixed at 40 eV for the detailed scans. A charge neutralizer (CN) was used to compensate for the surface charge. Samples were not conductive and C1s was used as the peak reference. The binding energy (BE eV) was corrected with the C1s (284.6 eV) as standard. X-ray diffraction (XRD) measurements were conducted on a Rigaku D/Max 2100 Powder X-Ray Diffractometer (Cu K^+ radiation) instrument and scanned from 10º to 85º with a step size of 0.005º and a step rate of 6 s.

Synthesis of diblock copolymer Poly(ethylene oxide)-*b*-poly(2-(methacryloyloxy)ethyl ferrocenecarboxylate) (PEO-*b*-PMAEFc-Br). PEO-Br (1.00 g, 0.20 mmol), MAEFc (4.12 g, 12.01 mmol), Cu(I)Br (34.3 mg, 0.23 mmol), bpy (75.0 mg, 0.48 mmol) were added to a to a 50-mL Schlenk flask and degassed by purging with nitrogen. Distilled toluene (20 mL) was added to a 50 mL round bottom flask and degassed by bubbling the solution with nitrogen gas for 30 min. The toluene was then transferred to the schlenk line flask and the mixture was further degassed by nitrogen bubbling for 5 min. The reaction was stirred at room temperature for 15 min before the flask was placed in an oil bath preheated to 90 ^oC. An initial sample was taken in order to accurately determine the reaction conversion by ^1H NMR. Samples were periodically

taken over the course of the polymerization to determine percent conversion by ^{1}H NMR. The polymerization was quenched when it reached 40% conversion by placing the Schlenk flask in an ice bath. The mixture was diluted with THF and passed through a short neutral alumina plug, concentrated, precipitated into diethyl ether three times and vacuum dried at room temperature overnight. The degree of polymerization was determined to be 25 by ^{1}H NMR analysis. MW_{PMAEFc}=8300. $MW_{PEO\text{-}b\text{-}PMAEFc}$=13300. Yield = 2.3 g. ^{1}H NMR (CD_2Cl_2), δ (TMS, ppm): 4.19-4.82 (m, 325 H, C_5H_5-Fe-C_5H_4-C(=O)OCH_2CH_2), 3.63 (s, 452 H, -OCH_2CH_2-), 0.8-2.2 (m, 75 H, -CH_2-C(CH_3)). GPC: Mn = 12600, PDI = 1.17.

Poly(ethylene oxide)-*b*-poly(2-(methacryloyloxy)ethyl ferrocenecarboxylate)-*b*-poly(styrene) (PEO-*b*-PMAEFc-*b*-PS) by ATRP. PEO-*b*-PMAEFc-Br (1 eq.) and Cu(I)Br (0.1 eq) were placed in a 10 mL schlenk line flask and purged with nitrogen for 20 minutes. Styrene (s eq.), PMDETA (1.2 eq), and 2 mL toluene were added to a 5 mL pearl shaped flask and degassed nitrogen bubbling for 20 minutes. The monomer, ligand, and solvent were then transferred to the schlenk line flask and further degassed by nitrogen bubbling for 5 minutes. The reaction was stirred at room temperature for 15 min before the flask was placed in an oil bath preheated to 90 ^{o}C. An initial sample was taken in order to accurately determine the reaction conversion by ^{1}H NMR. Samples were periodically taken over the course of the polymerization to determine percent conversion by ^{1}H NMR. The polymerization was quenched when it reached 80% conversion by placing the Schlenk flask in an ice bath. The mixture was precipitated into methanol three times and vacuum dried at room temperature overnight. The degree of polymerization was determined by ^{1}H NMR analysis. ^{1}H NMR (CD_2Cl_2), δ (TMS, ppm):

6.30-7.20 (m, PS Ph), (4.19-4.82 (m, C_5H_5-Fe-C_5H_4-C(=O)OCH_2CH_2), 3.63 (s, -OCH_2CH_2-), 0.8-2.2 (m, PMAEFc $CH_2C(CH_3)$ and PS CH_2-CH).

Preparation of Thin Films. The triblock copolymers were spin coated from 1.5wt% toluene solution onto silicon wafer substrates. The thin films were then solvent annealed under controlled humidity as reported earlier.[48,49] The films were annealed for 12h under saturated toluene vapor supplied by a neighboring solvent reservoir in a sealed chamber. After the solvent annealing process, selected films were treated by UV/Ozonolysis for 2 h and further pyrolysis at 1200 ºC for 20 min.

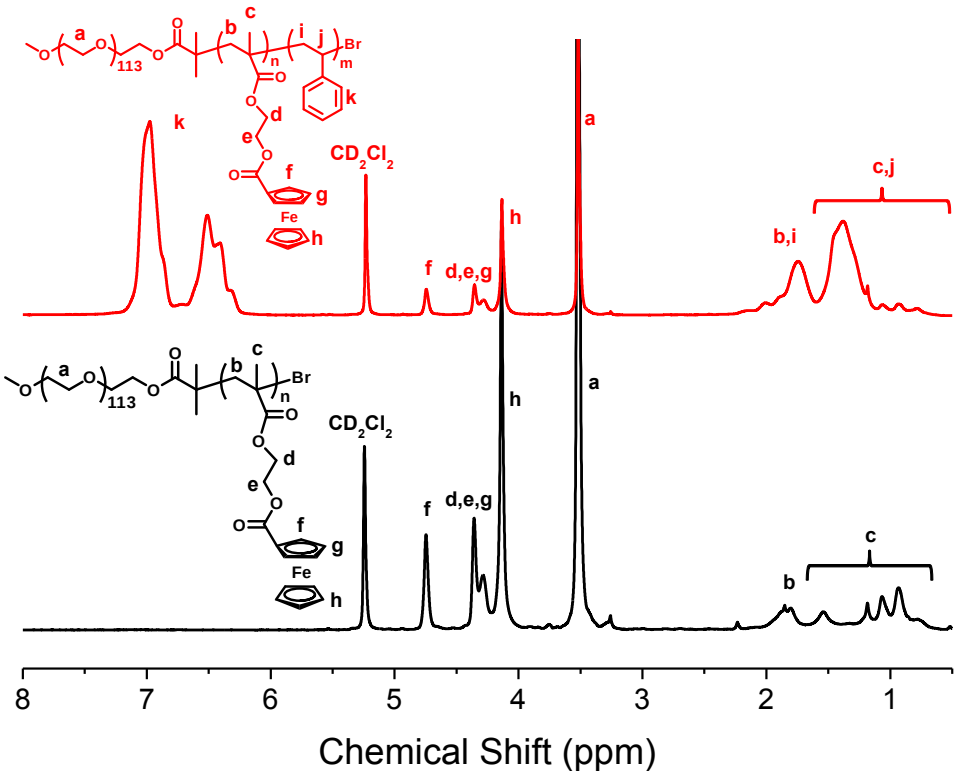

Figure 4.4. ^{1}H NMR spectra for diblock copolymer PEO-*b*-PMAEFc-Br and triblock copolymer PEO-*b*-PMAEFc-*b*-PS.

Table 4.1. Characterization for triblock copolymers **3a-3c**.

Polymer	M_n (PS), g/mol[a]	M_n (total), g/mol[a]	Wt% PS	PDI[b]	Morphology
3a	12100	25400	47.6%	1.42	Disordered
3b	56000	69300	80.8%	1.39	Cylindrical
3c	92600	105900	87.4%	1.59	Disordered

[a]Determined from ^{1}H NMR.
[b]Determined from GPC.

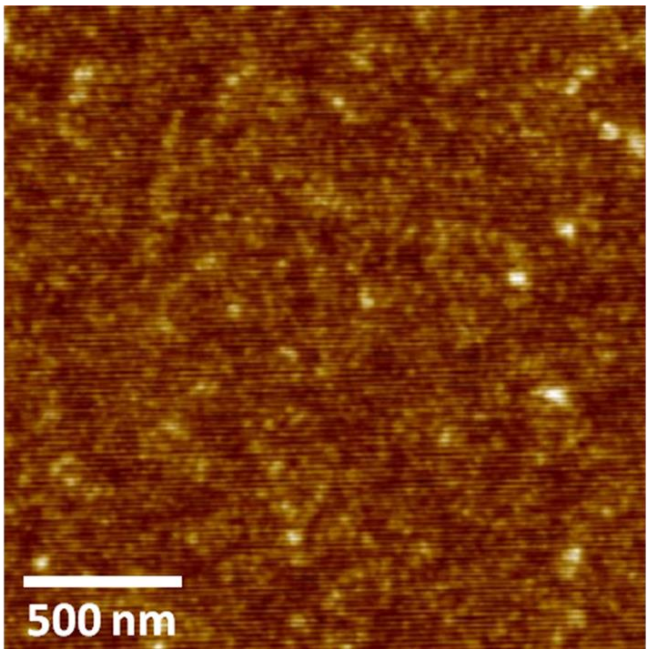

Figure 4.5. AFM image (height) of triblock copolymer **3a**.

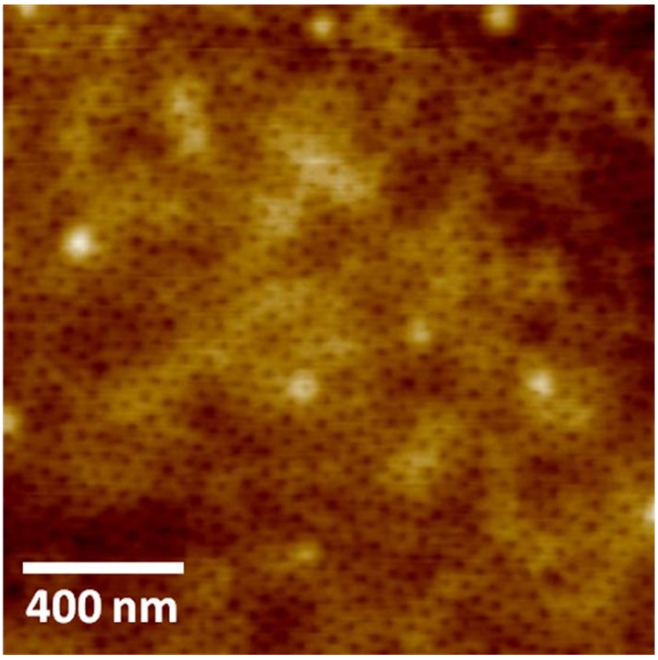

Figure 4.6. AFM image (height) of triblock copolymer **3c**.

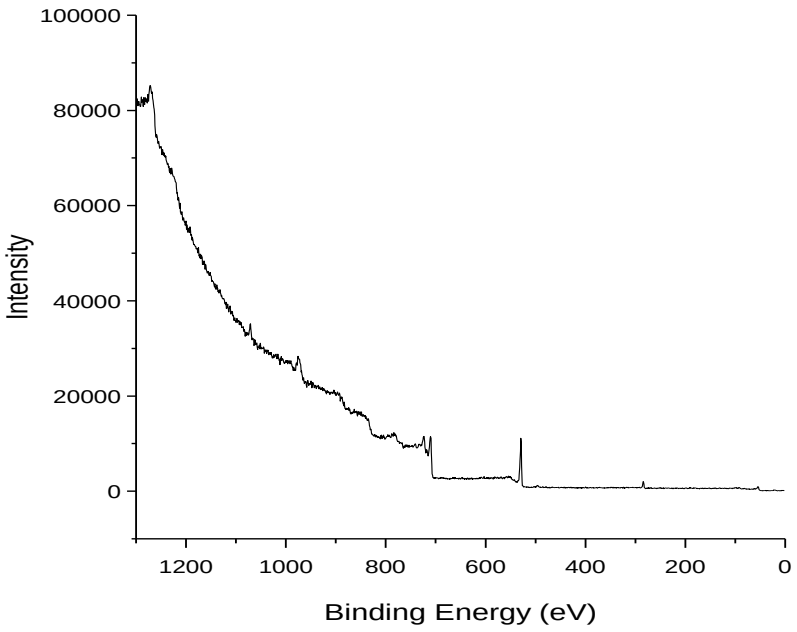

Figure 4.7. XPS spectrum of iron oxide nanoparticles after UV/O and pyrolysis of triblock copolymer PEO-*b*-PMAEFc-*b*-PS (**3b**).

Table 4.2. XRD comparison (peak positions in degree) between our iron oxide nanoparticles and reported α-Fe_2O_3.

Nanoparticles (this work)	α-Fe_2O_3 (reported)[50,51]
24.13	24.138
33.16	33.158
35.62	35.162
39.31	39.27
40.84	40.855
43.51	43.515
49.45	49.48
54.19	54.091
57.58	57.590
62.44	62.451
64.00	63.991

4.5 CONCLUSIONS

In conclusion, well-defined ferrocene-containing triblock copolymers were prepared by sequential ATRP. We utilized solvent annealing with controlled humidity to obtain highly ordered hexagonal arrays of cylinders of block copolymers in thin films, which were furthered used as templates to prepare ordered iron oxide nanoparticles after UV/ozonolyis and pyrolysis. XPS and XRD characterizations indicated the formation of α-Fe_2O_3 nanoparticles. This process should be easily expanded to other metal-containing block copolymers, which is an area of future exploration.

4.6 ACKNOWLEDGEMENTS

This work was supported by the University of South Carolina and Global Research Collaboration Program of Semiconductor Research Corporation (Task ID 2222.001).

4.7 REFERENCES

1. Alivisatos, A. P. *Science* **1996,** 271, 933-937.
2. Cui, Y.; Bjork, M. T.; Liddle, J. A.; Sonnichsen, C.; Boussert, B.; Alivisatos, A. P. *Nano Lett.* **2004,** 4, 1093-1098.
3. Lee, J.-S.; Cho, J.; Lee, C.; Kim, I.; Park, J.; Kim, Y.-M.; Shin, H.; Lee, J.; Caruso, F. *Nat. Nanotechnol.* **2007,** 2, 790-795.
4. Lu, W.; Lieber, C. M. **2007,** 6, 841-850.
5. Ruiz, R.; Kang, H.; Detcheverry, F. A.; Dobisz, E.; Kercher, D. S.; Albrecher, T. R.; de Pable, J. J.; Nealey, P. F. *Science* **2008,** 321, 936-939.
6. Park, M.; Harrison, C.; Chaikin, P. M.; Register, R. A.; Adamson, D. H. *Science* **1997,** 276, 1401-1404.
7. Bita, I.; Yang, J. K. W.; Jung, Y. S.; Ross, C. A.; Thomas, E. L.; Berggren, K. K. *Science* **2008,** 321, 939-943.
8. Tang, C.; Lennon, E. M.; Fredrickson, G. H.; Kramer, E. J.; Hawker, C. J. *Science* **2008,** 322, 429-432.
9. Kim, H.-C.; Park, S.-M.; Hinsberg, W. D. *Chem. Rev.* **2010,** 110, 146-177.
10. Cheng, J. Y.; Ross, C. A.; Smith, H. I.; Thomas, E. L. *Adv. Mater.* **2006,** 18, 2505-2521.
11. Hardy, C. G.; Tang, C. **2012,** 50, DOI: 10.1002/polb.23174.
12. Leibler, L. **1980,** 13, 1602-1617.
13. Bates, F. S.; Fredrickson, G. H. *Annu. Rev. Phys. Chem.* **1990,** 41, 525-557.
14. Bates, F. S.; Fredrickson, G. H. *Phys. Today* **1999,** 52, 32-38.
15. Mansky, P.; Liu, Y.; Huang, E.; Russell, T. P.; Hawker, C. J. *Science* **1997,** 275, 1458-1460.
16. Segalman, R. A.; Yokoyama, H.; Kramer, E. J. *Adv. Mater.* **2001,** 13, 1152-1155.
17. Kim, S. H.; Misner, M. J.; Xu, T.; Kimura, M.; Russell, T. P. *Adv. Mater.* **2004,** 16, 226-231.
18. Tang, C.; Tracz, A.; Kruk, M.; Zhang, R.; Smilgies, D.-M.; Matyjaszewski, K.; Kowalewski, T. *J. Am. Chem. Soc.* **2005,** 127, 6918-6919.
19. Tang, C.; Wu, W.; Smilgies, D.-M.; Matyjaszewski, K.; Kowalewski, T. *J. Am. Chem. Soc.* **2011,** 133, 11802-11809.
20. Kim, S. H.; Misner, M. J.; Russell, T. P. *Adv. Mater.* **2004,** 16, 2119-2123.
21. Gu, X.; Liu, Z.; Gunkel, I.; Chourou, S. T.; Hong, S. W.; Olynick, D. L.; Russell, T. P. **2012**, DOI: 10.1002/adma.201202361.
22. Park, S.; Lee, D. H.; Xu, J.; Kim, B.; Hong, S. W.; Jeong, U.; Xu, T.; Russell, T. P. *Science* **2009,** 323, 1030-1033.

23. Bang, J.; Kim, S. H.; Drockenmuller, E.; Misner, M. J.; Russell, T. P.; Hawker, C. J. *J. Am. Chem. Soc.* **2006,** 128, 7622-7629.
24. Bang, J.; Kim, B. J.; Stein, G. E.; Russell, T. P.; Li, X.; Wang, J.; Kramer, E. J.; Hawker, C. J. **2007,** 40, 7019-7025.
25. Park, S. C.; Jung, H.; Fukukawa, K.-i.; Campos, L. M.; Lee, K.; Shin, K.; Hawker, C. J.; Ha, J. S.; Bang, J. **2008,** 46, 8041-8048.
26. Tang, C.; Bang, J.; E. Stein, G.; Fredrickson, G. H.; Hawker, C. J.; Kramer, E. J.; Sprung, M.; Wang, J. **2008,** 41, 4328-4339.
27. Rao, J.; Paunescu, E.; Mirmohades, M.; Gadwal, I.; Khaydarov, A.; Hawker, C. J.; Bang, J.; Khan, A. *Polym. Chem.* **2012,** 3, 2050-2056.
28. Killops, K. L.; Gupta, N.; Dimitriou, M. D.; Lynd, N. A.; Jung, H.; Tran, H.; Bang, J.; Campos, L. M. **2012,** 1, 758-763.
29. Tang, C.; Hur, S.; Stahl, B. C.; Sivanandan, K.; Dimitriou, M.; Pressly, E.; Fredrickson, G. H.; Kramer, E. J.; Hawker, C. J. *Macromolecules* **2010,** 43, 2880-2889.
30. Tang, C.; Sivanandan, K.; Stahl, B. C.; Fredrickson, G. H.; Kramer, E. J.; Hawker, C. J. *ACS Nano* **2010,** 4, 285-291.
31. Lee, D. H.; Shin, D. O.; Lee, W. J.; Kim, S. O. *Adv. Mater.* **2008,** 20, 2480-2485.
32. Fried, T.; Shemer, G.; Markovich, G. *Adv. Mater.* **2001,** 13, 1158-1161.
33. Manners, I. *Science* **2001,** 294, 1664-1666.
34. Nguyen, P.; GÃ³mez-Elipe, P.; Manners, I. *Chem. Rev.* **1999,** 99, 1515-1548.
35. Kuila, B. K.; Rama, M. S.; Stamm, M. *Adv. Mater.* **2011,** 23, 1797-1800.
36. Shin, D. O.; Lee, D. H.; Moon, H.-S.; Jeong, S.-J.; Kim, J. Y.; Mun, J. H.; Cho, H.; Park, S.; Kim, S. O. *Adv. Funct. Mater.* **2011,** 21, 250-254.
37. Ghoshal, T.; Maity, T.; Godsell, J. F.; Roy, S.; Morris, M. A. *Adv. Mater.* **2012,** 24, 2390-2397.
38. Hardy, C. G.; Ren, L.; Tamboue, T. C.; Tang, C. *J. Polym. Sci. Pol. Chem.* **2011,** 49, 1409-1420.
39. McIntyre, N. S.; Zetaruk, D. G. *Anal. Chem.* **1977,** 49, 1521-1529.
40. Mills, P.; Sullivan, J. L. *J. Phys. D: Appl. Phys.* **1983,** 16, 723-732.
41. Zhang, S.; Wu, W.; Xiao, X.; Zhou, J.; Ren, F.; Jiang, C. *Nanoscale Res. Lett.* **2011,** 6, 89.
42. Bennett, R. D.; Miller, A. C.; Kohen, N. T.; Hammond, P. T.; Irvine, D. J.; Cohen, R. E. *Macromolecules* **2005,** 38, 10728-10735.
43. Hyeon, T.; Lee, S. S.; Park, J.; Chung, Y.; Na, H. B. *J. Am. Chem. Soc.* **2001,** 123, 12798-12801.
44. Yun, S.-H.; Sohn, B.-H.; Jung, J. C.; Zin, W.-C.; Lee, J.-K.; Song, O. *Langmuir* **2005,** 21, 6548-6552.
45. Sohn, B.-H.; Choi, J.-M.; Yoo, S. I.; Yun, S.-H.; Zin, W.-C.; Jung, J. C.; Kanehara, M.; Hirata, T.; Teranishi, T. *J. Am. Chem. Soc.* **2003,** 125, 6368-6369.
46. C. G. Hardy, L. Ren, T. C. Tamboue and C. Tang, *J. Polym. Sci., Part A: Polym. Chem.*, 2011, **49**, 1409-1420.
47. C. Tang, E. M. Lennon, G. H. Fredrickson, E. J. Kramer and C. J. Hawker, *Science*, 2008, **322**, 429-432.
48. C. Tang, J. Bang, G. E. Stein, G. H. Fredrickson, C. J. Hawker, E. J. Kramer, M. Sprung and J. Wang, *Macromolecules*, 2008, **41**, 4328-4339.

49. C. Tang, S.-m. Hur, B. C. Stahl, K.Sivanandan, M.Dimitriou, E. Pressly, G. H. Fredrickson, E. J. Kramer, C. J. Hawker, *Macromolecules*, 2010, **43**, 2880-2889.
50. B. K. Kuila, M. S. Rama and M. Stamm, *Adv. Mater.*, 2011, **23**, 1797-1800.
51. S. Zhang, W. Wu, X. Xiao, J. Zhou, F. Ren and C. Jiang, *Nannoscale Res. Lett.*, 2011, **6**, 89.

CHAPTER 5

OLIGOANILINE-CONTAINING SUPRAMOLECULAR BLOCK COPOLYMER NANODIELECTRIC MATERIALS[†]

[†] Hardy, C. G.; Islam, M. S.; Gonzalez-Delozier, D.; Ploehn, H. J.; Tang, C. *Macromolecular*. *Rapid Communications* **2012**, *33*, 791-797. Reprinted here with permission of publisher.

5.1 ABSTRACT

We report a new generation of nanodielectric energy storage materials based on supramolecular block copolymers. In our approach, highly polarizable, conducting nanodomains are embedded within an insulating matrix through block copolymer microphase separation. An applied electric field leads to electronic polarization of the conducting domains. The high interfacial area of microphase-separated domains amplifies the polarization, leading to high dielectric permittivity. Specifically, reversible addition fragmentation transfer (RAFT) polymerization was used to prepare block copolymers with poly(methyl acrylate) (PMA) as the insulating segment and a strongly acidic dopant moiety, poly-(2-acrylamido-2-methyl-1-propanesulfonic acid) (PAMPSA), as the basis for the conducting segment. The PAMPSA block was complexed with an oligoaniline trimer to form a dopant-conjugated moiety complex that is electronically conductive after oxidation. For the undoped neat block copolymers, the increase of the PMA block length leads to a transition in dielectric properties from ionic conductor to dielectric capacitor with polarization resulting from migration of protons within the isolated PAMPSA domains. The oligoaniline-doped copolymers show remarkably different dielectric properties. At frequencies above 200 kHz, they exhibit characteristics of dielectric capacitors with much higher permittivity and lower dielectric loss than the corresponding undoped copolymers.

5.1 INTRODUCTION

High performance dielectric materials have attracted tremendous attention due to their applications throughout such industries as telecommunications, computing, test and measurement, defense, and aerospace.[1-4] In particular, there is much demand for the

development of pulse power, which requires accumulating much energy over a relatively long period of time and releasing it very quickly thus increasing the available instantaneous power.[5, 6] Many of these applications require the use of large capacitors with high energy density and low dissipation. High energy density dielectric capacitors would help to reduce the volume, weight, and cost of the electric power system. To achieve this, Equation (**1**) indicates that both high permittivity (ε_r) and high dielectric breakdown field strength (V_{bd}) are extremely important to volumetric energy density $\boldsymbol{U_{max}}$ (ε_0 is the permittivity of vacuum).[3]

$$U_{max} = 0.5\varepsilon_0 \varepsilon_r V_{bd}^2 \qquad (1)$$

Traditionally, ceramic capacitors are used for pulse power applications due to their thermal stability and high dielectric constant of ceramic materials such as barium titanate, lead magnesium niobate and lead titanate.[7, 8] However, due to low dielectric breakdown field strength, these materials usually exhibit low energy density. An alternative is the use of polymer materials since many polymers used in dielectric capacitors have high dielectric breakdown field strength (e.g. BOPP with V_{bd} = 700 MV/m).[9, 10] However, most of these polymers have low dielectric constant (ε_r = 2-5). Poly(vinylidene fluoride) (PVDF) and its random copolymers are more attractive materials due to their higher dielectric constant (ε_r = 10–20) and high breakdown strength.[7, 11-18] However, high dielectric loss limits their use in high rate, high performance charge/discharge applications. On the other hand, with constant dielectric plasmon energy ($\hbar\varpi_p$, dictated by number of effective valence electrons, which is nearly constant), any increase of permittivity would reduce polymer bandgap (E_g) (Equation

(**2**)), which increases free charge carrier concentration and eventually induces current leakage and dielectric loss.

$$\varepsilon_r = [1 + (\hbar \varpi_p / E_g)^2] / \varepsilon_0 \qquad (2)$$

An intuitive strategy is to mix both ceramic and polymeric materials as heterogeneous composites.[19-27] However, poor compatibility between the organic polymer matrix and inorganic fillers leads to aggregation and defects, ultimately resulting in leakage and high dielectric loss.[28] Compared with organic-inorganic composites, all-organic dielectric composite materials have advantages of facile processability, light weight and probably low cost. Common all-organic composite approaches involve the use of high dielectric constant organic particulates embedded in a polymer matrix.[29-35] Similar to the organic-inorganic composite approach, a potential problem facing simple blends of organic particulates and polymer matrix is the tendency of undesirable macrophase separation.

π-conjugated macromolecules including oligoaniline (OANI)[36-39] and polyaniline (PANI)[30-32, 35] have previously been used as conductive fillers in polymers.[29, 33, 34, 40, 41] Conducting PANI particles have been used as high dielectric constant fillers to prepare all-organic dielectric composites.[30, 31] The PANI particles can be physically dispersed in a matrix polymer, which shows an impressive increase in dielectric constant. However, PANI particulates have low solubility and a highly brittle nature, resulting in poor compatibility with the polymer matrix. Recently, oligomer aniline (or oligoaniline, OANI) has been grafted onto chain ends of a polymer.[42] This approach showed a large enhancement in the dielectric constants. However, because the OANI was confined at the polymer chain ends, there was limited control over the compositions of the polymers.

Scheme 5.1. Nanodielectric materials using microphase-separated block copolymers consisting of an insulating poly(methyl acrylate) matrix, and dispersed and conductive domains formed via ionic interactions between poly(2-acrylamido-2-methyl-1-propanesulfonic acid) segment and oligoaniline.

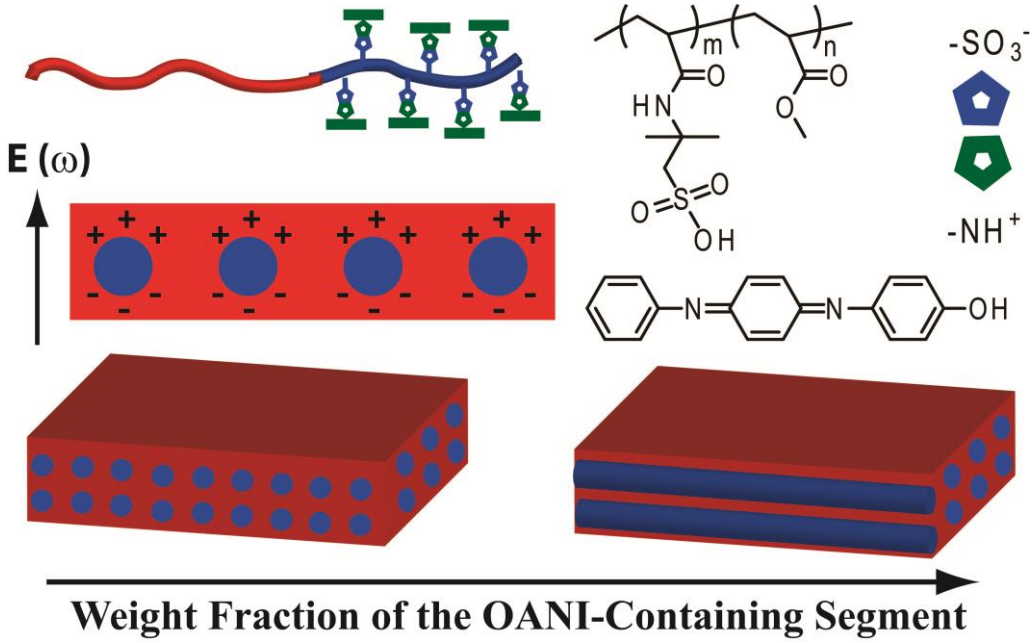

The goal of this work is the design of microphase-separated block copolymers that store energy via electronic conduction and interfacial polarization. These materials are constructed by spontaneous microphase separation that forms dispersed and conductive nanoscale domains embedded in an insulating polymeric matrix. These all-organic nanostructures are expected to achieve full interfacial compatibility and high interfacial areas. One block (blue) forms nanodomains with high electronic conductivity, while the other block (red) insulates the conductive domains to prevent percolation and to minimize inter-domain conduction (Scheme 5.1). Under an external electric field, electronic conduction will induce "nanodipoles" along the phase boundary due to space charge accumulation at the domain interfaces. The nanoscale size of phase-separated domains greatly amplifies the interfacial area per unit volume, resulting in dielectric

materials with energy storage dominated by internal interfacial polarization. Dielectric properties can be tailored by manipulation of chemical structures and molecular compositions of block copolymers.

Herein we report our initial findings on the preparation and characterization of the first nanodielectric materials based on oligoaniline-containing supramolecular block copolymers. Because of the high conductivity of aniline segments along with the ease in processability and tunability of block copolymers, we prepared block copolymers with a highly insulating segment (poly(methyl acrylate)) and a segment containing a strongly acidic dopant moiety (poly-(2-acrylamido-2-methyl-1-propanesulfonic acid) (PAMPSA)) that actively interacts with OANI, forming a dopant-conjugated moiety complex. The OANI-containing block copolymers are expected to produce phase-separated microdomains, in which highly polarizable and conductive OANI-containing domains are dispersed in an insulating PMA matrix.

5.3 Results and Discussion

As shown in Scheme 5.2, block copolymers poly(2-acrylamido-2-methylpropanesulfonic acid)-*b*-poly(methyl acrylate) (PAMPSA-*b*-PMA) were synthesized by reversible addition fragmentation transfer (RAFT) polymerization using cumyl dithiobenzoate (CDB) as the transfer agent.[43, 44] Briefly, PAMPSA was synthesized by reacting AMPSA, CDB and azobisisobutyronitrile (AIBN) in methanol at 65 ^{o}C. The obtained PAMPSA (**1**) was then used as a macroinitiator to chain-extend with methyl acrylate in the presence of AIBN and methanol at 65 ^{o}C. The same PAMPSA macroinitiator was used to prepare a series of diblock copolymers PAMPSA-*b*-PMA (**2-4**), in which the molecular weight of the PMA block was varied in order to target various

morphologies. Spherical and cylindrical morphologies were of particular interest, as the OANI-containing nanodomains would be well isolated from each other in order to prevent the formation of a conductive percolation pathway.

Figure 5.1A shows the proton NMR spectrum of homopolymer **1**. The degree of polymerization (DP) of homopolymer **1** was calculated from the ^{1}H NMR end group analysis by comparing the integration between the phenyl end group (7.1-7.6 ppm) and the -C*H*- group from the polymer backbone (1.6-2.1 ppm) of PAMPSA. The block lengths of diblock copolymers **2-4** were determined by comparing the integration values from the -C*H*- of the polymer backbone (2.4-2.6 ppm) with the backbone -CH_2- and methyl protons from PMA (1.4-2.1 ppm) after chain extension with methyl acrylate (Figure 5.1B). As shown in Figure 5.1C, Gel Permeation Chromatography (GPC) traces of polymers **1-4** showed clear shift from macroinitiators to block copolymers. Monomodal traces indicated that all macroinitiators participated in the chain extension reaction. Characterization results for polymers **1-4** are listed in Table 5.1. The thermal properties of polymers **1-4** were characterized using Differential Scanning Calorimetry (DSC) and Thermogravimetric Analysis (TGA). Homopolymer 1 showed a glass transition temperature (T_g) at 92 ^{o}C. Block copolymers **2-4** showed two T_gs at 92 ^{o}C and between -20-5 ^{o}C, corresponding to PAMPSA and PMA, respectively (Figure 5.5). TGA studies showed that all polymers were stable up to 150 ^{o}C (with 5% weight loss, Figure 5.6).

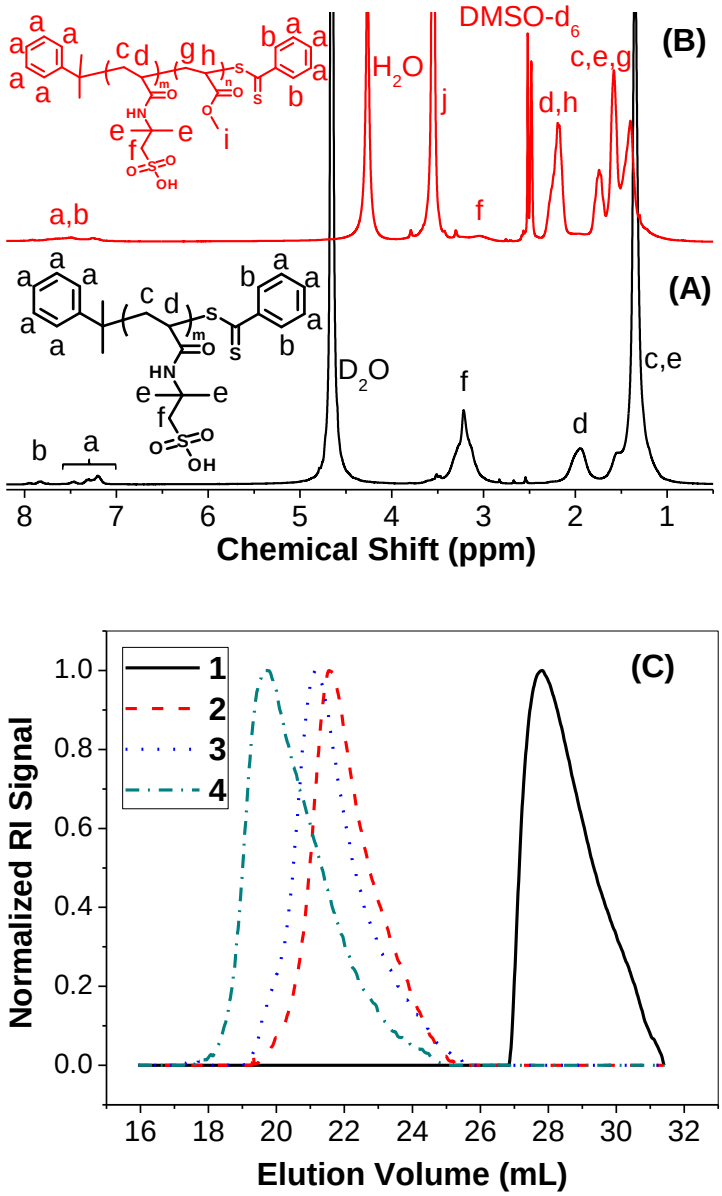

Figure 5.1. (A) and (B) ^{1}H NMR spectra of homopolymer PAMPSA (**1**) in D_2O and diblock copolymer PAMPSA-*b*-PMA (**2**) in DMSO-d_6; and (C) GPC traces of polymers **1**-**4**.

Table 5.1. Characterization of polymers **1**-**4**.

Polymer	DP_{PAMPSA} (NMR)	DP_{PMA} (NMR)	M_n (g/mol, NMR)	wt% PMA	PDI (GPC)
1	48	-	9900	-	1.18
2	48	392	43600	77.24	1.21
3	48	785	77400	87.17	1.30
4	48	1927	175600	94.34	1.42

A hydroxy-terminated oligoaniline trimer (OANI-OH) was prepared by reacting *N*-phenyl-*p*-phenylenediamine with hydroquinone in the presence of zinc chloride at 180 ^{o}C followed by refluxing in HCl solution. The resulting mixture was filtered and the solids were stirred in a 1M NH_4OH solution with hydrazine hydrate to reduce any oxidized imine nitrogen atoms to the amine state (^{1}H and ^{13}C NMR, Figures 5.7 and 5.8). The oxidation states of OANI-OH were investigated by UV-vis spectroscopy. In the fully reduced state, only one absorption peak around 310 nm was observed. This peak has been attributed to the π- π* transition of the benzenoid ring. As a model study, OANI-OH in *N, N'*-dimethylformamide (DMF) was oxidized by addition of ammonium persulfate in 1 M HCl. As the oxidation takes place, two peaks appear at 397 nm and 572 nm. The peak at 572 nm is attributed to charge transfer from the benzenoid ring to the quinoid ring (Scheme 5.3).[45-49] Upon further oxidation, the intensity of these two peaks increase while the π- π* transition peak decreases in intensity and shifts from 310 nm to 301 nm. The final oxidative state of OANI-OH as prepared by ammonium persulfate in 1 M HCl is shown in Figure 5.2A.

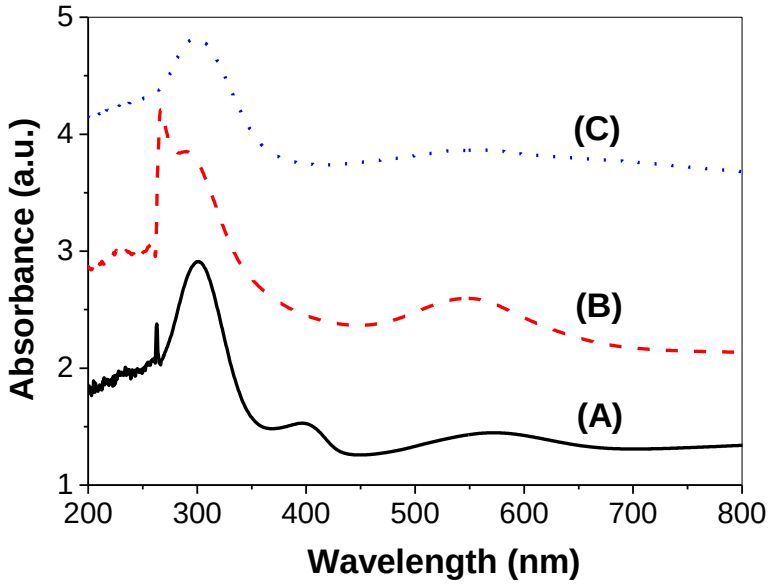

Figure 5.2. UV/Vis spectra of OANI-OH oxidized by: (A) $(NH_4)_2S_2O_8$ in 1 M HCl; (B) $(NH_4)_2S_2O_8$ in AMPSA; and (C) $(NH_4)_2S_2O_8$ in block copolymer.

OANI-OH oxidation was then performed by addition of ammonium persulfate in the presence of 1 eq. 2-acrylamido-2-methylpropanesulfonic acid (AMPSA). The oxidation showed a transition of the π- π* transition peak of the benzenoid ring from 310 nm to a less intense peak around 298 nm. Also, the appearance of a peak around 555 nm was observed (Figure 5.2B). It has been previously shown that PANI in the emeraldine state can complex with side-chain PAMPSA by electrostatic interactions between the imine groups from the PANI and the sulfonic acid groups of the PAMPSA.[43, 44] In order to complex polymers **2**-**4** with OANI-OH, the polymers were first dissolved in DMF before OANI-OH (1 eq. per SO_3H unit) was added. Once the polymer and OANI-OH were dissolved, ammonium persulfate was added in order to oxidize the OANI. The solutions were stirred at 70 ^oC for 48 hours. UV-Vis spectra of the oxidation of OANI-OH in the presence of polymer **2** are shown in Figure 5.2C. It should be noted that the π-

π* peak transitioned from 310 to 300 nm and there was appearance of a peak around 560 nm, indicating complexation of the OANI-OH to the side-chain sulfonic acid moiety. Finally, the solutions were dialyzed against deionized H_2O in order to remove any residual salts. Complete UV-Vis spectra of polymers **2**-**4** before and after dialysis against water are shown in the supporting information (Figures 5.9). It should be noted that the peaks at 300 and 560 nm remain after dialysis, indicating that the OANI complexation with the side-chain sulfonic acid moiety was preserved after the removal of salts.

The dielectric properties of the undoped PAMPSA-*b*-PMA block copolymers as well as the copolymers doped with OANI and oxidized with ammonium persulfate were characterized. Figure 5.3A shows the relative permittivity for undoped block copolymers **2**-**4** with different PMA block length. Undoped copolymer **2** (containing 23 wt% PAMPSA) has a high relative permittivity at low frequencies, but the permittivity decreases considerably with increasing frequency. The shape of the permittivity curve for copolymer **2**, specifically the significant polarization relaxation (permittivity decrease) at intermediate frequencies, suggests Maxwell-Wagner interfacial polarization associated with buildup of space charge at domain boundaries.[40] The high polarization at low frequencies results from the high concentration of sulfonic acid protons from the PAMPSA block which migrate and accumulate at internal domain boundaries. Higher frequencies permit less migration and thus result in lower polarization. Copolymers **3** and **4** show qualitatively different behavior, as relative permittivity values are much lower than that of copolymer **2**, and nearly independent of frequency below 200 kHz (copolymer **3**) and 10 MHz (copolymer **4**). Clearly, the permittivity values decrease with the decrease of PAMPSA wt% due to the reduced number of protons available for

polarization. The difference in the frequency dependence, however, could be due to a difference in copolymer domain structure and morphology. If the PAMPSA domains in copolymers **3** and **4** are smaller and more isolated (most likely spherical morphology), then one might expect polarization to be saturated across a wide frequency range as seen in Figure 5.3A. With the decrease of domain size (from copolymer **3** to **4**, or from 13 to 6 wt% PAMPSA), relaxation of interfacial polarization would be expected to move to higher frequency.

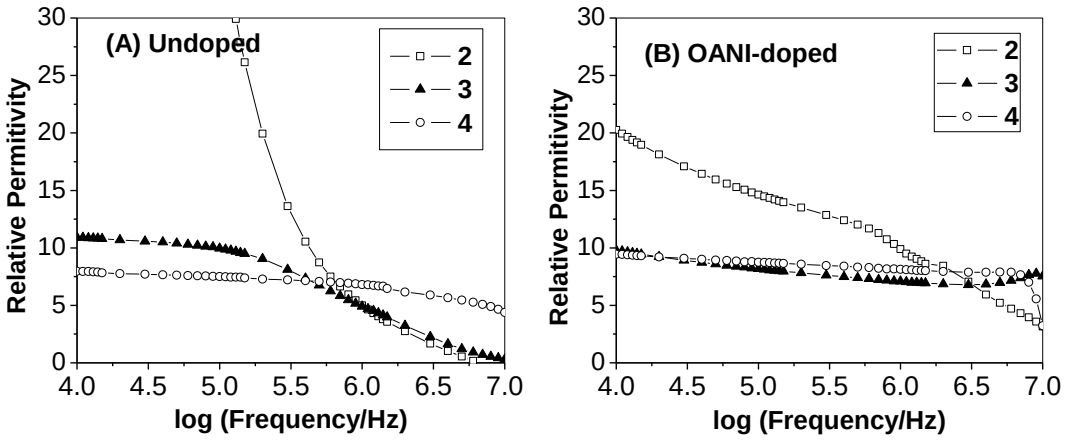

Figure 5.3. Relative permittivity versus frequency for (A) undoped PAMPSA-*b*-PMA block copolymers and (B) OANI-doped PAMPSA-*b*-PMA block copolymers after the removal of salts.

Figure 5.3B shows the relative permittivity of copolymers **2**-**4** doped with OANI, oxidized with ammonium persulfate and then dialyzed to remove salts. Copolymer **2** shows the greatest impact of OANI doping due to its high PAMPSA content (23 wt%). At frequencies below 200 kHz, doped copolymer **2** has much lower relative permittivity than undoped copolymer **2**, likely due to the absence of sulfonic acid protons in the former. Below 200 kHz, doping decreases the permittivity of copolymer **3** by 10-20% compared to the undoped state, but it increases the permittivity of copolymer **4** by 10-

20%. These subtle changes probably result from a combination of different factors (sulfonic acid protons, conjugation, etc.). At frequencies greater than 500 kHz, the doped form of copolymers **2**-**4** all have significantly higher permittivity values than the corresponding undoped polymers. The change is greatest for copolymer **3** which has a PAMPSA-OANI content (13 wt% PAMPSA) between those of copolymers **2** and **4**. This suggests that the OANI-doped PAMPSA domains are primarily responsible for the higher permittivity values at high frequencies. We believe this confirms the synthesis of all-organic nanodielectric materials based on electronically-conducting microdomains.

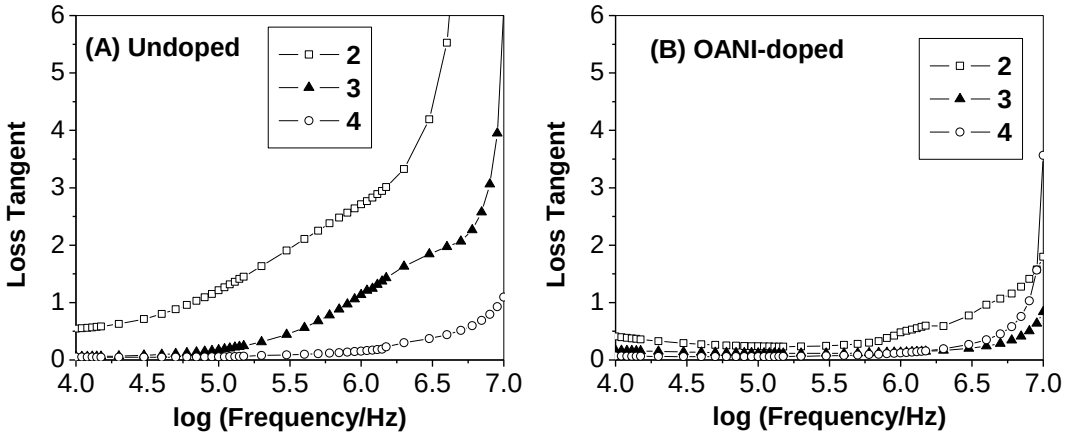

Figure 5.4. Loss tangent (dielectric loss) versus frequency for (A) undoped PAMPSA-*b*-PMA block copolymers and (B) OANI-doped PAMPSA-*b*-PMA block copolymers after the removal of salts.

As shown in Figure 5.4A, the loss tangents of undoped PAMPSA-*b*-PMA block copolymers **2**-**4** increase significantly as the PMA block length decreases (PAMPSA wt% increases). For copolymer **2**, the loss tangent is above 0.5 at all frequencies and rises sharply above 100 kHz, indicating that this material behaves more like a conductor than a capacitor. This is seen more clearly in Figure 5.11A showing the specific conductivities of these materials. In contrast, copolymers **3** and **4** have loss tangents below 0.2 up to

about 100 kHz and 1.5 MHz, respectively. These materials behave more like capacitors at low frequencies, although the polarization produced by ionic migration results in significant dielectric loss. Dielectric losses at high frequencies may be due to molecular relaxation processes activated by the applied field interacting with the PAMPSA anion. This hypothesis is supported by the observation that loss tangent increases sharply with PAMPSA wt% at frequencies above 100 kHz.

The dielectric loss shows much different behavior for the OANI-doped copolymers (Figure 5.4B). The loss tangent of doped copolymer **2** is much less than that of the undoped material at all frequencies. Likewise, for frequencies greater than 100 kHz, doped copolymer **3** also shows a dramatic decrease in loss tangent compared to undoped copolymer **3**. Unlike the undoped materials, the doped copolymers **2** and **3** behave like capacitors at frequencies up to more than 1 Mz. These results are likely explained by the absence of sulfonic acid protons in the doped materials. Additional corroboration can be found in the specific conductivity data for the doped copolymers (Figure 5.11B). OANI doping significantly reduces the conductivities of copolymers **2** and **3** compared to the respective undoped materials for frequencies greater than 100 kHz. On the other hand, Figure 5.4B shows negligible difference in the loss tangents for undoped and doped copolymers **4**, probably due to very low content of PAMPSA (and OANI) (6 wt% PAMPSA). Overall, the significant change in permittivity and loss tangent between undoped and doped copolymers **2** and **3** suggests that the presence of isolated, conjugated domains in the OANI-doped copolymers leads to different polarization and loss mechanisms that dominate at high frequencies.

It should be worthy to note that without the dialysis to remove ammonium persulfate salts, the dielectric properties of doped block copolymers exhibit contribution from the salts. Compared to doped block copolymers without salts, the existence of salts results in significant increase of both relative permittivity and loss tangent, particularly at lower frequencies (Figure 5.10). This suggests that low frequency polarization in the OANI-doped materials might be due to ionic migration of the persulfate salt with charge accumulation at domain boundaries.

5.4 EXPERIMENTAL

Materials. All reagents were purchased from Alfa Aesar and Aldrich and used as received unless otherwise noted. Methyl acrylate was distilled before use. Hydroquinone was recrystallized from toluene before use. Cumyl dithiobenzoate was prepared according to the literature.[50,51]

Characterization. ^{1}H NMR (300 MHz) and ^{13}C NMR (100 MHz) spectra were recorded on a Varian Mercury 300 spectrometer with tetramethylsilane (TMS) as an internal reference. GPC was performed at 50^{o}C on a Varian system equipped with a Varian 356-LC refractive index detector and a Prostar 210 pump. The columns were STYRAGEL HR1, HR2 (300 × 7.5 mm) from Waters. HPLC grade DMF was used as eluent with 0.01 wt% LiBr at a flow rate of 0.8 mL/min. Polystyrene standards were used for calibration. Mass spectrometry was conducted on a Waters Micromass Q-Tof mass spectrometer, and the ionization source was positive ion electrospray. UV-vis was carried out on a Shimadzu UV-2450 spectrophotometer with a 10.00-mm quartz cuvette using dimethylformamide (DMF) as solvent and monochromatic light of various wavelengths over a range of 190-900 nm. FTIR spectra were recorded on a PerkinElmer

Spectrum 100 FTIR spectrometer equipped with a Universal ATR sampling accessory. Thermal transitions of the polymers were recorded using DSC on a TA Instruments Q2000 in a temperature range from -70 to 150 ^{o}C at heating and cooling rates of 10 ^{o}C/min under constant nitrogen flow at a rate of 50 mL/min. Samples (between 3-8 mg) were added to aluminum hermetic pans and sealed. The data were collected on the second heating run. TGA was conducted on a TA Instruments Q5000 using a heating rate of 10 ^{o}C/min from 40 to 1000 ^{o}C under constant nitrogen flow.

Dielectric Properties. Polymer samples were dissolved in dimethylformamide (DMF) at concentrations of 0.168 g/mL (undoped copolymers) or 0.034 g/mL (doped, washed copolymers) and poured into aluminum pans. The solvent was removed by evaporation at 70°C under reduced pressure (125 mm Hg absolute) for 24 h. This temperature and pressure accelerated the evaporation of DMF (153°C normal boiling point) without producing solvent bubbles. After solvent evaporation, all films were annealed at 120°C in air for 24 h and then cooled for another 24 h. For copolymers **2-4** listed in Table 5.1, these procedures resulted in films with uniform thickness and free of bubbles, cracks, or other defects. Film thicknesses were measured at multiple positions with a micrometer; measured thicknesses ranged from 4 to 30 μm.

Strips of aluminum pan bearing copolymer films were cut using scissors; the aluminum pan served as the bottom electrode for dielectric measurements. Circular gold electrodes (area 1.13 cm^2) were deposited on the films' top surface by sputter coating in an argon atmosphere through a shadow mask.

The films' complex impedance was measured at varying frequency (typically 10^2 to 1.2×10^7 Hz) using an impedance analyzer (Agilent model 4192A LF).[52-54]

Measurements were carried out on 3-5 specimens of each sample to ensure reproducibility. For measurements in "impedance" mode, the data were interpreted using a parallel RC circuit model expected to describe a "leaky" capacitor.[55] Specifically, measured values of impedance magnitude $|Z|$ and phase angle θ lead to the real and complex parts of the relative permittivity given by[56]

$$\varepsilon_r' = \frac{-\sin(\theta)}{2\pi f C_0 |Z|} \qquad \text{and} \qquad \varepsilon_r'' = \frac{\cos(\theta)}{2\pi f C_0 |Z|}$$

where f is frequency in Hz, $C_0 = \varepsilon_0 A/t$, and A and t are the film area and thickness. The loss tangent [tan(δ), also called the dielectric loss], is defined as

$$\tan\delta = \frac{\varepsilon_r''}{\varepsilon_r'} = \cot\theta$$

The impedance analyzer was also used in "conductivity" mode to directly measure conductivity, which was multiplied by A/t to give specific conductivity values.

Synthesis of Block Copolymer PAMPSA-*b*-PMA. Cumyl dithiobenzoate (0.33 g, 1.21 mmol), 2-acrylamido-2-methylpropanesulfonic acid (25.00 g, 120.77 mmol), AIBN (0.02 g, 0.12 mmol), and 50 mL dry methanol were added to a 100 mL schlenk line flask and degassed by 5 cycles of freeze-pump-thaw. An initial sample was taken before the flask was submerged in a 65°C oil bath. Samples were periodically taken to monitor conversion by ^{1}H NMR. When conversion reached ~50%, the reaction flask was cooled by liquid nitrogen and diluted with methanol. The solution was dialyzed against methanol to remove any unreacted monomer. Homopolymer **1** was collected and vacuum dried, resulting in a pink powder. The degree of polymerization was determined using ^{1}H NMR by comparing the phenyl groups of the RAFT end group with the -C*H*- signal from the polymer backbone (1.6-2.1 ppm) (DP = 48, MW = 9936). To prepare

block copolymers **2-4**, homopolymer **1** was used as a macroinitiator. In a typical chain extension, PAMPSA, methyl acrylate, AIBN, dry methanol, and distilled anisole were added to a schlenk line flask and degassed by 5 cycles of freeze-pump-thaw. An initial sample was taken for ^{1}H NMR before adding the schlenk line flask to a 65^{o}C oil bath. The chain extension was monitored by ^{1}H NMR and the reactions were quenched when the target percent conversion was reached by cooling in liquid nitrogen. The reaction solutions were precipitated into diethyl ether and vacuum dried at room temperature. The degree of polymerization of the PMA block was calculated from ^{1}H NMR by comparing the integration of the -C*H*- of the polymer backbone (2.4-2.6 ppm) with the backbone -CH_2- and methyl protons from PMA (1.4-2.1 ppm) after chain extension with methyl acrylate with the known integration values for the homopolymer. ^{1}H NMR (**1**, D_2O, δ): 7.1-7.8 (m, Ph from RAFT end group), 2.9-3.1 (s, C$H_2$$SO_3$H), 1.6-2.1 (s, CH_2C*H*), 0.9-1.6 (m, CH_2CH). ^{1}H NMR (**2-4**, DMSO-d_6, δ): 7.1-7.8 (m, Ph from RAFT end group), 2.9-3.1 (s, C$H_2$$SO_3$H), 2.0-2.4 (m, CH_2C*H*), 1.0-1.8 (m, CH_2CH, -OCH_3).

Synthesis of Hydroxy-Terminated Oligoaniline Trimer (OANI-OH). *N*-phenyl-*p*-phenylenediamine (50.00 g), hydroquinone (57.00 g), and zinc chloride (7.40 g) were added to a 500 mL reaction vessel equipped with a mechanical stirrer and condenser. The reaction vessel was purged with nitrogen and heated to 180^{o}C and stirred for 5 hours. The reaction vessel was cooled to 60^{o}C before 1M HCl (300 mL) was added. The reaction was then heated and allowed to reflux for 3 hours. The suspension was then filtered and washed with deionized water. The solids were collected and stirred in a solution of hydrazine hydrate in 1M ammonium hydroxide for 15 hours. The mixture was filtered and washed with deionized water. The solids were collected and

recrystallized from toluene 3-5 times. The product was collected, vacuum dried, and analyzed by ^{1}H NMR (Figure 5.7), ^{13}C NMR (Figure 5.8), FT-IR, UV-Vis, and mass spectometry. ^{1}H NMR (**1**, DMSO-d_6, δ): 8.91 (s, 1H, -O*H*), 7.65 (s, 1H, -N*H*-), 7.48 (s, 1H, -N*H*-), 6.5-7.3 (m, 13H, Ph). ^{13}C NMR (DMSO-d_6, δ): 151.65, 146.10, 140.18, 136.19, 134.65, 129.49, 121.41, 120.10, 118.14, 116.91, 116.14, 114.79. FTIR (cm^{-1}): 3367, 3024, 1600, 1509, 1451, 1300, 1219, 819. MS (EI), m/z calcd for $C_{18}H_{16}N_2O$: 276.16; found: 276.

Scheme 5.2. Synthesis of block copolymer poly(2-acrylamido-2-methyl-1-propanesulfonic acid)-*b*-poly(methyl acrylate) by reversible addition fragmentation transfer (RAFT) polymerization.

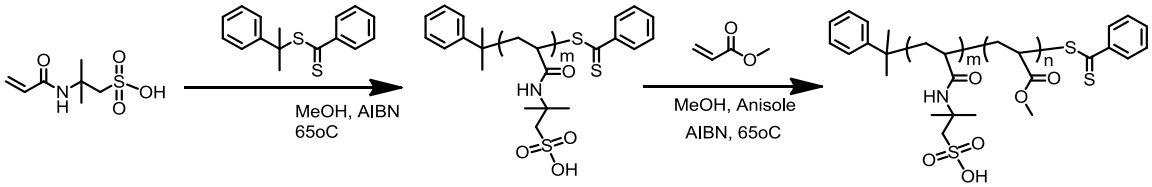

Scheme 5.3. Possible oxidation states of OANI-OH

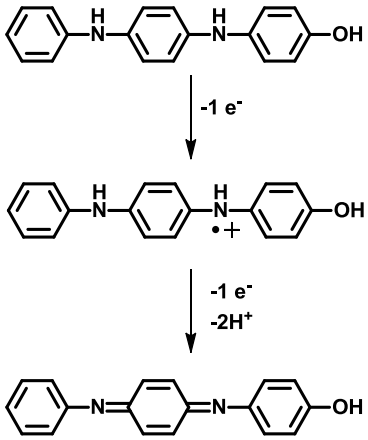

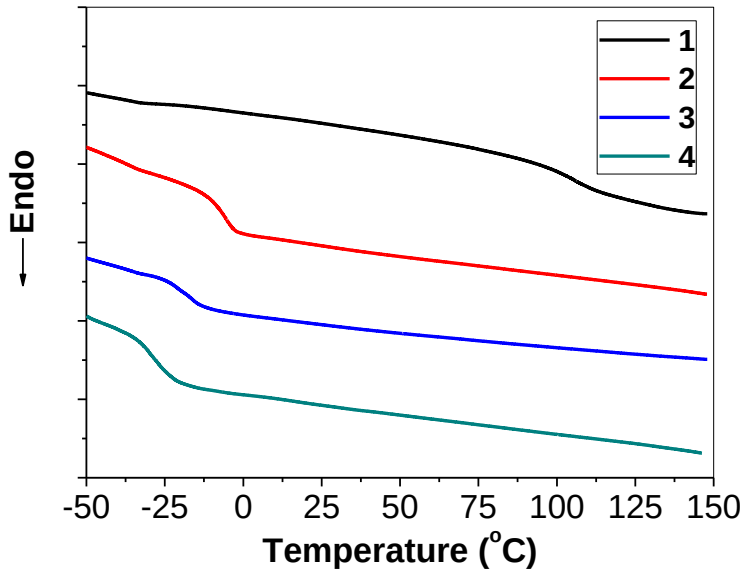

Figure 5.5. DSC overlay of polymers **1**-**4**.

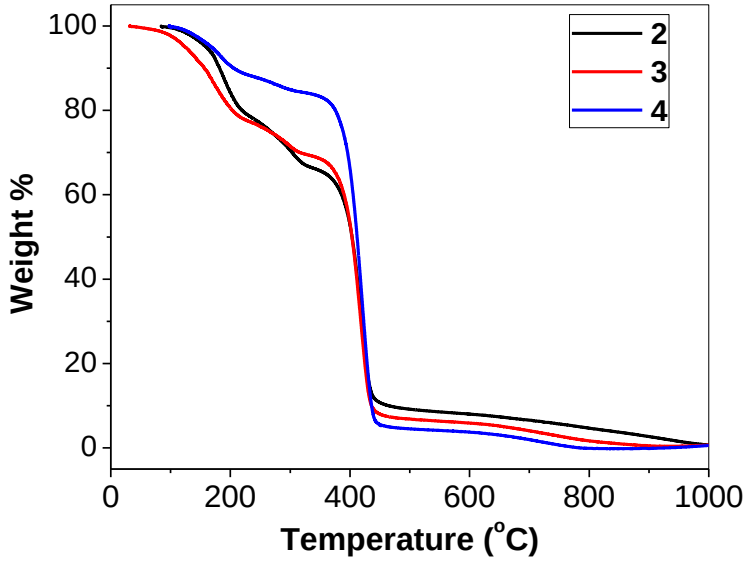

Figure 5.6. TGA overlay of polymers **2**-**4**.

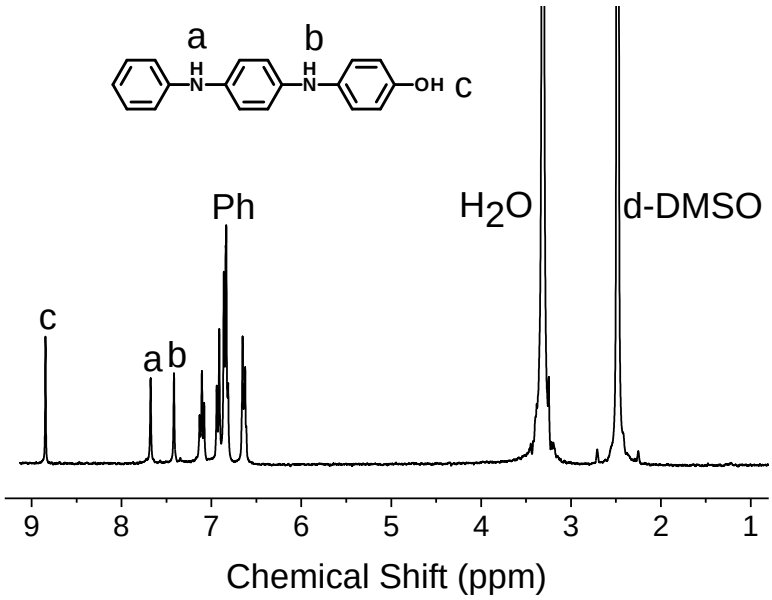

Figure 5.7. ^{1}H NMR spectrum of OANI-OH in DMSO-d_6.

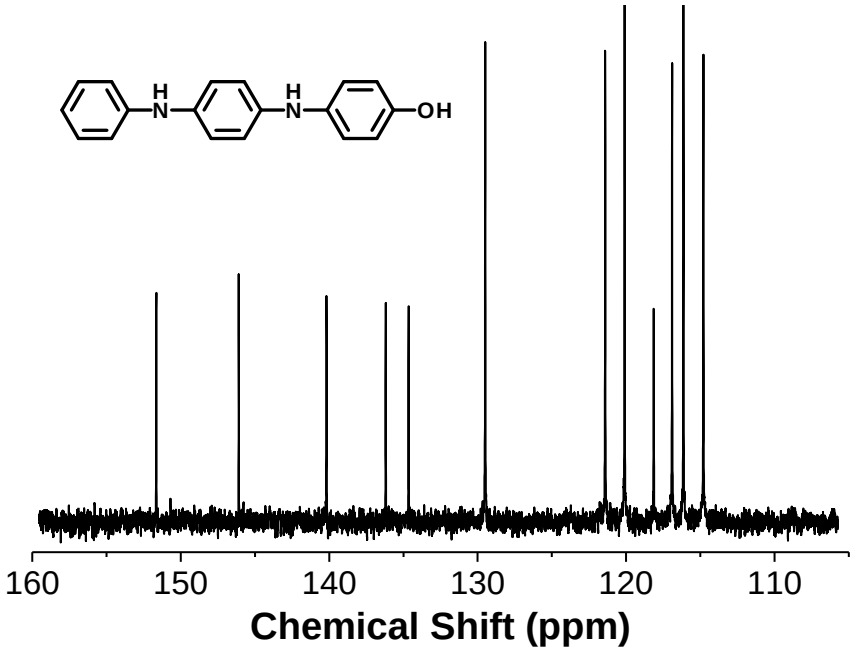

Figure 5.8. ^{13}C NMR spectrum of OANI-OH in DMSO-d_6.

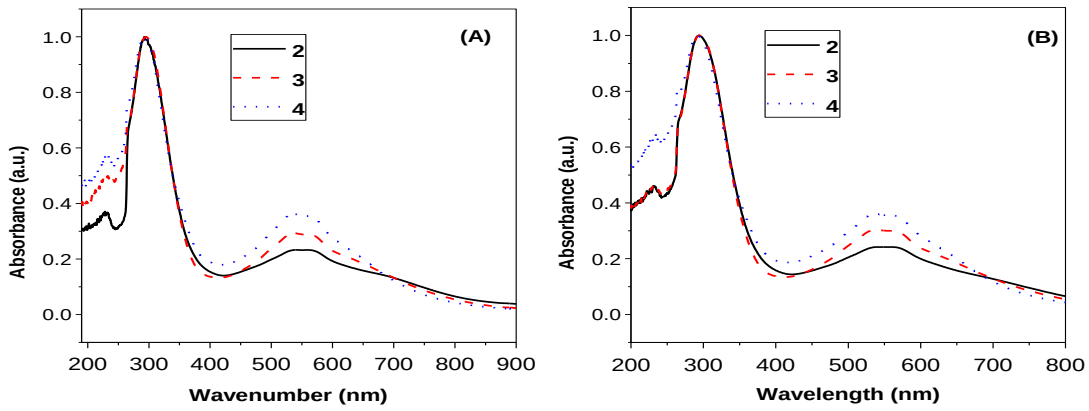

Figure 5.9. UV/Vis spectra of OANI-containing block copolymers: (A) before washing away ammonium persulfate salts; (B) after washing away ammonium persulfate salts.

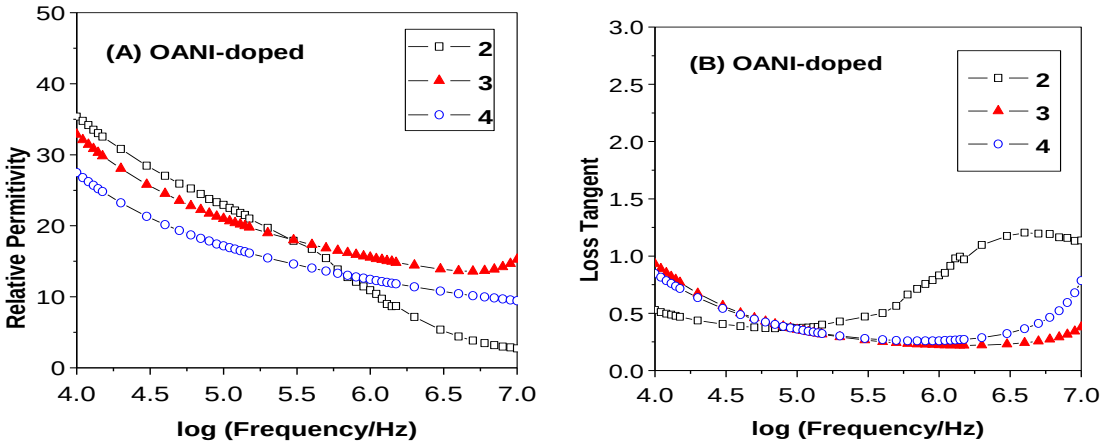

Figure 5.10. (A) Relative permittivity versus frequency; and (B) Loss tangent (dielectric loss) versus frequency for OANI-doped PAMPSA-*b*-PMA block copolymers without washing away ammonium persulfate salts.

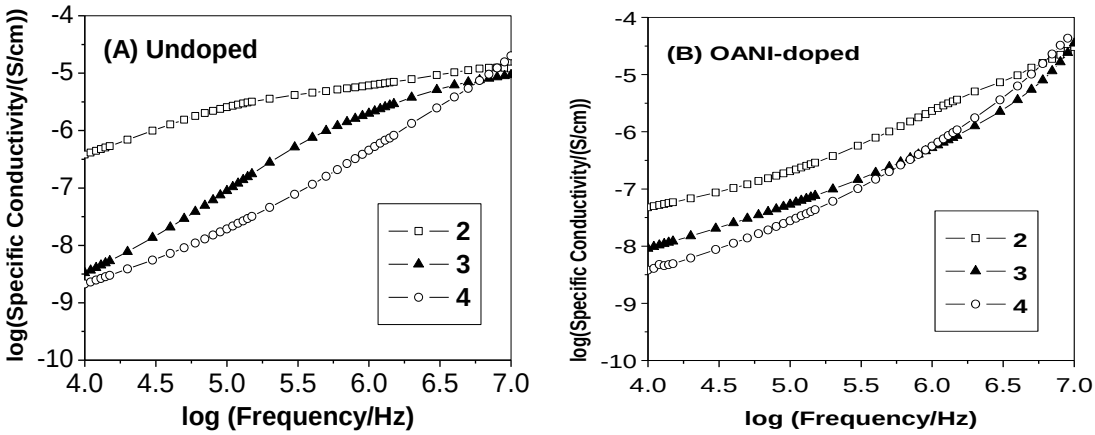

Figure 5.11. Specific conductivity versus frequency for (A) undoped PAMPSA-*b*-PMA block copolymers and (B) OANI-doped PAMPSA-*b*-PMA block copolymers after washing away ammonium persulfate salts

5.5 CONCLUSION

In summary, we prepared the first microphase-separated block copolymers as nanodielectric materials. Well-defined sulfonic acid-containing block copolymers PAMPSA-*b*-PMA were prepared by RAFT. These block copolymers were doped with oligoaniline. Undoped block copolymers and doped supramolecular block copolymers were further evaluated for their dielectric properties. Compared with undoped neat block copolymers, oligioaniline-doped supramolecular block copolymers exhibited higher permittivity and much lower dielectric loss, indicating dominant interfacial polarization at the microphase domains.

5.6 ACKNOWLEDGEMENT

We are grateful of the support by the Office of Naval Research (N000141110191). We thank Prof. Brian Benicwicz and Dr. Brandon Cash for helpful discussions on the synthesis of oligoaniline.

5.7 REFERENCES

1. Barber, P.; Balasubramanian, S.; Anguchamy, Y.; Gong, S.; Wibowo, A.; Gao, H.; Ploehn, H. J.; zur Loye, H.-C. *Materials* **2009,** 2, 1697-1733.
2. Nalwa, H., *Handbook of Low and High Dielectric Constant Materials and Their Applications;*. Academic Press: London, UK, 1999.
3. Wang, Q.; Zhu, L. *J. Polym. Sci. B Polym. Phys.* **2011,** 49, 1421-1429.
4. Ducharme, S. *ACS Nano* **2009,** 3, 2447-2450.
5. Jain, P.; Rymaszewski, E. J., *Thin Film Capacitors for Packaged Electronic*. National Academics: Washington, D.C., 2003.
6. Slenes, K. M.; Winsor, P.; Scholz, T.; Hudis, M. *IEEE Trans. Magn.* **2001**, 324-327.
7. Zhang, Q. M.; Bharti, V.; Zhao, X. *Science* **1998,** 280, 2101-2104.
8. Ihlefeld, J.; Laughlin, B.; Hunt-Lowery, A.; Borland, W.; Kingon, A.; Maria, J.-P. *J. Electroceram.* **2005,** 14, 95-102.
9. Starkweather, H. W.; Avakian, P.; Matheson, R. R.; Fontanella, J. J.; Wintersgill, M. C. *Macromolecules* **1992,** 25, 6871-6875.
10. Ho, J.; Ramprasad, R.; Boggs, S. *IEEE Trans. Dielectr. Electr. Insul.* **2007,** 14, 1295.
11. Lovinger, A. J. *Science* **1983,** 220, 1115.
12. Chu, B.; Lin, M.; Neese, B.; Zhou, X.; Chen, Q.; Zhang, Q. M. *Appl. Phys. Lett.* **2007,** 91, 1222909-1.
13. Chu, B.; Zhou, X.; Ren, K.; Neese, B.; Lin, M.; Wang, Q.; Bauer, F.; Zhang, Q. M. *Science* **2006,** 313, 334.
14. Wu, S.; Lin, M.; Lu, S. G.; Zhu, L.; Zhang, Q. M. *Appl. Phys. Lett.* **2011,** 99, 132901-132903.
15. Lu, Y.; Claude, J.; Neese, B.; Zhang, Q.; Wang, Q. *J. Am. Chem. Soc.* **2006,** 128, 8120-8121.
16. Chen, X.-Z.; Li, Z.-W.; Cheng, Z.-X.; Zhang, J.-Z.; Shen, Q.-D.; Ge, H.-X.; Li, H.-T. *Macromol. Rapid Commun.* **2011,** 32, 94-99.
17. Thakur, V. K.; Tan, E. J.; Lin, M.-F.; Lee, P. S. *J. Mater. Chem.* **2011,** 21, 3751-3759.
18. Zhang, Z.; Chung, T. C. M. *Macromolecules* **2007,** 40, 783.
19. Shen, Y.; Lin, Y.; Li, M.; Nan, C. W. *Adv. Mater.* **2007,** 19, 1418-1422.
20. Kim, P.; Jones, S. C.; Hotchkiss, P. J.; Haddock, J. N.; Kippelen, B.; Marder, S. R.; Perry, J. W. *Adv. Mater.* **2007,** 19, 1001-1005.
21. Kim, P.; Doss, N. M.; Tillotson, J. P.; Hotchkiss, P. J.; Pan, M.-J.; Marder, S. R.; Li, J.; Calame, J. P.; Perry, J. W. *ACS Nano* **2009,** 3, 2581-2592.
22. Li, J.; Khanchaitit, P.; Han, K.; Wang, Q. *Chem. Mater.* **2010,** 22, 5350-5357.
23. Li, J.; Claude, J.; Norena-Franco, L. E.; Seok, S. I.; Wang, Q. *Chem. Mater.* **2008,** 20, 6304-6306.
24. Li, J.; Seok, S. I.; Chu, B.; Dogan, F.; Zhang, Q.; Wang, Q. *Adv. Mater.* **2009,** 21, 217-221.
25. Guo, N.; DiBenedetto, S. A.; Tewari, P.; Lanagan, M. T.; Ratner, M. A.; Marks, T. J. *Chem. Mater.* **2010,** 22, 1567-1578.

26. Guo, M.; Yan, X.; Kwon, Y.; Hayakawa, T.; Kakimoto, M.; Goodson, T. *J. Am. Chem. Soc.* **2006,** 128, 14820.
27. Xu, J.; Wong, C. P. *Appl. Phys. Lett.* **2005,** 87, 082907.
28. Calame, J. P. *J. Appl. Phys.* **2006,** 99, 084101-08411.
29. Guo, M.; Hayakawa, T.; Kakimoto, M.-a.; Goodson, T. *J. Phys. Chem. B* **2011,** 115, 13419-13432.
30. Huang, C.; Zhang, Q. M.; deBotton, G.; Bhattacharya, K. *Appl. Phys. Lett.* **2004,** 84, 1757632-1757635.
31. Huang, C.; Zhang, Q. M.; Su, J. *Appl. Phys. Lett.* **2003,** 82, 1575505-1575508.
32. Huang, C.; Zhang, Q.-M. *Adv. Mater.* **2005,** 17, 1153-1158.
33. Molberg, M.; Crespy, D.; Rupper, P.; Nuesch, F.; Manson, J.-A. E.; Lowe, C.; Opris, D. M. *Adv. Funct. Mater.* **2010,** 20, 3280-3291.
34. Zhang, Q. M.; Li, H.; Poh, M.; Xia, F.; Cheng, Z.-Y.; Xu, H.; Huang, C. *Nature* **2002,** 419, 284-287.
35. Huang, C.; Zhang, Q. *Adv. Funct. Mater.* **2004,** 14, 501-506.
36. Cui, L.; Chao, D.; Lu, X.; Zhang, J.; Mao, H.; Li, Y.; Wang, C. *Polym. Int.* **2010,** 59, 975-979.
37. Zhang, J.; Chao, D.; Cui, L.; Liu, X.; Zhang, W. *Macromol. Chem. Phys.* **2009,** 210, 1739-1745.
38. Chao, D.; Jia, X.; Liu, H.; He, L.; Cui, L.; Wang, C.; Berda, E. B. *J. Polym. Sci. Pol. Chem.* **2011,** 49, 1605-1614.
39. He, L.; Chao, D.; Jia, X.; Liu, H.; Yao, L.; Liu, X.; Wang, C. *J. Mater. Chem.* **2011,** 21, 1852-1858.
40. Raju, G. G., *Dielectrics in Electric Fields*. Marcel Dekker: New York, 2003.
41. Stoyanov, H.; Kollosche, M.; McCarthy, D. N.; Kofod, G. *J. Mater. Chem.* **2010,** 20, 7558-7564.
42. Liang, S.; Claude, J.; Xu, K.; Wang, Q. *Macromolecules* **2008,** 41, 6265-6268.
43. McCullough, L. A.; Dufour, B.; Matyjaszewski, K. *Macromolecules* **2009,** 42, 8129-8137.
44. McCullough, L. A.; Dufour, B.; Tang, C.; Zhang, R.; Kowalewski, T.; Matyjaszewski, K. *Macromolecules* **2007,** 40, 7745-7747.
45. Chen, R.; Benicewicz, B. C. *Macromolecules* **2003,** 36, 6333-6339.
46. Buga, K.; Pokrop, R.; Zagorska, M.; Demadrille, R.; Genoud, F. *Synth. Met.* **2005,** 153, 137-140.
47. Liu, S.; Zhu, K.; Zhang, Y.; Zhu, Y.; Xu, J. *Mater. Lett.* **2005,** 59, 3715-3719.
48. Rozalska, I.; Kulyk, P.; Kulszewicz-Bajer, I. *New J. Chem.* **2004,** 28, 1235-1243.
49. Sun, Z. C.; Jing, X. B.; Wang, X. H.; Li, J.; Wang, F. S. *Synth. Met.* **2001,** 119, 313-314.
50. K. B. Guice, S. R. Marrou, S. R. Gondi, B. S. Sumerlin, *Macromolecules* **2008**, 41, 4390.
51. Y. Mitsukami, M. S. Donovan, A. B. Lowe, C. L. McCormick, *Macromolecules* **2001**, 49, 1605.
52. A. V. Bolotnikov, A. E. Grekov, P. G. Muzykov, T. S. Sudarshan, *IEEE Trans. Electron Devices* **2007**, 54, 1540.
53. A. V. Bolotnikov, P. G. Muzykov, T. S. Sudarshan, *Appl. Phys. Lett.* **2008**, 93, 052101.

54. P. G. Muzykov, A. V. Bolotnikov, T. S. Sudarshan, *Solid State Electron.* **2009**, 53, 14.
55. C. Huang, Q. Zhang, *Adv. Funct. Mater.* **2004**, 14, 501.
56. G. G. Raju, "Dielectrics in Electric Fields", Marcel Dekker, New York, 2003.

CHAPTER 6

CONVERTING AN ELECTRICAL INSULATOR INTO A DIELECTRIC CAPACITOR: END-CAPPING POLYSTYRENE WITH OLIGOANILINE[†]

[†] Hardy, C. G.; Islam, M. S.; Gonzalez-Delozier, D.; Morgan, J. E.; Cash, B.; Benicewicz, B. C.; Ploehn, H. J.; Tang, C. *Chemistry of Materials* **2013**, 25, 799-807. Reprinted here with permission of publisher.

6.1 ABSTRACT

We report a simple and low-cost strategy to enhance the dielectric permittivity of polystyrene by up to an order of magnitude via incorporating an oligoaniline trimer moiety at the end of the polymer chains. The oligoaniline-capped polystyrene was prepared by a copper-catalyzed click reaction between azide-capped polystyrene and an alkyne-containing aniline trimer, which was doped by different acids. By controlling molecular weight of polystyrene, the end-capped polymers can be induced to form nanoscale oligoaniline-rich domains embedded in an insulating matrix. Under an external electric field, this led to an increase in dielectric polarizability while maintaining a low dielectric loss. At frequencies as high as 0.1 MHz, the dielectric permittivity and dielectric loss (tan δ) were ~22.8 and ~0.02, respectively. This strategy may open a new avenue to increasing the dielectric permittivity of many other commodity polymers while maintaining relatively low dielectric loss.

6.1 INTRODUCTION

Dielectric polymer film-based capacitors have shown promise in applications including portable electronic devices, hybrid electric vehicles, pulse power devices and energy storage due to their light weight, low cost, and excellent processability.[1-13] Particularly, pulse power devices require accumulating much energy over a relatively long period of time and releasing it very quickly, thus increasing the available instantaneous power.[14-24]

Insulating commodity polymers play an important role in dielectric capacitors since most have very high dielectric breakdown strength, high volume availability, and low cost. Among various dielectric polymers, biaxially oriented polypropylene (BOPP)

is the industrial standard polymer for fabrication of capacitors because of its high breakdown strength (>700 MVm^{-1}) and low dielectric loss (tan δ ~0.0002 at 1 kHz). However, BOPP has a low dielectric permittivity (ε_r = 2.2), ultimately leading to low energy densities (ca. 1-1.2 J/cm^3).[25, 26] Similarly, many other commodity dielectric polymers including polystyrene, polyethylene, polyvinyl chloride and polycarbonate have high breakdown strength (~ 450-850 MV/m) and low dielectric permittivity (ε_r ~2.0-5.0 at 1kHz).[14, 15]

There is a crucial need to develop dielectric polymers with high dielectric permittivity while maintaining low dielectric loss. Poly(vinylidene fluoride) (PVDF) and its polymer derivatives have shown great promise since they have both high dielectric breakdown strength (500~700 MVm^{-1}) and moderate permittivity (ε_r = 10-20 at 1.0 KHz).[26-33] Recent studies have focused on modifying the chemical structure of PVDF with bulky fluorinated comonomers to prepare random fluorinated copolymers such as poly((vinylidene fluoride)-*r*-(chlorotrifluoroethylene)) (P(VDF-CTFE)).[26, 28, 29, 33-37] Though these random copolymers are capable of high breakdown strength, fast energy discharge rates and relatively low dielectric loss (e.g. tan δ ~0.02 at 1 kHz), their dielectric permittivity drops sharply at high frequency.[34]

Recently, a class of "molecular composites" has been developed, in which a conductive π-conjugated macromolecule is directly attached to the polymer backbone.[19, 38-43] Delocalization of electrons across the π-network can produce high interfacial polarization upon charge displacement, ultimately resulting in large dielectric responses. The Wang group was the first to attach oligoaniline octamer moieties to the ends of a ferroelectric polymer.[41] This resulted in a "dumbbell-shaped" copolymer containing

terminal oligoaniline units. The addition of 10 weight percent oligoaniline units increased the dielectric permittivity from 12 to 85 at 1 kHz. However, the addition of more than 10 wt% aniline resulted in significant increases in dielectric loss, presumably due to electron conduction across the film. Stoyanov *et al*. prepared a block copolymer in which one domain was complexed with polyaniline.[39] While there were improvements in permittivity (from 2 to 8 at 1 kHz and from 2 to 7 at 1 MHz) between 1.0-1.8 wt% polyaniline, additions of above 2.0 wt% polyaniline resulted in abrupt increases in conductivity. At this point complexation of the polyaniline with the polymer backbone was exhausted, and likely resulted in continuous conductive pathways across the film. Cui. *et al.* prepared a poly(ethylene oxide)-polyoligoaniline alternating copolymer that contained oligoaniline repeat units in the polymer main chain.[40] The copolymer films showed high dielectric permittivity ($\varepsilon_r \sim 70$ at 1 MHz), but also exhibited extremely high dielectric loss ($\tan \delta = 2.72$).

Clearly, chemically integrating the conductive domain into the polymer chain inhibits aggregation, thus reducing dielectric loss. However, the loading content of the conductive domain remains limited, since increases in the π-conjugated fraction eventually result in conductivity abruptly increasing to high levels. To address this issue, we have recently taken a new approach to developing dielectric materials by creating interfacially-dominated polymeric materials based on nanophase-separated block copolymers.[44] While the minor block forms nanodomains with high dielectric polarizability, the majority matrix block insulates the conductive domains to avoid percolation and minimize inter-domain conduction. Under an external electric field, electronic conduction induces nanodipoles along the phase boundary due to space charge

accumulation at the domain interfaces. Specifically, we prepared a series of diblock copolymers in which the major fraction was an insulating poly(methyl acrylate) block while the minor fraction had a side chain containing a sulfonic acid moiety, which was complexed with an oligoaniline trimer through supramolecular interactions. We observed both enhanced dielectric properties (ε_r = 11 at 1 MHz) and decreased dielectric loss (tan δ = 0.5 at 1 MHz) for the oligoaniline-complexed diblock copolymer compared to the uncomplexed diblock copolymer (ε_r = 5 at 1 MHz and tan δ = 2.7 at 1 MHz). However, this approach was limited, as the sulfonic acid on the side chain of the block copolymer was the only possible dopant for oligoaniline.

In this paper, we report a new, simple, and low cost approach that could be generalized to enhance dielectric permittivity of many commodity polymers, which has not yet been considered for high performance dielectric capacitor materials. This approach is based on capping the ends of polystyrene chains with oligoaniline through a click reaction between azide-terminated polystyrene and an alkyne-containing aniline trimer. The oligoaniline is then doped with various acids, including large organic acids such as dodecylbenzenesulfonic acid (DBSA) and camphorsulfonic acid (CSA). Due to the chemical incompatibility, it is expected that highly polar oligoaniline will self-assemble into nanoscale domains (i.e. a few nm) dispersed in non-polar polystyrene matrix (Scheme 6.1). Such highly polarizable nanodomains would make a positive contribution towards increasing the overall dielectric permittivity. Indeed, we observed that a small fraction of oligoaniline increased the dielectric permittivity of polystyrene by up to an order of magnitude while the dielectric loss remained low.

Scheme 6.1. Oligoaniline end-functionalized polystyrene and its contribution to increasing dielectric permittivity.

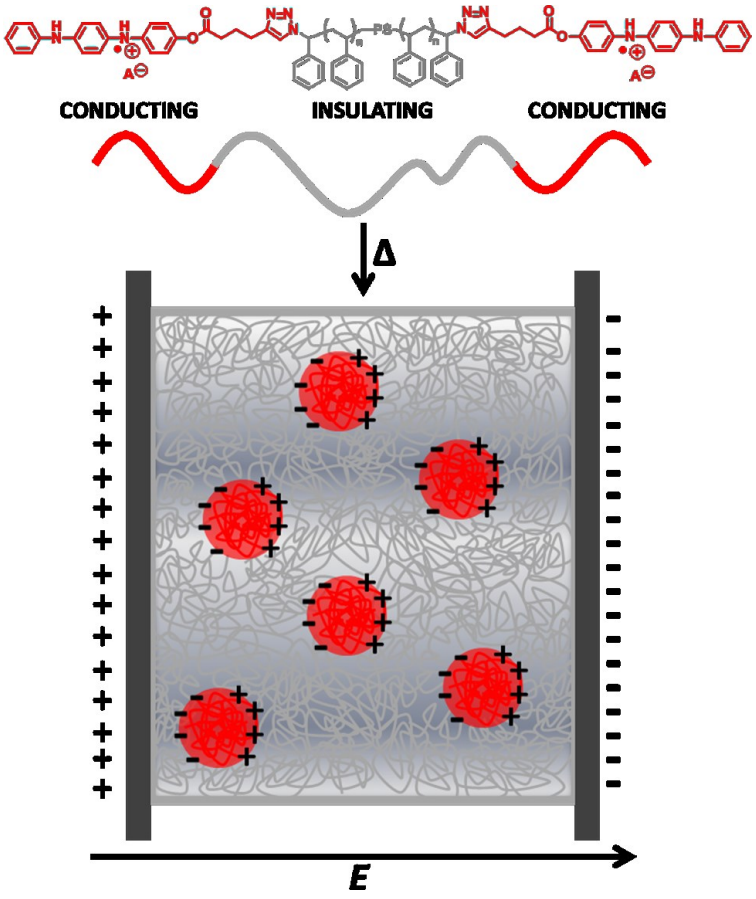

6.2 EXPERIMENTAL

Materials. All reagents were purchased from Alfa Aesar and Aldrich and used as received unless otherwise noted. Styrene was distilled before use. Hydroxy-terminated oligoaniline trimer (OANI-OH) was prepared according to a reported procedure.[44] Difunctional bromine- and azide-terminated polystyrene was prepared according to a procedure previously reported.[45]

Characterization. ^{1}H NMR (300 MHz) and ^{13}C NMR (100 MHz) spectra were recorded on a Varian Mercury 300 spectrometer with tetramethylsilane (TMS) as an internal reference. Gel permeation chromatography (GPC) was performed at 50^{o}C on a

Varian system equipped with a Varian 356-LC refractive index detector and a Prostar 210 pump. The columns were STYRAGEL HR1, HR2 (300 × 7.5 mm) from Waters. HPLC grade DMF with 0.01 wt% LiBr was used as eluent at a flow rate of 1.0 mL/min. Polystyrene standards were used for calibration. Mass spectrometry was carried out on a Waters Micromass Q-Tof mass spectrometer, with a positive ion electrospray as the ionization source. UV-vis spectroscopy was carried out on a Shimadzu UV-2450 spectrophotometer, scanning monochromatic light in the range of 190-900 nm. A quartz cuvette with a path length of 10.00 mm was used, and the solvent was dimethylformamide (DMF). FTIR spectra were recorded on a PerkinElmer Spectrum 100 FTIR spectrometer equipped with a Universal ATR sampling accessory. Thermal transitions of the polymers were measured by differential scanning calorimetry (DSC) using a TA Instruments Q2000 in a temperature range from -70 to 150 ^{o}C at heating and cooling rates of 5 ^{o}C/min under constant nitrogen flow at a rate of 50 mL/min. Samples (between 3-8 mg) were placed in aluminum hermetic pans and sealed. The data were collected on the second heating run.

Small-Angle X-ray Scattering (SAXS) data were acquired on a Bruker-AXS Nanostar-U instrument equipped as follows: copper rotating anode x-ray source (wavelength, □ = 0.154 nm, 6 KW supply 0.1 × 1 mm filaments) operated at 50 KV, 24 mA; Montel focusing optic; collimating assembly of 3 pinholes: (1) 750 μM, (2) 400 μM, and (3) 1000 μM, spacing (1-to-2) 925 mm, (2-to-3) 485 mm; extended sample chamber with x-y stage (where the beam is the z axis), secondary beam path 1050-1060 mm; beam path between focusing optic and detector under vacuum (< 0.1 mBar); 2-dimensional detector: Hi-star, multiwire proportional chamber, 1024 × 1024 pixels; control software:

Bruker SAXS v. 4.1.36; detector flood-field and spatial calibrations use 55Fe source; sample-to-detector distance calibrated using silver behenate. Bulk film samples were placed in a hole of copper spacer (1 mm thick) and then sandwiched between two sheets of Kapton films. The samples were then placed in the evacuated sample chamber at room temperature with a typical exposure time of 20 minutes. Data were integrated over the full circle of azimuthal angle values in the 2D SAXS scattering images with an increment of 0.01 degrees 2θ. Finally, the intensity I(q) was plotted against q = 4□/□ sin(□/2).

Films for dielectric characterization were prepared by dissolving polymer samples in toluene (67 mg/mL) and casting in heavy-gauge aluminum pans. The solvent was removed by evaporation at 65°C under slightly reduced pressure (635 mm Hg absolute) for 24 h, producing films with uniform thickness without solvent bubbles, cracks, or other defects. Film thicknesses were measured at multiple positions with a micrometer; measured thicknesses ranged from 2 to 25 μm. Strips of aluminum pan bearing copolymer films were cut using scissors; the aluminum pan served as the bottom electrode for dielectric measurements. Circular gold electrodes (area 1.13 cm^2) were deposited on the films' top surfaces by sputter coating in an argon atmosphere through a shadow mask.

The films' complex impedance using an impedance analyzer (Agilent model 4192A LF).[46-48] Measurements were carried out at low applied voltage (typically 10 mV) and varying frequency (typically 10^2 to 1.2×10^7 Hz) for 3-5 specimens of each sample to ensure reproducibility. A parallel RC circuit model expected to describe a "leaky" capacitor was used to determine the real and complex parts of the relative permittivity and the loss tangent from measured values of impedance magnitude and phase angle.

Polarization measurements at higher applied voltages were carried out using a Premier II ferroelectric polarization tester (Radiant, Inc.) using the same film specimens prepared for impedance testing. Films made from pure polystyrene (Aldrich, 192,000 g/mol) were also characterized. Polarization data (*D* vs. *E*) were acquired for applied voltages ranging from 1 to 199 V and cycle frequencies of 100 Hz and 1 kHz. The maximum applied field strength ranged from 15 to 300 kV/cm, depending on film thickness and the sample conductivity. Stored energy density $\hat{W} = \int E\,dD$ was determined by numerical integration of the *D*-*E* data.

Synthesis of oligoaniline-alkyne (OANI-alkyne, 2). 5-Hexynoic acid chloride was prepared by heating 5-hexynoic acid (8.0 mL, 73 mmol) in thionyl chloride (8 mL, 110 mmol). After refluxing for 12 hours, the product was collected by vacuum distillation. Hydroxy-terminated oligoaniline trimer (9.42 g, 34.1 mmol) was dissolved in 30 mL dry THF and the flask was purged with nitrogen. Triethylamine (7.1 mL, 51 mmol) was added and the solution was cooled to 0 ^{o}C. A solution of 5-hexynoic acid chloride (5.48 g, 37.5 mmol) in 10 mL dry THF was added over 30 minutes. After stirring at room temperature overnight, the reaction mixture was filtered and concentrated to dryness. The solids were dissolved in dichloromethane and extracted with water twice. The aqueous layers were combined and extracted with dichloromethane three times. The organic layers were combined and stirred over anhydrous sodium sulfate. The solution was filtered and the filtrate was concentrated to dryness. The resulting solids were stirred in refluxing hexanes overnight. The red/brown liquid was filtered, leaving a dark purple solid. The product was collected, vacuum dried, and analyzed by NMR, FT-IR, and mass spectrometry. Yield: 10.2 g, 81.0 %. ^{1}H NMR (**2**, DMSO-d_6, δ): 7.92 (s, 1H, Ph-NH-Ph-

N*H*-), 7.88 (s, 1H, Ph-N*H*-Ph-NH), 6.65-7.19 (m, 13H, Ph), 2.84 (t, 1H, CΞC*H*), 2.61 (t, 2H, OC(O)CH_2), 2.25 (td, 2H, CH_2CΞCH), 1.78 (quin, 2H, $CH_2CH_2CH_2$). ^{13}C NMR (**2**, DMSO-d_6, δ): 172.21 (*C*=O), 145.28, 143.12, 142.79, 136.95, 129.54, 122.70, 120.16, 120.07, 118.79, 115.96, and 115.52 (C_q of Ph), 84.08 (CH_2*C*ΞCH), 72.39 (CH_2CΞ*C*H), 32.79 (C=O*C*H_2), 23.85 ($CH_2CH_2CH_2$), 17.58 (CH_2CH_2C). FTIR (cm^{-1}): 3388, 3294, 3052, 2965, 2916, 1736, 1600, 1511, 1380, 1310, 1225, 1197, 1167, 1144, 861, 817, 749, 692. MS (EI), m/z calcd for $C_{24}H_{22}N_2O_2$: 370.17; found: 370.

Synthesis of oligoaniline-terminated PS (OANI-PS-OANI, 5). Oligoaniline groups were added onto the end of the PS polymer chains through a click reaction with oligoaniline-alkyne (**2**) and the terminal azide groups from polymer **4**. Cu(I)Br (0.1 equiv) was charged into a round bottom flask and purged with nitrogen for 30 minutes. OANI-alkyne (**2**, 2 equiv), N_3-PS-N_3 (**4**, 1 equiv N_3), and PMDETA (0.15 equiv) were added to a pear shaped flask, dissolved in THF, and bubbled with nitrogen for 30 minutes. The mixture in the pear shaped flask was transferred to the round bottom flask and stirred at room temperature overnight. The reaction mixture was concentrated to dryness, dissolved in dichloromethane, and extracted with water three times. The organic layer was dried over anhydrous sodium sulfate, filtered, and concentrated. The solution was then precipitated into methanol two times. The solid product was collected by filtration and vacuum dried overnight. Products **5a** and **5b** were analyzed by ^{1}H NMR and FTIR. ^{1}H NMR (**3a**, CD_2Cl_2, δ): 6.2-7.2 (br, Ph), 3.28 (br, OC(O)CH_2), 3.16, (br, $N_{triazole}$CH(Ph)CH_2), 2.61 (br, CH_2C$C_{triazole}$), 2.46 (br, $CH_2CH_2CH_2$), 1.1-2.4 (br, CH_2C*H*Ph). FTIR (cm^{-1}): 3391, 3027, 2923, 2849, 1732, 1659, 1601, 1495, 1451, 1023, 906, 756, 697 .

Doping of OANI-PS-OANI with HCl (6), DDBS (7), and CSA (8). Fractions (0.2 g) of polymers **5a** and **5b** were dissolved in dry DMF (3 mL) and passed through microfilters (pore size 0.2 μm). HCl, DBSA, or CSA (50 equiv per OANI group) was added to the polymer solutions. Ammonium persulfate (50 equiv per OANI group) was also added to each solution. The solutions were then stirred at 70 ^{o}C for 48 hours. Once cooled, dichloromethane (40 mL) was added and the mixture was extracted with deionized water three times. The organic layer was stirred over anhydrous sodium sulfate, filtered, and concentrated to dryness. A small sample of each doped polymer was taken for analysis by UV-Vis spectroscopy. The remainder of the sample was dissolved in toluene (3 mL).

6.3 Results and Discussion

Synthesis of Oligoaniline-terminated PS. Oligoaniline-terminated polystyrene (OANI-PS-OANI, **5**) was prepared as outlined in Scheme 6.2. To add an alkyne-group onto the termini of the oligoaniline moiety, 5-hexynoic acid was refluxed in oxalyl chloride, effectively converting the acid group to an acid chloride. The resulting 5-hexynoic acid chloride was then reacted with the hydroxy-ended oligoaniline trimer (**1**) under basic conditions to give an alkyne-terminated oligoaniline trimer (OANI-alkyne, **2**). The purity of **2** was confirmed by NMR, FTIR, and mass spectrometry. Besides the appearance of the alkyl chain protons from the addition of the hexynoic acid group in the proton NMR between 1.78-2.84 ppm, there was also observed the disappearance of the hydroxide proton from compound **1** at 8.91 ppm and a shift of the amine protons from 7.65 ppm and 7.48 ppm for compound **1** to 7.92 ppm and 7.88 ppm for compound **2** (Figure 6.1). FTIR analysis showed the appearance of sharp bands at 3388 and 1736 cm^{-1}

for compound **2**, correlating to an alkyne group and an ester group, respectively. These results from proton NMR and FTIR, along with mass spectrometry, confirmed that product **2** was successfully prepared through the halide displacement reaction.

Scheme 6.2. Synthesis and doping of oligoaniline-functionalized polystyrene.

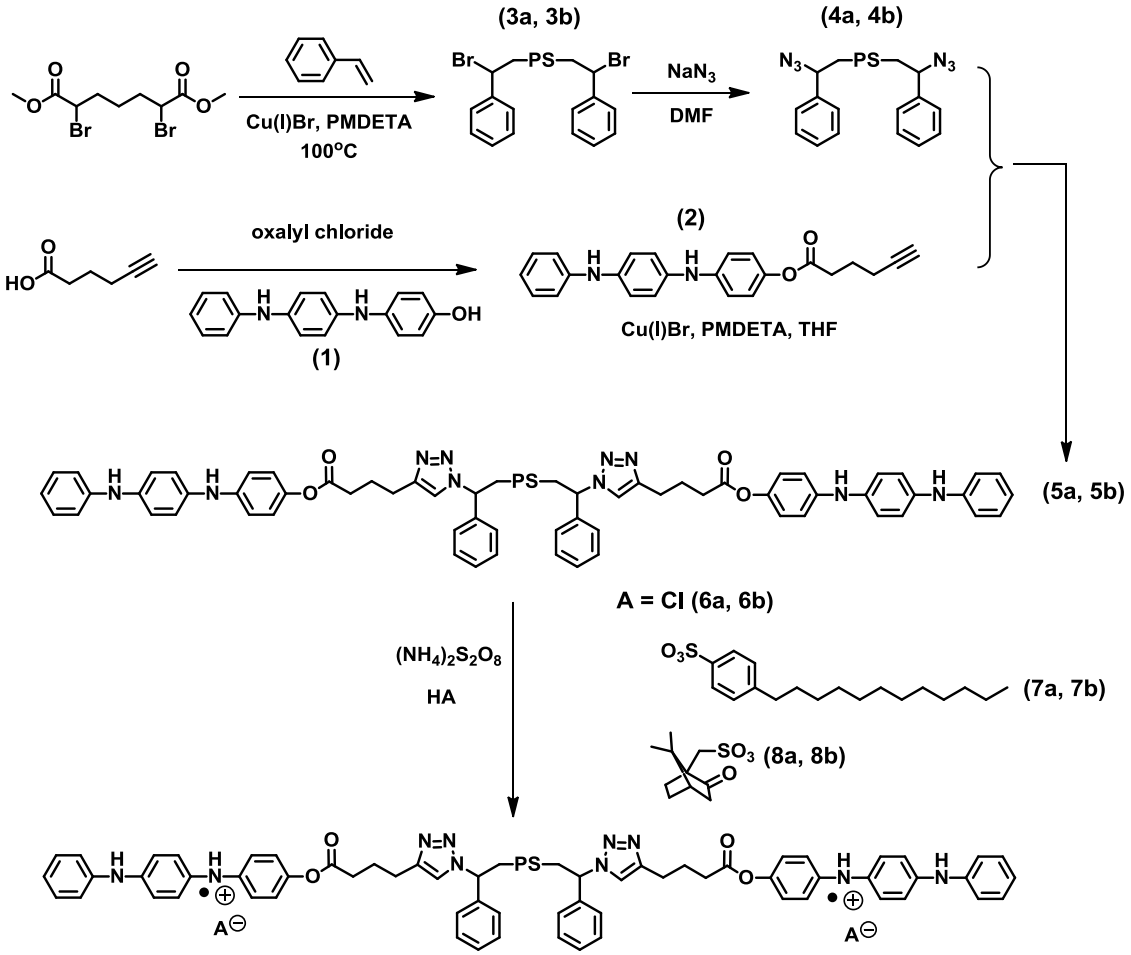

Polystyrene was prepared by atom transfer radical polymerization (ATRP) using a difunctional initiator so that both ends of the PS would contain bromine atoms.[45, 49] Specifically, dimethyl 2,6-dibromoheptanedioate was used as the difunctional initiator and the molar ratio of [initiator]:[Cu(I)Br]:[PMDETA] was 1:1:1.1. Both high (**3a**) and

low (**3b**) molecular weight PS homopolymers were prepared by adjusting the feed ratio of monomer to initiator. Both polymerizations were stopped below 60% monomer conversion to limit coupling termination reactions and to ensure that all polymer chain ends contained a bromine atom. Both difunctional PS polymers had low polydispersity indices (PDI < 1.1). The final molecular weight could be accurately determined by GPC analysis, as the system was calibrated using PS standards. The final molecular weight and PDI are shown in Table 6.1. The terminal bromine groups on difunctional PS homopolymers **3a** and **3b** obtained by ATRP were converted to azide groups by reaction with sodium azide.[45] The transformation from bromide to azide end groups was confirmed using FTIR, as a sharp band appeared at 2094 cm^{-1}, which is typical for an azide stretching mode.

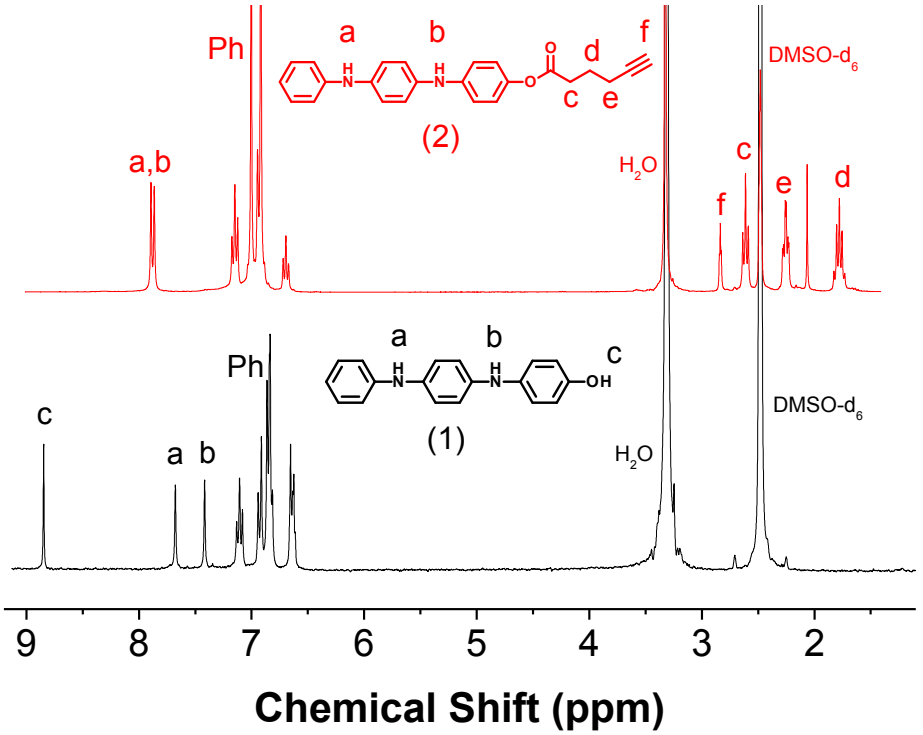

Figure 6.1. ^{1}H NMR spectra of hydroxy-terminated (**1**) and alkyne-terminated (**2**) oligoaniline.

Table 6.1. Preparation of bromide and azide end-functionalized polymers.

Entry	Polymer	[Monomer]: [Initiator]	M_n, g/mol (NMR)[1]	M_n, g/mol (GPC)[2]	PDI (GPC)
3a	Br-PS-Br	480:1	29,000	29,800	1.05
3b	Br-PS-Br	98:1	6,200	6,300	1.04
4a	N_3-PS-N_3	--	--	29,800	1.06
4b	N_3-PS-N_3	--	--	6,300	1.08

[1]Calculated by ^{1}H NMR using monomer conversion. [2]Calculated by GPC calibrated by polystyrene standards.

To prepare the oligoaniline-terminated PS, a click reaction was performed on the azide-terminated PS (**4a** and **4b**) with the oligoaniline-alkyne (**2**) using copper (I) bromide and PMDETA in THF. The excess oligoaniline-alkyne and residual copper bromide were removed by extraction with water followed by precipitating into a large excess of methanol two times. The disappearance of the alkyne stretch at 3294 cm^{-1} and the azide band at 2094 cm^{-1}, the appearance of a band at 1504 cm^{-1}, which is typical of a triazole group, and the appearance of a small, broad peak at 3391 cm^{-1} from the amine groups of the oligoaniline confirmed the addition of the oligoaniline onto the PS chain end (Figure 62).

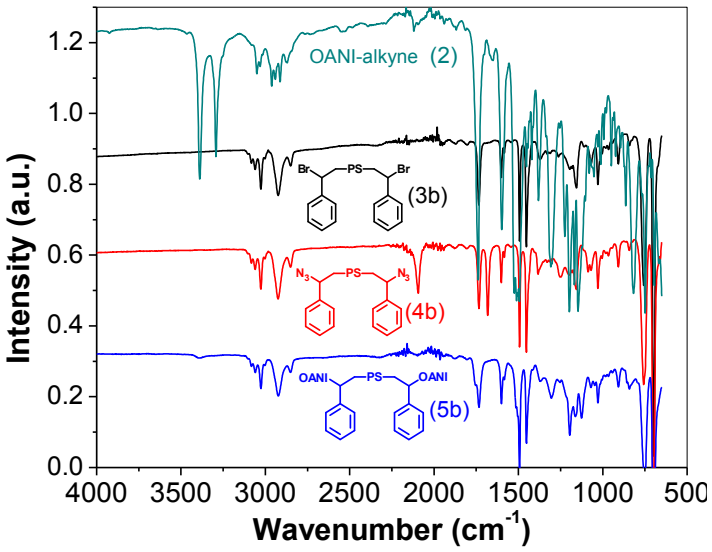

Figure 6.2. FTIR overlay for oligoaniline-alkyne (OANI-alkyne, **2**), bromide- (**3b**), azide- (**4b**), and oligoaniline- (**5b**) end functionalized polystyrene.

Doping with Acids. The oxidation states of the oligoaniline trimer were previously investigated by UV-Vis spectroscopy.[44, 50-54] Briefly, when oligoaniline is in the fully reduced form, only one absorption peak at 310 nm is observed in a solution of DMF. When an oxidant (e.g. ammonium persulfate) and an acid dopant are added, the oxidized oligoaniline displays a peak around 570 nm due to the charge transfer from the benzenoid ring to the quinoid ring. Additionally, the peak that was at 310 nm shifts to 301 nm. As these peaks are very prominent, UV-Vis was again used to confirm the oxidation and complexation of oligoaniline when doping with acids. Polymers **5a** and **5b** were doped with HCl (**6a** and **6b**), dodecylbenzenesulfonic acid (DBSA, **7a** and **7b**), and camphorsulfonic acid (CSA, **8a** and **8b**), as summarized in Table 6.2. An excess of acid as well as ammonium persulfate were added to the polymer solution (**5a** and **5b**) and stirred at 70 ^{o}C for 48 hours to ensure that all oligoaniline moieties were oxidized and doped with the corresponding acid. Removal of excess acids is crucial, as it has been

previously shown that any free acid can result in increased dielectric loss in final dielectric materials due to ionic conduction.[44] To ensure that all excess free acids and remaining ammonium persulfate were removed, the polymer solutions were dissolved in dichloromethane and extracted with deionized water three times. The organic layer was then dried over sodium sulfate, filtered, and vacuum dried. Small samples of the final doped polymers (**6a**-**8b**) were analyzed by UV-Vis. As an example of confirmation of the doping process, the UV-Vis spectra for the lower molecular weight doped polymers **5b**, **6b**, **7b**, and **8b** are shown in Figure 6.3. Polymers **5a**, **6a**, **7a**, and **8a** exhibited similar UV-Vis spectra, as listed in Table 6.2. The oxidation and doping process was clearly observed with the shift of the π-π* peak from 310 nm to around 300 nm, as well as the appearance of peaks around 390 nm and 525 nm.

Table 6.2. Preparation of oxidized and doped oligoaniline-ended PS.

Entry	Polymer	Oxidant	Dopant	Absorbance Peaks (nm)[1]	Wt. % OANI/acid[2]
5a	**5a**	None	None	310	1.81%
5b	**5b**	None	None	310	7.94%
6a	**5a**	$(NH_4)_2S_2O_8$	HCl	300, 395, 524	1.93%
6b	**5b**	$(NH_4)_2S_2O_8$	HCl	300, 395, 524	8.41%
7a	**5a**	$(NH_4)_2S_2O_8$	DBSA	298, 385, 520	2.84%
7b	**5b**	$(NH_4)_2S_2O_8$	DBSA	298, 385, 520	12.02%
8a	**5a**	$(NH_4)_2S_2O_8$	CSA	299, 383, 529	2.56%
8b	**5b**	$(NH_4)_2S_2O_8$	CSA	299, 383, 529	10.91%

[1]Values from UV-Vis. [2]Calculated assuming complete doping of oligoaniline.

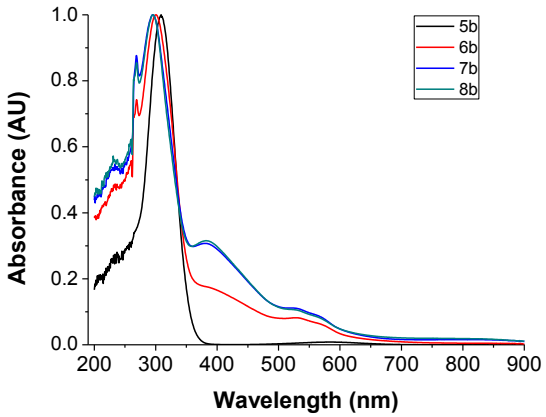

Figure 6.3. UV/Vis spectra for polymers **5b-8b**.

Dielectric Properties. The dielectric properties of oligoaniline-capped PS (OANI-PS-OANI), undoped and doped with various acids, were characterized using impedance spectroscopy and polarization testing. Impedance measurements yield the relative permittivity as a function of frequency (Figure 6.4) for polymers **3a-8b**. The higher molecular weight (~30,000 g/mol) Br-terminated polystyrene **3a** has a relative permittivity of about 2.7, nearly independent of frequency. Upon converting the end-group from Br to OANI units, the relative permittivity for polymer **5a** increases to a value of about 3.5, again constant across the 10^3-10^6 Hz frequency range. Polymer **6a**, in which the OANI units are doped with HCl, shows a slight increase in relative permittivity (ε_r = 3.9-4.1 between 10^3-10^6 Hz) compared to polymer **5a**. In the same frequency range, the permittivity of polymer **7a** (OANI-PS-OANI doped with DBSA) increases to values between 6-9; polymer **8a**, (OANI-PS-OANI doped with CSA) shows greater enhancement of permittivity with values in the 8.8-12 range.

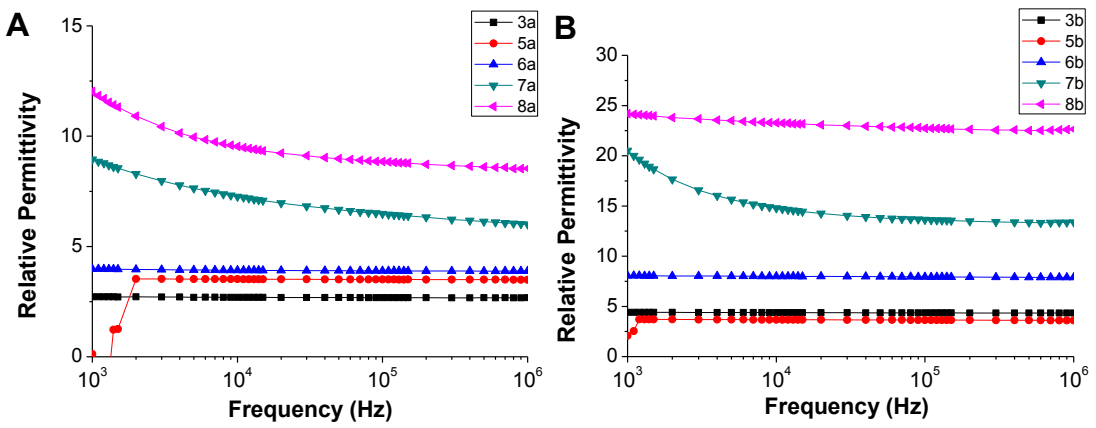

Figure 6.4. Relative permittivity versus frequency for polymers (**A**) **3a-8a** and (**B**) **3b-8b**.

Lower molecular weight oligoaniline-capped PS polymers show similar trends but larger enhancement in permittivity. The lower molecular weight (~6,000 g/mol) Br-terminated polystyrene **3b** has a nearly constant permittivity of about 4.3. Undoped polymer **5b** has permittivity value of about 3.6. HCl-doped polymer **6b** has permittivity values around 8; DBSA doped polymer **7b** had permittivity between 13.3-20; and CSA doped polymer **8b** had permittivity values between 22.6-24.2 across the range of 10^3-10^6 Hz. The permittivity of polymer **8b** is nearly one order of magnitude higher than that of polystyrene homopolymer, indicating the significant impact of the oligoaniline chain end when doped by the large organic acid, CSA. The greater enhancement in permittivity for the lower molecular weight OANI-PS-OANI polymers can be attributed to their higher fraction of aniline. The weight percents of the oligoaniline/acid complex relative to the total molecular weight of the polymers are summarized in Table 6.2.

As shown in Figure 6.5, the loss tangents for all polymers, including the acid doped polymers, remain below 0.6 across the range 10^3-10^6 Hz. For CSA-doped polymers **8a** and **8b** with highest permittivity, the dielectric loss at frequency 0.1 MHz

was only 0.05 and 0.02, respectively. This was substantially lower than other oligoaniline-containing ferroelectric copolymers as previously reported.[39-41]

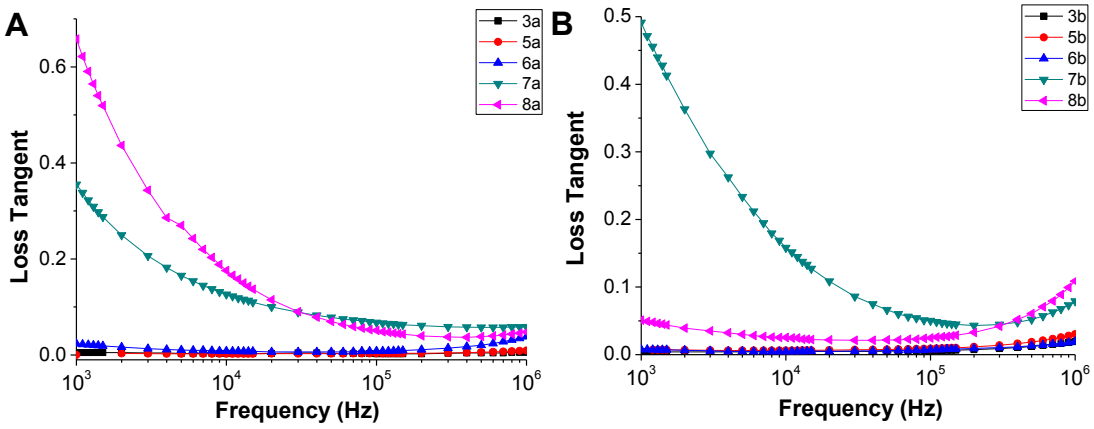

Figure 6.5. Loss tangent (dielectric loss) versus frequency for (**A**) polymers **3a-8a** and (**B**) polymers **3b-8b**.

Past experimental and theoretical studies have shown that bulky organic acids can have a large effect on the conductivity in polyaniline and oligoaniline films.[55, 56] A recent study utilizing density functional theory (DFT) found that organic acid CSA has much stronger interactions with the nitrogen atoms of oligoaniline than HCl, resulting in more stable complexes.[57] This suggests that organic acids produce more charge transfer between the dopant and the oligoaniline complex, allowing for greater electron transfer, and ultimately enhanced conductivity. As shown in Figure 6.6, polymers **7a-8b**, which contain oligoaniline units doped by large organic acids (DBSA and CSA), display much higher levels of electrical conductivity than HCl-doped polymers **6a** and **6b**. Polymers **7a-8b** display conductivities two orders of magnitude greater than **6a**,**b** at low frequencies (10^3 Hz), and an order of magnitude greater at high frequencies (10^6 Hz). These higher levels of conductivity directly correlate to higher levels of permittivity across the range of 10^3-10^6 Hz (Figure 6.4).

In addition, DBSA- and CSA-doped polymers **7a-8b** display relative permittivities that decrease noticeably with increasing frequency. Bulky DBSA and CSA anions complexed with oligoaniline create relatively large dipoles that may undergo orientational polarization and contribute to the permittivity, especially at low frequencies. Orientational polarization might be responsible for the energy dissipation observed at low frequencies for polymers **7a-8b** (Figure 6.5). Orientational polarization relaxes at higher frequencies (>10^4 Hz), where the enhanced dielectric responses likely result primarily from electronic polarization. Again, organic acids DBSA and CSA facilitate greater charge separation and local space charge buildup at the interface between conducting and insulating segments. These results are consistent with previous work which utilized large organic acids to dope polyaniline and oligoaniline-containing polymers to prepare highly conductive aniline-based films.[41, 58]

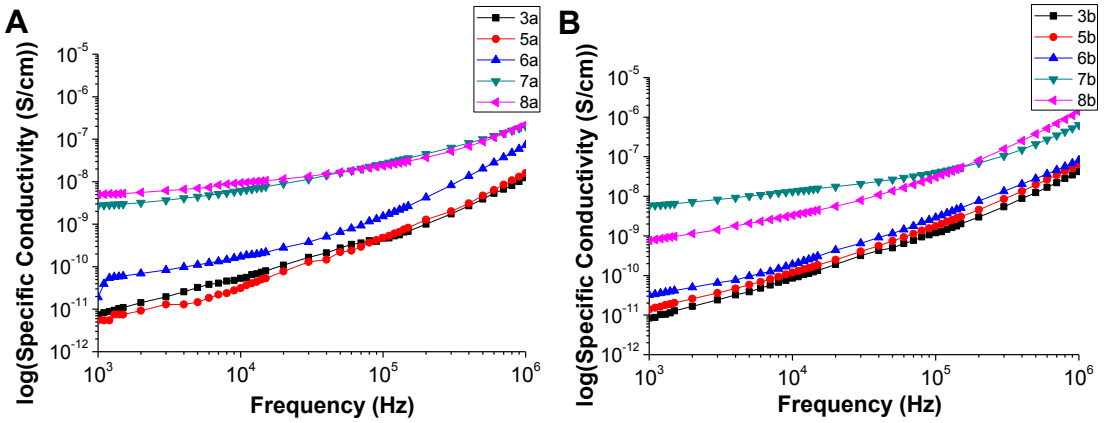

Figure 6.6. Conductivity versus frequency for (**A**) polymers **3a-8a** and (**B**) polymers **3b-8b**.

Figure 6.7 shows results from polarization testing at low to moderate voltages (1-199 V), in contrast to the impedance results obtained at very low applied voltage (typically 10 mV). As expected, the polarization curves for PS homopolymer are nearly

linear with low hysteresis. In contrast, all acid-doped OANI-capped PS polymers show significantly enhanced dielectric polarization compared to PS homopolymer, as evidenced by the slopes of the *D*-*E* curves in Figure 6.7. This shows that acid-doped OANI-capped PS polymers have much higher energy storage capacity than PS homopolymer.

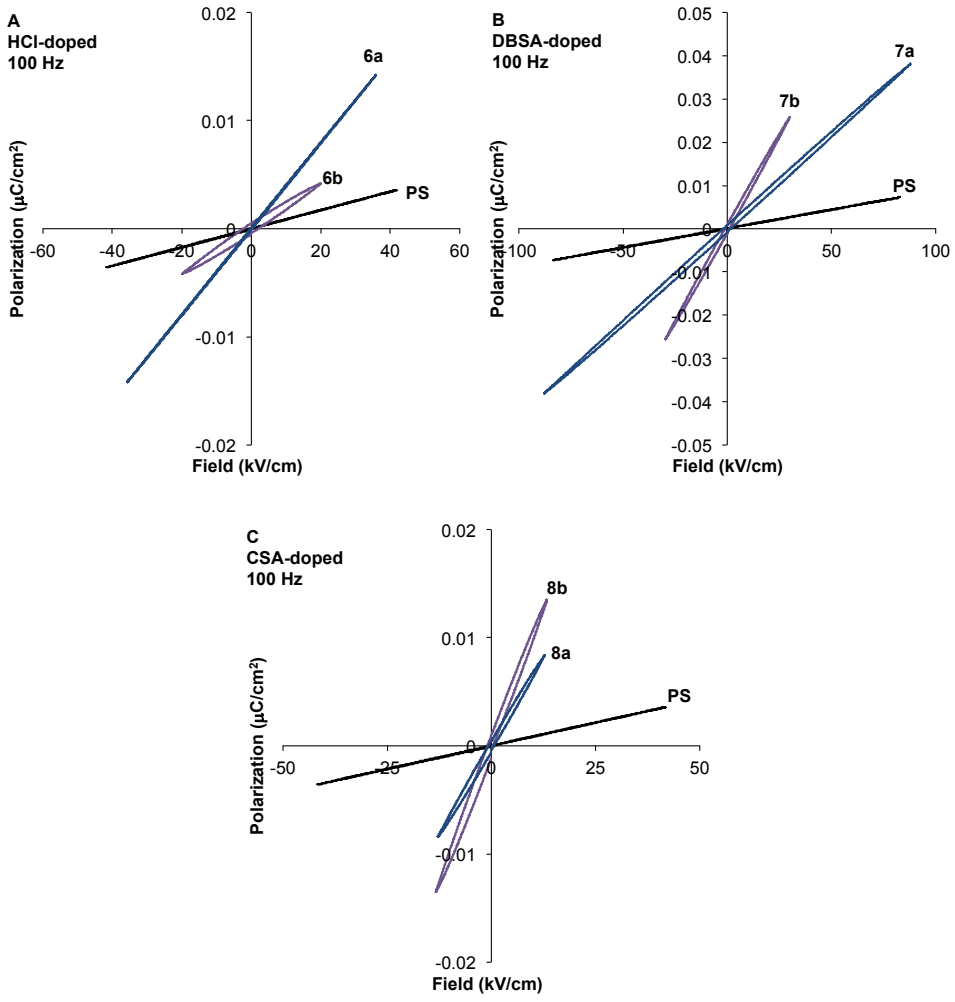

Figure 6.7. Dielectric polarization versus applied electric field for PS and OANI-capped PS doped with (A) HCl, (B) DBSA, and (C) CSA. All measurements carried out with 100 Hz cycle frequency.

Figure 6.8 shows the stored energy density of acid-doped OANI-capped PS relative to that of pure PS measured at the same electric field polarization. The higher molecular weight polymers (**6a**, **7a**, **8a**), containing 2-3% OANI (Table 6.2), have stored energy densities that are 4-8 times higher than PS homopolymer. For lower molecular weight polymers (**7b**, **8b**), doped with DBSA or CSA and having 11-12% OANI, the relative energy densities increase further, to 10-12 times higher than that of PS. However, the relative energy density of polymer **6b** (HCl-doped, 8.41% OANI) decreases relative to that of polymer **6a**, although it is still more than twice as large as the energy density stored in PS homopolymer at the same applied field strength. This trend can be seen in Figure 6.7A, in which the *D*-*E* curve for polymer **6b** has a smaller slope than that of polymer **6a**.

The *D*-*E* curves in Figure 6.7 also show that all acid-doped OANI-capped PS polymers manifest more nonlinearity and hysteresis than PS homopolymer. In general, the energy loss percentage (not shown here) increases with OANI content and maximum applied electric field, and decreases with increasing polarization cycle frequency.

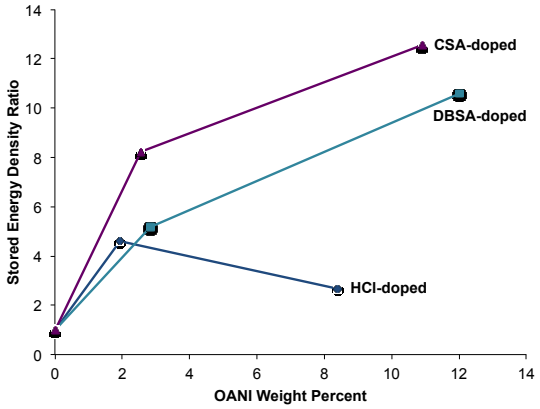

Figure 6.8. Stored energy density ratio ($\hat{W}_{\text{OANI-PS}}$ divided by $\hat{W}_{\text{PS}}$ measured at the same frequency and field strength) as a function of OANI weight percent.

The significant enhancement of the permittivity of polystyrene by the chain-end group could be explained by the presence of oligoaniline-rich domains dispersed in the polystyrene matrix. The formation of these nanoscale domains would significantly enhance the interfacial area of highly polarizable nanodipoles. This hypothesis is further supported by the higher permittivity of low molecular weight PS compared to that of higher molecular weight PS when doped with same reagents, as the weight fraction of oligoaniline plus dopant in the lower molecular weight PS was in the range of 8-12 wt%, which was sufficient to have nanoscale phase separation between chain ends and the polystyrene matrix (Scheme 6.1). However, this phase separation would be much less prominent in high molecular weight PS as the weight fraction of oligoaniline plus dopant was only around 2 wt%, which would lead to totally disorganized systems. To support this hypothesis, SAXS measurement was carried out on polymers **6a-8b**. For the high molecular weight polymers **6a**, **7a**, and **8a**, no ordered peaks were observed, as shown in Figure 6.9A. Given that polymers **6a**, **7a**, and **8a** had only 2 wt% oligoaniline/acid dopant, these polymers probably formed homogeneous systems. However, for the low molecular weight polymers **6b**, **7b**, and **8b**, a weak correlation peak at the 5 nm length scale ($d = 2\pi/q$) was observed (Figure 6.9B). Since there were no additional higher order peaks present, it can be concluded that these polymers did not form well-ordered nanodomains of oligoaniline/acid dopant complex, but rather disordered domains with broad interfaces between them and polystyrene matrix. Nevertheless, these results suggest that these highly polarizable nanodomains led to significant enhancements in dielectric permittivity.

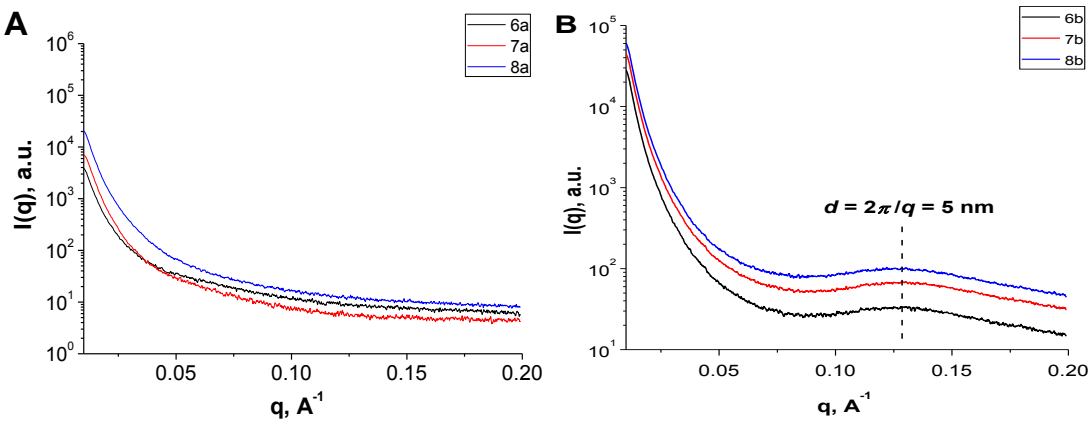

Figure 6.9. SAXS plots of polymers (**A**) **6a-8a** and (**B**) **6b-8b**.

6.5 Conclusions

In conclusion, we prepared oligoaniline end-functionalized polystyrene polymers via click chemistry between azide-ended polystyrene and alkyne-containing oligoaniline. The oligoaniline units were doped by various acids, including HCl, DBSA, and CSA. The dielectric properties of these oligoaniline-ended PS polymers indicated that doping with large, organic acids resulted in increases of up to an order of magnitude in permittivity and energy storage density relative to PS, while maintaining a relatively low dielectric loss, especially in the high frequency range. Given its simplicity, this novel strategy could be generalized to improve dielectric permittivity of many other commodity polymers.

6.6 Acknowledgment

This work was supported by the Office of Naval Research (award N000141110191) and the University of South Carolina.

6.7 References

1. Barber, P.; Balasubramanian, S.; Anguchamy, Y.; Gong, S.; Wibowo, A.; Gao, H.; Ploehn, H. J.; zur Loye, H.-C. *Materials* **2009,** 2, 1697-1733.

2. Carpi, F.; Gallone, G.; Galantini, F.; De Rossi, D. *Adv. Funct. Mater.* **2008,** 18, 235-241.
3. Ducharme, S. *ACS Nano* **2009,** 3, 2447-2450.
4. Guo, M.; Hayakawa, T.; Kakimoto, M.-a.; Goodson, T. *J. Phys. Chem. B* **2011,** 115, 13419-13432.
5. Huang, C.; Zhang, Q. *Adv. Funct. Mater.* **2004,** 14, 501-506.
6. Huang, C.; Zhang, Q.-M. *Adv. Mater.* **2005,** 17, 1153-1158.
7. Huang, C.; Zhang, Q. M.; deBotton, G.; Bhattacharya, K. *Appl. Phys. Lett.* **2004,** 84, 1757632-1757635.
8. Huang, C.; Zhang, Q. M.; Su, J. *Appl. Phys. Lett.* **2003,** 82, 1575505-1575508.
9. Molberg, M.; Crespy, D.; Rupper, P.; Nuesch, F.; Manson, J.-A. E.; Lowe, C.; Opris, D. M. *Adv. Funct. Mater.* **2010,** 20, 3280-3291.
10. Nalwa, H., *Handbook of Low and High Dielectric Constant Materials and Their Applications;*. Academic Press: London, UK, 1999.
11. Wang, Q.; Zhu, L. *J. Polym. Sci. B Polym. Phys.* **2011,** 49, 1421-1429.
12. Zhang, Q. M.; Li, H.; Poh, M.; Xia, F.; Cheng, Z.-Y.; Xu, H.; Huang, C. *Nature* **2002,** 419, 284-287.
13. Zhu, L.; Wang, Q. **2012,** 45, 2937-2954.
14. Jain, P.; Rymaszewski, E. J., *Thin Film Capacitors for Packaged Electronic*. National Academics: Washington, D.C., 2003.
15. Osaka, T.; Datta, M., *Energy Storage Systems for Electronics*. Gordon and Breach: Amsterdam, The Netherlands, 2001.
16. Kim, P.; Doss, N. M.; Tillotson, J. P.; Hotchkiss, P. J.; Pan, M.-J.; Marder, S. R.; Li, J.; Calame, J. P.; Perry, J. W. *ACS Nano* **2009,** 3, 2581-2592.
17. Kim, P.; Jones, S. C.; Hotchkiss, P. J.; Haddock, J. N.; Kippelen, B.; Marder, S. R.; Perry, J. W. *Adv. Mater.* **2007,** 19, 1001-1005.
18. Li, J.; Khanchaitit, P.; Han, K.; Wang, Q. *Chem. Mater.* **2010,** 22, 5350-5357.
19. Li, J.; Seok, S. I.; Chu, B.; Dogan, F.; Zhang, Q.; Wang, Q. *Adv. Mater.* **2009,** 21, 217-221.
20. Guo, N.; DiBenedetto, S. A.; Kwon, D.-K.; Wang, L.; Russell, M. T.; Lanagan, M. T.; Facchetti, A.; Marks, T. J. *J. Am. Chem. Soc.* **2007,** 129, 766-767.
21. Guo, N.; DiBenedetto, S. A.; Tewari, P.; Lanagan, M. T.; Ratner, M. A.; Marks, T. J. *Chem. Mater.* **2010,** 22, 1567-1578.
22. Dang, Z. M.; Lin, Y. H.; Nan, C. W. *Adv. Mater.* **2003,** 15, 1622-1625.
23. Calame, J. P. *J. Appl. Phys.* **2006,** 99, 084101-08411.
24. Li, J.; Claude, J.; Norena-Franco, L. E.; Seok, S. I.; Wang, Q. *Chem. Mater.* **2008,** 20, 6304-6306.
25. Starkweather, H. W.; Avakian, P.; Matheson, R. R.; Fontanella, J. J.; Wintersgill, M. C. *Macromolecules* **1992,** 25, 6871-6875.
26. Chu, B.; Lin, M.; Neese, B.; Zhou, X.; Chen, Q.; Zhang, Q. M. *Appl. Phys. Lett.* **2007,** 91, 1222909-122910.
27. Lovinger, A. J. *Science* **1983,** 220, 1115-1121.
28. Wu, S.; Lin, M.; Lu, S. G.; Zhu, L.; Zhang, Q. M. *Appl. Phys. Lett.* **2011,** 99, 132901-132903.
29. Chu, B.; Zhou, X.; Ren, K.; Neese, B.; Lin, M.; Wang, Q.; Bauer, F.; Zhang, Q. M. *Science* **2006,** 313, 334.

30. Guan, F.; Pan, J.; Wang, J.; Wang, Q.; Zhu, L. *Macromolecules* **2009,** 43, 384-392.
31. Guan, F.; Wang, J.; Pan, J.; Wang, Q.; Zhu, L. *Macromolecules* **2010,** 43, 6739-6748.
32. Guan, F.; Wang, J.; Yang, L.; Tseng, J.-K.; Han, K.; Wang, Q.; Zhu, L. *Macromolecules* **2011,** 44, 2190-2199.
33. Chen, X.-Z.; Li, Z.-W.; Cheng, Z.-X.; Zhang, J.-Z.; Shen, Q.-D.; Ge, H.-X.; Li, H.-T. *Macromol. Rapid Commun.* **2011,** 32, 94-99.
34. Lu, Y.; Claude, J.; Neese, B.; Zhang, Q.; Wang, Q. *J. Am. Chem. Soc.* **2006,** 128, 8120-8121.
35. Thakur, V. K.; Tan, E. J.; Lin, M.-F.; Lee, P. S. *J. Mater. Chem.* **2011,** 21, 3751-3759.
36. Guan, F.; Yang, L.; Wang, J.; Guan, B.; Han, K.; Wang, Q.; Zhu, L. *Adv. Funct. Mater.* **2011,** 21, 3176-3188.
37. Zhong, G.; Zhang, L.; Su, R.; Wang, K.; Fong, H.; Zhu, L. *Polymer* **2011,** 52, 2228-2237.
38. Chao, D.; Jia, X.; Liu, H.; He, L.; Cui, L.; Wang, C.; Berda, E. B. *J. Polym. Sci. Pol. Chem.* **2011,** 49, 1605-1614.
39. Stoyanov, H.; Kollosche, M.; McCarthy, D. N.; Kofod, G. *J. Mater. Chem.* **2010,** 20, 7558-7564.
40. Cui, L.; Chao, D.; Lu, X.; Zhang, J.; Mao, H.; Li, Y.; Wang, C. *Polym. Int.* **2010,** 59, 975-979.
41. Liang, S.; Claude, J.; Xu, K.; Wang, Q. *Macromolecules* **2008,** 41, 6265-6268.
42. He, L.; Chao, D.; Jia, X.; Liu, H.; Yao, L.; Liu, X.; Wang, C. *J. Mater. Chem.* **2011,** 21, 1852-1858.
43. Zhang, J.; Chao, D.; Cui, L.; Liu, X.; Zhang, W. *Macromol. Chem. Phys.* **2009,** 210, 1739-1745.
44. Hardy, C. G.; Islam, M. S.; Gonzalez-Delozier, D.; Ploehn, H. J.; Tang, C. *Macromol. Rapid Commun.* **2012,** 33, 791-797.
45. Gao, H.; Louche, G.; Sumerlin, B. S.; Jahed, N.; Golas, P.; Matyjaszewski, K. *Macromolecules* **2005,** 38, 8979-8982.
46. Bolotnikov, A. V.; Muzykov, P. G.; Grekov, A. E.; Sudarshan, T. S. *IEEE Trans. Electron Devices* **2007,** 54, 1540-1544.
47. Bolotnikov, A. V.; Muzykov, P. G.; Sudarshan, T. S. *Appl. Phys. Lett.* **2008,** 93, 052101-052103.
48. Muzykov, P. G.; Bolotnikov, A. V.; Sudarshan, T. S. *Solid-State Electron.* **2009,** 53, 14-17.
49. Matyjaszewski, K.; Tsarevsky, N. V. *Nat. Chem.* **2009,** 1, 276-288.
50. Chen, R.; Benicewicz, B. C. *Macromolecules* **2003,** 36, 6333-6339.
51. Buga, K.; Pokrop, R.; Zagorska, M.; Demadrille, R.; Genoud, F. *Synth. Met.* **2005,** 153, 137-140.
52. Liu, S.; Zhu, K.; Zhang, Y.; Zhu, Y.; Xu, J. **2005,** 59, 3715-3719.
53. Rozalska, I.; Kulyk, P.; Kulszewicz-Bajer, I. *New J. Chem.* **2004,** 28, 1235-1243.
54. Sun, Z. C.; Jing, X. B.; Wang, X. H.; Li, J.; Wang, F. S. *Synth. Met.* **2001,** 119, 313-314.

55. Casanovas, J.; Canales, M.; Ferreira, C. A.; Alemaì□n, C. *J. Phys. Chem. A* **2009,** 113, 8795-8800.
56. Udeh, C. U.; Fey, N.; Faul, C. F. J. *J. Mater. Chem.* **2011,** 21, 18137-18153.
57. Yang, G.; Hou, W.; Feng, X.; Jiang, X.; Guo, J. *Int. J. Quantum. Chem.* **2008,** 108, 1155-1163.
58. MacDiarmid, A. G.; Epstein, A. J. *Synthetic Met.* **1995,** 69, 85-92.

CHAPTER 7

LINEAR DIBLOCK COPOLYMER PEO-B-PS WITH A PHOTOCLEAVABLE LINKER: APPROACHING THE LOWER SIZE LIMIT OF ORDERED NANOPORES

7.1 ABSTRACT

This chapter discusses the preparation of highly dense, highly ordered nanoporous films by utilizing low molecular weight block copolymers PEO-*b*-PS with a photocleavable, *ortho*-nitrobenzyl linker between the two blocks. A lower limit in molecular weight was realized, below which films completely dewet during annealing, even after complexing the PEO domain with LiCl. Films using PEO with a molecular weight of 2000 $g \cdot mol^{-1}$ led to the formation of pores with diameter and center-to-center distances of 10 nm and 20 nm, respectively, after incorporation of LiCl. Block copolymers using PEO with a molecular weight of 750 $g \cdot mol^{-1}$ completely dewet during annealing, even after complexing with high ratios of LiCl.

7.2 INTRODUCTION

Block copolymers have been used to prepare highly ordered nanoscale domains upon self-assembly and can be utilized in the "bottom-up" fabrication of nanoengineered materials and devices.[1] The molecular characteristics of block copolymers dictate the self-assembly process and are critical in the formation of well-defined nanostructures.[2] These microphase separated structures are mostly dictated by three experimental parameters: the degree of polymerization (N), the volume fraction of the blocks (f), and

the Flory–Huggins interaction parameter (χ).[3-5] The chemical nature of the block segments determines χ, which in turn describes the segment-segment interactions. The emerging role of block copolymer lithography in the fabrication of various devices has led to significant challenges in the creation of small features with a high degree of order.[6] Smaller feature size, uniform porous films, faster processing time, and long-range order are a few of the main requirements demanded by the nanotechnology industry as outlined in the International Technology Roadmap for Semiconductors.[7-9] The feature sizes of self-assembled nanodomains is directly influenced by the molecular weight (N) of block copolymers. There, decreasing the molecular weight N would reduce feature sizes. However, there is a limit as to how low the molecular weight a linear block copolymer for a given block copolymer system can be before it passes the order-disorder transition (ODT) and is incapable of forming microphase separated structures.

It has been well demonstrated that poly(ethylene oxide)-*block*-polystyrene (PEO-*b*-PS) can form long-range ordered nanostructures in thin films through a solvent annealing process under controlled humidity.[10] Hexagonally-packed cylinders of PEO in a matrix of PS can align perpendicular to the surface when the volume fraction of PEO is between 0.15-0.35. Traditionally, removing the minor PEO cylindrical domains to obtain nanoporous films has been problematic, as harsh, acidic conditions have typically been required.[11, 12] Sacrificial blocks in block copolymers have been used to prepare nanoporous films after degrading the middle block.[7] However, the preparation of well-defined block copolymers is time consuming and limited to degradable polymers. More recently, incorporation of degradable functional groups at the junction between the two blocks has been realized as a more efficient method of cleaving block copolymers. Trityl

ethers, disulfides, acetals, hydrazones, metallo-supramolecular, and ionic linkages have been utilized at the junction between diblock copolymer PEO-*b*-PS to form nanoporous films.[13-21] However, most of these techniques either involve acidic conditions or long soaking times (> 4 days) in order to degrade or rearrange the linker and remove the PEO cylindrical domain.

Recently, block copolymers PEO-*hv*-b-PS with *ortho*-nitrobenzyl (ONB) photocleavable linkers (*hv*) have been prepared.[22-26] Upon self-assembly, thin films of these block copolymers were exposed to UV irradiation to rearrange the ONB linker and effectively cleave the PS and PEO blocks. Nanoporous PS films were obtained upon washing away the cylindrical PEO domain with water or methanol. In early reports, the degree of ordering was somewhat limited, as grain sizes of less than 0.1 μm^2 were obtained. A recent report utilizing PEO-*hv*-*b*-PS was capable of obtaining highly ordered nanoporous arrays.[24] The average diameter and pitch of the pores were ~20 nm and ~40 nm, respectively.

In this work we have prepared highly ordered nanoporous thin film based on PEO-*hv*-*b*-PS diblock copolymers in which there is an ONB linker between the two blocks. Commercially available PEOs were first modified to contain an ONB unit. Subsequently, well defined PEO-*hv*-*b*-PS diblock copolymers were prepared by atom transfer radical polymerization (ATRP). Highly ordered nanoporous thin films were obtained through solvent annealing and photodegradation of the ONB junction. Furthermore, we have decreased the total molecular weight of the block copolymer systems in order to decrease both the diameter and spacing of the nanopores. A minimum total molecular weight was realized that allowed for microphase separation of

linear PEO-*b*-PS diblock copolymers. This work represents the highest density of ordered nanoporous thin films prepared from linear PEO-*b*-PS diblock copolymers to date.

7.3 EXPERIMENTAL

Materials. All reagents were purchased from Alfa Aesar and Aldrich and used as received unless otherwise noted. Styrene was distilled before use. Tetrahydrofuran (THF) and dimethylformamide (DMF) were dried over molecular sieves and distilled before use.

Characterization. ^{1}H NMR (300 MHz) and ^{13}C NMR (100 MHz) spectra were recorded on a Varian Mercury 300 spectrometer with tetramethylsilane (TMS) as an internal reference. Gel permeation chromatography (GPC) was performed at 30 ^{o}C on a Waters system equipped with a 515 HPLC pump, a 2410 refractive index detector, and three Styragel columns (HR1, HR3, HR4 in the effective molecular weight range of 100–5000 g·mol^{-1}, 500–30,000 g·mol^{-1}, and 5000–500,000 g·mol^{-1}, respectively). HPLC grade THF was used as eluent at a flow rate of 1.0 mL/min. Polystyrene standards were used for calibration. Mass spectrometry was carried out on a Waters Micromass Q-Tof mass spectrometer, with a positive ion electrospray as the ionization source. UV-vis spectroscopy was carried out on a Shimadzu UV-2450 spectrophotometer, scanning monochromatic light in the range of 190-900 nm. A quartz cuvette with a path length of 10.00 mm was used, and the solvent was dimethylformamide (DMF). FTIR spectra were recorded on a PerkinElmer Spectrum 100 FTIR spectrometer equipped with a Universal ATR sampling accessory.

α-Methoxy-ω-toluenesulfonyl-PEO (PEO-OTs, 2). PEO-OH (1 eq.) was dissolved in 20 mL dry THF, purged with nitrogen, and cooled to 0°C. Triethylamine (25 eq.) was then added and the solution was stirred for 15 minutes. A solution of 4-toluenesulfonyl chloride (25 eq.) in dry THF (10 mL) was added dropwise to the reaction mixture. After stirring at 0°C for 30 minutes, the solution was stirred at room temperature overnight. The solvent was then removed by rotary evaporation. The solids were dissolved in DCM and extracted with deionized H_2O twice. The aqueous layers were combined and extracted with DCM three times. The organic layers were combined, dried over anhydrous sodium sulfate, filtered, concentrated, and precipitated into diethyl ether two times. The resulting white powder was collected by filtration and vacuum dried (~90% yield). ^{1}H NMR (CD_2Cl_2), δ (TMS, ppm): 7.78 (dd, 2H, Ar*H*), 7.34 (dd, 2H, Ar*H*), 4.15 (t, 2H, -C*H*$_2$SO$_2$Ar-), 3.47-2.77 (br, , -C*H*$_2$C*H*$_2$-), 2.45 (ArC*H*$_3$).

PEO-*hv*-OH (3). Sodium hydride (5 eq.) was suspended in 30 mL dry THF and the reaction flask was purged with nitrogen. A solution of 5-hydroxy-2-nitrobenzyl alcohol (4 eq.) in dry THF (10 mL) was slowly added to the reaction flask and stirred for 15 minutes. PEO-OTs (1 eq.) in dry THF (10 mL) was then added dropwise to the reaction flask, stirred at room temperature for 15 minutes and refluxed overnight. After cooling the solution to room temperature, the reaction was quenched by the addition of 10 mL deionized H_2O. The reaction workup was similar to that for product **2**. (3.7 g, 93% yield). ^{1}H NMR (CD_2Cl_2), δ (TMS, ppm): 8.20 (dd, 1H, Ar*H*), 7.42 (s, 1H, Ar*H*), 6.95 (dd, 1H, Ar*H*), 4.92 (s, 2H, ArC*H*$_2$OH), 4.25 (t, 2H, -C*H*$_2$OAr-), 3.47-2.77 (br, -C*H*$_2$C*H*$_2$-).

PEO-*hv*-Br (4). PEO-*hv*-OH (1 eq.) and 4-dimethylaminopyridine (DMAP, 0.020 g, 0.16 mmol) were added to a 100 mL round bottom flask equipped with a stir bar and purged with nitrogen. Dry dichloromethane (50 mL) was added and the reaction mixture was stirred until all the solids dissolved. The reaction mixture was then cooled to 0^{o}C before triethylamine (4 eq.) was added. A solution of 2-bromoisobutyryl bromide (4 eq.) in dry dichloromethane (15 mL) was added dropwise to the cooled solution. The solution was stirred at 0^{o}C for 30 minutes, then at room temperature overnight. The reaction was then quenched by the addition of deionized H_2O (10 mL). The reaction workup was similar to that for product **2**. (~90% yield). ^{1}H NMR (CD_2Cl_2), δ (TMS, ppm): 8.20 (dd, 1H, Ar*H*), 7.42 (s, 1H, Ar*H*), 6.95 (dd, 1H, Ar*H*), 5.61 (s, 2H, ArC*H*$_2$OC(O), 4.25 (t, 2H, -C*H*$_2$OAr-), 3.47-2.77 (br, -C*H*$_2$C*H*$_2$-), 1.98 (s, 6H, C(O)(C*H*$_3$)$_2$Br.

PEO-*hv*-*b*-PS (5). Copper (I) bromide (1 eq.) was charged in a 10 mL schlenk line flask and purged with nitrogen. PEO-*hv*-Br (1 eq.), styrene (*x* eq.), and N,N,N',N'',N''-pentamethyldiethylenetriamine (PMDETA, 1.5 eq.) were added to a 5 mL pearl shaped flask, degassed by bubbling nitrogen through the solution for 20 minutes, and transferred to the schlenk line flask. The solution was then allowed to stir at room temperature for 20 minutes before a sample was taken for NMR analysis. The schlenk line flask was then added to an oil bath preheated to 90^{o}C. The polymerization was monitored by proton NMR and the reaction was stopped at the desired monomer conversion by cooling in an ice bath and then diluting the solution with THF. The solution was then precipitated into methanol twice. The solid white product was

collected by filtration and vacuum dried. ^{1}H NMR (CD_2Cl_2), δ (TMS, ppm): 6.02-7.38 (br, Ar*H*), 3.47-2.77 (br, -C*H*$_2$C*H*$_2$-), 1.02-2.26 (br, -C*H*$_2$C*H*-).

Preparation of Thin Films. The PEO-*hv*-*b*-PS diblock copolymers were spin-coated (3000 RPM, 60 s) from toluene solutions (1.5 wt%) onto silicon substrates that were coated with a 100 nm thick SiO_2 layer. The thin films were then annealed overnight under a saturated toluene atmosphere before being exposed to a high relative humidity (>85%) atmosphere for 15 minutes.

7.4 Results and Discussion

Poly(ethylene oxide) (PEO) ATRP macroinitiators containing an *ortho*-nitrobenzyl (ONB) groups were prepared using PEOs with molecular weights of 5000, 2000, and 750 Da. The synthetic route is shown in Scheme 7.1, and follows a previously reported route which utilized a PEO with molecular weight of 5000 Da. The hydroxy end-group of commercially available poly(ethylene glycol) monomethyl ethers (**1a-c**) were converted into α-methoxy-ω-toluenesulfonyl-PEO (PEO-OTs, **2**) in >90% yield by reaction with 4-toluenesulfonyl chloride. The products were analyzed by proton NMR (Figure 7.1), FTIR (Figure 7.2), and GPC (Table 7.1). Successful attachment of the tosyl group was evident by the appearance of signature tosyl protons including two doublet aromatic signals at 7.34 and 7.78 ppm and a singlet signal (-ArOC*H*$_3$) at 2.45 ppm in the proton NMR. The appearance of a triplet at 4.15 ppm correlates to the methylene group adjacent to the tosyl group (-C*H*$_2$SO$_2$Ar-), which is further evidence that the polymer chain end reacted. FTIR showed the disappearance of the hydroxy functional group (3200-3700 cm^{-1}), confirming reaction of the terminal hydroxy group.

Scheme 7.1. Synthesis of diblock copolymer PEO-*hv*-*b*-PS.

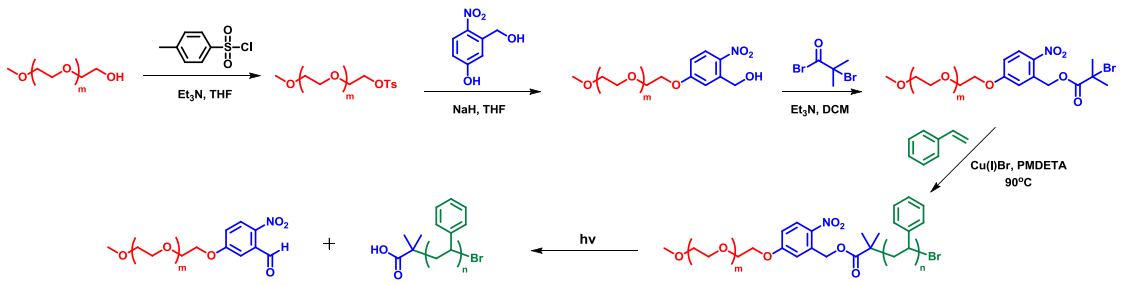

A substitution reaction of 5-hydroxy-2-nitrobenzyl alcohol and PEO-OTs (**2a-c**) introduced the ONB group onto one end of the PEO chain, resulting in polymers PEO-*hv*-OH (**3a-c**) in > 90% yield. Compounds **3a-c** were also analyzed by proton NMR (Figure 7.1), FTIR (Figure 7.2), and GPC (Table 7.1). The complete disappearance of all three tosyl proton signals, the appearance of three new aromatic signals at 8.20, 7.42, and 6.95 ppm (Ar-H), and the appearance of a singlet at 4.92 ppm (ArCH_2OH) suggests the successful displacement of the tosyl group with the ONB group. Furthermore, the polymer end-chain methylene protons shifted from 4.15 to 4.25 ppm (-CH_2OAr), displaying a change in chemical environment from adjacent to the tosyl group to adjacent to the ONB group.

Finally, ATRP macroinitiators **4a-c** were prepared by reacting the primary alcohol of PEO-*hv*-OH (**3a-c**) with 2-bromoisobutyryl bromide in the presence of triethylamine. Characterization by proton NMR (Figure 7.1), FTIR (Figure 7.2), and GPC (Table 7.1) confirmed the products. The singlet corresponding to the methylene protons that were adjacent to the hydroxy group (ArCH_2OH, 4.92 ppm) shifted downfield to 5.61 ppm as the ester formed in products **4a-c**. Additionally, a singlet at 1.98 ppm (C(O)(CH_3)$_2$Br)

appeared corresponding to the methyl groups of the tertiary alkyl halide. A carbonyl stretch in the FTIR spectra at 1690 cm^{-1} confirmed the ester formation.

Chain extension of ATRP macroinitiators **4a-c** with styrene using Cu(I)Br and PMDETA at 90^{o}C was monitored by proton NMR. Samples were taken throughout the polymerizations and the monomer conversion was obtained by calculating the decrease in styrene monomer signals at 5.74 and 5.22 ppm as compared to the PEO backbone protons at 3.47-3.77 ppm. The chain extension was stopped at the desired monomer conversion and precipitated into methanol twice to remove any remaining monomer and copper catalyst. The degree of polymerization of PS was determined by proton NMR by comparing the aromatic signals from PS (6.02-7.38 ppm) with the methylene protons from PEO (3.47-2.77 ppm). The GPC traces for copolymers **5a-c** showed clean shifts from macroinitiators **4a-c** with a low PDIs (<1.25). The polymer compositions are given in Table 7.1.

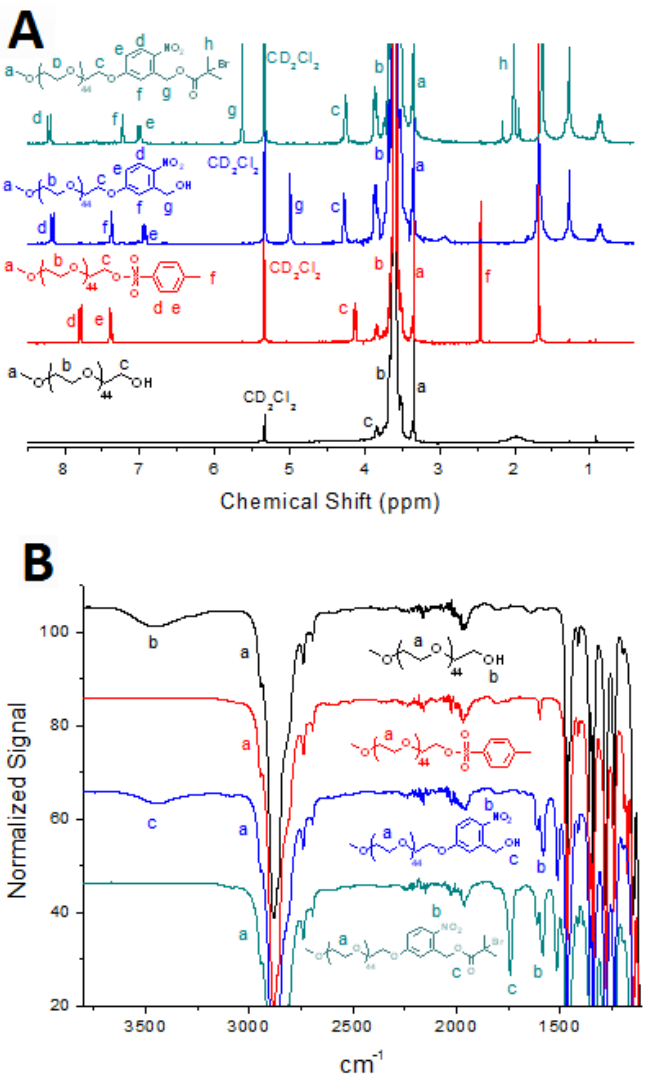

Figure 7.1. ^{1}H NMR spectra (**A**) and FT-IR spectra (**B**) of polymers **1b**-**4b**.

1.5 wt% solutions of block copolymers **5a-g** in toluene were spin-coated onto silicon substrates. The thin films were then annealed in a saturated toluene atmosphere for 7 hours before being exposed to a high humidity (>85% RH) atmosphere. The annealed thin films were characterized by AFM. Hexagonally packed cylinders with long-range order (>3x3 μm^2) were obtained for block copolymer **5a**, which contained PEO with molecular weight of 5000 Da (MW_{total}=23100 $g \cdot mol^{-1}$, 21.6 wt% PEO). The

average diameter and center-to-center distance for the solvent annealed film of polymer **5a** was 22 nm and 32 nm, respectively, as seen in Figure 7.2A. Block copolymer **5b**, which contains PEO with molecular weight of 2000 Da and a total molecular weight of 18600 g·mol^{-1} (10.7 wt% PEO) also formed highly ordered films with average diameter and center-to-center distance of 10 nm and 28 nm, respectively (Figure 7.2B). The low weight percent of PEO and the appearance of local domains of square packing suggested that the morphology consisted of body centered cubic packed spheres of PEO in a matrix of PS.[8] Polymers **5c** (MW_{PEO}=2000, MW_{total}=9600, 20.9 wt% PEO) and **5e** (MW_{PEO}=750, MW_{total}=2950, 25.4 wt% PEO) resulted in disorganized or dewet films after annealing.

Previous reports utilizing solvent annealing of PEO-*b*-PS diblock copolymers with low total molecular weights also observed no microphase separation after annealing.[2, 27] This is due to the dependence of microphase separation on the product of the Flory-Huggins interaction parameter and the total molecular weight (χN). For PEO-*b*-PS systems, χ can be determined by equation 1:

$$\chi_{PS\text{-}b\text{-}PEO} = -0.007 + 21.3/T \qquad \text{(Equation 1)}$$

where T is the temperature. For polymer **5a** (MW_{total}=23100 g·mol^{-1}) and **5b** (MW_{total}=18600 g·mol^{-1}), $\chi N \sim 21.2$ and 17.1, respectively, and well-defined microphase separated structures are formed after annealing. However, for polymers **5c** (MW_{total}=9600 g·mol^{-1}) and **5e** (MW_{total}=2950 g·mol^{-1}), $\chi N \sim 8.8$ and 2.71, respectively, no microphase separation is observed after annealing. This agrees with a previous report, as weak microphase separated structures were observed for a PEO-*b*-PS polymer with $\chi N \sim 16.8$ and no microphase separated structures were observed when $\chi N \sim 10.1$.[27] In

previous reports, increasing the segregation strength, χ, was achieved by complexing the ether linkages in the PEO domain with a salt additive (LiCl).[2, 27] This resulted in apparent increase in χ by the formation of highly ordered microphase separated films after solvent annealing. Similar to these previous reports, polymers **5c** and **5e** were complexed with LiCl to increase the segregation strength of the low molecular weight block copolymers.

Table 7.1. Compositions of polymers **5a-g**.

Polymer Entry	M_n PEO	M_n PS[a]	PDI[b]	M_n PS[c]	Wt. % PEO	[O]:[Li][d]	χN[e] (Bulk)
5a	5000	19000	1.21	18100	21.6%	--	21.2
5b	2000	16900	1.25	16600	10.7%	--	17.1
5c	2000	9000	1.26	7600	20.9%	--	8.8
5d	2000	9000	--	7600	20.9%	0.03	>10.5
5e	750	2600	1.18	2200	25.4%	--	2.71
5f	750	2600	--	2200	25.4%	0.03	2.71<x<10.5
5g	750	2600	--	2200	25.4%	0.125	2.71<x<10.5

[a]Determined by ^{1}H NMR. [b]Determined from GPC before photoexposure, calibrated by PS standards. [c]Determined from GPC after photoexposure, calibrated by PS standards. [d]Ratio of repeat units of ethylene oxide to LiCl. [e]Calculated from Equation 1.

When polymer **5c** was complexed with LiCl in a molar ratio of [O]:[Li+]=1:0.03, highly ordered films were observed after solvent annealing (polymer **5d**, Figure 7.2C). Similar to previous reports detailing the solvent annealing conditions for higher molecular weight PEO-*b*-PS systems, there was a direct correlation between the humidity

level during annealing and the direction of ordering in the microphase separated films. When the humidity level was above 70%, highly ordered perpendicular cylinders were formed, as seen in Figure 7.2C. The diameter and center-to-center distances for the perpendicular cylinders were 10 nm and 20 nm, respectively. When the humidity level was below 70%, parallel cylinders were formed, as seen in Figure 7.2D. The average widths of the cylinders were 10 nm with an average center-to-center distance of 20 nm. We were unable to obtain any microphase separated films after annealing polymer **5e** (MW_{total}=2950 g·mol^{-1}), even after complexing with LiCl in ratios as high as 1:0.125 (Polymers **5e-f**), as macrophase separation left completely dewet films after annealing.

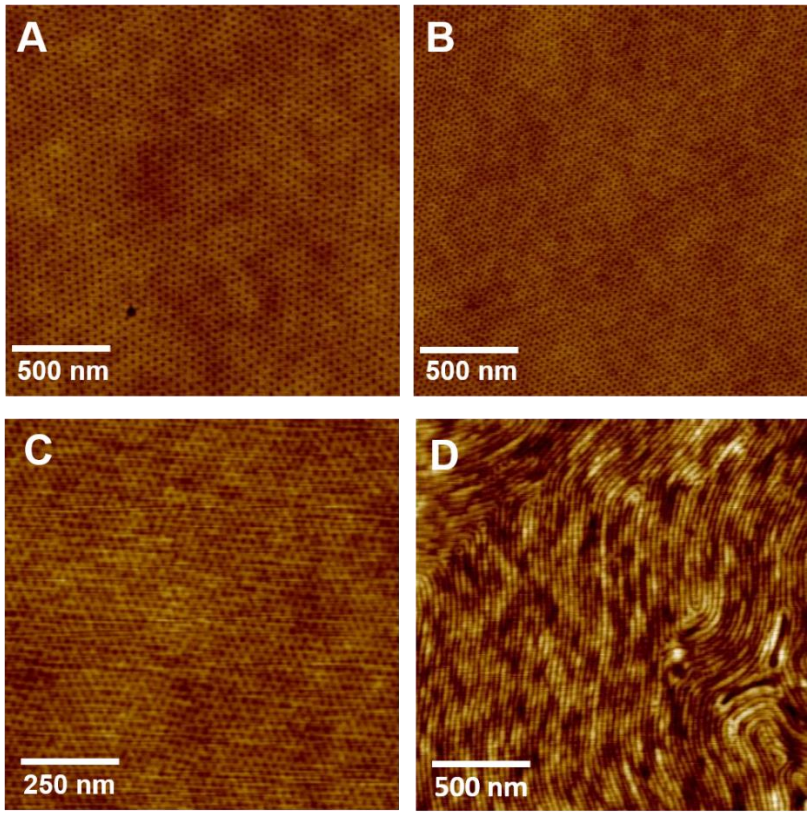

Figure 7.2. AFM images of microphase separated films after high humidity (90% RH) solvent annealing of polymers **5a** (**A**), **5b** (**B**), and **5d** (**C**). AFM image of microphase separated film after low humidity (50% RH) of polymer **5d** (**D**).

In order to determine a sufficient amount of ultraviolet light exposure time degrade the photocleavable ortho-nitrobenzyl (ONB) linker, an experiment was carried out in which block copolymer **5a** was cast in a small vial and exposed to ultraviolet light. The polymer was dissolved in dichloromethane and the absorption properties were studied by UV-Vis after each dose of photoexposure. A medium wavelength lamp (308 nm) was used, as the ONB has high absorption between 300-325 nm. As the *ortho*-nitrobenzyl group rearranges to an *ortho*-nitrosobenzaldehyde group, the absorption band at 310 nm decreases and a new band at 350 nm appears, as seen in Figure 7.3. After 16 minutes of exposure, the band at 310 nm reached a minimum and the band at 350 nm reached a maximum, suggesting complete rearrangement of the ONB moiety. At this point, the photoirradiated polymer **5a** was evaluated with GPC. The diblock copolymer PEO-*hv*-*b*-PS (polymer **5a**) before and after photoexposure are shown in Figure 7.4. After photoexposure, a monomodal polymer species was observed, which has a lower molecular weight than before photoexposure. The molecular weight of the lower molecular weight peak after photoexposure matches the molecular weight of the PS obtained by NMR analysis for diblock copolymer **5a**, as shown in Table 7.1. Clearly, after photoexposure, the diblock copolymer **5a** is cleaved at the ONB junction, yielding homopolymers PEO and PS.

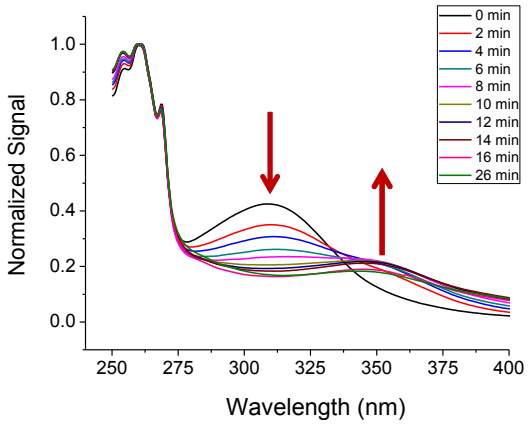

Figure 7.3. UV-Vis spectra of photocleavable polymer **5a** as a function of exposure time.

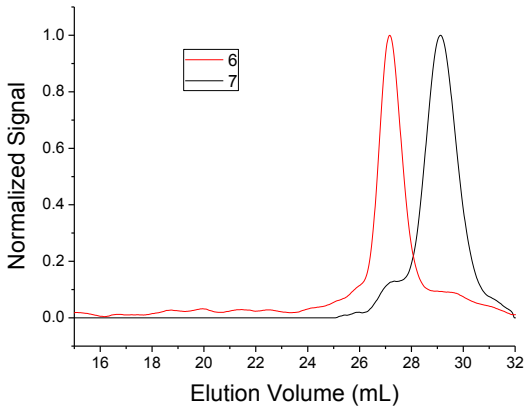

Figure 7.4. GPC traces of polymer **5a** before (**A**) and after (**B**) 26-minute photoexposure.

To prepare highly ordered nanoporous films, the ordered PEO-*hv*-*b*-PS films were exposed to ultraviolet light for 30 minutes. After soaking in diluted acetic acid for 5 minutes, the films were dipped in water, ethanol, and finally dried before imaged by AFM. The films from block copolymers **5a** and **5d** remained highly ordered, as seen in Figure 7.5. Similar to the films before photoexposure and washing, the average diameter and center-to-center distances for nanoporous films of polymer **5a** were 22 nm and 32 nm, respectively. The average diameter and center-to-center distances for nanoporous films of polymer **5d** were 10 nm and 20 nm, respectively. To ensure that the ONB

moiety was cleaved and the PEO cylinder was washed away, top-down and cross-sectional SEM was carried out for polymers **5a** and **5d**. Before photoexposure and washing of polymer **5a**, no features could be seen by SEM. After photoexposure and washing, highly ordered arrays of nanopores were observed by top-down SEM for polymer **5a** (Figure 7.5c). To prove that the nanopore continued through the entire film, cross-sectional SEM was performed. Figures 7.5d (polymer **5a**) and 7.5e (polymer **5d**) clearly show that the films contain nanopores that span through the entire film for PEO-*hv*-*b*-PS polymers after annealing, photoexposure, and washing. Nanoporous films originating from polymer **5d** represent the smallest reported highly ordered hexagonal arrays of pores in thin films resulting from PEO-based block copolymers.

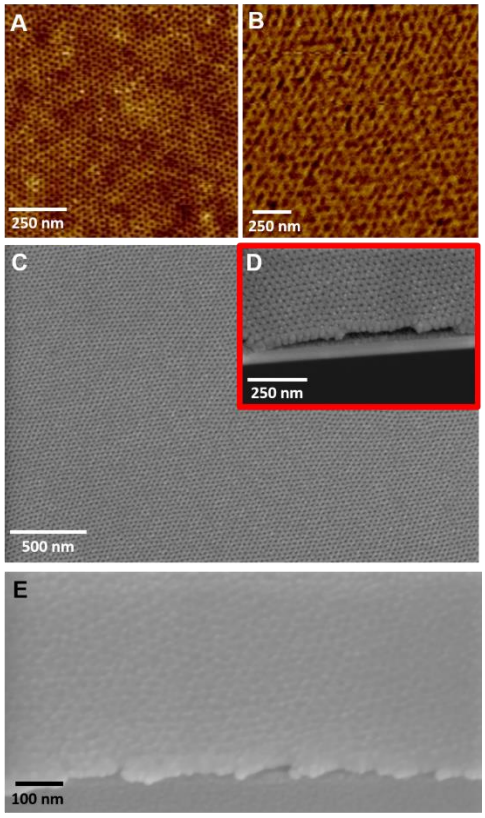

Figure 7.5. AFM phase images of nanoporous films resulting from polymer **5a** (**A**) and **5d** (**B**). Top-down (**C**) and cross-sectional SEM images (45°, **D, E**) of nanoporous films from polymer **5a** (**C, D**) and **5d** (**E**).

7.5 Conclusion

In conclusion, we prepared highly dense, ordered nanoporous films using low molecular weight PEO-*b*-PS diblock copolymers that had an ortho-nitrobenzyl (ONB) photocleavable linker between the blocks. Through use of low molecular weight blocks copolymers complexed with LiCl, microphase separation was observed after solvent annealing. Nanopores spanning through the polymer film were observed with diameter and center-to-center distances of 10 nm and 20 nm, respectively.

7.5 Acknowledgements

This work was supported by the Global Research Collaboration Program of Semiconductor Research Corporation (Task ID 2222.001).

7.6 References

1. Lu, W.; Lieber, C. M. *Nat. Mater.* **2007,** 6, 841-850.
2. Kim, H.-C.; Park, S.-M.; Hinsberg, W. D. *Chem. Rev.* **2009,** 110, 146-177.
3. Bates, F. S.; Fredrickson, G. H. *Phys. Today* **1999,** 52, 32-38.
4. Bates, F. S.; Fredrickson, G. H. *Annu. Rev. Phys. Chem.* **1990,** 41, 525-557.
5. Fredrickson, G. H.; Bates, F. S. *Annu. Rev. Mater. Sci.* **1996,** 26, 501-550.
6. Stoykovich, M. P.; Müller, M.; Kim, S. O.; Solak, H. H.; Edwards, E. W.; de Pablo, J. J.; Nealey, P. F. *Science* **2005,** 308, 1442-1446.
7. Bang, J.; Kim, S. H.; Drockenmuller, E.; Misner, M. J.; Russell, T. P.; Hawker, C. J. *J. Am. Chem. Soc.* **2006,** 128, 7622-7629.
8. Tang, C.; Lennon, E. M.; Fredrickson, G. H.; Kramer, E. J.; Hawker, C. J. *Science* **2008,** 322, 429-432.
9. Ryu, D. Y.; Ham, S.; Kim, E.; Jeong, U.; Hawker, C. J.; Russell, T. P. *Macromolecules* **2009,** 42, 4902-4906.
10. Kim, S. H.; Misner, M. J.; Russell, T. P. *Adv. Mater.* **2004,** 16, 2119-2123.
11. Rzayev, J.; Hillmyer, M. A. *Macromolecules* **2004,** 38, 3-5.
12. Rzayev, J.; Hillmyer, M. A. *J. Am. Chem. Soc.* **2005,** 127, 13373-13379.
13. Yu, H.; Stoffelbach, F.; Detrembleur, C.; Fustin, C.-A.; Gohy, J.-F. *Eur. Polym. J.* **2012,** 48, 940-944.
14. Satoh, K.; Poelma, J. E.; Campos, L. M.; Stahl, B.; Hawker, C. J. *Polym. Chem.* **2012,** 3, 1890-1898.
15. Glassner, M.; Blinco, J. P.; Barner-Kowollik, C. *Polym. Chem.* **2011,** 2, 83-87.
16. Ryu, J.-H.; Park, S.; Kim, B.; Klaikherd, A.; Russell, T. P.; Thayumanavan, S. *J. Am. Chem. Soc.* **2009,** 131, 9870-9871.
17. Rao, J.; Khan, A. *Polym. Chem.* **2013,** 4, 2691-2695.

18. Mugemana, C.; Gohy, J.-F.; Fustin, C.-A. *Langmuir* **2012,** 28, 3018-3023.
19. Rao, J.; De, S.; Khan, A. *Chem. Commun.* **2012,** 48, 3427-3429.
20. Goldbach, J. T.; Russell, T. P.; Penelle, J. *Macromolecules* **2002,** 35, 4271-4276.
21. Goldbach, J. T.; Lavery, K. A.; Penelle, J.; Russell, T. P. *Macromolecules* **2004,** 37, 9639-9645.
22. Kang, M.; Moon, B. *Macromolecules* **2008,** 42, 455-458.
23. Schumers, J.-M.; Gohy, J.-F.; Fustin, C.-A. *Polym. Chem.* **2010,** 1, 161-163.
24. Zhao, H.; Gu, W.; Sterner, E.; Russell, T. P.; Coughlin, E. B.; Theato, P. *Macromolecules* **2011,** 44, 6433-6440.
25. Gamys, C. G.; Schumers, J.-M.; Vlad, A.; Fustin, C.-A.; Gohy, J.-F. *Soft Matter* **2012,** 8, 4486-4493.
26. Schumers, J.-M.; Vlad, A.; Huynen, I.; Gohy, J.-F.; Fustin, C.-A. *Macromol. Rapid Commun.* **2012,** 33, 199-205.
27. Xu, J.; Hong, S. W.; Gu, W.; Lee, K. Y.; Kuo, D. S.; Xiao, S.; Russell, T. P. *Adv. Mater.* **2011,** 23, 5755-5761.

CHAPTER 8

HIGH QUALITY FILMS WITH SUB-10 NM FEATURE SIZES UTILIZING GRAFTED BLOCK COPOLYMERS

8.1 ABSTRACT

This chapter discusses the preparation of highly ordered microphase separated films utilizing a grafted block copolymer with PS-*b*-PEO diblock copolymers on the side-chain. High quality films with highly ordered nanostructures were obtained when the molecular weight of the side-chain block copolymer was extremely low. Previous studies utilizing linear diblock copolymer PS-*b*-PEO observed severe dewetting for low molecular weight systems. This problem is avoided in the grafted block copolymer system, as enhanced chain entanglement between adjacent polymer chains ensures a high quality film after annealing. Furthermore, the block copolymers on the side-chain dictate the feature sizes of the microphase separated films when the backbone length is kept low, as hexagonally packed cylinders of PEO in a matrix of PS with diameter and center-to-center distances of 10 and 20 nm, respectively, were possible.

8.2 INTRODUCTION

In the near future, the semiconductor industry will face a major hurdle in continuing to decrease the size of integrated circuit components, as the photolithographic techniques currently employed in complementary metal oxide semiconductor transistors are reaching their lower limit.[1] Block copolymer nanolithography is a promising

technique to drive further device miniaturization due to the nanometer-scale length size of structures obtained after self-assembly.[1, 2] However, significant challenges remain to be solved before block copolymer nanolithography can be realized as a practical solution to the semiconductor industries problems. Smaller feature size, uniform porous films, and long-range order are a few of the main requirements demanded by the nanotechnology industry as outlined in the International Technology Roadmap for Semiconductors.[1, 3-7] The size of the nanodomains after block copolymer self-assembly are ultimately defined by the molecular weight of block copolymer. Therefore, decreasing the molecular weight would reduce feature sizes. However, there is a limit as to how low the molecular weight of a linear block copolymer system (χ is constant for any given system) can be before it passes the order-disorder transition (ODT) and is incapable of forming microphase separated assemblies. Equally, block copolymers systems with a high χ can utilize lower molecular weight polymers before the ODT is reached. However, during the annealing phase, macroscopic phase separation occurs for low molecular weight linear block copolymers systems due to limited polymer chain entanglement.

Long-range order and orientational control has been achieved with A-B, A-B-A, A-B-C, or A-B/B'-C block copolymer systems through various processing strategies including topographical and chemical graphoepitaxy, external fields, temperature gradients, and solvent annealing.[1, 2, 8, 9] As discussed in the previous chapter, solvent annealing of poly(ethylene oxide)-*block*-polystyrene (PEO-*b*-PS) block copolymer systems is a fast and cheap technique which gives rise to long-range ordered nanostructures in thin films. However, for all linear block copolymers there exists vast

film dewetting during annealing of low molecular weight systems.[10] We recently found a lower molecular weight threshold for microphase separated films based on linear diblock copolymer PEO-*b*-PS.[10] Below a certain molecular weight, the polymer film would macroscopically dewet from the substrate during the solvent annealing process due to limited inter-chain entanglement of the linear block copolymer system.

Grafted block copolymers (or brush copolymers) have recently received much attention due to their ability to form nanostructures not possible from linear block copolymer systems.[11-19] The highly-dense side-chains and large cross-sectional areas inherent with grafting high molecular weight polymers from a common backbone limit the amount of intermolecular chain entanglement, and thus, spontaneously form wormlike or spherical conformations.[20-22] Such structures have been utilized as carriers for encapsulation and as templates for uniform nanoparticle preparation. Additionally, grafted block copolymers have been utilized to prepare microphase separated spherical, cylindrical, and lamellae structures with domain sizes above 100 nm, which have applications in photonics as optical materials.[23, 24] These grafted block copolymer systems typically have long backbones between 1000 – 2500 repeat units. The molecular weight of the side-chains are low, typically between 2,000 – 10,000 $g \cdot mol^{-1}$, ultimately resulting in extremely high molecular weight polymers, generally between 1,000,000 – 6,000,000 $g \cdot mol^{-1}$.

In this work, we have utilized grafted block copolymers in which the side-chains consist of low molecular weight PEO-*b*-PS diblock copolymers to prepare films with feature sizes *below* what is possible for the linear diblock copolymer analogues. By keeping the backbone length below 20 repeat units, the polymer system is not forced into

a wormlike conformation during self-assembly. While macrophase separation led to dewet films for linear diblock copolymers with the same molecular weight as the grafted copolymer side-chains, the grafted block copolymers system retained high quality films due to increased chain entanglement between adjacent polymer chains. Furthermore, the feature sizes of the microphase separated structures of the grafted block copolymer system was similar to those of the linear diblock copolymer analogues, suggesting that for grafted block copolymer systems with low backbone lengths, the block copolymer on the side-chain determines the feature sizes upon self-assembly.

8.3 EXPERIMENTAL

Materials. All reagents were purchased from Alfa Aesar and Aldrich and used as received unless otherwise noted. Styrene was distilled before use. Tetrahydrofuran (THF) and dimethylformamide (DMF) were dried over molecular sieves and distilled before use. Grubbs 3rd generation catalyst (G3), N-[3-Hydroxylpropyl]-*cis*-5-Norbornene-*exo*-2,3-Dicarboximide (NPH), and 5-hexynoic acid chloride were prepared according to previous reports.[25-27]

Characterization. ^{1}H NMR (300 MHz) and ^{13}C NMR (100 MHz) spectra were recorded on a Varian Mercury 300 spectrometer with tetramethylsilane (TMS) as an internal reference. Gel permeation chromatography (GPC) was performed at 30 ^{o}C on a Waters system equipped with a 515 HPLC pump, a 2410 refractive index detector, and three Styragel columns (HR1, HR3, HR4 in the effective molecular weight range of 100–5000 g·mol^{-1}, 500–30,000 g·mol^{-1}, and 5000–500,000 g·mol^{-1}, respectively). HPLC grade THF was used as eluent at a flow rate of 1.0 mL/min. Polystyrene standards were used for calibration. Mass spectrometry was carried out on a Waters Micromass Q-Tof mass

spectrometer, with a positive ion electrospray as the ionization source. FTIR spectra were recorded on a PerkinElmer Spectrum 100 FTIR spectrometer equipped with a Universal ATR sampling accessory.

Norbornene-terminated ATRP initiator (N-[3-propyl-2-bromo-2-methylproponate]-*cis*-5-Norbornene-*exo*-2,3-Dicarboximide, NP-Br, 2). NPH (**1**, 0.31 g, 1.4 mmol) was added to a 100 mL round bottom flask equipped with a stir bar and purged with nitrogen. Dry tetrahydrofuran (25 mL) was added and the reaction was cooled to 0^{o}C before triethylamine (0.39 mL, 2.8 mmol) was added. A solution of 2-bromoisobutyryl bromide (0.26 mL, 2.1 mmol) in dry tetrahydrofuran (15 mL) was added drop wise to the cooled solution. The solution was stirred at 0^{o}C for 30 minutes, then at room temperature overnight. The mixture was filtered and concentrated to dryness. The solids were then dissolved in either DCM or water. The DCM was extracted with deionized H_2O twice. The aqueous layers were combined and extracted with DCM three times. The organic layers were combined, dried over anhydrous sodium sulfate, filtered, concentrated, and the products were separated using column chromatography (silica gel, eluent: DCM). The product was collected, concentrated, and vacuum dried. Yield: 0.40 g, 76.9%. ^{1}H NMR (CD_2Cl_2), δ (TMS, ppm): 6.30 (s, 2H, C*H*=C*H*), 4.15 (t, 2H, $CH_2CH_2OC(O)$), 3.59 (t, 2H, NCH_2CH_2), 3.33 (s, 2H, C*H*C(O)N), 2.69 (s, 2H, CH_2CH), 1.88-2.08 (m, 8s, $CH_2CH_2CH_2$ + $(CH_3)_2C(O)$), 1.51 and 1.23 (dd, 2H, CH_2CH). ^{13}C NMR (CD_2Cl_2), δ (TMS, ppm): 177.7 (*C*ON), 171.3 (*C*(O)O), 137.7 (*C*H=*C*H), 63.2 ($CH_2CH_2OC(O)$), 56.2 ($C(CH_3)_2Br$), 47.8 ($CH_2CHCHCO$), 45.2 ($CH_2CHCHCO$), 42.7 ($CH_2CHCHCO$), 35.2 (NCH_2CH_2), 30.5 ($C(CH_3)_2Br$), 26.8 (NCH_2CH_2). FTIR (cm^{-1}): 2980, 1760, 1690, 1465, 1440, 1390, 1340, 1110, 1170, 890, 720.

Bromine-terminated NP-polystyrene (NP-PS-Br, 3). Copper (I) bromide (1 eq.) was charged into a 10 mL schlenk line flask and purged with nitrogen. NP-Br (**2**, 1 eq.), styrene (*n* eq.), and N,N,N',N'',N''-pentamethyldiethylenetriamine (PMDETA, 1.5 eq.) were added to a 5 mL pearl shaped flask, degassed by bubbling nitrogen through the solution for 20 minutes, and transferred to the schlenk line flask. The solution was then allowed to stir at room temperature for 20 minutes before a sample was taken for NMR analysis. The schlenk line flask was then added to an oil bath preheated to 90°C. The polymerization was monitored by proton NMR and the reaction was stopped at the desired monomer conversion by cooling in an ice bath and then diluting the solution with THF. The solution was then precipitated into methanol twice. The solid white product was collected by filtration and vacuum dried. ^{1}H NMR (CD_2Cl_2), δ (TMS, ppm): 6.35-7.33 (br, Ar*H*), 6.30 (s, 2H, C*H*=C*H*), 3.59 (t, 2H, NCH_2CH_2), 3.33 (s, 2H, C*H*C(O)N), 2.69 (s, 2H, CH_2C*H*), 1.0-2.4 (br, -CH_2C*H*-). FTIR (cm^{-1}): 3090, 3050, 3020, 2960, 2840, 1700, 1590, 1490, 1460.

Azide-terminated NP-polystyrene (NP-PS-N_3, 4). The terminal bromine groups were converted to azide groups through reaction with NaN_3 in DMF as previously reported.[27] ^{1}H NMR (CD_2Cl_2), δ (TMS, ppm): 6.35-7.33 (br, Ar*H*), 6.30 (s, 2H, C*H*=C*H*), 3.59 (t, 2H, NCH_2CH_2), 3.33 (s, 2H, C*H*C(O)N), 2.69 (s, 2H, CH_2C*H*), 1.0-2.4 (br, -CH_2C*H*-). FTIR (cm^{-1}): 3090, 3050, 3020, 2960, 2840, 2100, 1700, 1590, 1490, 1460.

Alkyne-terminated poly(ethylene oxide) (PEO-alkyne, 5). Polyethylene glycol monomethyl ether (1 equiv.) was dissolved in 30 mL dry THF and the flask was purged with nitrogen. Triethylamine (1.5 equiv.) was added and the solution was cooled to 0 °C.

A solution of 5-hexynoic acid chloride (1.5 equiv.) in 10 mL dry THF was added over 30 minutes. After stirring at room temperature overnight, the reaction mixture was filtered and concentrated to dryness. The solids were dissolved in dichloromethane and extracted with water twice. The aqueous layers were combined and extracted with dichloromethane three times. The organic layers were combined and stirred over anhydrous sodium sulfate. The solution was filtered, concentrated, and precipitated into diethyl ether three times. The product was collected by centrifuge and vacuum dried. ^{1}H NMR (CD_2Cl_2), δ (TMS, ppm): 4.22 (t, 2H, $CH_2CH_2COC(O)$), 3.4-3.8 (m, -OCH_2CH_2-), 3.35 (s, 3H, -OCH_3), 2.48 (t, 2H, $C(O)CH_2CH_2$), 2.25 (td, 2H, $CH_2CH_2C\equiv CH$), 2.02 (t, 1H, $C\equiv CH$), 1.84 (quin, 2H, $CH_2CH_2CH_2$). FTIR (cm^{-1}): 3290, 3070, 2880, 1710, 1450, 1290.

Norbornene-terminated diblock copolymer PS-*b*-PEO (NP-*g*-(PS-*b*-PEO), 6). Cu(I)Br (0.1 equiv.) was charged into a round bottom flask and purged with nitrogen. PEO-alkyne (**5**, 2 equiv.), NP-PS-N_3 (**4**, 1 equiv.), and PMDETA (0.15 equiv.) were added to a pear shaped flask, dissolved in THF, and bubbled with nitrogen for 30 minutes. The mixture in the pear shaped flask was transferred to the round bottom flask and stirred at 40 ^{o}C overnight. The reaction mixture was then concentrated to dryness, dissolved in dichloromethane, and extracted with water three times. The organic layer was dried over anhydrous sodium sulfate, filtered, and concentrated. The solution was then precipitated into methanol two times. The product was collected by centrifuge and vacuum dried overnight. ^{1}H NMR (CD_2Cl_2), δ (TMS, ppm): 6.35-7.33 (br, Ar*H*), 6.30 (s, 2H, C*H*=C*H*), 4.22 (t, 2H, $CH_2CH_2COC(O)$), 3.4-3.8 (m, -OCH_2CH_2-), 3.35 (s, 3H, -

OC*H*$_3$), 2.69 (s, 2H, CH_2CH), 2.48 (t, 2H, C(O)C*H*$_2$CH$_2$), 1.0-2.4 (br, -C*H*$_2$C*H*-). FTIR (cm^{-1}): 3090, 3050, 3020, 2960, 2840, 1700, 1590, 1490, 1460.

Grafted block copolymer poly(norbornene-graft-(PS-*b*-PEO)) (PNP-*g*-(PS-*b*-PEO), 7). Grubbs 3rd generation catalyst (1 equiv.) and anhydrous DMF (1 mL) were added to a schlenk line flask and bubbled with nitrogen for 10 minutes. NP-*g*-(PS-*b*-PEO) (**6**, *p* equiv.) was added to a pear shaped flask, dissolved in DMF (4 mL), and bubbled with nitrogen for 10 minutes. The mixture in the pear shaped flask was transferred to the schlenk line flask and stirred at 600 ^{o}C. The polymerization was monitored by GPC and terminated by addition of ethyl vinyl ether (5 equiv.) when all macromonomer **6** was consumed. The reaction mixture was precipitated into diethyl ether two times. The solid product was collected by centrifuge and vacuum dried overnight. ^{1}H NMR (CD_2Cl_2), δ (TMS, ppm): 6.35-7.33 (br, Ar*H*), 5.42 and 5.60 (br, C*H*=C*H*), 4.22 (br, $CH_2CH_2COC(O)$), 3.4-3.8 (m, -OC*H*$_2$C*H*$_2$-), 3.35 (br, -OC*H*$_3$), 2.69 (br, CH_2CH), 2.48 (br, C(O)C*H*$_2$CH$_2$), 1.0-2.4 (br, -C*H*$_2$C*H*-).

Preparation of Thin Films. The NP-*g*-(PEO-*b*-PS) (**6**) linear diblock copolymers and PNP-*g*-(PEO-*b*-PS) (**7**) grafted block copolymers were spin-coated (3000 RPM, 60 s) from toluene solutions (1.5 wt%) onto silicon substrates that were coated with a 100 nm thick SiO_2 layer. The thin films were then annealed overnight under a saturated toluene atmosphere before being exposed to a high relative humidity (>85%) atmosphere for 15 minutes.

8.4 Results and Discussion

Polystrene-*block*-poly(ethylene oxide) PS-*b*-PEO diblock copolymers were grafted from a norbornene backbone through a combination of ATRP, “click” chemistry,

and ROMP. The synthetic route is shown in Scheme 8.1 and begins by first synthesizing compound **2**, which has a norbornene unit that can be polymerized by ROMP, as well as tertiary alkyl halide, which can serve as an ATRP initiating site. This was carried out by reacting the terminal primary alcohol of compound **1** with 2-bromoisobutyryl bromide in the presence of triethyl amine. The product was confirmed by NMR and FT-IR. The chemical shift of the methylene protons adjacent to the alcohol in compound **1** clearly shifted downfield from 3.53 ppm to 4.15 ppm as the ester formed for compound **2** (Figure 8.1A). Additionally, a singlet appeared at 1.90 ppm, which corresponds to the methyl groups of the tertiary alkyl halide. The large, broad peak corresponding to the hydroxy functional group (3200-3700 cm^{-1}) in FTIR was not present for compound **2**, and a new peak at 1690 cm^{-1} appeared, typical for an ester, confirming the transformation of the alcohol to an ester.

Scheme 8.1. Synthesis of grafted block copolymer PNB-*g*-(PS-*b*-PEO) (**7**).

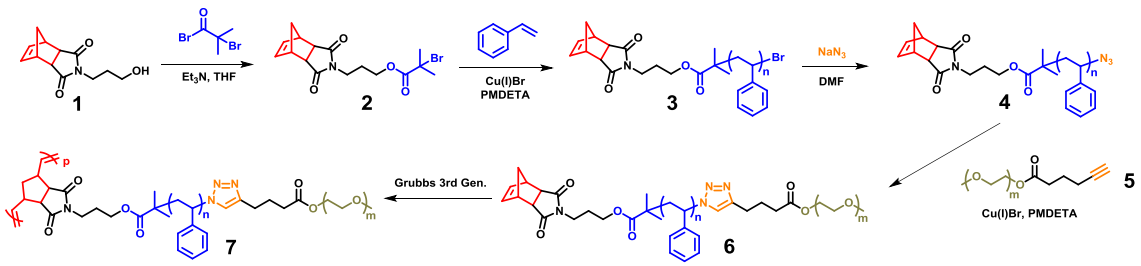

NP-Br (**2**) was then used to initiate the polymerization of styrene using Cu(I)Br and PMDETA at 90 ^{o}C. The polymerizations were monitored by ^{1}H NMR, as monomer conversion was calculated by comparing the ratio of decrease of the vinyl peaks at 5.74 and 5.22 ppm to the aromatic peaks between 6.00 and 7.40 ppm. The chain extensions were stopped at the desired percent monomer conversion. The molecular weight and

polydispersities of the polymers were determined by GPC, as the system was calibrated using PS standards (Table 8.1). NP-PS-N_3 (**4**) was obtained after reacting the terminal bromine group of NP-PS-Br (**3**) with sodium azide in DMF. Extractions against water and precipitations into diethyl ether removed residual sodium azide. The azide on the end of the polymer chain was confirmed by FTIR, as a sharp band appeared at 2100 cm^{-1}, which is common for an azide stretch (Figure 8.3C).

Commercially available monohydroxy-terminated poly(ethylene oxide) was reacted with 5-hexynoic acid in the presence of triethyl amine to prepare PEO-alkyne (**5**). ^1H NMR clearly shows the appearance of the presence of the methylene and alkyne protons between 1.78 and 2.85 ppm (Figure 8.2). PEO-alkyne (**5**) was then reacted with NP-PS-N_3 (**4**) in a copper catalyzed alkyne-azide cycloaddition using a Cu(I)Br/PMDETA catalyst system. The reaction was monitored by GPC, and was stopped once all NP-PS-N_3 (**4**) was consumed. Two precipitations into methanol removed all residual PEO-alkyne, as confirmed by GPC (Figure 8.4). Clean shifts to higher molecular weight from homopolymer **4** to end-functionalized diblock polymer **6** was observed in GPC (Figures 8.4 and 8.5). Additionally, ^1H NMR revealed shifts characteristic for both PS (6.35-7.33, 1.0-2.4 ppm) and well as PEO (3.4-3.8 ppm), while also having the norbornene end-group and methylene mid-group peaks (6.30, 2.69, and 2.48 ppm), as seen in Figure 8.1C. FTIR revealed the disappearance of the azide and alkyne stretches. Typically, a triazole stretching vibration is seen at 1500 cm^{-1}. However, this stretching was not noticed, likely due to the large steric bulk of the polymer chains on either side of the triazole unit (Figure 8.3D).

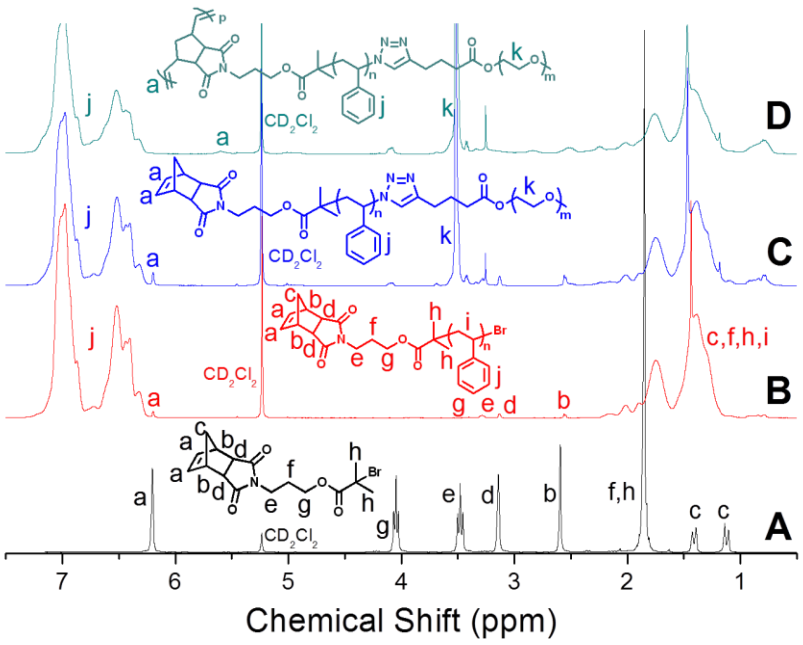

Figure 8.1. ^{1}H NMR spectra for compound **2** and polymers **3a**, **6a**, and **7a**.

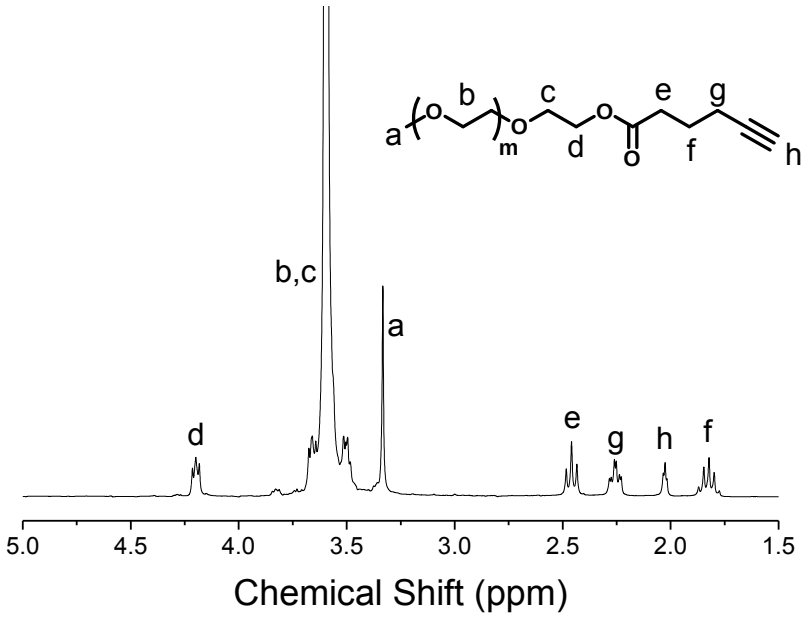

Figure 8.2. ^{1}H spectra NMR for polymer **5a**.

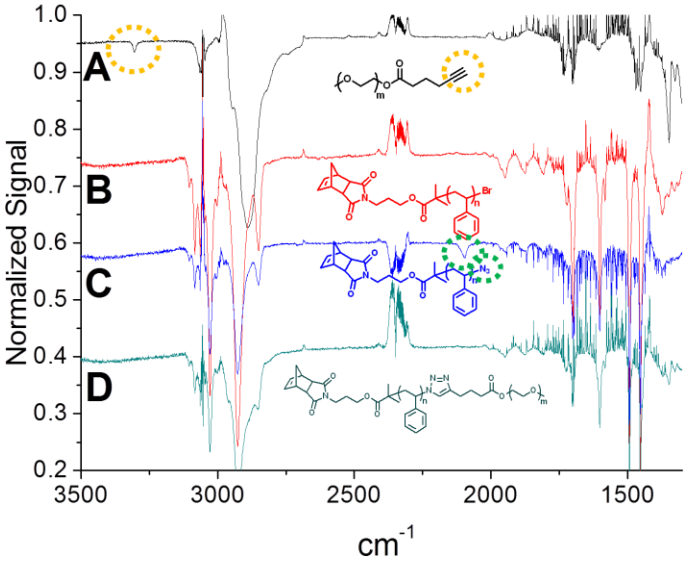

Figure 8.3. FTIR spectra for polymers **3a**-**6a**.

Grubbs 3rd generation catalyst was used to polymerize norbornene-functionalized diblock copolymer **6** in DMF at 60 °C. The polymerization was monitored by GPC, and was quenched with ethyl vinyl ether once all macromonomer was consumed. The polymer was then precipitated into diethyl ether twice before being characterized. ^{1}H NMR revealed the disappearance of the monomer alkene at 6.30 ppm and the appearance of two peaks at 5.42 and 5.60 ppm, which correspond to the polymer alkenes. As seen in Figures 8.4 and 8.5, the GPC traces of grafted block copolymer **7** cleanly shifted to a higher molecular weight with no residual macromonomer. Furthermore, the polydispersity of the grafted block copolymer remained below 1.3, demonstrating that a combination of ATRP, click chemistry, and ROMP resulted in well-defined polymers. The polymer compositions are given in Table 8.1.

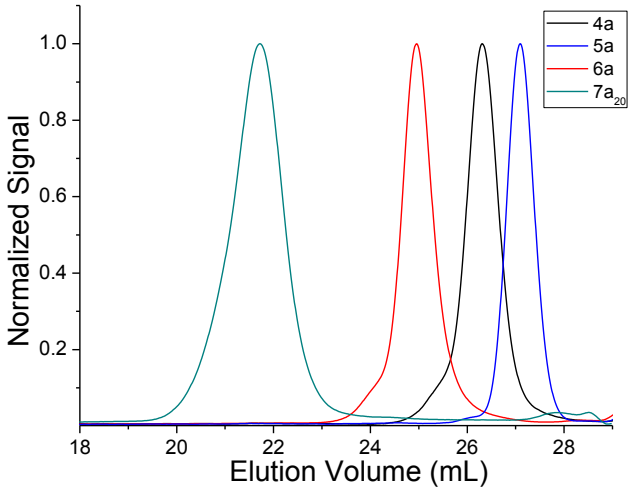

Figure 8.4. GPC traces for polymers **4a-7a$_{20}$**.

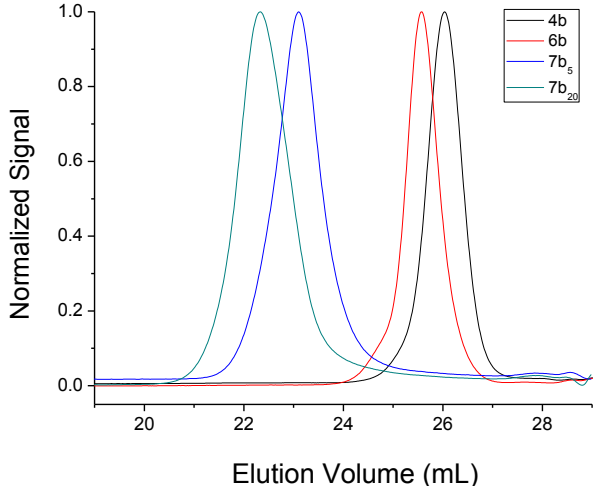

Figure 8.5. GPC traces for polymers **5b-7b$_{20}$**.

Table 8.1. Characterization of polymers **3-7**.

Polymer Entry	M_n	PDI [a]	DP PNP	Wt. % PEO	Wt. % PS	Wt. % Backbone
3a	6400[a]	1.15	--	--	--	--
3b	2400[a]	1.11	--	--	--	--
5a	2000[b]	1.05	--	--	--	--
5b	750[b]	1.08	--	--	--	--
6a	8690	1.13	--	23.02	73.65	3.34
6b	3440	1.13	--	21.80	69.77	8.43
7a$_5$	43500[c]	1.26	5	23.02	73.65	3.34
7a$_{20}$	173800[c]	1.30	20	23.02	73.65	3.34
7b$_5$	17300[c]	1.17	5	21.80	69.77	8.43
7b$_{20}$	68900[c]	1.17	20	21.80	69.77	8.43

[a]Determined from GPC calibrated by PS standards. [b]From supplier. [c]Calculated from feed ratio.

1.5 wt % solutions of block copolymers **6** and **7** in toluene were spin-coated onto silicon substrates. The thin films were then annealed in a saturated toluene atmosphere overnight before being exposed to a high humidity (>85% RH) atmosphere for 15 minutes. Complete film dewetting occurred for linear diblock copolymers **6a** and **6b**, as the molecular weights were too low to allow for enough intermolecular chain entanglement necessary to retain films (Figure 8.6A). Similar to the previous chapter, linear diblock copolymers **6a** and **6b** were complexed with LiCl. The resulting film for polymer **6a** after solvent annealing was partially dewet, as seen in Figure 8.6B. When the

ether linkages in PEO bind with Li^+, the χ between the PEO/Li and PS blocks is increased due to the ionic nature of the PEO/Li block. Furthermore, the lithium atoms can loosely coordinate between multiple PEO chains.[1, 28] This, to an extent, allows for enhanced inter-chain entanglement, as the lithium atom serves as a type of binding agent between polymer chains. However, the films for polymer **6b** after annealing fully dewet, revealing that the cation-ether interactions are limited in increasing inter-chain entanglement. Grafted block copolymers $\mathbf{7a_5}$ and $\mathbf{7a_{20}}$ retained high quality films after solvent annealing, as seen in Figure 8.6C.

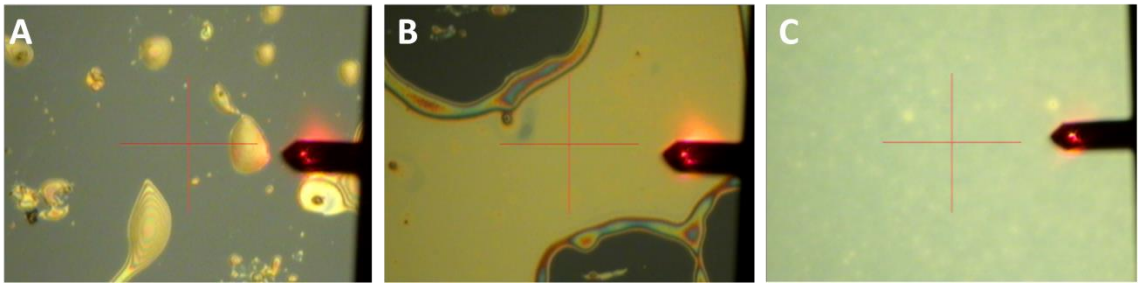

Figure 8.6. Optical microscopy images of low weight linear block copolymer **6b** without (A) and with (B) complexation with LiCl. (C) Optical image of grafted block copolymer $\mathbf{7a_{20}}$.

The diameter and center-to-center distance of the cylinders from **6a** complexed with lithium, $\mathbf{7a_5}$ and $\mathbf{7a_{20}}$ were 10 and 20 nm, respectively (Figure 8.7). Remarkably, the feature sizes of the hexagonally-packed arrays of cylinders for linear block copolymer **6a** complexed with lithium were the same as what was observed for grafted block copolymer $\mathbf{7a_5}$ and $\mathbf{7a_{20}}$. This demonstrates that when the backbone length is equal to or less than 20 repeat units, the feature sizes of the microphase separated nanostructures are due to the block characteristics of the diblock copolymers grafted onto the side-chain of the polymer brush.

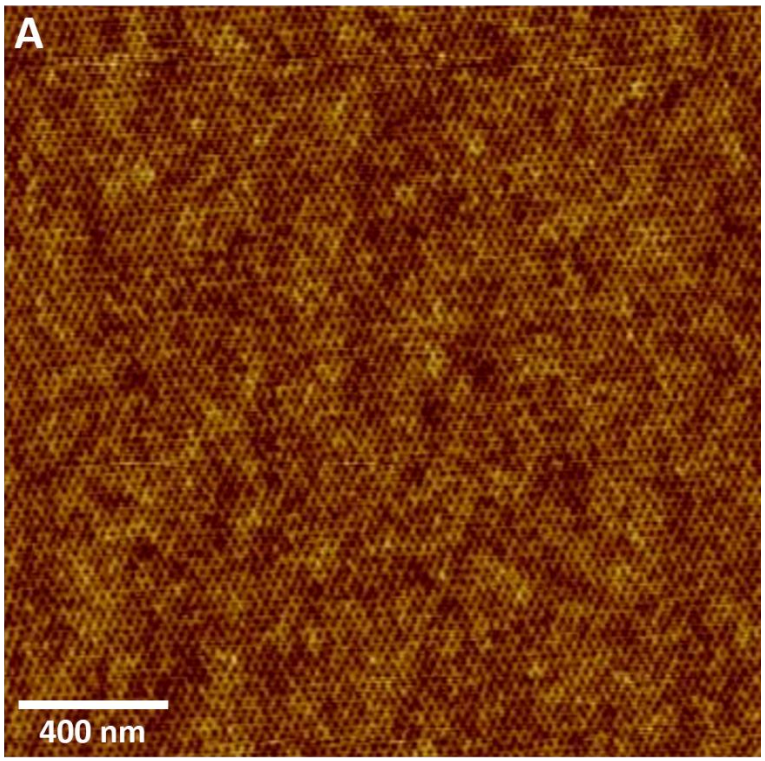

Figure 8.7. (A,B) AFM phase images of polymer **7a$_{20}$**.

PEO with molecular weight of 750 g·mol^{-1} was utilized to prepare grafted block copolymers **7b$_5$** and **7b$_{20}$**. The polymer compositions are shown in Table 8.1 and GPC traces in Figure 8.5. Complete film dewetting occurred for linear diblock copolymer **6b** after solvent annealing, as seen in Figure 8.7A. Even after complexing with LiCl in high ratios, no noticeable film was obtained after solvent annealing. Grafted block copolymers **7b$_5$** and **7b$_{20}$** retained high quality films after solvent annealing. However, microphase separation was limited without any long-range order, as seen in Figure 8.8. This is likely due to the extremely low molecular weight of the side-chain copolymers, which causes the ODT to occur. Also, the end-group may interfere with microphase separation, as the norbornene-initiator constitutes 8.43 wt% of grafted block copolymers

7b$_5$ and **7b$_{20}$** (Table 8.1). This may be enough to hinder ordering during the microphase separation process. Current studies are focused on utilizing low molecular weight PS-*b*-PEO diblock copolymers ($3{,}150 < x < 8{,}400$ g·mol^{-1}) on the side chain of a grafted block copolymer to determine what is the lowest possible molecular weight that leads to well-defined microphase separated structures. Furthermore, the backbone length for the grafted block copolymer systems are also being studied to find the upper and lower requirements for obtaining well-defined microphase separated structures utilizing such systems.

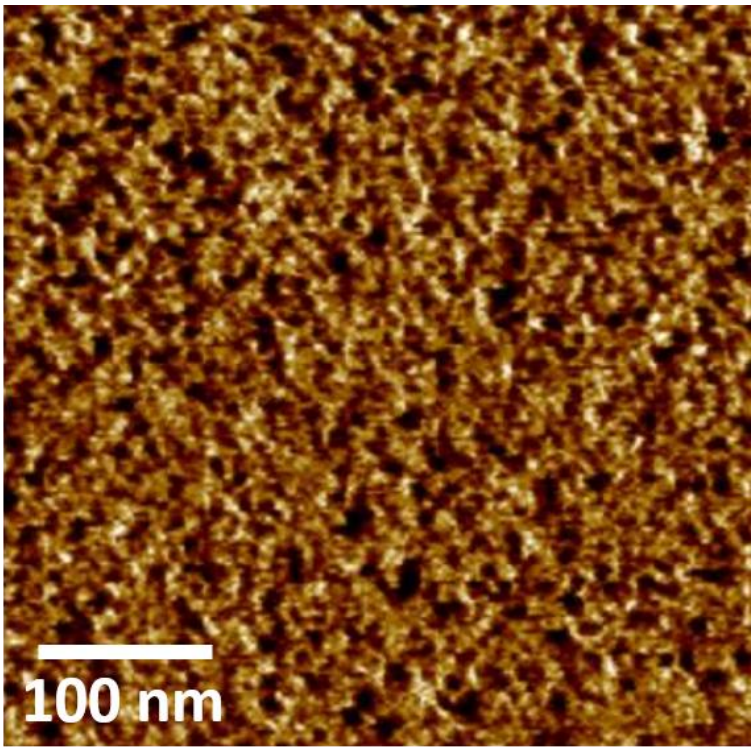

Figure 8.8. AFM phase image of polymer **7b$_{20}$** after solvent annealing.

8.5 Conclusions

In conclusion, we prepared grafted block copolymers using a polynorbornene-based backbone with PS-b-PEO diblock copolymers as the side-chains. By keeping the DP of the polymer backbone low, the polymer chains were able to rearrange and form highly ordered hexagonally-packed cylinders of PEO within a matrix of PS upon solvent annealing. The grafted copolymer system produced low feature sizes, while retaining high film quality after annealing.

8.6 Acknowledgements

This work was supported by the University of South Carolina and Global Research Collaboration Program of Semiconductor Research Corporation (Task ID 2222.001).

8.7 References

1. Park, S.; Lee, D. H.; Xu, J.; Kim, B.; Hong, S. W.; Jeong, U.; Xu, T.; Russell, T. P. *Science* **2009,** 323, 1030-1033.
2. Tang, C.; Lennon, E. M.; Fredrickson, G. H.; Kramer, E. J.; Hawker, C. J. *Science* **2008,** 322, 429-432.
3. Bang, J.; Kim, S. H.; Drockenmuller, E.; Misner, M. J.; Russell, T. P.; Hawker, C. J. *J. Am. Chem. Soc.* **2006,** 128, 7622-7629.
4. Ryu, D. Y.; Ham, S.; Kim, E.; Jeong, U.; Hawker, C. J.; Russell, T. P. *Macromolecules* **2009,** 42, 4902-4906.
5. Bita, I.; Yang, J. K. W.; Jung, Y. S.; Ross, C. A.; Thomas, E. L.; Berggren, K. K. *Science* **2008,** 321, 939-943.
6. Ross, C. *Annu. Rev. Mater. Res.* **2001,** 31, 203-235.
7. Ruiz, R.; Kang, H.; Detcheverry, F. A.; Dobisz, E.; Kercher, D. S.; Albrecher, T. R.; de Pable, J. J.; Nealey, P. F. *Science* **2008,** 321, 936-939.
8. Hardy, C. G.; Ren, L.; Ma, S.; Tang, C. *Chem. Commun.* **2013,** 49, 4373-4375.
9. Chuang, V. P.; Gwyther, J.; Mickiewicz, R. A.; Manners, I.; Ross, C. A. *Nano Lett.* **2009,** 9, 4364-4369.
10. Hardy, C. G. Functional Block Copolymers for Applications in Advanced Materials, Energy Storage, and Lithography. University of South Carolina, Columbia, SC, 2013.

11. Feng, C.; Li, Y.; Yang, D.; Hu, J.; Zhang, X.; Huang, X. *Chem. Soc. Rev.* **2011,** 40, 1282-1295.
12. Le, D.; Morandi, G.; Legoupy, S.; Pascual, S.; Montembault, V.; Fontaine, L. **2013,** 49, 972-983.
13. Charvet, R.; Novak, B. M. *Macromolecules* **2004,** 37, 8808-8811.
14. Kriegel, R. M.; Rees, W. S.; Weck, M. *Macromolecules* **2004,** 37, 6644-6649.
15. Cheng, C.; Khoshdel, E.; Wooley, K. L. *Macromolecules* **2007,** 40, 2289-2292.
16. Airaud, C. d.; Héroguez, V. r.; Gnanou, Y. *Macromolecules* **2008,** 41, 3015-3022.
17. Xie, M.; Dang, J.; Han, H.; Wang, W.; Liu, J.; He, X.; Zhang, Y. *Macromolecules* **2008,** 41, 9004-9010.
18. Le, D.; Montembault, V.; Soutif, J. C.; Rutnakornpituk, M.; Fontaine, L. *Macromolecules* **2010,** 43, 5611-5617.
19. Li, Z.; Ma, J.; Cheng, C.; Zhang, K.; Wooley, K. L. *Macromolecules* **2010,** 43, 1182-1184.
20. Cheng, C.; Qi, K.; Khoshdel, E.; Wooley, K. L. *J. Am. Chem. Soc.* **2006,** 128, 6808-6809.
21. Börner, H. G.; Beers, K.; Matyjaszewski, K.; Sheiko, S. S.; Möller, M. *Macromolecules* **2001,** 34, 4375-4383.
22. Cheng, C.; Khoshdel, E.; Wooley, K. L. *Nano Lett.* **2006,** 6, 1741-1746.
23. Runge, M. B.; Bowden, N. B. *J. Am. Chem. Soc.* **2007,** 129, 10551-10560.
24. Gu, W.; Huh, J.; Hong, S. W.; Sveinbjornsson, B. R.; Park, C.; Grubbs, R. H.; Russell, T. P. *ACS Nano* **2013,** 7, 2551-2558.
25. Ren, L.; Zhang, J.; Bai, X.; Hardy, C. G.; Shimizu, K. D.; Tang, C. *Chem. Sci.* **2012,** 3, 580-583.
26. Sanford, M. S.; Love, J. A.; Grubbs, R. H. *Organometallics* **2001,** 20, 5314-5318.
27. Hardy, C. G.; Islam, M. S.; Gonzalez-Delozier, D.; Morgan, J. E.; Cash, B.; Benicewicz, B. C.; Ploehn, H. J.; Tang, C. *Chem. Mater.* **2013,** 25, 799-807.
28. Xu, J.; Hong, S. W.; Gu, W.; Lee, K. Y.; Kuo, D. S.; Xiao, S.; Russell, T. P. *Adv. Mater.* **2011,** 23, 5755-5761.

CHAPTER 9

CONCLUSIONS

9.1 DISSERTATION SUMMARY

Incorporating desired functional groups into the side-chain, end-chain, and/or linker between polymer chains allows for spatial confinement of the functional group either within a specific domain or at the border between domains within a microphase separated block copolymer system. The first part of this dissertation focused on incorporating ferrocene units into the side-chain of homopolymers and block copolymers. Chapter 2 offered a review into metallocene-containing polymers that had been prepared by various living and controlled polymerization techniques. Chapter 3 detailed the preparation of several ferrocene-containing (meth)acrylate monomers and their polymerization by atom transfer radical polymerization. The thermal and electronic properties of the ferrocene-containing monomers and polymers were characterized. In Chapter 4, triblock copolymers were prepared which incorporated ferrocene into the side-chain of one domain. Upon self-assembly, highly ordered hexagonal arrays of ferrocene-containing cylinders were formed. After removing all organic material by pyrolysis or uv/ozonolysis, highly ordered arrays of iron oxide nanoparticles were obtained and characterized.

The second part of this dissertation dealt with preparing oligoaniline-functionalized block copolymers for use as all-organic nanodielectric materials. Chapter 5 summarized incorporating oligoaniline moieties into the side-chain of a diblock

copolymer. Upon self-assembly, the oligoaniline formed conductive domains within an insulating matrix which led to enhanced dielectric properties. In Chapter 6, oligoaniline units were added to the chain ends of polystyrene. For low molecular weight systems, microphase separation led to small domains of conductive oligoaniline. This system led to enhanced dielectric permittivity while retaining a low dielectric loss.

The third part of this dissertation involved preparing highly dense, ordered arrays of nanopores for use as templates in lithography. In Chapter 7, diblock copolymer PEO-*b*-PS with a photocleavable *ortho*-nitrobenzyl unit between the two blocks was prepared. Upon self-assembly, photoexposure, and PEO removal, highly ordered nanopores were formed. It was found that films could not be retained for low molecular weight systems, as limited inter-chain entanglement led to dewet films after annealing. In the pursuit of further decreasing the feature sizes while retaining film stability, grafted block copolymers in which PEO-*b*-PS diblock copolymers were grafted from a common backbone were prepared. By limiting the backbone length, enhanced inter-chain entanglement led to high quality films after annealing. For such systems, the domain sizes were dictated by the molecular weight of the block copolymers on the side-chain.

9.2 FUTURE WORK

The first part of this dissertation focused on incorporating ferrocene into the side-chain of block copolymers. Other than ferrocene, we have also incorporated cobaltocenium into block copolymer systems.[1-9] Cobaltocenium is cationic, and therefore, requires a counterion to be stable. We have found that by changing the counterion, the solubility, physical, and thermal properties can be systematically varied. Recently, new applications of cobaltocenium-containing polymers have been realized in

the medicinal field, as cobaltocenium-containing polymers utilizing halides as counterions show excellent anti-cancer and anti-microbial characteristics. More classes of counterion should be incorporated into cobaltocenium-containing polymers, including counterions that have multiple ionic sites, which could lead to cross-linked hydrogels. Additionally, other than ferrocene and cobaltocenium, there has been minimal work in preparing other metallocene-containing polymers. Incorporating ruthenocene, rhodocene, chromocene, titanocene, and zirconocene, amongst others, could lead to materials with unanticipated magnetic, catalytic, and electronic properties.

The second part of this thesis focused on preparing all-organic nanodielectric materials from block copolymers functionalized with oligoaniline. While dielectric permittivity was increased, there was also increases in dielectric loss. This likely results from the counterion present upon doping the oligoaniline structure to form a conductive state. We have recently started exploring other conductive polymers that do not need to be doped to an ionic state. Oligothiophene has shown great promise, as dielectric permittivity is increased while retaining low dielectric loss.[10] There is a lot of potential in incorporating other conjugated structures into one domain of a block copolymer, including polyacetylene, polyphenylene vinylene, and polyphenylene sulfide. Further functionalization of the conjugated repeat unit with alkyl chains or fluorinated chains may lead to enhanced dielectric properties.

The third part of this dissertation summarized recent work in utilizing block copolymer systems to prepare highly ordered templates for nanolithography. We found the lowest molecular weight of diblock copolymer PEO-*b*-PS in which films can be retained after annealing. We attribute the macroscopic dewetting of low molecular

weight films to the limited inter-chain polymer entanglement. To address this issue, we prepared grafted block copolymer systems in which the side-chains are block copolymers. Such systems retain high quality films after annealing due to increased inter-chain polymer entanglement. To expand this research thrust, star block copolymers, miktoarm star copolymers, brush copolymers, and multi-segmented block copolymers can be prepared (Figure 9.1). All of these systems utilize a central core or polymer backbone to link low molecular weight linear block copolymers. Much attention should be paid to the linking structure, as it was observed in Chapter 8 that the polymer end-group was having an impact on the microphase separation. Large end-groups have an increased volume fraction in low molecular weight block copolymers, which may interfere with polymer chain packing. A simple star block copolymer in which a small molecule with multiple branching sites may prove an ideal structure, as the star core will make a minimal impact on the overall volume fraction.

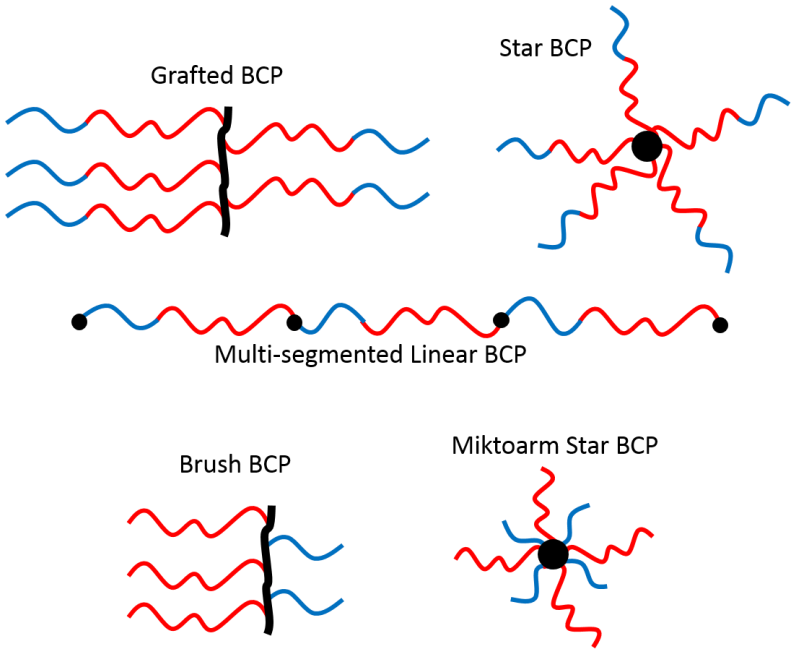

Figure 9.1. Various block copolymer systems.

9.3 REFERENCES

1. Ren, L.; Hardy, C. G.; Tang, C. *J. Am. Chem. Soc.* **2010,** 132, 8874-8875.
2. Ren, L.; Hardy, C. G.; Tang, S.; Doxie, D. B.; Hamidi, N.; Tang, C. *Macromolecules* **2010,** 43, 9304-9310.
3. Ren, L.; Zhang, J.; Bai, X.; Hardy, C. G.; Shimizu, K. D.; Tang, C. *Chem. Sci.* **2012,** 3, 580-583.
4. Ren, L.; Zhang, J.; Hardy, C. G.; Doxie, D.; Fleming, B.; Tang, C. *Macromolecules* **2012,** 45, 2267-2275.
5. Ren, L.; Zhang, J.; Hardy, C. G.; Ma, S.; Tang, C. *Macromol. Rapid Commun.* **2012,** 33, 510-516.
6. Zhang, J.; Pellechia, P. J.; Hayat, J.; Hardy, C. G.; Tang, C. *Macromolecules* **2013,** 46, 1618-1624.
7. Zhang, J.; Ren, L.; Hardy, C. G.; Tang, C. *Macromolecules* **2012,** 45, 6857-6863.
8. Zhang, J.; Yan, Y.; Chance, M. W.; Chen, J.; Hayat, J.; Ma, S.; Tang, C. *Angew. Chem. Int. Ed.* **2013**.
9. Yan, Y.; Zhang, J.; Qiao, Y.; Tang, C. *Macromol. Rapid Commun.* **2013**, n/a-n/a.
10. Qiao, Y.; Islam, M. S.; Han, K.; Leonhardt, E.; Zhang, J.; Wang, Q.; Ploehn, H. J.; Tang, C. *Adv. Funct. Mater.* **2013**, n/a-n/a.

APPENDIX A

COPYRIGHT RELEASES

JOHN WILEY AND SONS LICENSE TERMS AND CONDITIONS

Nov 19, 2013

This is a License Agreement between Christopher G Hardy ("You") and John Wiley and Sons ("John Wiley and Sons") provided by Copyright Clearance Center ("CCC"). The license consists of your order details, the terms and conditions provided by John Wiley and Sons, and the payment terms and conditions.

All payments must be made in full to CCC. For payment instructions, please see information listed at the bottom of this form.

License Number	3272550708385
License date	Nov 19, 2013
Licensed content publisher	John Wiley and Sons
Licensed content publication	Israel Journal of Chemistry
Licensed content title	Side-Chain Metallocene-Containing Polymers by Living and Controlled Polymerizations
Licensed copyright line	Copyright © 2012 WILEY-VCH Verlag GmbH & Co. KGaA, Weinheim
Licensed content author	Christopher G. Hardy,Lixia Ren,Jiuyang Zhang,Chuanbing Tang
Licensed content date	Feb 15, 2012
Start page	230
End page	245
Type of use	Dissertation/Thesis
Requestor type	Author of this Wiley article
Format	Print and electronic
Portion	Full article
Will you be translating?	No
Total	0.00 USD
Terms and Conditions	

Figure A.1. Copyright release for Chapter 2.

JOHN WILEY AND SONS LICENSE
TERMS AND CONDITIONS

Nov 19, 2013

This is a License Agreement between Christopher G Hardy ("You") and John Wiley and Sons ("John Wiley and Sons") provided by Copyright Clearance Center ("CCC"). The license consists of your order details, the terms and conditions provided by John Wiley and Sons, and the payment terms and conditions.

All payments must be made in full to CCC. For payment instructions, please see information listed at the bottom of this form.

License Number	3272550592875
License date	Nov 19, 2013
Licensed content publisher	John Wiley and Sons
Licensed content publication	Journal of Polymer Science Part A: Polymer Chemistry
Licensed content title	Side-chain ferrocene-containing (meth)acrylate polymers: Synthesis and properties
Licensed copyright line	Copyright © 2011 Wiley Periodicals, Inc.
Licensed content author	Christopher G. Hardy,Lixia Ren,Tuedjo C. Tamboue,Chuanbing Tang
Licensed content date	Jan 18, 2011
Start page	1409
End page	1420
Type of use	Dissertation/Thesis
Requestor type	Author of this Wiley article
Format	Print and electronic
Portion	Full article
Will you be translating?	No
Total	0.00 USD
Terms and Conditions	

Figure A.2. Copyright release for Chapter 3.

Self-assembly of well-defined ferrocene triblock copolymers and their template synthesis of ordered iron oxide nanoparticles

C. G. Hardy, L. Ren, S. Ma and C. Tang, *Chem. Commun.*, 2013, **49**, 4373
DOI: 10.1039/C2CC36756D

Figure A.3. Copyright release for Chapter 4.

JOHN WILEY AND SONS LICENSE TERMS AND CONDITIONS

Nov 19, 2013

This is a License Agreement between Christopher G Hardy ("You") and John Wiley and Sons ("John Wiley and Sons") provided by Copyright Clearance Center ("CCC"). The license consists of your order details, the terms and conditions provided by John Wiley and Sons, and the payment terms and conditions.

All payments must be made in full to CCC. For payment instructions, please see information listed at the bottom of this form.

License Number	3272551014297
License date	Nov 19, 2013
Licensed content publisher	John Wiley and Sons
Licensed content publication	Macromolecular Rapid Communications
Licensed content title	Oligoaniline-Containing Supramolecular Block Copolymer Nanodielectric Materials
Licensed copyright line	Copyright © 2012 WILEY-VCH Verlag GmbH & Co. KGaA, Weinheim
Licensed content author	Christopher G. Hardy,Md. Sayful Islam,Dioni Gonzalez-Delozier,Harry J. Ploehn,Chuanbing Tang
Licensed content date	Feb 14, 2012
Start page	791
End page	797
Type of use	Dissertation/Thesis
Requestor type	Author of this Wiley article
Format	Print and electronic
Portion	Full article
Will you be translating?	No
Total	0.00 USD
Terms and Conditions	

Figure A.4. Copyright release for Chapter 5.

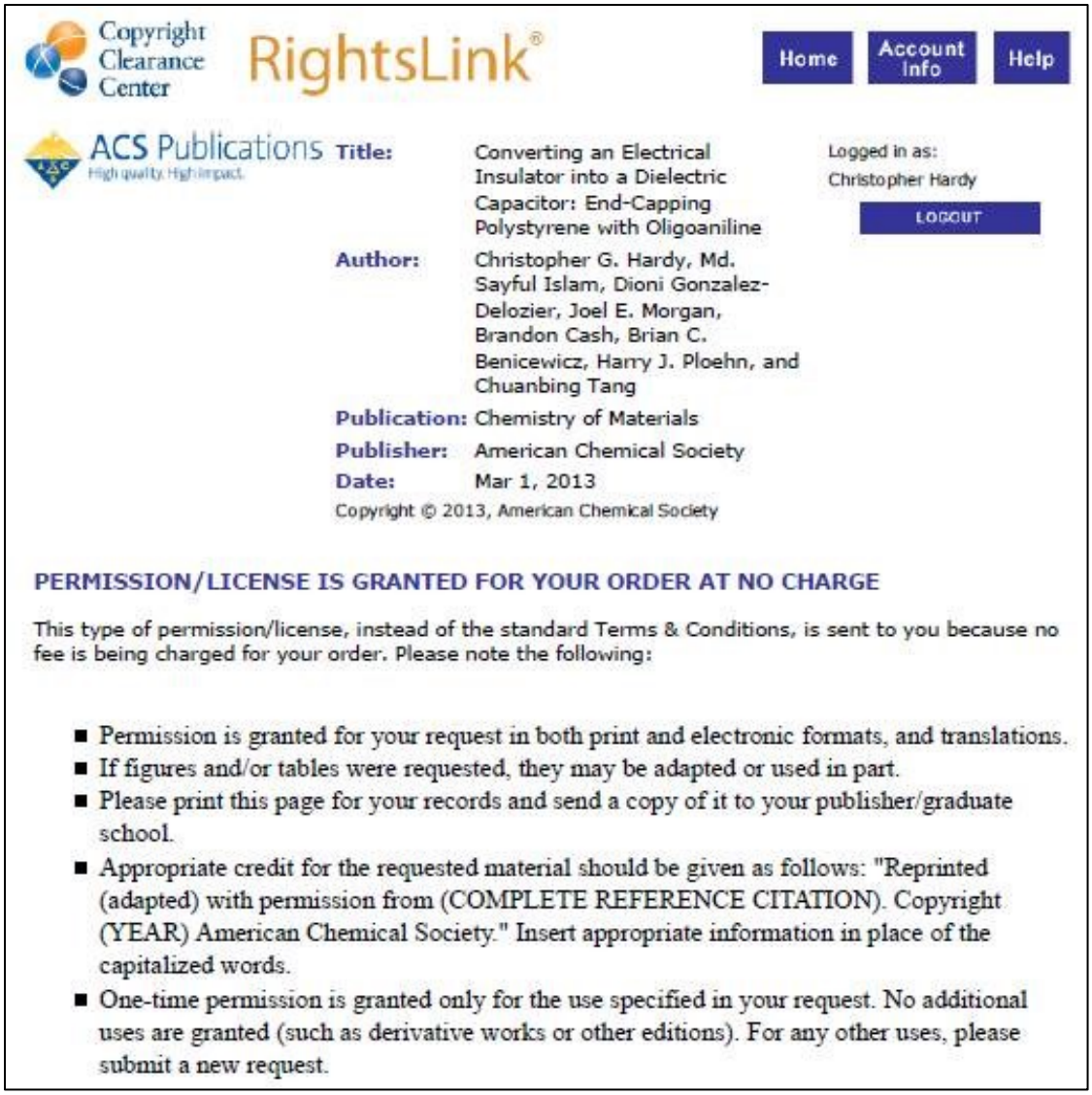

Copyright Clearance Center RightsLink®

Home | Account Info | Help

ACS Publications
High quality. High impact.

Title: Converting an Electrical Insulator into a Dielectric Capacitor: End-Capping Polystyrene with Oligoaniline

Logged in as:
Christopher Hardy
LOGOUT

Author: Christopher G. Hardy, Md. Sayful Islam, Dioni Gonzalez-Delozier, Joel E. Morgan, Brandon Cash, Brian C. Benicewicz, Harry J. Ploehn, and Chuanbing Tang

Publication: Chemistry of Materials

Publisher: American Chemical Society

Date: Mar 1, 2013

Copyright © 2013, American Chemical Society

PERMISSION/LICENSE IS GRANTED FOR YOUR ORDER AT NO CHARGE

This type of permission/license, instead of the standard Terms & Conditions, is sent to you because no fee is being charged for your order. Please note the following:

- Permission is granted for your request in both print and electronic formats, and translations.
- If figures and/or tables were requested, they may be adapted or used in part.
- Please print this page for your records and send a copy of it to your publisher/graduate school.
- Appropriate credit for the requested material should be given as follows: "Reprinted (adapted) with permission from (COMPLETE REFERENCE CITATION). Copyright (YEAR) American Chemical Society." Insert appropriate information in place of the capitalized words.
- One-time permission is granted only for the use specified in your request. No additional uses are granted (such as derivative works or other editions). For any other uses, please submit a new request.

Figure A.5. Copyright release for Chapter 6.